JOURNAL OF ENERGY IN SOUTHERN AFRICA

Volume 26 Number 2 • May 2015

Sponsored by the Department of Science and Technology

Sponsored by the
Department of Science & Technology

This journal is accredited by the South African Department of Higher Education and Training for university subsidy purposes. It is abstracted and indexed in Environment Abstract, Index to South African Periodicals, and the Nexus Database System.

The journal has also been selected into the Science Citation Index Expanded by Thomson Reuters, and coverage begins from Volume 19 No 1. It is also on the Scientific Electronic Library Online (SciELO) SA platform and is managed by the Academy of Science of South Africa (ASSAf).

It is the policy of the Journal to publish papers covering the technical, economic, policy, environmental and social aspects of energy research and development carried out in, or relevant to, Southern Africa. Only previously unpublished work will be accepted; conference papers delivered but not published elsewhere are also welcomed. Short comments, not exceeding 500 words, on articles appearing in the Journal are invited. Relevant items of general interest, news, statistics, technical notes, reviews and research results will also be included, as will announcements of recent publications, reviews, conferences, seminars and meetings.

Those wishing to submit contributions should refer to the guidelines given on the inside back cover.

The Editorial Committee does not accept responsibility for viewpoints or opinions expressed here, or the correctness of facts and figures.

Website: www.erc.uct.ac.za

 ISSN 1021 447X

JOURNAL OF ENERGY IN SOUTHERN AFRICA

Volume 26 Number 2 • May 2015

CONTENTS

Suppressed demand in the clean development mechanism: conceptual and practical issues

Randall Spalding-Fecher
Carbon Limits AS, Norway

Abstract
One of the challenges of applying greenhouse gas emission accounting approaches in poor communities is that the current consumption of many household services (e.g. heating and cooking, lighting and potable water) may not reflect the real demand for those services. This could be the result of lack of infrastructure, lack of natural resources or poverty, particularly the high costs of these services relative to household incomes. The situation of 'suppressed demand' creates a problem for setting emissions baselines against which to compare project performance, and has negatively affected CDM project development in Africa, Least Developed Countries and other regions with very few CDM projects. Ironically, although new large-scale power plants do not have to show that they actually displace other plants (existing or new), many small-scale energy projects can only claim credit for displacing historical (very low level) emissions from households. While the CDM rules are evolving to consider suppressed demand, much more can be done to catalyse investment in these types of climate change mitigation projects in poor communities. Furthermore, making progress will require significant expert and stakeholder input to ensure that simplification is balanced with maintaining overall environmental integrity.
Keywords: Clean development mechanism, climate change mitigation, suppressed demand, energy services, poverty

1. Introduction

When adopting the Kyoto Protocol in 1997, Parties to the United Nations Framework Convention on Climate Change (UNFCCC) established the clean development mechanism (CDM) with the twin goals of contributing to the sustainable development of developing countries and assisting developed countries to meet their emission limitation targets. This has meant that the rules for the CDM have had to address not only technical issues around greenhouse accounting but also the how the rules and procedures affect development in host countries. For any project-based mitigation activity under the CDM, the crux of the emissions reduction analysis is determining what would have happened in the absence of the mitigation mechanism or incentive. This includes determining the appropriate 'baseline' for a given project activity (i.e. technology development and emissions without the project activity), as well as the interlinked concept of determining whether the project activity is 'additional' (Ellis *et al.*, 2007; Gillenwater and Seres, 2011; Schneider, 2009).

One of the challenges of applying greenhouse gas (GHG) accounting approaches in poor communities is that the current consumption of many household services (e.g. heating and cooking, lighting and potable water) may not reflect the real demand for those services. This could be the result of a lack of infrastructure, lack of natural resources, or poverty, particularly the high costs of these services relative to household incomes. The situation of 'suppressed demand' creates a problem for setting baselines, because the CDM rules say that the baseline scenario selected for a project should provide the same level of service and quality as the project scenario (Winkler and Thorne, 2002). This is clearly not the case if the project scenario provides a much higher service level, owing to low historical consumption. At the same time, the CDM rules state that, 'the baseline may include a scenario where future anthropogenic emissions by sources are projected to rise above current levels, due to the spe-

cific circumstances of the host Party' (UNFCCC, 2006 para. 46), and in 2009 the Parties to the Kyoto Protocol directed the CDM Executive Board (EB) to, 'further explore the possibility of including in baseline and monitoring methodologies, as appropriate, a scenario where future anthropogenic emissions by sources are projected to rise above current levels due to specific circumstances of the host Party' (UNFCCC, 2009). This article examines how suppressed demand has been addressed so far in the CDM system, as well as discussing the need for and implications of increasing the use of suppressed demand in GHG accounting within the CDM.

2. Background and definitions

Household energy services for poor non-electrified communities are an important example of the need to consider suppressed demand, because historical energy consumption may not be a good proxy for future energy demand.[1] Even if we know the energy source used historically (e.g. kerosene for lighting), the quantity of fuel used historically may not represent the actual energy *service* demand. Energy services include lighting, cooking, space heating and motive power. These are measured not with energy units (kWh or GJ) but in units that reflect the actual service delivered (e.g. lumens of lighting, average indoor temperature, or litres of water heated to a certain temperature) (Modi *et al*., 2006; Sovacool, 2011). This distinction is very important because, for the same energy consumption and emissions, two different technologies can deliver vastly different energy service levels.

There are two main reasons why historical energy consumption may not be a good proxy for future energy consumption or future energy service level demand after electrification. These same two concepts could be applied to any other project type that provides services qualitatively and quantitatively different from historical service levels:

- Firstly, as incomes grow over time, energy service demand and consumption would increase, so that even without access to electricity it is likely that energy consumption in the 'without project scenario' would rise over time. This is the 'income effect'.
- Secondly, and more importantly, the combination of low household incomes and high unit costs of energy services can mean that individual households cannot afford sufficient energy services for their basic needs. In other words, since households face a budget constraint and must trade off purchasing energy services with other household needs, poor households may be forced to choose levels of energy services that are inadequate to meet their basic needs. If the households had access to a less expensive energy service (i.e. because of the availability of a less expensive source with lower unit cost, such as electric versus kerosene lighting), those households would consume significantly more energy services *even without a change in total household income*. This is the 'price effect' and it is due to a combination of lack of physical access to an energy source or technology (i.e. the lack of infrastructure barrier cited earlier) and a high unit cost of existing energy services. The price effect is similar to the 'rebound effect' described in the literature on energy efficiency (Greening *et al.,* 2000; Lin *et al.*, 2013).

Both the income effect and the price effect have been described as 'suppressed demand' for energy services that must be considered in setting the baseline for CDM projects that target energy services for poor communities (Gold Standard, 2011; Thorne *et al.,* 2010; UNFCCC, 2011; Winkler and Thorne, 2002). The two concepts, however, have different implications for how to construct an alternative baseline scenario. In addition, the income effect is accepted as a way to adjust historical energy use to create a baseline, while the price effect has only recently been explicitly implemented in approved accounting methodologies under the CDM. The implications for the baseline of these two components of suppressed demand are as follows:

- Baseline service level increase due to the 'income effect': If the main issue was the growth of energy consumption over time as *incomes* increase, and the costs of the energy service are fairly constant, then an appropriate baseline could start with historical energy consumption and increase this each year after project implementation, proportional to the increase in average household income in the target community (i.e. assuming an elasticity of demand for energy relative to income of 1). This is similar to the concept of a 'trend-adjusted' energy use projection in approved small-scale methodology 'AMS I.A Electricity generation by the user'. It could also include, for example, the household investing in more-efficient lighting technologies, owing to increased access to capital (e.g. kerosene pressure lamps, which are more expensive than hurricane lamps and therefore rarely used by the poorest communities).
- Baseline service level increase due to the 'price effect': The second concept, whereby historically households have not been able to purchase adequate levels of energy services, implies that a change in the *unit cost* of those services (e.g. $/lumen-hour, not $/kWh) could lead to an immediate and significant increase in energy service demand. Switching from kerosene lighting to electric lighting, for example, can reduce the unit cost of lighting by 90% or more and consumption of lighting services (lumens) may

jump by a factor of 40 (ESMAP, 2002; IEG, 2008).

The CDM Gold Standard, as part of the development of an improved cook-stove methodology, has considered the concept of suppressed demand: 'Where a group of people are deprived of a reasonable level of human development in comparison to their peers, and the opportunity to achieve a satisfactory level of service is available through carbon financing calculated from the baseline level of service of their peers or from the project level of service achievable, then the appropriate adjustment to the baseline can be made' (Gold Standard, 2011). This is an example of the price effect. The Gold Standard biogas-digester methodology has a similar definition of suppressed demand to the one provided here.

'Satisfied demand' is the level of energy services that would be reached with access to better quality and more affordable services and increases in income. In other words, satisfied demand is the level of energy service demand of households in a given area when the income effect and the price effect have been overcome. A CDM activity may overcome the 'price effect' by introducing a technology that dramatically reduces the unit cost of an energy service (e.g. CFLs with grid electricity). While a CDM project will not overcome the income effect directly, this is most likely much smaller and also has already been considered a reasonable adjustment to make to the baseline in cases such as the methodology for electricity generation by the user mentioned above.

Another way of understanding the relationship between these concepts is the following: the reason historical energy service levels are not a good proxy for the 'without project' baseline is that 'satisfied demand' for those services has been 'suppressed' by both an 'income effect' and a 'price effect'. The difference between satisfied demand and the actual observed level of demand is the sum of these two effects. This means that there are multiple options for setting a baseline, depending on the degree to which suppressed demand is considered. In addition, another option for the baseline is a 'minimum service level', which would reflect the minimum necessary to provide for adequate, basic human needs.

The concept of a minimum service level is common not only in the energy sector (see review of targets and measures in Bazilian *et al.*, 2010) but across many sectors, from the Millennium Development Goals (MDGs), to proposals for minimum levels of clean water per household, adequate household comfort levels (related to space heating and cooling), adequate nutritional levels and even 'threshold' poverty levels that represent a household's ability to achieve MDG service levels (Baer *et al.*, 2008; Falkenmark, 1989; Howard and Bartram, 2003; Modi *et al.*, 2006; Thorne *et al.*, 2010). This concept is also included in the EB-approve 'Guidelines on the consideration of suppressed demand in CDM methodologies' (UNFCCC, 2012, 2011).

Figure 1 illustrates the service levels of these different baseline concepts, showing how the suppressed demand effects discussed above and minimum service level compared with historical service levels. The 'income effect' line simply shows the gradual expected increase in service demand resulting from increasing household income within the affected communities (assuming per capita income is growing, which is not true for all developing countries). In other words, it is the service level without the income effect suppressing that demand. The 'income and price effect' line shows the step change in service levels that would occur if the services were suddenly as inexpensive (per unit) as they will be once the project activity has been implemented. For example, in the Philippines the estimated cost of lighting with kerosene is 36 US cents per kilolumen-hour (klmh), while the cost of lighting with grid electricity is 0.75 US cents per klmh (ESMAP, 2002). If the household had been able to pay 0.75 US cents per klmh for kerosene lighting historically, they would have consumed far more lighting services.[2] This is why the 'income and price effect' line has a significantly higher service level than historical consumption. Note that this line still slopes upwards, as household incomes grow. The 'satisfied demand' line is the level of services at which the entire income and price effect has been removed over a longer time period (e.g. 10 years). The 'minimum service level' line is flat because it reflects a standard 'adequate'[3] demand for basic services for a typical rural community, rather than being based on the current income of the households in that community. The minimum service level is lower than satisfied demand because most households would want more than the most basic services if they could afford it.

Figure 2 illustrates how *project* service levels could compare to the baseline scenario alternatives. Project service levels are much higher than historical service levels because of the impact that the CDM project has on the unit cost of services. Service levels could reach the minimum service level almost immediately owing to dramatically lower unit costs, but may still take time to reach satisfied demand because of the income level of the households or other specific characteristics of the community (e.g. energy taxes and subsidies, or appliance prices).

Energy consumption (GJ or kWh, as opposed to service level) in each scenario depends on the technology used to provide the service. For example, providing the minimum service level with the proj-

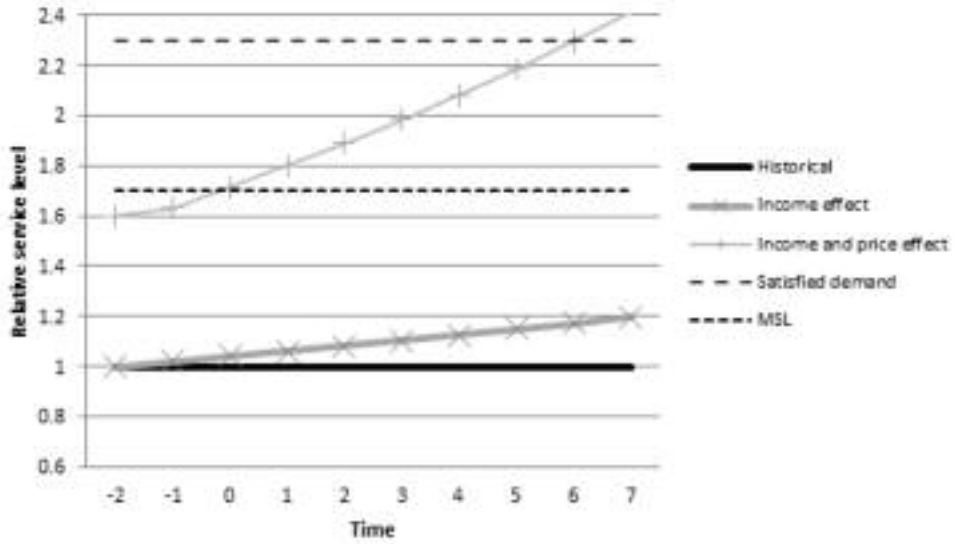

Note: Time is relative to the start of a CDM project activity. MSL = minimum service level.

Figure 1: Relative service levels for different baseline assumptions about suppressed demand effects and minimum service level
Source: Author's analysis

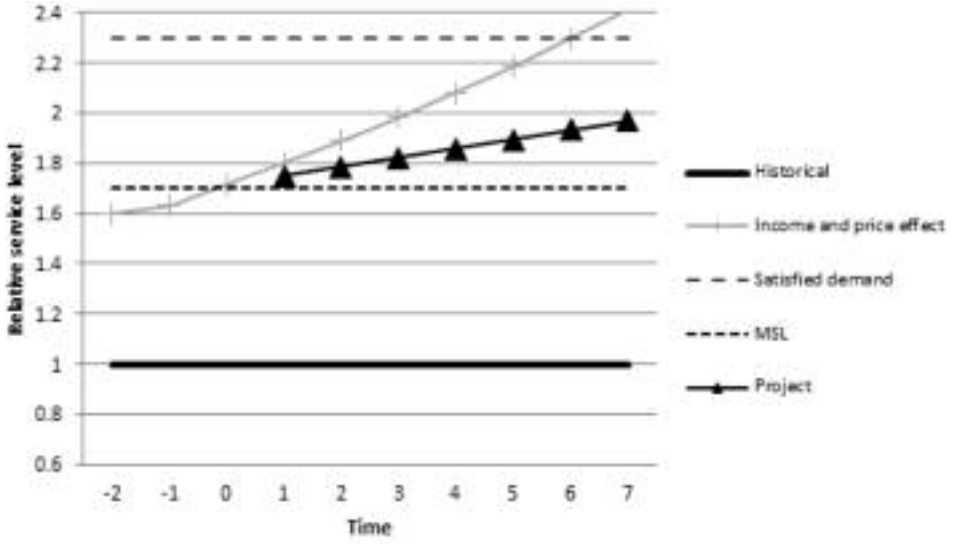

Note: Time is relative to start of CDM project activity. MSL = minimum service level. Income effect line has been removed for simplification.

Figure 2: Baseline and project service levels under different assumptions of suppressed demand effects and minimum service level
Source: Author's analysis

ect technology would use less energy than providing the same service with the historical technology. The project scenario might provide several times the service level of historical technology, but use less energy – in fact, this is what we would expect. Over time, however, the project scenario might use more energy than the household historically used, because the service level delivery is so much higher. This is particularly true if the project activity is grid electricity from a fossil fuel-based electricity grid. Figure 3 illustrates this possibility. The energy consumption of the baseline scenario alternatives in Figure 3 is shown using historical technology and is so marked 'hist', while the project scenario obviously uses the project technology. This shows how the project technology can meet the minimum service level and still be below historical energy consumption, because the project technology is so much more efficient at meeting the minimum service level. Of course, this figure does not provide an exact representation of these levels for all projects, but rather shows the possible relative differences. The relative emission levels would follow a similar pattern to the energy consumption levels, but obviously adjusted for the emission intensity of the fuels. The calculation of CERs would be very different if

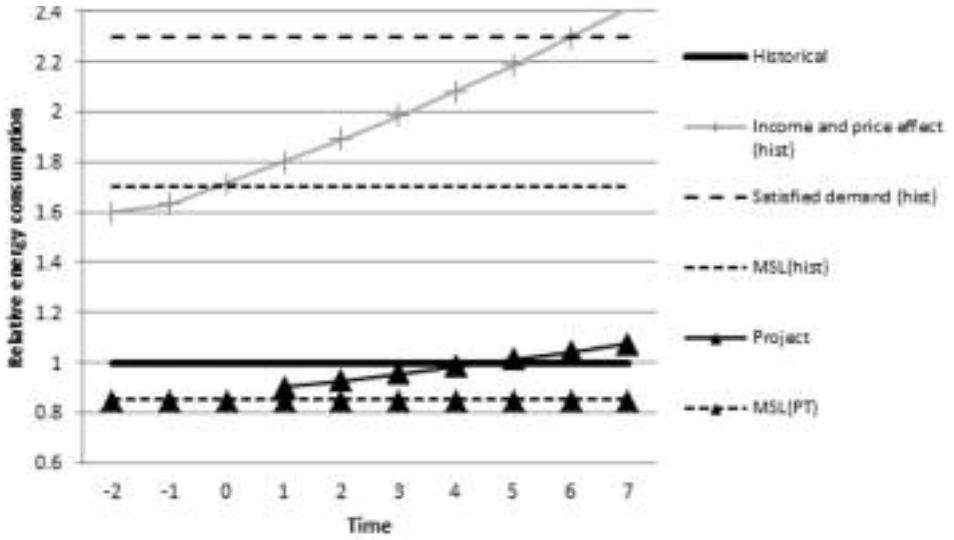

Note: The energy consumption levels are marked with (hist) to indicate the efficiency of the historical technology. For example, the minimum service level can be provided at a much lower energy consumption using project technology (PT). This implicitly assumes that the project technology is much more efficient than baseline technologies.

Figure 3: Baseline and project energy consumption under different scenarios (historical versus project technology)
Source: Author's analysis

comparing the project with the minimum service level using historical technology, instead of using actual historical energy consumption to calculate baseline emissions.

3. Suppressed demand under the CDM

Suppressed demand has been implicitly considered in some methodologies for greenfield projects, which do not use any historical consumption or production levels for the baseline. For example, ACM2 'Consolidated baseline methodology for grid-connected electricity generation from renewable sources' and AMS I.D 'Grid-connected renewable electricity generation', the most widely used methodologies, do not require the project participant to demonstrate that the CDM plant actually displaces another plant or that production is reduced elsewhere. The renewable power plant is essentially compared to the mix of power plants that would have been run or built to meet *additional demand* that exists but is currently not met owing to supply constraints. In the case of a geothermal or low power density hydropower plant (which both have some project emissions), this could mean that *total* emissions from the electricity grid actually increase as a result of the project, even though the emission *intensity* of electricity generation declines. This is reasonable, given the continuous and rapid growth in demand for electricity in almost all developing countries, and because of the large development benefits from increased access to and consumption of electricity.

Historically, this approach has not been applied to household energy services. Until recently, in the only methodology for household-scale renewable electricity provision, historical energy use was one of the baseline options, with the others being a diesel generator producing the same electricity or the electricity consumption in the closest grid-connected communities. While the last option could have addressed suppressed demand, the cost of monitoring was prohibitive for a small project. The diesel generator option was also problematic because the default emission factor used in the methodology was for a 200 kW capacity generator or larger. This implied that the most realistic alternative to household-scale renewable electrification was a local diesel mini-grid, when the capital cost for the latter would clearly be beyond the reach of that community even if the demand for energy services were there.

New methodologies and approaches are now emerging, along with important guidelines from the EB, to address suppressed demand. In early 2011 a methodology for water purification was approved (AMS II.AV) which used project water-consumption levels to determine baseline emissions, even if the households did not boil that much water historically owing to lack of time and income. For rural electrification, AMS I.L (for household-scale off grid) and AMS III.BB (for grid connection) approved in 2012 both explicitly define a minimum service level and baseline technology for household lighting and household total electricity use and use a default baseline emission factor to represent that minimum service level. Baseline emissions therefore do not require monitoring, which simplifies the monitoring process considerably.

In July 2011 the EB approved guidelines on the treatment of suppressed demand in CDM method-

ologies (UNFCCC, 2011e), and these were revised in July 2012 following inputs from stakeholders (UNFCCC, 2012). The guidelines provide methodological approaches for identifying the baseline technology/measure where there is suppressed demand and identifying the baseline service level used to calculate baseline emissions. The EB defined the minimum service level as, 'the service level that is able to meet basic human needs…basic housing, basic energy services including lighting, cooking, drinking water supply…. In some situations, this service level may not have been provided prior to the implementation of the CDM project activity'. The guidelines apply to any situation, 'when a minimum service level, as defined above, was unavailable to the end user of the service prior to the implementation of the project activity'. The guidelines outline the approach and principles for setting a minimum service level, 'that satisfies basic human needs and makes possible the development of the type of project'. The following guidance is also provided:

1. The minimum service level should be realistic and reasonable.
2. For establishing a minimum service level, the following approaches may be used:
   (a) National/international peer-reviewed research or relevant studies (e.g. the World Health Organization recommendations on per capita safe drinking water);
   (b) Benchmarks that take into account that emissions will rise to achieve the international/national development goals.
3. Further, in setting the minimum service level, the following should be taken into account:
   (a) Environmental integrity of the emission reductions has to be safeguarded;
   (b) Climatic zones may be taken into account where feasible;
   (c) Normative decisions have to be clearly referenced and explained;
   (d) Decisions regarding suppressed demand have to be re-evaluated and updated periodically based on recent data to ensure they are based on realistic assumptions.

The EB developed a work programme on suppressed demand, which included identifying methodologies for revision, public and expert consultation, revising methodologies and revising the guidelines themselves (UNFCCC, 2011i). The criteria for choosing these methodologies to revise included the opportunity to enhance the regional distribution of CDM projects, the wide use of the methodology by communities, whether minimum service levels can be considered in that technology area, and the exclusion of methodologies addressing industrial gases, processes and large-scale grid power generation (UNFCCC, 2012a).

Table 1 overleaf shows the methodologies where suppressed demand has been explicitly considered, in three different categories. The first group is from the work plan contained in the EB report, where the EB had requested the Secretariat and relevant support panels to explore how to incorporate suppressed demand. The second group is methodology revisions where the proponent of the revision motivated the change based on the Suppressed Demand Guidance. The final group is new methodologies that were developed after the approvals of the Suppressed Demand guidance and incorporated those ideas, as documented in the UNFCCC Methodology Guidebook (UNFCCC, 2013). Of the original 10 methodologies in the EB work plan, 5 were revised or replaced, while an additional 8 methodologies fall into the second and third categories. While the proportion of project activities influenced by these methodologies is very small, a significant share of CDM Programmes of Activities (PoAs) are utilising the revised or new methodologies.

4. Implications and concerns

The main concern raised by stakeholders regarding accounting for suppressed demand is that increasing baseline emission levels beyond historical emission levels could inflate the number of CERs issued and therefore undermine the environmental integrity of the CDM (e.g. Kollmuss, 2012). This concern does not imply that the household-level projects are not important, or that they are currently treated fairly, but that perhaps the CDM is not the best mechanism to address these project types. The current discussions around Results Based Financing (RBF) for mitigation, including the establishment of the Climate Initiative for Development (Ci-DEV) (www.ci-dev.org/) to address energy access issues, are looking at how payment levels could be increased even without changing the accounting for GHG impacts (ESMAP 2013).

The risks of increased crediting depends on the rate at which project beneficiaries would increase their emissions without the project, and how the minimum service level or other benchmark service level is set for that technology. If minimum service levels are set at levels that are achievable within a reasonable time frame (e.g. five to 10 years), this reduces the risk of inflating CER issuance. On the other hand, stakeholders have not criticised the greenfield power methodologies mentioned earlier for allowing crediting without actually displacing other power generation (current or future) and these are the most widely used CDM methodologies. There is an underlying equity issue here and a need for consistency across sectors and methodologies.

A related concern is that, even if the minimum service level is agreed, the choice of baseline tech-

Table 1: Methodologies explicitly addressing suppressed demand or part of EB work plan on suppressed demand

Source: Fenhann (2014)

				Pipeline	
Meth no.	*Meth name*	*Revised*	*When*	*Projects*	*PoAs*
	From EB67 work plan List of Meths				
AM0025	Alternative waste treatment processes	ACM22	EB69	126	5
AM0046	Distribution of efficient light bulbs to households	No		2	0
AM0086	Installation of zero energy water purifier for safe drinking water application	No	EB70	1	0
AM0094	Distribution of biomass based stove and/or heater for household or institution	No	EB70	0	0
ACM0014	Treatment of wastewater	Yes	EB77	47	1
ACM0016	Mass Rapid Transit Projects	No		15	1
AMS I.A	Electricity generation by the user	Yes	EB69	50	17
AMS I.E	Switch from non-renewable biomass for thermal applications by the user	Not nec.	EB70	27	58
AMS II.E	Energy efficiency and fuel switching measures for buildings	No		44	5
AMS III.AR	Substituting fossil fuel based lighting with LED/CFL lighting systems	Yes	EB68	4	14
	Additional revisions referring to Suppressed Demand				
AM0091	Energy efficiency technologies and fuel switching in new and existing buildings	Yes	EB77	0	0
AMS II.G	Energy efficiency measures in thermal applications of non-renewable biomass	Yes	EB70	45	68
AMS III.F	Avoidance of methane emissions through composting	Yes	EB67	103	21
	New methodologies where EB noted Suppressed Demand				
ACM0022	Alternative waste treatment processes	New	EB69	11	
AMS II.R	Energy efficiency space heating measures for residential buildings	New	EB73	0	0
AMS I.L	Electrification of rural communities using renewable energy	New	EB66	0	2
AMS III.BB	Electrification of communities through grid extension or new mini-grids	New	EB67	0	0
AMS III.AV	Low greenhouse gas emitting safe drinking water production systems	New	EB60/62	0	11
Total with revisions or new related to suppressed demand				413	197
Total pipeline				12011	452*

* PoA Design Documents submitted which may include multiple methodologies and include 23 PoAs replaced by new versions. Total number of methodology citations in all PoAs submitted is 888.

Note: Pipeline is as of 1 March 2014; PoA = CDM Programme of Activities. EBXX = EB meeting number.

nology has a dramatic influence on the baseline emissions. For example, the small-scale water purification methodology (AMS III.AR) allows the project participants to use boiling with non-renewable biomass as the baseline technology, even though many households may use low or non-energy intensive solutions (e.g. chlorination).

While some case studies are available on specific project types and how the concept of suppressed demand might be applied (GERES & CDC Climat, 2011; Thorne, 2012), there is no research yet on the overall impact on carbon credit generation or emission reductions that could come from including suppressed demand in baselines. The methodologies prioritized for revision represent only 4% of the CDM pipeline so far, and 13% of the PoA pipeline, so clearly there is scope to expand their use. While there may be some tension between increasing the CDM's contribution to sustainable development and ensuring that emission reductions are 'real' and 'measurable', recognizing the future growth in emissions and incorporating that into baselines is clearly a priority for the Parties to the Kyoto Protocol given the decision at the Copenhagen Conference that initiated the EB's effort. So in this sense, this may be more a political decision than a technical or scientific decision.

A final concern is how to establish the minimum service levels in a way that is 'realistic and reasonable but not overly conservative'. This may require not only substantial expert input but also more stakeholder consultation than methodologies typically have received in the past. Because setting minimum service levels is a normative decision and involves expert judgement, the process must be transparent and thorough. This is similar to the challenge faced in setting standardized baselines.

5. Conclusions

The concept of suppressed demand, although often mentioned in the discussions about the CDM, should be defined more clearly, to distinguish between 'income effects' and 'price effects'. This would guide further methodological development

in a way that could promote the more rapid uptake of clean energy technologies in poor communities as CDM projects. The guidance provided by the EB, and the subsequent revisions of methodologies and newly approved methodologies, is important steps forward. Further guidance is needed, however, on several key issues. These include the following:

- Limiting methodological changes to account for suppressed demand to the technologies and sectors that directly address household-level services.
- Developing a clear plan for approving 'minimum service levels' and baseline technology choices, including which stakeholders and experts will be involved and how.
- Providing guidance on the time frame within which the 'minimum service levels' should be achievable.
- Ensuring that the 'minimum service levels' are universal and not country specific.
- Using the methodology revision process to establish consistency across all sectors.
- Providing guidance on how often the 'minimum service level' and/or baseline technology should be reviewed and, if necessary, updated.

Notes

1. While the concept of suppressed demand could be applied to other sectors, such as industrial and commercial energy use, these are conceptually different for two reasons: the budget constraint is related access to capital issues rather than to poverty, and the difference in the price of energy service options available tends to be much smaller than for households (e.g. consider different commercial lighting options, as opposed to a household situation where kerosene wick lamps up to high efficiency bulbs are all options).
2. The difference in GHG-related external costs between these two services depends on both the delivery technology and the service level. Lighting with a 60W incandescent and a kerosene hurricane lamp, for example, might have fairly similar emissions over the course of the year, but the incandescent bulb would provide almost 20 times the service level (e.g. lux-hours) even when use the same number of hours.
3 The Guidelines provide different options for justifying the adequacy of the proposed service level, including: (1) The service level provided prior to the implementation of the project activity, (2) The service level provided under the project activity, and (3) A minimum service level derived from 'globally applicable conservative thresholds.' The latter may be based on, for example, 'national/international peer-reviewed research or relevant studies,' or, 'benchmarks that take into account that emissions will rise to achieve the international/national development goals.'

References

Baer, P., Athanasiou, T., Kartha, S., and Kemp-Benedict, E., (2008). The Greenhouse Development Rights Framework. The right to development in a climate constrained world (No. Second edition). Heinrich Böll Foundation, Christian Aid, EcoEquity and the Stockholm Environment Institute, Berlin.

Bazilian, M., Nussbaumer, P., Cabraal, A., Centurelli, R., Detchon, R., Gielen, D., Rogner, H., Howells, M., McMahon, H., Modi, V., Nakicenovic, N., O'Gallachoir, B., Radka, M., Rijal, K., Takada, M., and Ziegler, F., (2010). Measuring energy access: Supporting a global target. Earth Institute, Columbia University, New York.

Ellis, J., Corfee-Morlot, J., and Winkler, H., (2007). CDM: Taking stock and looking forward. *Energy Policy* 35, 15–28.

ESMAP, (2002). Rural Electrification and Development in the Philippines: Measuring the Social and Economic Benefits. Energy Sector Management Assistance Programme, World Bank, Washington, D.C.

ESMAP, (2013). Results-Based Financing in the Energy Sector: An Analytical Guide. Energy Sector Management Assistance Programme, World Bank, Washington, D. C.

Falkenmark, M., (1989). The massive water scarcity threatening Africa-why isn't it being addressed. *Ambio* 18, 112–118.

Fenhann, J., (2014). UNEP Risø CDM/JI Pipeline Analysis and Database, 1 February 2014 [WWW Document]. URL www.cdmpipeline.org (accessed 12.5.13).

GERES & CDC Climat, (2011). Three case studies of suppressed demand in CDM projects: case studies on development projects in the carbon market. GERES and CDC Climat, Aubange, France.

Gillenwater, M., and Seres, S., (2011). The Clean Development Mechanism: a review of the first international offset programme. *Greenh. Gas Meas. Manag.* 1, 179–203. doi:10.1080/20430779.2011.647014.

Gold Standard, (2011). Technologies and Practices to Displace Decentralized Thermal Energy Consumption [WWW Document]. URL http://www.cdmgoldstandard.org/wp-content/uploads/2011/10/GS_110411_TPDDTEC_Methodology.pdf. (accessed 7.3.12).

Greening, L.A., Greene, D.L., and Difiglio, C., (2000). Energy efficiency and consumption – the rebound effect – a survey. *Energy Policy* 28, 389–401.

Howard, G., and Bartram, J., (2003). Domestic Water Quantity, Service, Level and Health. World Health Organisation, Geneva.

IEG, (2008). The welfare impacts of rural electrification: a reassessment of the costs and benefits. An IEG impact evaluation. Independent Evaluation Group, World Bank, Washington, D. C.

Kollmuss, A., (2012). Suppressed Demand. An NGO Perspective. Presented at the UNFCCC Sustainable Development Methodologies Workshop, CDM Watch, Bonn.

Lin, B., Yang, F., and Liu, X., (2013). A study of the

rebound effect on China's current energy conservation and emissions reduction: Measures and policy choices. Energy 58, 330–339. doi:10.1016/j.energy.2013.06.018.

Modi, V., McDade, S., Lamment, D., and Saghir, J., (2006). Energy Services for the Millennium Development Goals (No. Millennium Project). Energy Sector Management Assistance Programme, United Nations Development Programme, UN Millennium Project, and World Bank, New York.

Schneider, L., (2009). Assessing the additionality of CDM projects: practical experiences and lessons learned. *Clim. Policy* 9, 242–254. doi:10.3763/cpol.2008.0533.

Sovacool, B.K., (2011). Conceptualizing urban household energy use: Climbing the 'Energy Services Ladder'. *Energy Policy* 39, 1659–1668. doi:10.1016/j.enpol.2010.12.041.

Thorne, S., (2012). Operationalising Suppressed Demand. Presentation to First Sustainable Development Mechanisms Joint Workshop. 24 March 2012 [WWW Document]. URL http://cdm.unfccc.int/stakeholder/workshops/jws/sdm_jws/presentations/jws_pres32.ppt (accessed 6.21.12).

Thorne, S., Mqadi, L., Winkler, H., Wamukonya, N., Michaelowa, A., and La Rovere, E.L., (2010). Energy poverty and suppressed demand for energy services – case study of low cost housing in South Africa. Unpublished working draft. SouthSouthNorth Project, Cape Town.

UNFCCC, (2006). Decision 3/CMP.1 Modalities and procedures for a clean development mechanism as defined in Article 12 of the Kyoto Protocol. FCCC/KP/CMP/2005/8/Add.1 [WWW Document]. URL http://cdm.unfccc.int/Reference/COPMOP/08a01.pdf (accessed 6.21.12).

UNFCCC, (2009). Decision 2/CMP.5. Further guidance relating to the clean development mechanism. FCCC/KP/CMP/2009/21/Add.1. United Nations Framework Convention on Climate Change.

UNFCCC, (2011). Guidelines on the consideration of suppressed demand in CDM methodologies (version 01). EB62 Report. Annex 6. United Nations Framework Convention on Climate Change, Bonn.

UNFCCC, (2012). Guidelines on the consideration of suppressed demand in CDM methodologies (version 02). EB68 Report. Annex 2. United Nations Framework Convention on Climate Change, Bonn.

UNFCCC, (2013). CDM Methodology Booklet. Information up to EB75 November 2013. United Nations Framework Convention on Climate Change, Bonn.

Winkler, H., and Thorne, S., (2002). Baselines for suppressed demand: CDM projects contribution to poverty alleviation. *South Afr. J. Econ. Manag. Sci.* 5, 413–429.

Received 13 June 2014; revised 12 March 2015

Proposal for improved nuclear fuel utilisation and economic performance by utilising thorium

Marina du Toit
Eskom and PhD student, Post Graduate School for Nuclear Science and Engineering, North West University, South Africa

Sunil Chirayath
Nuclear Security Science & Policy Institute, Texas A&M University and Nuclear Engineering Department, TAMU

Abstract
A systematic and strategic nuclear power reactor deployment roadmap has been developed for South Africa within the national strategic plan, utilizing thorium-based fuel. The roadmap was developed through analysis of economical, strategic and historical aspects. The accumulated advantages of thorium-based fuels are summarized, which could form the initiative to implement thorium-based nuclear fuels in South Africa.
A timeline (which forms the basis of the roadmap) was constructed and consists of three different phases. Phase 1 starts in 2015 and extends to 2030. Phase 2 starts in 2031 and ends in 2044 whilst Phase 3 is from 2045 to 2060. Each phase is discussed with regard to construction, implementation and research activities. This roadmap starts at current pressurized water reactors (PWRs) and advances to future reactor technologies, using an evolutionary approach.
In addition to the results reported in this paper, the economic advantages to introducing thorium as a fertile component in PWR fuels as compared to once-through conventional uranium-only cycles is explored (Du Toit & Cilliers, 2014). The economic evaluation compares uranium fuel to thorium-uranium fuel in terms of the fuel cycle costs, reactor downtime costs due to refuelling and income derived from electricity sales.

Keywords: thorium-based fuels, PWR, roadmap, fuel cycle, nuclear power in South Africa

1 Introduction

The world is facing the reality of increasing electricity demand and depleting natural resources. The recent focus on clean energy and security-of-supply has forced countries to diversify their electricity grid in order to become less dependent on fossil fuels such as coal, gas and oil. Uranium supplies, like any natural resource, are limited and uranium carries the risk of price escalations. Diversity of fuel sources other than uranium needs to be considered for nuclear power to be sustainable into a long future.

Nuclear technology for electricity production has received increased attention in South Africa (SA), especially after the South African government published the IRP2010 (Integrated Resource Plan) (SA, 2010). The South African IRP2010 requires building of new nuclear power reactors (most likely PWRs) with a generation capacity of 9 600 MWe before the end of 2030. New reactors are planned and the rate of building is restricted to one reactor every 18 months, the first reactor is scheduled for commissioning in 2023. South African policy, aimed at an increased nuclear power share, can be attributed to the depletion of coal resources, a move away from coal based electric generation as base-load power, to diversify and to focus on increasing electricity generation from carbon emission-free resources.

Uranium mined from its ore is the common fuel used in nuclear power reactors for electricity generation and to a lesser extent plutonium (a by-product in used uranium fuel). Thorium is another potential material which can be used in reactors to breed fissile fuel material, ^{233}U (man-made isotope of uranium compared to natural uranium isotopes, ^{235}U and ^{238}U). Transmutation of thorium (^{232}Th) to ^{233}U fuel through neutron irradiation in a nuclear reactor can be seen as a driver for fuel sustainability in nuclear power reactors. The challenge is that the uranium (^{233}U) bred from thorium has to be recov-

ered and the process must also be economically competitive compared to the uranium (^{235}U + ^{238}U) produced through mining and enrichment. Uranium resources are expected to deplete, being the sole resource for supplying fuel to about 435 nuclear power reactors currently in operation and 71 under construction worldwide, which will bring up the prominence of thorium (WNA, 2014).

Thorium deployment in nuclear power reactors has been studied during the 1950s, but was not commonly employed due to the abundance and also lower cost of mining uranium (Trellue *et al*., 2011). There is a renewed interest in thorium for reasons elaborated in Section 1.1 and the International Atomic Energy Agency (IAEA) has released several reports on thorium utilization in nuclear reactors (IAEA, 2000; IAEA, 2002; IAEA, 2003; IAEA, 2005). The feasibility of mixing thorium and plutonium fuel in existing PWRs has been the focus of some recent studies (Trellue *et al.,* 2011; Fridman & Kliem, 2011; Bjork, 2012). This fuel mix is especially used to optimize the plutonium destruction rate (Schram & Klaassen, 2007). Mixed thorium and uranium fuels in PWRs have been studied (Herring *et al.,* 2001; Weaver & Herring, 2002; Wilson et al., 2009). Thorium-plutonium mixed oxide fuel pins of Boiling Water Reactor (BWR), Pressurized Heavy Water Reactor (PHWR) and Advanced Heavy Water Reactor (AHWR) design have been tested in Indian research reactors, CIRUS and DHRUVA (BARC, 2014). The total thorium resources in SA are estimated at around 55,000 tonnes (Van Rooyen *et al*., 2012).

This study develops a roadmap for electricity generation from nuclear fuel resources in South Africa, utilizing thorium as a fuel. The advantages to implement thorium-based fuels are discussed. The roadmap is then developed and discussed to provide scope for policy-makers and government. The assumptions in developing the roadmap in three phases are described and each phase is described in terms of construction, implementation and research activity needs.

The economic advantages of introducing thorium as a fertile component in PWR fuels are explored as compared to once-through conventional uranium-only cycles (Du Toit & Cilliers, 2014). The economical evaluation and comparison of uranium fuel and thorium-uranium fuel in terms of the fuel cycle costs, reactor downtime costs due to refuelling and income derived from electricity generation are presented.

1.1 Advantages of thorium-based fuel

The advantages of thorium-based fuels are summarized in this section and all these advantages underlie the initiative to *implement* thorium-based fuels in South African nuclear power reactors.

Thorium is said to be between three to four times more abundant than uranium (Trellue *et al.,* 2011; WNA, 2011). Thorium-based fuels have greater potential to produce more fuel material (uranium) in reactors compared to uranium-based fuels producing fuel material plutonium (Kang-Mok & Myung-Hyung, 2005). Uranium produced from thorium has better fuel properties to enhance reactor safety, and to efficiently generate electricity (Trellue et al., 2011). Thorium dioxide (ThO_2) is more stable and robust than Uranium dioxide (UO_2) in fuel fabrication fuel from a metallurgical (Caner & Dugan, 2000) and chemical point of view. ThO_2-UO_2 and ThO_2-PuO_2 fuel combinations have better heat-transfer properties leading to lower fuel failures (Bjork, 2012). The higher melting point of ThO_2 aids in better utilization of fuel (Trellue *et al.,* 2011) and higher fuel utilization will extend refuelling time of the reactors, which in turn, reduces the fuel requirements and reduces used fuel management efforts. Extended re-fuelling cycles also reduce the reactor downtime for re-fuelling, which increases the reactor availability and capacity factors.

Thorium-based fuels are found to better alleviate the nuclear weapons material proliferation concerns compared to that of uranium-plutonium mixed oxide fuel (Herring *et al.,* 2001). Mixed oxides of ThO_2-PuO_2 fuel can achieve two times higher plutonium destruction rates compared to UO_2-PuO_2. This reduces the material attractiveness of plutonium (with regard to proliferation) in the used ThO_2-PuO_2 fuel because of reduced plutonium inventory (Trellue *et al.,* 2011). The uniformity of power production within the reactor core is a desirable reactor safety feature and is found to be better in ThO_2-UO_2 and ThO_2-PuO_2 fuelled reactors (Fridman & Kliem, 2011).

Based on the economic and technical advantages, along with the historic examples that suggests evolutionary introduction of new technology tend to be more successful than revolutionary changes. An evolutionary approach in the development of the aforementioned roadmap is taken by recommending the introduction ThO_2–UO_2 fuel assemblies in place of pure UO_2 fuel assemblies in the existing Pressurized Water Reactor (PWR) which results in a better fertile to fissile material conversion ratio, longer re-fuelling cycles and ultimately a reduction in operating cost. These changes result in slightly different operating parameters but the operating philosophy remains unchanged (Du Toit, 2012).

2. Roadmap

The advantages of thorium-based fuel and the historical, economical, strategic and technical aspects are taken into account to develop a nuclear power roadmap for South Africa and to provide the scope for policy-makers.

The roadmap consists of three different phases. Phase 1 starts in 2015 and extends to 2030. Phase 2 starts in 2031 and ends in 2044 and Phase 3 from 2045 to 2060. Each phase is discussed with regard to construction, implementation and research needs. This roadmap will progress and advance to future technologies using an evolutionary approach.

2.1 Assumptions

1. Six reactors are planned with a building rate of one reactor every 18 months; the first reactor being envisaged for commissioning in 2023 (SA, 2010). It is assumed that there will be a one-year delay and the first reactor will start operation in 2024.
2. The reactor construction duration is assumed to be four years (Koomey & Hultman, 2007).
3. It is estimated to take ten to fifteen years for introducing new fuels into modern reactors and it is assumed that the thorium-based fuel cycle could be deployed in the newly built reactors within the next fifteen years, which is comparable to the period that was required to implement mixed oxide fuel in PWRs elsewhere (Hesketh & Worall, 2010).
4. It is assumed that South Africa will start to build its own fuel production, fabrication- and fuel reprocessing plants in 19 years', which is two years after the 6th new reactor, will have been commissioned. This will correspond to the suggestion from Eskom Holdings SOC Limited to develop the fuel cycle facilities together with the reactor programme.
5. The used UO_2 fuel in PWRs is cooled for five years before it is chemically reprocessed to recover useful plutonium and uranium (Rose *et al.,* 2011).
6. The reprocessing duration after the cooling period is assumed to be two years (Shelley *et al.,* 2000).
7. The construction of the reprocessing facility would take up to ten years (Schneider et al., 2009).
8. It is assumed that the lifetime of the two PWRs currently operating in Koeberg, SA will be extended from 40 years to 60 years.
9. A new Accelerator Driven System (ADS), envisaged to incinerate nuclear waste and to produce electricity, needs a minimum of 40 years to be designed, built and reach commercial maturity (Hesketh & Worall, 2010). It is assumed that the first ADS will operate 45 years from now.
10. The annual discharge of recyclable plutonium from a standard PWR is about 250kg (Galperin *et al.,* 1997).

All of these assumptions result in a timeline as shown in Figures 1 and 2, depending on the scenarios chosen in Phase 2. These timelines form the basis of the roadmap and will now be discussed in more detail.

2.2 Phase 1 (2015-2030)

Phase 1 describes the starting point of the roadmap to implement thorium-based fuels in PWRs as well as the construction of the six planned reactors.

2.2.1 Construction

The first reactor starts construction in 2019 and will be commissioned in 2024, followed by three new reactors online in 2025, 2026 and 2027. The remaining two reactors will be commissioned in 2029 and 2030. During this time, South Africa

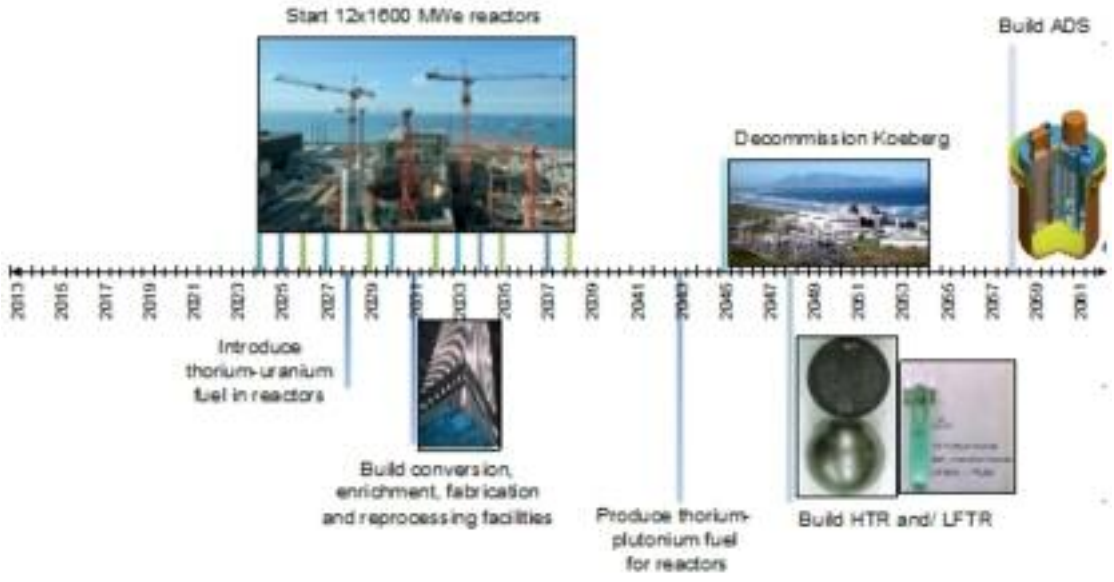

Figure 1: Thorium fuel introduction roadmap for Scenario A

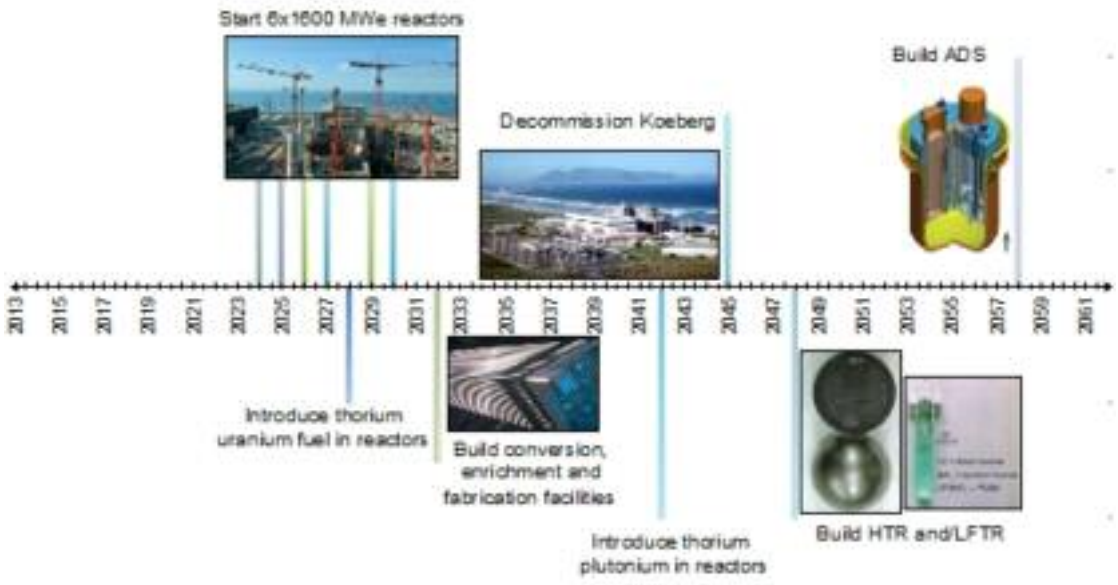

Figure 2: Thorium introduction roadmap for Scenario B

should obtain as much as possible experience and skills from the vendor/vendors building these reactors. Local contractors and manufacturers should be involved in the nuclear expansion programme and start to work independently on the last two reactors.

2.2.2 Implementation

In 2028, thorium-based fuels would be introduced in the one completed reactor, assuming the construction period to be four years for each new reactor. The choice for the thorium-based fuel for Phase 1 would be, once through ThO_2-UO_2 fuel with special coating and fuel cladding materials, increasing coolant water inside the reactor as well as reactor control materials like boron.

The reason for choosing ThO_2-UO_2 fuel than ThO_2.PuO_2 fuel is, because there is more open literature on investigations of the former than the latter (Schram & Klaassen, 2007). Also, uranium mining has already been established in SA, and currently SA has no plutonium (Pu) reprocessing facility to recycle Pu to use in ThO_2-PuO_2 fuels. ThO_2-UO_2 fuel has also proved to be more economical than ThO_2-PuO_2 fuel unless the cost of plutonium reprocessing and the corresponding fuel fabrication could be reduced. The proposed fuel cycle with thorium deployment is shown in Figure 3.

2.2.3 Research requirements

During Phase 1, investigations should focus on ThO_2-UO_2 and ThO_2-PuO_2 fuel deployment challenges such as;

- Reactor performance characterization with ThO_2-UO_2 fuel instead of the conventional UO_2 fuel used in PWRs.
- Reactor performance characterization with ThO_2-PuO_2 fuel instead of the conventional UO_2 fuel used in PWRs.
- Reducing the reprocessing cost to deploy ThO_2-PuO_2 fuels in PWRs in the future.
- Research and Development into the planning, construction of a fuel fabrication facility and a reprocessing facility, from here on called *fuel cycle facilities*.

The implementation of the required fuel cycle facilities (excluding the nuclear reactors) is projected at a cost of $6.15 billion (Balack, 2010). The applications for funding to support the fuel cycle

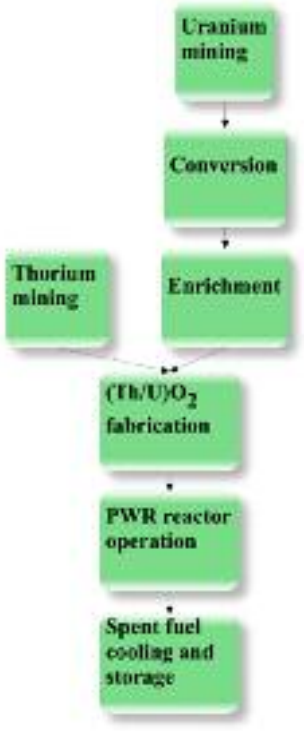

Figure 3: Fuel cycle for thorium deployment in Phase 1 of the roadmap

facilities development should be in progress at this time. The option to develop thorium-based fuels should be pursued in collaboration with other international partners.

As shown in Figures 1 and 2, other than PWRs, it is proposed to deploy technologically different but newer types of nuclear power reactors in SA. They are High-Temperature Reactors, Liquid Fluoride Thorium Reactors and Accelerator Driven System. Research should commence on these newer nuclear power systems as well.

The manufacture of fuels based on uranium (^{233}U), recovered through chemical reprocessing of thorium fuel discharged from the reactors has challenges associated with it, which could turn out to be very expensive than conventional natural uranium ($^{235+238}U$) fuel fabrication. Hence, research should also focus on streamlining the ^{233}U-based fuel fabrication process and reducing the chemical reprocessing cost of such fuels, by simplifying this process, or by a combination of all these factors (Lung & Gremm, 1998; BARC, 2014).

2.3 Phase 2 (2031-2044)

Two different scenarios are sketched for Phase 2, the first (scenario A) assuming that government decides to continue the nuclear reactor building programme after 2030 (refer to Figure 1). The second scenario assumes that the nuclear reactor building programmes stop in 2030 with no support to build a used fuel reprocessing plant (refer to Figure 2).

2.3.1 Phase 2A

Phase 2A focuses on the construction of the uranium enrichment and fuel fabrication plants to produce ThO_2-UO_2. The main reasons for building local fuel cycle facilities are to make sure of security of fuel supply and the usage of locally-mined uranium and thorium. Phase 2A also focuses on building a reprocessing facility and producing ThO_2-PuO_2 fuel. It should be noted that reprocessing is an expensive and sensitive step in the fuel cycle and depends on the local demand. The cost of conversion, enrichment, fabrication and reprocessing plants is estimated at $6.2 billion (Balack, 2010).

2.3.1.1 Construction

Construction on the nuclear fuel cycle facilities (including plants for conversion, enrichment, fabrication and used fuel reprocessing) will start in 2031 and construction is assumed to continue for 10 years. In 2041, the fuel cycle facilities should be online and be ready to recycle plutonium (Pu) and produce ThO_2-PuO_2 fuel. It is assumed that the same building schedule for nuclear reactors be followed as in Phase 1 starting with the commissioning of the first reactor in 2035. The construction of these six reactors will be easier at this time due to the experience gained from the first six reactors.

2.3.1.2 Implementation

ThO_2-PuO_2 fuel could be introduced in reactors by middle of 2043, assuming a reprocessing period of two years and another six months for fuel fabrication. The choice for the thorium-based fuel for Phase 2 would be ThO_2-PuO_2. The reasons for choosing ThO_2-PuO_2 are due to the used fuel accumulation at the currently operating PWRs at Koeberg and at new plants as well so as to reduce the waste stockpiles. According to simplified calculations, the accumulated plutonium can supply approximately 12 re-fuelling cycles of the reactor.

ThO_2-PuO_2 fuel improves proliferation resistance reduces waste with no new plutonium and relieves some of the uranium requirements. The reactor-grade (RG) plutonium is recycled from current Koeberg used fuel and mixed with thorium. The proposed fuel cycle is shown in Figure 4.

It should be noted that South Africa agreed that they would not reprocess their used fuel to recover plutonium. Commercial possibilities to reprocess used fuel overseas should be arranged. SA can also import reprocessed plutonium for the ThO_2-PuO_2 fuel option, but concerns about plutonium diversion for non-peaceful uses can cause impediments to this import.

Figure 4: Fuel cycle for Phase 2A of the roadmap

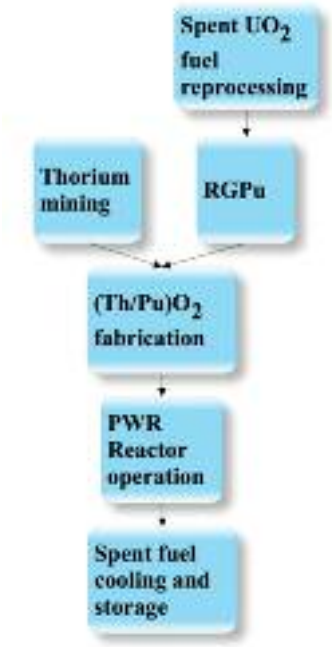

2.3.1.3 Research requirements

The behaviour of ThO_2-PuO_2 fuel in the new PWRs should be investigated, analysed and optimized.

The option to develop thorium-based fuels, not only for SA, but also in the future for the whole world should be researched (BARC, 2014). As

shown in Figures 1 and 2, it is proposed to implement HTRs, LFRs and ADS in future. Research on these nuclear power systems (HTRs, LFTRs and ADS) should be complete and should be moving into the design stages.

A permanent and sustainable fuel cycle involves utilizing uranium (^{233}U) bred from thorium-based cycles. The manufacture of ^{233}U-based fuels has challenges and needs to be made cost-effective and safe through R&D focusing on streamlining the fuel fabrication process and reducing the reprocessing cost of such fuels, by simplifying this process, or by a combination of all these factors (Kang-Mok & Myung-Hyung, 2005).

2.3.2 Phase 2B

The only difference here compared to Phase 2A is that chemical reprocessing of used fuel is not envisaged here. The reason for this is that eight reactors in total may not validate the capital investment in such a reprocessing facility. The cost of implementing the conversion plant, enrichment plant and fuel fabrication plant is approximately $3.6 billion (Balack, 2010).

2.3.2.1 Construction

Construction of the nuclear fuel facilities (including conversion, enrichment and fabrication facilities) will start in 2032 and construction is assumed to continue for ten years. In 2042 the fuel facility should be online and ready to produce ThO_2-UO_2 (note the difference in this scenario, as uranium, instead of plutonium is mixed with thorium, due to the fact that plutonium will be hard to come by without a reprocessing plant).

2.3.2.2 Implementation

The implementation activity for Phase 2B is similar to Phase 1, as the fuel is now only produced locally in South Africa. In 2042, the locally produced ThO_2-UO_2 fuels would be introduced into the remaining reactors. The choice for the thorium-based fuel for Phase 2B would be that it is once through (no recycling) ThO_2-UO_2 fuel with a special coating and fuel cladding materials, with increasing coolant water inside the reactor as well as reactor control materials like boron. The proposed fuel cycle is shown in Figure 5.

2.3.2.3 Research requirements

The behaviour of ThO_2-UO_2 fuel in the new PWRs should be investigated, analysed, and optimized. The option to develop thorium-based fuels, not only for SA, but also internationally, should be researched and pursued. As shown in Figures 1 and 2, it is proposed to implement HTRs, LFTRs and ADS in future. Research should commence on these systems (HTRs, LFRs and ADS).

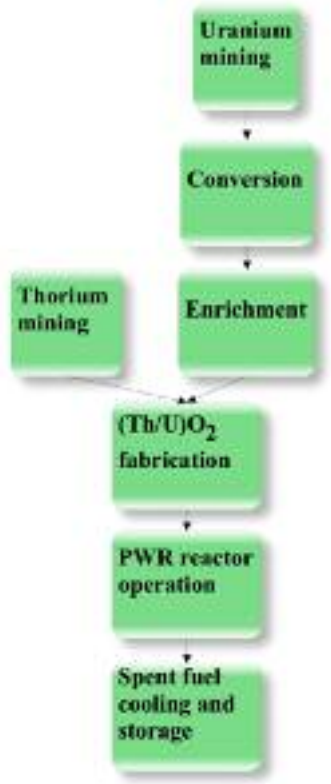

Figure 5: Fuel cycle for Phase 2B of the roadmap

2.4 Phase 3 (2045-2060)

Phase 3 consists of inducting (Th/^{233}U)O_2 into PWRs and building and planning thorium specific reactor designs such as the LFTR, ADS and the HTR. Please note that some of these reactors can reach commercial maturity before 2045, for instance, HTRs. HTRs and LFTRs both have continuous online re-fuelling, which completely eliminates the re-fuelling outage costs to the utility.

2.4.1 Construction

Koeberg would be decommissioned in 2045. HTRs and LFTRs should start construction in 2048. The number of reactor and reactor type would be based on the electricity demand and technological maturity. The ADS should start construction in 2058.

2.4.2 Implementation

ThO_2-PuO_2 fuel discharged from Phase 2 PWRs is cooled for five years and will be reprocessed to extract the uranium (^{233}U) produced from thorium. This extracted uranium can be used to manufacture ThO_2/$^{233}UO_2$ fuel and can be loaded into the periphery of PWR to compose so-called 'blanket' to help increase the re-fuelling time of the reactor. This cycle can be continued with the recycling of ^{233}U repeatedly (Si, 2009). The proposed fuel cycle is shown in Figure 6.

2.4.3 Research requirements

Research should focus on the optimisation of the

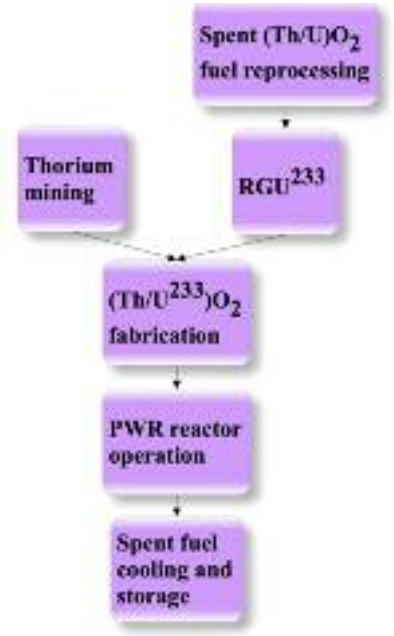

Figure 6: Fuel cycle for Phase 3 of the roadmap

entire current reactor systems as well as fuel performance. Possibilities to produce fuel for international markets should be explored.

3. Conclusions

A three-phase pragmatic approach is taken to develop an evolutionary strategic roadmap to introduce and implement thorium-based fuels in the South African nuclear power reactor building programme. It has been described in terms of construction, implementation and research activities. The strategic roadmap is based on historical, technical, strategic and economical aspects as well as based on the advantages of thorium-based fuels. An evolutionary strategy of introducing thorium-based fuels into existing and future reactor technologies is developed.

Thorium-based fuels can supplement uranium to diversify the natural nuclear fuel resources and increase the nuclear energy sustainability. Thorium-based fuels can incinerate plutonium, enhance fuel utilization and extend re-fuelling cycles of the reactor, which adheres to current governmental initiatives. SA can utilize local resources (Thorium, currently stockpiled) to enhance fuel utilization.

The thorium-based fuel implementation strategy fits in with the government policy and can pay for the front-end fuel cycle facilities by saving on fuel cycle costs and re-fuelling outage costs. The proposed strategy can help SA to become fuel-independent, help Eskom Holdings SOC Limited (current nuclear operator in SA) to keep the power on for longer period and create local job opportunities. Safety is increased with higher proliferation resistant fuels and advanced reactor technologies.

Acknowledgements

This work was supported by the South African utility, Eskom and the National Research Foundation (NRF).

References

Balack P.A. (2010). Framework for the cost of policy implementation of the South African nuclear expansion program. North-West University (Dissertation, M Eng).

BARC (Bhabha Atomic Research Centre), Department of Atomic Energy, Government of India (2014). Thorium fuel cycle in India. http://www.barc.gov.in/reactor/tfc.html Date of access: 04 May 2015.

Bjork K.I. (2012) Thorium-plutonium fuel for long operating cycles in PWR's – Preliminary calculations, Paper presented the Thorium and Rare Earths 2012, Cape Town, 22 February.

Caner M. & Dugan E.T. (2000). ThO2–UO2 annular pins for high burnup fuels. *Annals of nuclear energy*, 27 (2000) 759-770.

Du Toit M.H. & Cilliers A.C. (2014). Preliminary Economic Evaluation of Thorium-Based Fuels in PWRs, American Nuclear Society, Nuclear Technology 187:3 (2014) 260-269.

Du Toit, M.H. (2012). Introducing advanced thorium-based fuel cycles in SA: an evolutionary approach. North-West University (Dissertation, M Eng).

Fridman E. & Kliem S. (2011). Pu recycling in a full Th-MOX PWR core. Part I: Steady state analysis. *Nuclear engineering and design,* 241 (2011) 193-202.

Galperin A., Reichert P. & Radkowsky A. (1997). Thorium Fuel for Light Water Reactors Reducing Proliferation Potential of Nuclear Power Fuel Cycle. Science Global Security, 6, 265-290.

Herring J.S., Macdonald P.E., Weaver K.D &. Kullberg C. (2001). Low cost, proliferation resistant, uranium–thorium dioxide fuels for light water reactors. *Nuclear engineering and design,* 203, 65-85.

Hesketh K. & Worall A. (2010). The Thorium Fuel Cycle, An independent assessment by the UK National Nuclear Laboratory, Position Paper.

IAEA (International Atomic Energy Agency). (2000). Thorium based fuel options for generation of electricity developments in the 1990s. IAEA-TECDOC-1155.

IAEA (International Atomic Energy Agency). (2002). Thorium fuel utilization Options and Trends. IAEA-TECDOC-1319.

IAEA (International Atomic Energy Agency). (2003). Potential of thorium based fuel cycles to constrain plutonium and reduce long lived waste toxicity. IAEA-TECDOC-1349.

IAEA (International Atomic Energy Agency). (2005). Thorium fuel cycle — Potential benefits and challenges. IAEA-TECDOC-1350.

Kang-Mok B. & Myung-Hyung K. (2005). Core design for heterogeneous thorium fuel assemblies for PWR(I)-nuclear design and fuel cycle economy. *Nuclear Engineering and Technology,* 37, 91-100.

Koomey J. & Hultman N.E. (2007). A reactor-level analysis of busbar costs for US nuclear plants,

1970–2005. *Energy Policy,* 35, 5630–5642.
Lung M. & Gremm O. (1998). Perspectives of the Thorium Fuel Cycle, *Nuclear Engineering and Design,* 180, 133-146.
Rose S.J., Wilson J.N., Capellan N., David S., Guilemin P., Ivanov E., Schneider E.A., Deinert M.R & Cady K.B. (2011). Minimization of actinide waste by multi recycling of thoriated fuels in the EPR reactor. *Annals of Nuclear Energy*, 38 (2011) 2619–2624.
SA (SOUTH AFRICA). (2010). Integrated Resource Plan for Electricity 2010-2030. http://www.energy.gov.za/IRP/irp%20files/SO_IRP%202010%20Energy%20Forecast%20Final%20Report.pdf Date of access: 10 June 11.
Schneider E.A., Deinert M.R. & Cady K.B. (2009). Cost analysis of the US spent nuclear fuel reprocessing facility. *Energy Economics*, 31, 627–634.
Schram R.P.C. & Klaassen. (2007). Plutonium management with thorium-based fuels and inert matrix fuels in thermal reactor systems. *Progress in nuclear energy,* 49, 617-622.
Shelley A., Akie H., Takano H. & Sekimoto H. (2000). Radiotoxicity hazard of U free PuO2+ZrO2 and PuO2+ThO2 spent fuels in LWR. *Progress in Nuclear Energy*, 31, 317-382.
Si S. (2009). Roadmap Design for Thorium-Uranium Breeding Recycle in PWR, Shanghai Nuclear Engineering Research and Design Institute, Shanghai, China IAEA-CN-164-5S09.
Trellue H.R., Bathke C.G. & Sadasivan P. (2011). Neutronics and material attractiveness for PWR thorium systems using Monte Carlo techniques. *Progress in nuclear energy*, 53, 698-707.
Van Rooyen M., Mashai P. & Lydall M. (2012). Thorium: SA's most underestimated energy source? Paper presented at the Thorium and Rare Earths 2012, Cape Town, 22 February.
Weaver K.D. & Herring J.S. (2002). Performance of Thorium-Based Mixed Oxide Fuels for the Consumption of Plutonium in Current and Advanced Reactors. Paper presented at International Congress on Advanced Nuclear Power Plants (ICAPP), 2002 ANS Annual Meeting, 9 June.
Wilson J.N., Bidaud A., Capellan N., Chambon R., David S., Guillemin P., Ivanov E., Nuttin A &. Meplan O. (2009). Economy of uranium resources in a three-component reactor fleet with mixed thorium/uranium fuel cycles. *Annals of nuclear energy,* 36, 404-408.
WNA (World Nuclear Association). (2011). Thorium. http://www.world-nuclear.org/info/inf62.html Date of access: 30 Oct. 2011.
WNA (World Nuclear Association). (2014). http://www.world-nuclear.org/Nuclear-Basics/Global-number-of-nuclear-reactors/ Date of access: 5 Nov. 2014

Received 5 November 2014; revised 7 May 2014

Energy supply in Malawi: Options and issues

John L Taulo
Department of Mechanical & Mechatronic Engineering, Stellenbosch University, South Africa

Kenneth Joseph Gondwe
Department of Mechanical Engineering, University of Malawi, Blantyre, Malawi

Adoniya Ben Sebitosi
Department of Mechanical & Mechatronic Engineering, Stellenbosch University, South Africa

Abstract
Inadequate energy supply is one of the major problems confronting Malawi and limiting its social, economic and industrial development. This paper reviews the current status of energy supply and demand in Malawi; examines the major sources of energy, current exploitation status and their potential contribution to the electricity supply of the country; discusses key issues facing the energy sector; and identifies broad strategies to be implemented to tackle the energy supply challenges. Using secondary data for its critical analysis, the paper also presents modelling of long-term energy demand forecast in the economic sectors of Malawi using the Model for Analysis of Energy Demand (MAED) for a study period from 2008-2030. Three scenarios namely reference (REF), moderate growth (MGS) and accelerated growth (AGS) were formulated to simulate possible future long-term energy demand based on socio-economic and technological development with the base year of 2008. Results from all scenarios suggest an increased energy demand in consuming sectors with biomass being a dominant energy form in household and industry sectors in the study period. Forecast results reveal that energy demand will increase at an annual growth rate of 1.2% and reach 5160 ktoe in 2030 under REF scenario. The growth rates for MGS and AGS are projected at 1.5% each reaching 4639 ktoe and 5974 ktoe in 2030, respectively. The final electricity demand of about 105 ktoe in the base year will grow annually at average rates of 13.8%, 15.3% and 12.6% for REF, AGS and MGS, respectively. Over the study period 2008-2030 the annual electricity per capita will increase from about 111 kWh to 1062, 1418 and 844 kWh for the REF, AGS and MGS, respectively. The final energy intensity will decrease continuously from about 13.71 kWh/US$ in the base year to 3.88 kWh/US$, 2.98 kWh/US$ and 5.27 kWh/US$ for the REF, AGS and MGS, respectively in the year 2030. In conclusion, the paper outlines strategies that could be utilized to ensure adequate supply of modern energy which is a key ingredient for achieving sustainable social and economic growth.

Keywords: energy, energy supply, energy demand, scenario analysis, MAED, Malawi

1. Introduction

Energy supply has become a growing concern in Malawi and an important factor towards achieving growth and development. Future economic growth crucially depends on the long term availability of energy from sources that are affordable, accessible, and environmentally friendly. However, the country is faced with serious energy supply problems including, rising energy and electricity demand; insufficient power generation capacity; increasing high oil import bills; lack of investment in new power generation units; high transmission and distribution costs, transmission losses; poor power quality and reliability; heavily subsidized pricing; insufficient focus on alternative energy sources; and lack of access to modern electricity for a large segment of the population (MCC,2011).

In addition, the country faces a widening gap between electricity demand and supply which is being exacerbated by urbanisation, economic development, population growth and rural electrification (MCA, 2010). Electricity demand has been growing consistently at 6-8% per annum (GoM, 2010a). As a result, the existing system is greatly strained and the frequency of blackouts or brownouts is increasing, constraining industrial pro-

duction and provision of socioeconomic services as well as deterring foreign investment.

Furthermore, inefficient production and unsustainable use of biomass energy in Malawi is contributing to environmental degradation, such as high deforestation, desertification, and soil erosion. The use of wood, charcoal and crop residues as fuel also results in indoor air pollution which causes severe human health impacts directly to the users, especially rural women. Moreover, the task of gathering traditional supplies of fuelwood is time consuming and exhausting. This burden is borne by women and children, who are then diverted from other activities such as education and farming that could eventually have improved their productivity and living conditions. Thus, improving the energy supply situation and, in particular increasing access to electricity, are of prime concern in Malawi.

Very few studies on the country's energy sector and strategies for the future are presented in the literature. Kaunda (2013) investigated the energy situation and small scale hydropower potential and application status in Malawi. Kaunda and Mtalo (2013) presented work that studied the impacts of environmental degradation and climate change on power generation in Malawi. Although Gamula *et al.* (2013) provided an overview of the energy sector development in Malawi and the likely scenario in 2050, their study did not take into account fuel prices, technology costs as well as renewable energy potentials. Jumbe (2004) examined the relationship between electricity consumption and GDP for Malawi for the period 1970-1999. The study found bidirectional causality between electricity consumption and GDP. Openshaw (2010) studied biomass energy, employment generation, and its contribution to poverty alleviation. Despite these studies, there has been comparatively limited interest in examining the energy supply situation, options and issues associated with it in Malawi. Consequently, there has been a corresponding dearth of research. The present article aims at filling this gap in the literature.

This paper highlights the energy supply deficit the country faces and its impacts on social economic development against the background of rich endowment of renewable energy resources. It also critiques the constraints that are hindering growth in electric power generation, presents plausible alternative pathways and discusses on key issues that stakeholders must take on board to bring improvement in the energy supply.

2. Current status of energy demand and supply in Malawi

Malawi is located in South-east Africa and has a total area of 118 484 km^2 and a population of about 15.6 million inhabitants, with an annual growth rate of 2.8% (NSO, 2009). The GDP of the country in the year 2010 was US$5.7 billion with the following composition by sector: services 52%, 33% agriculture, and 15% industry. Agriculture contributes 60% of total export earnings and employs 84% of total labour force. The major export crops are tobacco, tea, sugarcane and cotton; tobacco alone accounts for about 67% of the export earnings from agriculture (World Bank, 2011). While the country's GDP has grown steadily by an average of 7% per annum over the last five years, electricity generation and supply has remained stagnant. With rapid increase in population and industry, energy needs are on the rise. Electricity shortages are estimated to cost the country around 2-3% of GDP (MCA, 2010).

Primary energy supplies of the country consist of hydropower, biomass, petroleum products, coal and other renewable energy sources.[1] Petroleum and petroleum products are imported and the country spends about 10 % of its foreign currency reserves on the import of petroleum products (GoM, 2003). On the other hand, the country's vast resource of renewable hydropower energy remains virtually unexploited. More than 84.7% of the total population in Malawi live in rural areas and has access only to wood and paraffin as major energy resources. Currently, the overall electrification rate in Malawi is 10%, with 37% of the urban population and only 2% of the rural population having access to electricity (NSO, 2009). Per capita consumption-often viewed as a key index of development- in the country, is only 290 kg of oil equivalent (kgoe) per person of primary energy compared to the averages of 563 kgoe for low income countries and the world average of 1820 kgoe (IEA, 2010). Similarly, the per capita consumption of electrical energy is still low, estimated at 93 kWh per year compared with 432 kWh and 2167 kWh per year for Sub-Saharan Africa and world averages, respectively (World Bank, 2001).

There is a strong correlation between human development index (HDI) and per capita electricity consumption. According to UNDP Human Development Report of 2013, Malawi's per capita consumption and its corresponding HDI of 0.418 is well below the sub-Saharan regional and global averages. Malawi needs to reach the first critical threshold of 500 kWh per year use.

Table 1 presents the distribution of primary energy supply for the years 1996 and 2008. Biomass remains the main primary energy source and accounted for 88.5% of the total energy supply for country. Petroleum fuels, electricity and coal supplied 6.4%, 2.4%, and 2.8%, respectively. Total primary energy supply in 1996 was 2741.32 kilo tonnes of oil equivalent (ktoe) and increased to 4125.97 ktoe in 2008 (GoM, 2010b).The major sources of traditional biomass are firewood, charcoal, and agricultural residues, and their shares in

energy supply are approximately 87%, 6.4% and 6.6%, respectively (Openshaw,2010). The share of commercial fuels including petroleum products, hydro and coal is 11.6%. The contribution of petroleum products in energy supply in Malawi has increased from 4.11% in 1999 to 6.4% in 2010.

Similarly, the contribution of coal in Malawi's primary energy supply in the country has increased from 1% in 1996 to 2.8% in 2010, primarily due to rapid expanding use of coal in industries. The contribution of renewable energy sources is only 0.3%, which is very low in comparison to other countries (GoM, 2010c). However, there is need to increase both coal and electricity consumption as a means of increasing the energy mix for the country. There has also been an increase in the percentage of households with access to electricity from 4% in 2005 to 10% in 2010. This is partly due to successful implementation of rural electrification program, which has increased the number of trading centres connected to electricity from 45 in 2005 to 182 in 2010. Furthermore, there has been a decline in the proportion of population using solid fuels from 94.8% in 2005 to 88.4% in 2010 (GoM, 2012).

Table 1: Primary energy supply share in Malawi

Primary energy supply	*Amount (ktoe)*		*Share (%)*	
	1996	2008	1996	2008
Biomass	2577.3	3640	89	88
Coal	50.16	98.68	2	2
Petroleum	200.1	280.07	7	7
Hydro	64.5	104.82	2	3
Solar	0	2.4	0	0
Total	2892.06	4125.97	100	100

Figures 1(a) and (b) show the final energy consumption per sector and fuel for the years 1996 and 2008. The household sector is the largest single consumer of final energy, with 3455 ktoe, followed by transport, industrial, agricultural and natural resources, and service with 201 ktoe, 180 ktoe, 168 ktoe and 106 ktoe, respectively. Rural households utilized the greatest proportion of the energy (77%) out of which 97% is of biomass origin and comprises mainly of firewood, charcoal and crop residues. The principal end uses of fuel are cooking and lighting. Firewood, charcoal and crop residues are used for cooking while paraffin is used for lighting. The main energy uses in the industrial sector are process heating, motive power, and lighting. Coal supplied 53.3% of total industrial energy demand, and electricity and biomass sources supplied 17.8% and 27.7% of the total energy demand, respectively (GoM, 2010c).

The energy consumption of the transport sector will be an important factor for the future of energy demand supply projection and has the potential to become the highest sector of energy consumption. The transport sector, in spite of consuming very little energy (5%) needs significant amounts of the country's foreign currency earnings to purchase this energy from abroad. The expenditure on petroleum fuels is growing through time because of price increases on the world petroleum market and the increment in vehicle imports. This is greatly influencing the trade balance of the country. Also the revenue to finance social services like health, education, and other infrastructure is significantly reduced by the pressure caused by the national transport energy expenditure.

3. Power energy status

3.1 Power generation capacity

Grid electricity is the main source of modern energy in Malawi. The major sources of electricity are hydropower and thermal. Table 2 shows the installed capacity of various generating plants and grid stations in Malawi. Total installed capacity for electricity generation as at March 2015 is 430 MW, in which 80% is contributed by the Electricity Supply Corporation of Malawi (ESCOM, 2011). The rest of the energy is supplied by the private sector at 19.6%. Total installed capacity of the grid

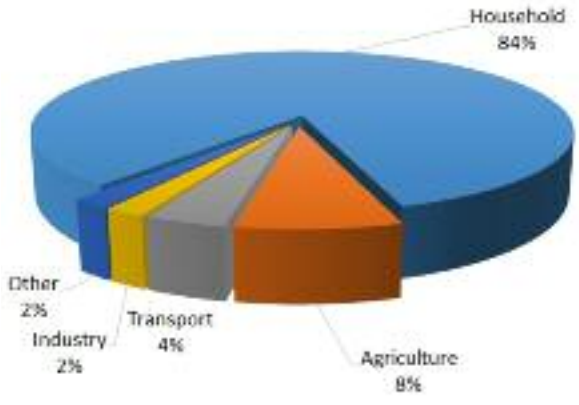

Figure 1(a): Total energy use, percent by sector, 1996

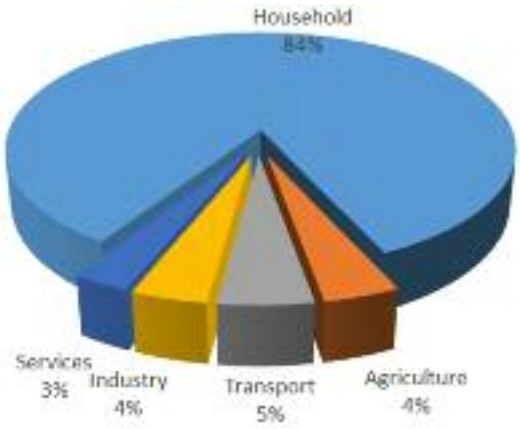

Figure 1(b): Total energy use, percent by sector, 2008

Table 2: Installed capacities (MW) of generating plants from different sources

Power plant	*Bagasse*	*Diesel*	*Hydro units*	*Solar/wind hybrid*	*Solar PV*	*Total*
Nkula A			3 x 8			24
Nkula B			5 x 20			100
Tedzani I			2 x 10			20
Tedzani II			2 x 10			20
Tedzani III			2 x 26.35			52.7
Kapichira I			2 x 32.4			64.8
KapichiraII			2 x 32.4			64.8
Wovwe			3 x 1.5			4.5
Mzuzu		1 x 1.1				1.1
Chizumulu		1 x 0.3				0.3
Likoma		3 x 0.25				0.75
Dwangwa	2 x 3.5					7
Nchalo	1 x 11.5					11.5
Kayerekera		1 x 10				10
Others		51.5		3 x 0.025		51.58
Lujeri			0.84			0.84
Lilongwe					0.87	0.87
Total	18.5	63.65	347.14	0.075	0.87	430.2

connected hydropower system and isolated small hydropower is around 351.8 MW and 4.5 MW, respectively (Gooneratne and Visser, 2010). The installed capacity and electricity generation of hydropower plants accounts for 80.2% and 98%, respectively, of the country's total power generation. In addition to this, there are a number of cogeneration and diesel power plants with a total installed capacity of 70 MW (GoM, 2010a), which are not connected to the grid and owned by the private sector. Currently, 0.3% power is produced from different renewable energy sources such as solar and solar/wind hybrid. The installed capacity of solar and solar/wind hybrid based power station is estimated to be 1 MW.

3.2 Electricity demand

Figure 2 shows electricity generation and demand between 1999 and 2011. Grid electricity has increased from 1031.8 to 1887.7 GWh between 1999 and 2011, representing an average annual increase of 6%. Between 1996 and 2011, the average maximum demand for electricity had increased from 190.2 MW to 277 MW. Currently the system average peak load is around 300 MW, while the available capacity is around 255 MW representing a deficit of 14%. Under the business as usual (BAU) scenario, the projected electricity demand will be 598 MW in 2015, 874 MW in 2020, 1193 MW in 2025, and 1597 MW in 2030 (GoM, 2010a). Further, an estimated step load increase of 37 MW per year is expected for up to 2020. The load fore-

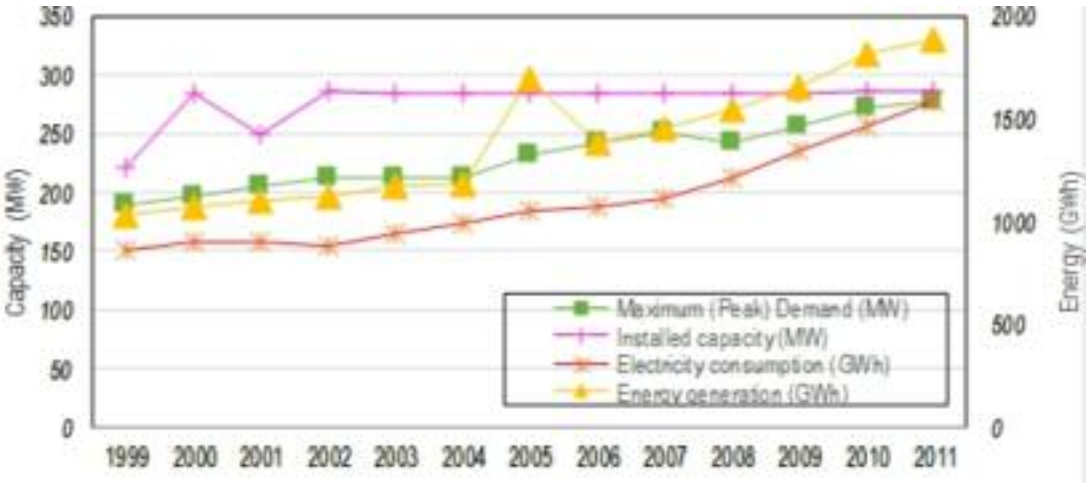

Figure 2: The total installed electricity-generation capacity and the peak demand in Malawi

casts also expects an average demand increase of 5 MW per year in the residential sector alone due to increased electrification. The supply and demand in the Malawi's power sector show a trend of significant shortage in the foreseeable future, due to an increase in demand averaging 7% per year (GoM, 2010c). The annual electricity consumer connections have continued to rise sharply over the last five years, increasing from 175, 167 in 2008/9 to 204, 955 in 2011/12 financial years (ESCOM, 2011). The total number of customers connected to electricity was 218,164 as of June 2012 representing 10% access, which still compares poorly to the average of 32% for developing countries (Kiplagat, Wang and Li, 2011).

3.3 Generation capacity expansion

Future generation plants consist of conventional hydro power schemes and coal fired stations as well as a nuclear power plant. Total planned generation capacity will grow from 430 MW in the base year to over 2764 MW (GoM, 2010a). Hydro will maintain its position as the main driver of the electricity sector in the short to medium term. Hydropower capacity is expected to increase from 351 MW in the base year to about 1985 MW by 2050. Coal and nuclear capacity are expected to increase from nil to 420 MW and 125 MW by 2050, respectively. Renewable energy technologies such as small hydro, geothermal and dendro thermal are not captured by the least economic cost based planning process being followed by government. However, it is estimated that a technical potential of about 150 MW of small hydropower (GoM, 1997), over 100 MW of dendropower (Venedaal, 1996) and over 200 MW (Gondwe et al., 2012) of geothermal power exists in the country. The expansion of grid connected small-hydro schemes and the introduction of dendro thermal systems and geothermal power systems would reduce the need for fossil fuel based power generation, resulting in reduced greenhouse gas emissions.

4. Energy outlook for Malawi

4.1 Scenario development

To analyse the future development of the Malawian energy and electrical demand, the computer program MAED (Model for Analysis of Energy Demand has been applied. MAED is a bottom-up approach model widely used for forecasting medium to long-term energy demands. It evaluates the future energy needs based on medium and long-term scenarios of socioeconomic, technological and demographic development in a country or region. Key consumption sectors that are considered in MAED comprises of industry, transport, household and service. The industry is further divided into sub-sectors that comprise of agriculture, construction, mining (ACM) and, manufacturing while transport sector is sub-divided into passenger and freight transport. Population is a major driver of energy demand, while its most important determinant is the level of economic activity and its structure measured by the total gross domestic product (GDP) alongside the various sectors of the economy. Population of Malawi is expected to grow from 13.077 million in 2008 to 19.696 million by 2030 at an average annual rate of 2.8%. The GDP growth rate is projected at 7% per year in the long term. The results of the study carried out using the MAED model are discussed in this section.

4.2 Simulation results and analyses

4.2.1 Total final energy demand projection

Figure 3 presents the projected total final energy demand from 2008 to 2030 for the three scenarios in this study: REF, AGS and MGS. The average annual growth rate will amount to 1.2%, 1.5% and 1.5% for REF, AGS and MGS, respectively. Total final energy demand will increase from 4125 ktoe in the base year to 5160, 5974 and 4639 ktoe in the year 2030 for REF, AGS and MGS, respectively. Results further show that energy balance for all scenarios will be dominated by biomass followed by electricity and imported energy (fossil and motor fuels). Biomass dominates both scenarios by having an average share of 39.5%, 34.7% and 43% of the total final energy demand for REF, MGS and AGS, respectively. Moreover, results indicate that imported energy have an average of 25.1% in 2030 for all scenarios. Electricity will command a share of 34.8%, 40.2% and 43% of final energy demand in REF, MGS and AGS scenarios, respectively in 2030.

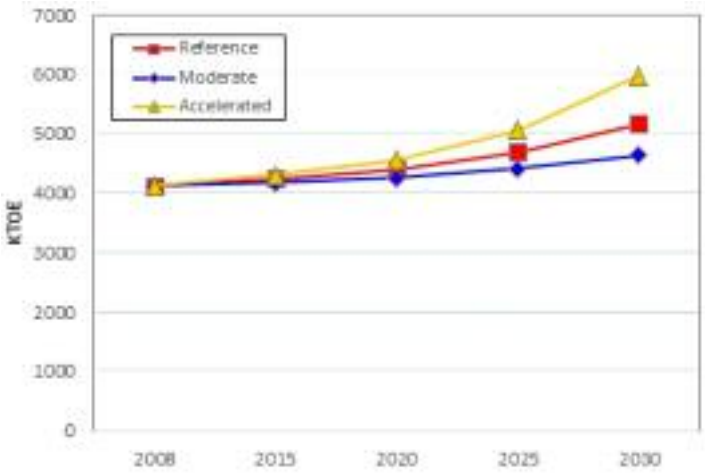

Figure 3: Total final energy demand projection in Malawi

4.2.2 Final energy demand by energy form

Table 3 shows the development of final energy demand distributed by the energy form of consumption. Compared to the REF and AGS scenarios, MGS show less projected energy demand growth rate as the final energy is less by 526 ktoe than REF whereas AGS is higher by 809 ktoe both

in 2030. The growth rate of biomass demand is estimated to amount at -3.03%, -2.96% and -3.13% for REF, AGS and MGS scenario respectively. Electricity demand annual growth rate is projected to increase at the rate of 13.78%, 15.29% and 12.6% for the REF, AGS and MGS scenario, respectively. Fossil fuel for thermal applications projected demand is expected to increase at 5.39%, 6.73% and 4.45% for the REF, AGS and MGS scenario, respectively. Motor fuels demand of about 264 ktoe will grow annually at average rates of 5.95%, 6.23% and 5.7%; reaching 941, 997.3 and 894.2 ktoe in 2030 for the REF, AGS and MGS scenario, respectively. Solar energy demand annual growth rate is projected to increase at a rate of 12.45%, 12.61% and 12.28% for the REF, AGS and MGS scenario, respectively.

4.2.3 Final energy demand by sector

Table 4 shows the REF, AGS and MGS scenario results for energy demand in different sectors for the period 2008-2030. The household sector is expected to dominate total final energy consumption demand over the outlook period, accounting for 55% share by 2030. Industry, transport and service demands are estimated to account for 25%, 16% and 5%, respectively, of the country's final energy demand by 2030. The household sector will have total final energy demand of 2859.22 ktoe in 2030 for REF scenario whereas AGS and MGS will have 3063.67 and 2859.22 ktoe, respectively. Transport sector depicts higher final energy demand in passenger transport as compared to freight transport in all scenarios. Final energy demand in transport sector in REF scenario for 2030 will be 497.93 ktoe for passenger transport as compared to 253.07 ktoe for freight transport. The analysis shows that manufacturing is the leading sub-sector in consumption of final energy demand as compared to agriculture, construction and mining (ACM) combined together, for all scenarios.

4.2.4 Electricity demand forecast

Figures 4 and 5 depict the comparison in electricity demand growth and peak projects for the REF, AGS and MGS scenarios. The share of electricity consumption will increase from 2.54% in the base year to about 34.81%, 40.25% and 30.8% for the REF, AGS and MGS, respectively. The final electricity demand of about 105 ktoe in the base year will grow annually at average rates of 13.8%, 15.3% and 12.6% for REF, AGS and MGS, respectively. According to these rates, the final electricity demand will reach 1798 ktoe for the REF, 2402 ktoe for the AGS and 1429 ktoe starting from the base year value.

The system peak demand in Malawi is forecasted to increase from the suppressed demand of 233 MW in the base year to 4274 MW in 2030 under REF scenario, which translates to an annual growth rate of 14%. The growth rates for AGS and MGS are projected at 15% and 13% reaching 5352 MW and 3622 MW, respectively. The system load factor decreases from 67.5% in the base year to 60.94%, 64.65% and 57.47% in REF, AGS and MGS, respectively. In order to meet the future demand,

Table 3: Energy demand by energy form

Energy source	*Growth rate (%)*			*2008 (ktoe)*	*2030 (ktoe)*		
	BAU	*AGS*	*MGS*	*Base year*	*BAU*	*AGS*	*MGS*
Traditional biomass	-3.03	-2.96	-3.13	3640	1849	1880	1806.6
Modern biomass	26.96	26.96	26.96	0	191	191	191
Electricity	13.78	15.29	12.6	105	1798	2402	1428.7
Solar thermal	7.06	8.96	5.14	1.03	4.62	6.8	3.1
Solar photovoltaic	12.45	12.61	12.28	1.4	18.5	19.1	17.9
Fossil fuel	5.39	6.73	4.45	114	362	477.6	296.9
Motor fuels	5.95	6.23	5.7	264	941	997.3	894.2

Table 4: Energy demand by sector

Sector	*Growth rate (%)*			*2008 (ktoe)*	*2030 (ktoe)*		
	BAU	*AGS*	*MGS*	*Base year*	*BAU*	*AGS*	*MGS*
Industry	6.07	8.18	4.0	357.02	1306.08	2014.33	846.83
Manufacturing	4.64	7.28	2.35	180.22	489.23	846.47	300.28
ACM	7.2	8.96	5.26	176.8	816.84	1167.86	546.55
Transport	6.02	6.04	6.04	206.55	747.66	750.5	750.99
Freight	4.27	4.39	4.39	98.37	246.98	253.07	253.07
Passenger	7.21	7.18	7.18	108.18	500.68	497.43	497.93
Household	-0.86	-0.55	-0.86	3455.34	2859.22	3063.67	2859.22
Service	3.99	3.65	2.46	106.58	251.97	234.72	181.77

the expansion of the electricity industry is necessary.

Table 5 depicts the comparison in electricity demand growth for REF, AGS and MGS scenarios. Sectorial consumption of electricity shows the growth rate of electricity demand for industry to be 14.28%, 16.96% and 11.67% for REF, AGS and MGS scenarios. Average growth rate for household is 14.7% for all scenarios. The electricity consumption in the base year was distributed to 44% for industry, 45% for household, and 11% for service. However, the more significant effect observed in the evolution of electricity is the shift from household to industry. Much of the increase is driven by higher demands for electricity in industry to sustain the high economic growth anticipated by the policy makers.

4.2.5 Final energy demand per capita

Figure 6 compares per capita energy demand for the REF, AGS and MGS scenarios. Results show decreasing trend in energy demand per capita. Energy demand per capita will decrease continuously from 3.669 MWh in the base year to 3.050 MWh, 3.527 MWh and 2.739 MWh for the REF, AGS and MGS, respectively in the year 2030. Annual growth rates of energy demand per capita of -0.84%, -0.18% and -1.32% are observed for REF, AGs and MGS scenarios respectively.

4.2.6 Energy intensity

Figure 7 compares the evolution of energy intensity for the REF, AGS and MGS scenarios. The analysis show energy intensity decreasing at -5.58% reaching 3.875 kWh/US$ in REF scenario by 2030 against base year value of 13.714 kWh/US$. The growth rates for AGS and MGS are projected at -6.7% and -4.25% reaching 2.982 kWh/US$ and 5.271 kWh/US$ in 2030, respectively. The projected decrease in energy intensity is brought about mainly by improvement in technological energy efficiency in industry, service, household and transport. A high decrease rate in the AGS scenario is due to these changes while low decrease in the MGS scenario is due to less improvement.

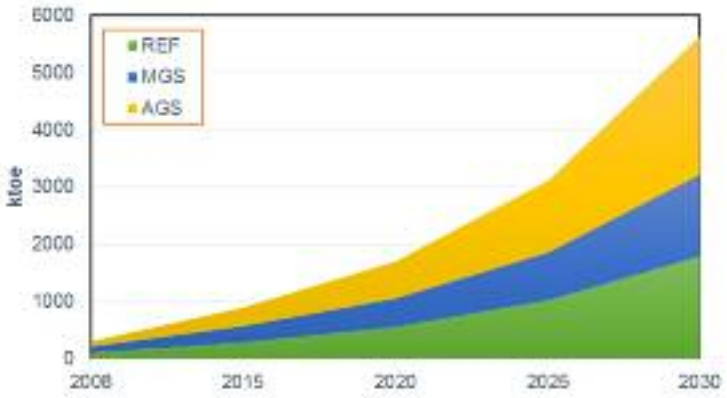

Figure 4: Projected electricity demand

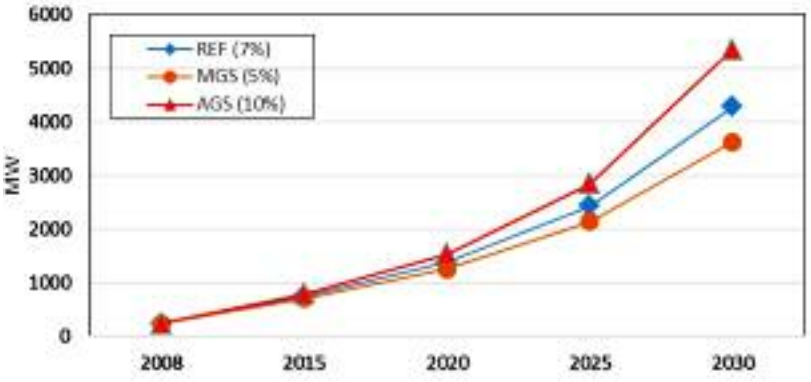

Figure 5: Electricity demand (peak) projections, MW

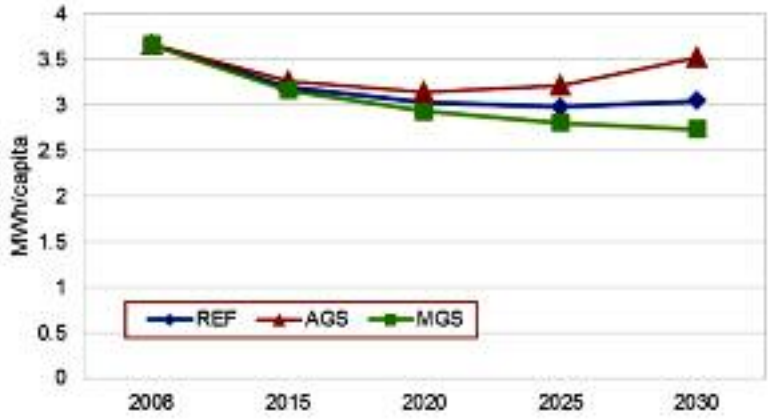

Figure 6: Final energy per capita

Table 5: Sectorial demand

Sector	*Growth rate (%)*			*2008 (ktoe)*	*2030 (ktoe)*		
	BAU	*AGS*	*MGS*	*Base year*	*BAU*	*AGS*	*MGS*
Industry	14.28	16.96	11.67	42.03	791.67	1320.33	476.4
Manufacturing	10.58	14.00	8.09	32.03	292.68	511.784	177.52
ACM	19.45	22.10	16.70	10.00	498.99	808.54	298.87
Transport	-	-	-	0	0.273	0.163	0.163
Freight	-	-	-	0	0.11	0	0
Passenger	-	-	-	0	0.163	0.163	0.163
Household	14.7	14.7	14.7	39.30	802.52	802.52	802.52
Service	10.29	11.88	8.76	23.59	203.53	278.73	149.67

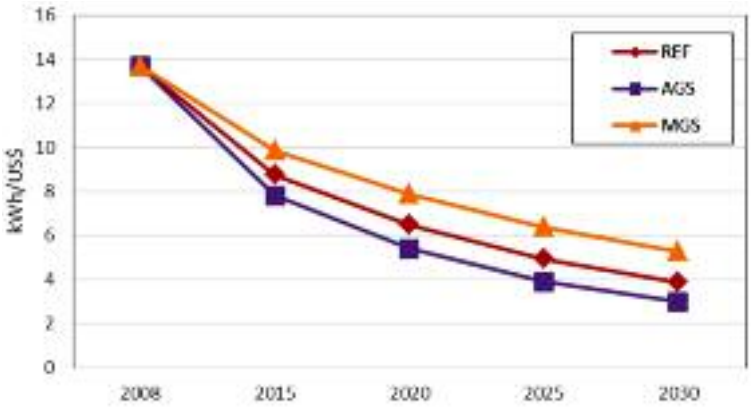

Figure 7: Energy intensity

5. Supply options and resources

5.1 Fossil fuel

5.1.1 Coal

Coal is Malawi's most abundant fossil resource. Probable coal reserves are estimated at 1 billion metric tonnes, 22 million of which are proven reserves of a bituminous type, with a high ash and low sulphur content. Coal deposits have been found in 15 dispersed locations in the country, the largest being at Ngana in the north, where total proven reserves[2] have been estimated at 16 million tonnes but could possibly reach as high as 70 million tonnes (GoM, 2010c). Further exploration work might increase the total reserves of coal in the country.

Coal mining started in 1985 and currently two fields are being mined in Rumphi district. Coal extraction is carried out primarily in open-pit mines. The production of coal in Malawi has increased from 34 100 metric tons in 2001 to 79 186 metric tons in 2010 (GoM, 2010c). At present coal is predominantly used as an energy source for process heat mainly in tobacco processing, textile and sugar production, and beer brewing as well as cement production. The country plans to install two coal-fired power stations at Zalewa and Salima with capacity of 300 MW and 100 MW respectively (Chiyembekeza, 2013). Compared to nuclear and solar, coal is preferable as energy source in Malawi due to its relatively low price and abundance. However, there will be need to invest in new production equipment, quality, environmental stewardship and transport infrastructure.

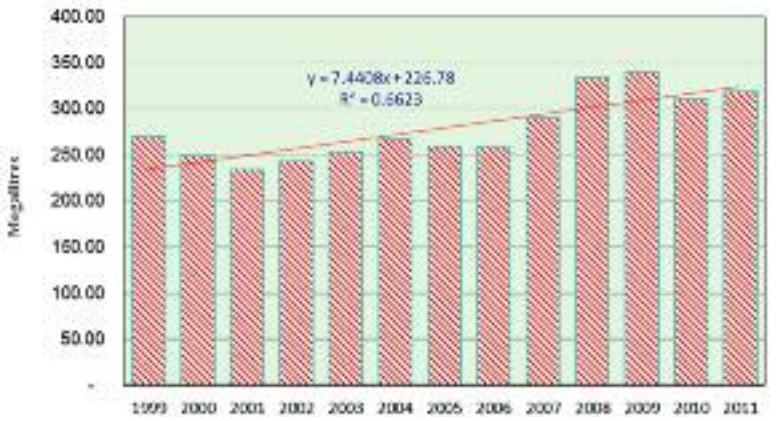

Figure 8: Consumption of petroleum products 1999-2011
Source: MERA

5.1.2 Hydrocarbon resources

Malawi does not have oil deposits, and relies entirely on imported petroleum products. However, some past studies have shown the existence of some hydrocarbon resources in the northern part of Lake Malawi and in the lower Shire Valley, although the quantities are not certain. Exploration work by two companies, Surestream Petroleum Limited and Simkara continues under agreements with the Government of Malawi. Currently, Malawi imports 97% of its refined petroleum products and the remaining 3% from locally produced ethanol fuel (NCST, 2011). The country imports about 8 000 barrels per day while the average daily fuel demand is currently estimated at 1.124 million litres which translates to 33.6 million litres per month or annual budget equivalent of US$366 million (Lanjesi, 2011). All petroleum products are imported into the country via three routes Dar Corridor (Tanzania), Nacala and Beira Corridor (Mozambique). The import bill has been continuously increasing in recent years which impose a serious financial burden on a developing country that already suffers the problem of huge public debt. The total annual import bill for the year 2005 accounted for 8.8% of the total imports. Imports of petroleum from the year 1999 onwards are given in Figure 8 (GoM, 2011). A major consumer of the liquid fuel is the transportation sector (89.99%), followed by domestic (5.25%), industry (2.87%), and agriculture (1.9%).

The demand for petrol and diesel is dependent on the growth of road infrastructure, the price of oil, the future efficiency of vehicles, the growth of alternate modes of transport and the emergence of substitutes like biofuels. Due to rapid growth of the number of vehicles, the demand for petroleum products will witness a growth in demand and it is expected to rise to more than 400 million litres by 2015, which will further increase to around 560 million litres by 2030 considering a high output growth (NCST, 2011).

5.1.3 Uranium

Nuclear technology has been playing an important role in medicine, industry, science, and food and agriculture, as well as power generation. Malawi has relatively small uranium reserves, therefore as a nuclear fuel of the future has a special importance for the country. The known recoverable resource of uranium in Malawi at Kayelekera Mine is estimated at 63 000 tons, which is equivalent to 378 tons of

U-235 (GoM, 2003).[3] Another deposit which is yet to be quantified is at Illomba in Chitipa district. If used to generate electricity in conventional reactors, these reserves would equate to 458.5 PJ of energy. Mining of uranium started in 2008 at Kayelekera but currently all the extracted uranium is exported to Canada for enrichment. The country's annual production output in 2010 was estimated at 790 tons of uranium (U308), which generated about $133.9 million, accounting for nearly 10% of Malawi's exports by value. Malawi is considering installing nuclear power to cope with future energy demand increases. Growing electricity demand, fluctuation of fossil fuel prices and climate change pressure bring all in favour of nuclear power. Under the Malawi Electricity Investment Plan, the first 125 MW nuclear power plant is expected to start operating by 2050 and will contribute to 4% of the total energy supply in Malawi (GoM, 2010a).

5.2. Renewable energy resources

Malawi has a large potential for renewable energy exploitation in a number of areas, the significant ones being solar energy, biomass, and hydropower with potential for geothermal and wind energy. Except for large scale hydropower, which serves as a major source of electricity, the current state of exploitation and utilization of the renewable energy sources in the country is very low, limited largely to pilot and demonstration projects. This section gives a review on the available energy potential of different renewable energy sources and the current status of exploitation is presented.

5.2.1 Hydro

Malawi has an estimated gross theoretical potential of 1670 MW and the average power generation of 15 000 GWh/year. The technical and economically feasible hydro capacity has been estimated at 6 000 and 7 000 GWh/year, respectively (Taulo, 2007). Current hydropower generation is about 17% of the nation's hydropower potential and represents 98% of total installed grid-connected electricity generation capacity. Hydropower potential of Malawi is concentrated on the Shire River. The capacity ranges from 18 to 140 MW. The estimated hydro potential of the Shire River is about 600 MW, equivalent to an annual production of 3500 GWh (ibid). In addition, several smaller rivers such as the Songwe, South Rukuru, Dwangwa and Bua, have limited potential at a number of sites estimated to total about 300-400 MW (WEC, 2002).

In addition, Malawi also has huge untapped small hydropower potential (with capacities of less than 10 MW each) which are spread out across the country. The gross theoretical small hydro potential of the country is 150 MW, out of which only 4.5 MW of the economically feasible potential has been developed (MEM, 1997). The exploitability of these is limited by their projected costs, but they could be useful for off-grid or stand-alone-mini grid electrification.

5.2.2 Solar energy

Solar energy presents considerable potential that can contribute to a large extent to fill the gap of energy needs in Malawi. The country receives about 2138 to 3087 hours of sunshine and 2133 kWh/m^2/year. The global solar radiation on a horizontal surface ranges between 4.3 kWh/m^2/day minimum and 7 kWh/m^2/day maximum. The annual daily mean global solar radiation is about 5.86 kWh/m^2/day, equivalent to 250 million tonnes of oil equivalent. Maximum irradiation of 6.5-7.0 kWh/m^2/day occurs in September – October and the minimum of 4.3-4.6 kWh/m^2/day occurs in January-February or in June-July according to location. Peak hourly solar radiation is more than 1000 kWh/m^2 during November to December (Chima, 1998). Considering that many parts of the country receive 8 to 12 hours of sunshine per day of 244 W/m^2, the potential for using solar for electricity generation is very high. The total available solar energy potential over the total geographical area (i.e. 94,280 km^2), of Malawi is calculated to be 356,284,837 MWh/year.

The solar resource in Malawi has been employed for various applications. Solar water heaters have been developed and are manufactured locally for domestic purposes. Total amount of installed solar water heaters in the country is estimated to have reached approximately 4 855 square meters. In addition, photovoltaic systems are also finding increasing use for various purposes such as lighting, water pumping, telecommunications repeater stations, refrigeration, and other appropriate applications. At present, there are more than10 000 photovoltaic systems installed in various parts of the country, with a total capacity of 165 kWp (CSR, 2005). There has been further growth, though small, in the SHS but no accurate figures are currently available. Six solar–wind hybrid systems have also been installed with Department of Energy Affairs support in Thyolo, Chiradzulu, Nkhata Bay, Mzimba, Nkhota-kota and Ntcheu (12 kW, each providing power for about 150 households). More recently, an 870 kWp solar photovoltaic plant has been commissioned at Lilongwe International Airport.

5.2.3 Wind energy

Wind energy has been used on a small scale to supply water for both livestock and irrigation in Malawi. Although there is a dearth of information on the wind energy characteristics of the country, it seems the wind speeds are moderate to low, typically in the range of 2.0 – 7.0 metres/second (GoM, 2003). Preliminary results from studies conducted by

Malawi's Meteorological Department suggest that the wind resource in Malawi cannot contribute significantly to a firm power generation; and that low speed aerogenerators could be operated for various applications such as milling of grains, pumping water and even lighting purposes in small remote villages around Malawi. It is particularly suited to water pumping as intermittent wind could still supply the needs when an adequate storage facility is incorporated. However, such assertion is contrasted by recent research findings which indicate that there is considerable potential for wind in the country. At present, the DoEA is collaborating with Malawi Renewable Energy Acceleration Programme (M-REAP) at the University of Malawi, an initiative funded by the Scottish Government, to undertake detailed wind measurements at five strategic sites as part of developing Malawi's wind atlas.

5.2.4 Biomass and bioenergy

Biomass in the form of wood fuel is the largest form of primary energy consumed in Malawi, accounting for 97% of the total primary energy supply in the country (GoM, 2010b). Major sources of biomass available include fuelwood and forestry residues, agricultural residues, animal dung, energy crops and municipal wastes. Forest reserves are the main sources of fuelwood and contribute nearly 75% of the total biomass supply (Jumbe and Angelsen, 2011). Forests cover 3.2 million hectares, approximately 36% of the total land area with total available biomass resources being 275.5 million tonnes (Kambewa and Chiwaula, 2010). Sustainable fuel wood supplies from forests are estimated to be 42.4 million cubic metres of solid wood equivalent. Total demand for biomass energy is estimated at 8.92 million total wood equivalent or 13.38 million cubic metres solid wood.

Total bioenergy potential in Malawi is estimated between 0.1 and 0.5 EJ/year (Zyl *et al*, 2010). Crop residues have the biggest energy potential about 161 910 TJ/year, followed by forest residues (48 744 TJ). In addition, there are approximately 23 million animals (cattle, goats, sheep, pigs and chickens) and their manure can be used for the production of biogas (FAO, 2010). This number of animals gives a theoretical potential for biogas production of 1,387,195 m^3 of biogas per day corresponding to 1100 GWh_{el}/year of electricity or 914.5 GWh_{th}/y of heat, assuming an average of 2.25 kWh/m^3. This is about 74% of the electricity consumed in Malawi (electricity consumption amounted to 1478 GWh in 2012). In view of rising consumption, which is expected to quadruple over 2008 to 2030, using biogas to generate electricity could be a sensible way of improving electricity supply mix in Malawi.

Annual average production of sugarcane in Malawi is estimated at 2.5 million tons/year leaving behind over 950 000 tons baggase which is a significant power source. There are two sugar mills in Malawi having potential to generate 62 MWe of electricity but currently only 18 MWe has been utilised. Bagasse–based electrical generation estimated at 251GWh, corresponds to about 25% of national electricity generation (UNEP, 2013). The country can also explore biogas potential of municipal solid waste (MSW) as well. Current estimated municipal solid waste (MSW) generation per day is 720 tons which gives theoretical potential for biogas production of 32,683 m^3/day corresponding to 70.6 MWh_{el}/y or 58.8 MWh_{th}/y (Karekezi *et al.,* 2003).

Moreover, agricultural residues such as rice straw, sugarcane and cassava pulp have the potential to produce approximately 46.5 million litres ethanol production for the country. This could possibly displace over 40% of Malawi's 2011 petrol consumption as transport fuel. Alternatively, the same amount of residue could provide 18.1 million litres per year of diesel to potentially offset 9.5% of natural diesel consumption in the transport sector. Presently, molasses-based ethanol amounting to 18 million litres/year, is being marketed as 10% blend with petrol. The total demand for ethanol is expected to be 33.6 million litres against present availability, resulting in scarcity of 15.6 million litres ethanol in the year 2015. Furthermore, biodiesel produced from energy crops such as *Jatropha curcas*, soya beans, cotton, sunflower and groundnuts has the potential to produce 50 million litres of biodiesel, equivalent to 583, 530 TJ/year of energy.

5.2.5 Geothermal energy

Geothermal energy has been extensively used for power generation and direct power applications in many countries of the world (Fridleifsson, 2003). As a consequence of Malawi's location in the East African Rift System (EARS), the country is endowed with significant potential reserves of geothermal energy. There are approximately 55 geothermal spots in Malawi, but three major ones identified for detailed investigation are: Chiweta, Mwankeja, and Nkhotakota. The combined geothermal potential from these major areas is 200 MWe (Gondwe *et al.,* 2012). As for geothermal projects, some studies have been conducted to design a prototype Geothermal Power Plant for producing electricity. One of the ongoing related projects is a 30 MW Geothermal Power Plant at exploring stage in Nkhotakota, to be upgraded to 100 MW depending on the results of exploration drilling.

6. Issues

Despite these options, there are several issues facing the energy sector and crucial to economic development. The main energy challenges that face Malawi presently is how to increase energy supplies to meet the needs of its growing population; also significant

is the need to repair and upgrade existing infrastructure for non-hydrocarbon energy sources. Meeting these challenges is critical to improving the nation's economy and raising the standard of living in Malawi.

6.1 Deforestation

Widespread inefficient production and use of traditional energy sources such as fuelwood and charcoal, has contributed to deforestation. Between 1990 and 2010, forest cover has declined from 41% to 34% (FAO, 2010). The resultant deforestation degrades catchment areas leading to siltation and reduced base flows in rivers. Use of biomass as a source of energy and clearing of natural woodlands for agricultural expansions are among factors that have contributed to the rate of deforestation.

6.2 Inadequate and unreliable power supply

Lack of adequate and reliable power is consistently cited by private sector firms as being among the top five constraints on Malawi's economic growth. There is insufficient power supply due to the current diminished generation capacity which is a direct result of low hydraulic head, siltation and weed infestation. Inevitably, the energy sector is also affected by extreme weather events such as droughts and floods, which negatively impact on hydropower generation along the Shire River. The water flow disruptions have been exacerbated by siltation caused by poor and unsustainable agriculture practices and deforestation in the catchment area, and invasive weeds such as water hyacinth.

6.3 Ensuring energy access

Very low electricity coverage throughout the country, especially in rural areas, is a critical challenge. In Malawi, about 10% of households are supplied with electricity from the national grid and most of these are in urban centres. Only 2% of rural households are electrified despite the fact that 85% of people in Malawi reside in rural areas. The situation is unlikely to improve in the short term. For Malawi, access goes beyond the grid power being available but also affordable. The MAREP effort could have easily yielded 20 to 25% access to grid electricity if the rural population was also economically empowered to afford paying for upfront costs of wiring, inspection and connection. This calls for an innovative model for rural energy access beyond the grid extension.

6.4 Security of energy supply

A key issue for Malawi's energy security is its dependence on imported petroleum products. The country is highly vulnerable to oil price shocks as it imports almost all of its 8 000 barrels of oil per day. There is no doubt that the challenge for Malawi's import dependence will increase at least in the short to medium term. Firstly, the country's demand is still growing, hence further import increase is inevitable; secondly, Malawi is a price taker in the global oil market, so any international price hike will have a direct impact on Malawi's current account and; finally, as seen recently, a depreciation of Malawi's currency will also push up the import bill. Additionally, the costs of transportation of the petroleum products from sea ports (Beira, Nacala, Dare Salaam and Durban) are high. There is also low storage capacity for petroleum products compared to national requirements. The Southern Africa region is projected to experience increased intensity and frequency of extreme climate events such as floods and droughts. Since 98% of national grid electricity is from hydro, Malawi's electricity supply is considered vulnerable to the impacts of climate variability and climate change.

6.5 Energy investment needs

The country's energy consumption is forecasted to grow at an average rate of 7% to sustain economic growth of 6% per annum to the year 2030. This increased energy demand would require significant investments in the energy infrastructure. This is especially necessary to provide modern energy to the large proportion of the country's population, whose energy demand is currently unmet. According to GoM (2010a), Malawi would need a total investment of US$2.1 billion on overall energy supply infrastructure from 2011 to 2030. This is a substantial amount, considering that the Malawi government annual budget for total capital expenditure is less than US$10million. Ensuring this scale of investment for the next two decades will be a challenge for Malawi, making private investment crucial.

6.6 Aging infrastructure

Aging transmission and distribution infrastructure causes high transmission and distribution losses and drives the power system to be highly vulnerable. Over 50% of the power generation plants in Malawi have passed their expected lifespans and hence require frequent maintenance in order to improve on efficiency of the machines. The average age profile for the transmission infrastructure is around 30 years. Additionally, the system experiences termite attacks and natural rotting of wood structures. Other problems include bush fires leading to burning of wooden poles, and even vandalism on both wood and steel tower structures.

6.7 High transmission and distribution losses

Transmission losses in Malawi continue to be amongst the highest in the world, and reducing losses or improving transmission efficiency is the main concern in the electric power sector. The overall

transmission losses are estimated to be currently 21%, with around 14% being technical losses (MCA, 2010). High losses in the distribution systems are mainly due to the aging systems, with inadequate investments over the past years resulting in unplanned extensions of distribution lines and the overloading of systems equipment such as transformers and conductors.

6.8 Operational aspects

Floating aquatic weeds and debris being transported in the Shire River have caused severe operational problems and damage to intake structures at the generation plants. Siltation of power plants reservoirs has also contributed immensely to the operational problems. In addition, theft and vandalism of ESCOM infrastructure; illegal connection of electricity; encroachment of ESCOM Way-leave; as well as illegal extension of electricity has resulted in contributed to huge financial losses.

7. Conclusion

This paper presents an overview of the current status of the energy sector in Malawi in terms of its total energy demand and supply, options and issues in the present and future. The study found that the present energy scenario of the country is not satisfactory, as the existing power shortage is at 14%. While there has been some progress in recent years, shortage of energy and lack of access continues to be a major constraint to economic growth. The persistent shortages of electricity indicate the need for improving performance of the energy sector in the country. To cope with the expected increase in electricity consumption, electricity generation capacity must increase. The country is also heavily dependent on biomass and importation of oil as a source of primary energy supply, and it is likely to remain so for decades. This dependence on expensive imported energy resources place a huge burden on the economy and air pollution is becoming a great environmental concern in the country. Therefore, the Malawi Government energy planners should take due consideration of social, economic and environmental factors to ensure a resilient and sustainable future energy mix for the country.

There is considerable opportunity for Malawi to meet its future demand and thus economic growing through renewable energy. Since renewable energy supply in Malawi is dominated by hydropower and biomass, the share of bioenergy is expected to increases with the expansion of other renewables. There is potential for solar and wind development. The paper also discussed some of the issues facing the energy sector in Malawi. Malawi is rapidly running out of generating capacity and must build new power stations soon. The only two indigenous sources for bulk electricity are hydro and coal, since oil reserves are unknown and small hydro, wind and solar power only have limited potential, developing new hydro power schemes is a probability.

The following strategies need to be considered to secure Malawi's energy supply:

1. Enlarge the use of domestic energy resources through promotion of renewable energy projects such as small hydro power; cogeneration with sugarcane, tea and timber factories, increased use of solar to generate electricity.
2. Diversify energy supply by interconnecting and importing electricity from Caborra Bassa in Mozambique as well as building coal-fired plants using modern cleaner technologies.
3. Continue with the development of Malawi's power sector by the optimal way, minimising the environmental impacts and expected investment and operational costs.
4. Accelerate energy conservation and efficiency including development of technical personnel and energy efficient technologies. For future interest, Malawi should pay more attention to the optimization of consumption of energy resources, power system and final energy consumption by the vector objectives, minimizing the cost of energy resources, environmental impact, operating costs and investment costs.
5. Reduce oil dependency by promoting plug-in hybrid engines, increase percentage of ethanol-petrol blend from 20% to higher levels, biofuels (as biodiesel or 100% ethanol) and other technologies. Fiscal incentives such as duty free importation of hybrid vehicles, government procurement of such vehicles for its fleet, and legislation on compulsory blending of fuel are likely to be helpful.

Acronyms and abbreviations

CSR	Centre for Social Research
ESCOM	Electricity Supply Corporation of Malawi
FAO	Food and Agricultural Organization
GDP	Gross Domestic Product
GoM	Government of Malawi
GWh	Giga Watt hour
Ktoe	Kilotonnes of oil equivalent
MAREP	Malawi Rural Electrification Programme
MCA	Millennium Challenge Account
MCC	Millennium Challenge Corporation
MERA	Malawi Energy Regulatory Authority
M-REAP	Malawi Renewable Energy Acceleration Programme
MSW	Municipal Solid Wastes
Mtoe	Million tonnes of oil equivalent
MW	Mega watts
MWe	Megawatt (electrical)
MWth	Megawatts (thermal)
NCST	National Commission for Science and Technology

NEP	National Energy Policy
NSO	National Statistical Office
UNDP	United Nations Development Programme
WEC	World Energy Council

Notes

1. In this paper, renewable energy technologies refer small hydro, geothermal, wind, cogeneration and biomass-based power generation, and solar technologies and exclude large hydropower.
2. Proven reserves are those for which further exploration is not required for mine planning
3. There are 85 kg of uranium in 100 kg of uranium oxide. Of these 85 kg, only 0.7% is U-235. i.e. there are 0.6 kg of u-235 in 100 kg of U_3O_8.

Acknowledgements

The authors gratefully acknowledge funding from the Department of Mechanical and Mechatronics Engineering, at Stellenbosch University. Further, they are indebted to the Ministry of Energy for their provision of much of the data used in this paper.

References

Chima, T. (1998). Study on Assessment of Alternative Energy Resources in Malawi. Consultancy Report, prepared for Department of Energy Affairs and Danish Aid for International Development Assistance.

Chiyembekeza, C. (2012). China invests $500m for electricity in Malawi, *The Nation*, Vol. 19. No.14, September 26, 2012.

CSR, (2005). Baseline Inventory/Development Impact of Solar Photovoltaic and Thermal Systems in Malawi, Final Report; Centre for Social Research, University of Malawi, Zomba.

ESCOM, (2011). Annual Report,' Electricity Supply Corporation of Malawi, Blantyre.

FAO, (2010). Global Forest Resources Assessment 2010: Country Report Malawi. Food and Agricultural Organization, Rome.

Fridleifsson, I.B., (2003). The Role of Geothermal Energy in the World. United Nations Geothermal Training Programme, Reykjavik, Iceland.

Gamula, G.E.T., Hui, L. & Peng, W. (2013. Contribution of the Energy Sector towards Global Warming in Malawi, *Energy and Power Engineering* (5): 284-292.

Gondwe, K., Allen, A., Georgsson, L., Loga, U., & Tsokonombwe, G. (2012). Geothermal Development in Malawi – a Country Update. Proceedings 4th African Rift Geothermal Conference, Nairobi, Kenya, 21-23 November 2012.

Gooneratne, F., & Visser, A. (2010). Malawi: Development of a large-Scale Energy Efficient Lighting Program – CFL Program Design and Implementation Plan, Final Report. The TI-UP Resource Centre.

Government of Malawi, (2003). Malawi Energy Policy. Ministry of Energy and Mining, Lilongwe.

Government of Malawi, (2010a). Malawi Electricity Investment Plan. Department of Energy Affairs, Lilongwe.

Government of Malawi, (2003). Malawi Energy Policy. Ministry of Energy and Mining, Lilongwe.

Government of Malawi, 2010b. Energy Demand Assessment for Malawi (Final Report to IAEA). Department of Energy Affairs, Lilongwe.

Government of Malawi, (2010c). Malawi State of Environment and Outlook Report: Environment for Sustainable Economic Growth. Ministry of Natural Resources, Energy and Environment, Lilongwe.

Government of Malawi, (2011). Annual Economic Report. Ministry of Economic Planning and Development.

Government of Malawi, (2012). Malawi Growth and Development Strategy II (2011-2016). Ministry of Economic Planning and Development, Lilongwe.

IEA, (2010). Key World Energy Statistics 2010. OECD/IEA, Paris.

Jumbe, B.L. & Angelsen, A. (2011). Modelling choice of fuelwood source among rural households in Malawi: A multinomial probit analysis, *Energy Economics* 33: 732-738.

Jumbe, C.B. (2004). Cointegration and casuality between electricity consumption and GDP/empirical evidence Evidence from Malawi, *Energy Economics* 26(1):61-68.

Kambewa, P. & Chiwaula, L. (2010). Biomass energy use in Malawi: A background paper prepared for the International Institute for Environment and Development (IIED) for an international workshop on biomass energy, 19-21 October 2010, Parliament House Hotel, Edinburgh.

Karekezi, S, Kimani, J, Maina, A, Wangeci, J & Mutiga, A. (2003). Overcoming Barriers to the Use of Renewable Energy and Energy Efficiency Systems in the Reforming Power Sector of Eastern Africa – Background paper for Eastern Africa Renewable Energy and Energy Efficiency Partnership (REEEP) Regional Consultation Workshop.

Kaunda, C.S. (2013). Energy situation, potential and application status of small-scale hydropower systems in Malawi. *Renewable and Sustainable Energy Reviews* (26): 1-19.

Kaunda, C.S., & Mtalo, F. (2013). Impacts of environmental degradation and climate change on electricity generation in Malawi. *International Journal of Energy and Environment* 4(1):481-496.

Kiplagat, J.K., Wang, R.Z., Li, &T.X. (2011). Renewable energy in Kenya: Resource potentials and status of exploitation. *Renewable and Sustainable Energy Reviews* 15: 2960-2973.

Koopmans, A., & Koppejan, J. (1997). Agricultural and Forest Residues-Generation, Utilization and Availability. Regional Consultation on Modern Application of Biomass Energy, Kuala Lumpur, Malaysia.

Lanjesi, D. (2011). Economic Forum Seminar Report on Procurement and Management of Fuel Supplies in Malawi. 20 October, 2011, Hotel Victoria, Blantyre.

MCA, (2010). Concept Paper for the Energy Sector.

Millennium Challenge Account, Malawi Country Office Secretariat, Lilongwe, Malawi.
MCC, (2011). Malawi Power System Project Studies – Final Feasibility Study Report. Millennium Challenge Corporation, Washington DC.
MEM, (1997). National Sustainable and Renewable Energy Programme. Ministry of Energy and Mining, Lilongwe, Malawi.
NCST, (2011). Ethanol Driven Vehicle Project-Assessment of the Use of Ethanol as an Alternative Vehicle Fuel to Petrol in Malawi. National Commission for Science and Technology (NCST), Lilongwe, Malawi.
NSO, (2009). Population and Housing Census: Main Report. National Statistical Office, Zomba, Malawi.
Openshaw, K. (2010). Biomass energy: Employment generation and its contribution to poverty alleviation. *Biomass and Bioenergy* (34): 365-378.
Taulo, J.L. (2007). A study on the utilization of small-scale hydropower for rural electrification in Malawi. Master's thesis, University of Cape Town.
UNDP, (2013). Human Development Report 2013. United Nations Development Programme (UNDP), New York, USA. Accessed on: http://hdr.undp.org.
UNEP, (2013). Emission Reduction Profile – Malawi. United Nations Environmental Programme, Denmark.
Venendaal, R. (1996). Malawi Power Production with Bio-mass: A Feasibility Study Report. Biomass Technology Group, Enschede, Netherlands.
WEC, (2002). Survey of Energy Resources: Hydropower, World Energy Council.
World Bank, (2011). World Development Indicators. The World Bank, Washington DC, USA.
World Bank, (2001). World Development Report 2000/2001: Attacking Poverty. Selected World Development Indicators, Table 10, Energy Use and Emissions (New York: Oxford University Press, 2001.
Zyl, V., Gorgens, J.F., Chimphango, A.F.A. & Chirwa, P.W.C. (2010). Bioenergy Potential in Sub-Saharan Africa. 17-19 March 2010, Stellenbosch University, South Africa.

Received 28 April 2014; revised 9 April 2015

Bio-oil yield potential of some tropical woody biomass

Edmund C Okoroigwe[1,2]

Zhenglong Li[3]

Shantanu Kelkar[3]

Christopher Saffron[3]

Samuel Onyegegbu[2]

1. National Centre for Energy Research and Development, University of Nigeria, Nsukka, Nigeria
2. Department of Mechanical Engineering, University of Nigeria, Nsukka, Nigeria
3. Department of Biosystems and Agricultural Engineering, Michigan State University, East Lansing, USA

Abstract
Six tropical biomass samples namely: Ogbono wood (Irvingia wombolu), Mango wood (Mangifera indica), Neem wood (Azadiracta indica), Ogbono shell (Irvingia wombolu), Ogirisi wood (Neubouldia laevis) and Tropical Almond wood (Terminalia catappa) were pyrolyzed in a bench scale screw reactor at 450oC. The physicochemical properties of the samples were determined prior to the pyrolysis experiments. The bio-oil and bio-char produced were similarly characterized using standard procedures established by American Standard and Test Methods (ASTM). The highest bio-oil yield of 66 wt% and least bio-oil yield of 53 wt% were obtained from Neem wood and Tropical Almond wood respectively. The characterization results of the products show that even though the moisture content of the bio-oil was quite higher than those of the original feedstock, their higher heating values were higher than those of the parent feedstock. Both characterization results show that the feedstock and their fast pyrolysis products are good materials for bioenergy production. The Gas Chromatography Mass Spectroscopy (GC-MS) analysis of the bio-oil shows the presence of useful chemicals such as phenols and levoglucosan, which could be harnessed for industrial applications.

Keywords: biomass, pyrolysis, bio-oil, characterization, energy, bio-char

1. Introduction

The rapid degradation of the environment due to climatic changes resulting from huge consumption of fossil fuels has led to the search and advocacy of biomass-based fuels as alternative or blend to fossil fuels thereby reducing the fossil fuel consumption gross index. The geographical spread of biomass vis-à-vis natural gas, oil and coal is a support for encouraging the use of biomass for energy production.

Biomass fast pyrolysis is one of the sources of the biofuels regarded as future generation fuels which are suitable for the environment (Dinesh *et al.,* 2006, Bui *et al*., 2009, Sivakumar *et al.,* 2010). Pyrolysis is the intermediate process in both combustion and gasification technologies involved in biomass to energy conversion. Knowledge of the pyrolysis characterization of biomass materials and their products are very important in the design of any conversion technology systems as well as a guide to selecting most suitable species for biofuel production from the biomasses (Tsamba *et al.,* 2006). Hence, the characterization of the parent feedstock is fundamental in pyrolysis technology. It is usually more cost effective to transport the fast pyrolysis products than transporting the bulk biomass from one place to the other compared to other conversion techniques.

Even though, virtually, every plant biomass can be pyrolyzed (Ingram *et al.,* 2008) some species are more suitable than the others under the same technical and operational conditions. In tropical Africa, there are huge wastes resulting from low mecha-

nized system of agriculture such as stalks, shells, shrubs or remains of felled trees and stumps. These are commonly burnt in the open as part of a land clearing method (Senjobi *et al*., 2007, Pantami *et al.,* 2010) to give way to farm operations. Similarly, logs of wood in the forest are hewed for fuelwood or burnt in the open (when dry) to make way for other uses of the forest. Wood shavings and sawmill wastes are similarly burnt as a way of disposing them (Azeez *et al.,* 2010). These contribute to the ranking of Africa as leader in biomass burning emission source (Andreae, 1991; Roberts, 2008). The emissions from the burning contribute to the climatic problems confronting our environment. If Africa's huge biomass potential is adequately utilized in bioenergy production, it will contribute immensely to the solution of global energy demand and economic problems of the developing nations.

The search for green energy has attracted a lot of interests in research, ranging from characterization of different biomass materials for their energy production potential (Satyanarayan et al., 2010; De Ramos *et al*., 2011), to actual production and upgrading of bioenergy-based products for fuel and chemical production. To date there is little or no evidence, in literature, of converting the tropical biomass species used in this work, to bioenergy. However, Azeez et al. (2010) pyrolyzed three tropical biomass materials – iroko (Chlophora excelsa L.), albizia (Albizia adianthifolia L.), and corncob (Zea mays ssp) obtained in Nigeria alongside two European species – spruce (Picea abies L.) and beech (Fagus sylvatica L), in a Fluidized Bed reactor and Py-GC/MS. In their work, the tropical biomass species showed some potential as sources of bioenergy and could compete favourably with temperate biomass species if pre-treatment operations such as removal of ash and extractives are carried out. In our work, six biomass species were characterized and pyrolyzed in a bench scale screw pyrolysis reactor with a view to determining their suitability for commercial bio-oil production. The products were characterized in order to determine their potential as sources of bioenergy. The pyrolysis of the biomass used in this work for bio-oil production and characterization has not been reported in literature to the knowledge of the authors.

2 Experimental

2.1 Feedstock selection

Six tropical woody biomass samples obtained within Nsukka urban and prepared at the National Centre for Energy Research and Development, University of Nigeria, Nsukka were used for the experiment. These include Ogbono wood (*Irvingia wombolu*), Mango wood *(Mangifera indica*), Neem wood (*Azadiracta indica*), Ogbono shell (*Irvingia wombolu*), Ogirisi wood (*Neubouldia laevis*) and Tropical Almond wood (*Terminalia catappa*). Ogbono wood tree is deciduous and can be as old as 60 years before it can be felled for wood production. Usually the fruit is made of edible pulp and cartilaginous seed housed in a woody shell. In some regions it a common economic tree that grows uncultivated in large numbers owned by families. For this work the specimen was cut from the mature tree about 15 to 20 years together with its shell. Mango trees can be planted in large plantations as a commercial tree. The specimen for this research was obtained from one estimated to be up to 25 to 30 years old even though not from a commercial farm. In tropical Nigeria, mango trees can be planted individually near residential homes only to be felled when its presence poses a safety threat to buildings. The wood can only be useful as fuelwood for combustion purposes. It could constitute as an environmental nuisance if not burnt immediately.

A Neem tree in Nigeria serves as an ornamental and medicinal plant depending on the purpose of its cultivation and the part of the plant of interest. It can be as old as 45 years before aging depending on the soil conditions. It grows in large quantities even though there is no existing 'Neem farm' in our country. Like the mango wood it can only be used as fuelwood for combustion purposes when felled. The sample for this research is from a mature tree that is not less than 20 years of age. The Ogirisi tree and the Tropical Almond tree are wild plants which are not cultivated for economic purposes other than for local fencing and ornamental shade respectively. They are both soft woods that cannot be used for wood production for structural purposes. Because they are fast growing they produce large wood. The ones used for this research were obtained from species that are not more than 10 years old. The samples were cut, air dried and milled to a particulate size less than 1 mm passing mesh 40 (425μm) using Wiley milling machine.

2.2 Feedstock characterization

The physicochemical analyses of the feedstock were carried out to determine the properties of the feedstock prior to the bench scale pyrolysis. The properties analyzed include the: moisture content, percentage ash, higher heating values (HHV); compositional analysis (lignin and structural carbohydrates) and elemental composition analyses to determine (C, H, N, O, S). The detailed procedures for these analyses are similar to those reported in (Okoroigwe *et al.,* 2012).

2.3 Pyrolysis experiment:

The bench scale pyrolysis experiment was performed with the screw reactor (Figure 1). The system is made of a biomass delivery unit being powered by a 1.5 horse power (Hp) electric motor and comprising: (1). The metering device (2), Made of a glass cylinder fitted into the 420 mm long stainless

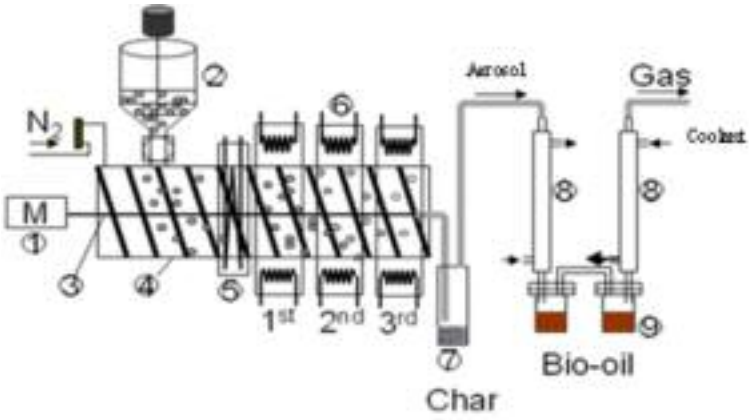

Figure 1: The schematic diagram of the reactor

steel barrel (4), housing the screw shaft (3). Nitrogen gas is delivered to the system on top of the hopper to ensure complete purging of air (oxygen) from the system before and during the pyrolysis process. The barrel is heated externally by six band heaters (6) of 750W each, fixed on the barrel. There are 3 heating zones for the pyrolysis process. Two band heaters form a heating zone equally spaced along the 420 mm heated zone of the reactor and set to raise the temperature of the barrel to a fixed value. As the electric motor drives the shaft, the biomass is smeared on the hot barrel wall which decomposes the biomass. Since the barrel outer wall is heated, heat transfer to the shaft and inside wall is by conduction and slight convection because of trapped gas. To prevent backflow of heat from the nearest band heaters to the hopper base and to prevent preheating of the biomass, a cooling system (5) is introduced by continuous flow of running water forming the feed cooling system.

The products recovery system of the reactor comprises the heated char trap (7) and the shell and tube heat exchanger (8) used to condense the vapour into liquid bio-oil in the Bio-oil containers (9). After the thermal decomposition of the biomass, aerosol (comprising the char and vapour) formed travel together to the char trap where char separation takes place. The char trap was heated using heating tapes rated 570 and 430 W in order to avoid pre-condensation of the vapour in the char trap. The liquid bio-oil was obtained by rapid quenching of the temperature of the vapour from about 450°C to about 2°C or less as obtained in different experiments. This was possible because two bio-oil collection containers were used. Both containers were each connected to a heat exchanger. The two containers were however interconnected by small tubing such that the products not collected in the first container due to inability to condense are collected in the second tube at much reduced temperature. The flow of the refrigerant is counter-current to the flow of the aerosol. The non- condensable gas exits from the last container by means of gas delivery pipe. Most of the liquid products condensed at the first condenser, while at much lower temperature a further liquid product was collected in the second condenser. The non-condensable gases were let out of the chamber by gas delivery tube and collected into gas trap bags for analysis with gas analysers. The exit gas temperature was monitored using k-type thermocouples at temperature 8 to 2°C. When tested for combustion, the mixture of gases burnt with blue flame implying the presence of flammable gases confirmed to be H_2, C_2H_4, and CH_4 by analysis of the gas using gas chromatographer.

2.4 Products characterization

The bio-oils were analysed for moisture and ash contents, density, pH, elemental composition, viscosity, and heating values. They were also analysed using GC/MS for the determination of chemical compounds present in the oils. For the char, only the heating value and ash content were determined using bomb calorimeter and electric furnace methods respectively. The elemental analysis for determination of Carbon, Hydrogen, Nitrogen, Oxygen and Sulphur content of the bio-oil samples was performed at Galbraith Labs Inc, Knoxville, Tennessee USA. The ASTM D5291-02 (Standard Test Methods for Instrumental Determination of Carbon, Hydrogen, and Nitrogen in Petroleum Products and Lubricants) and the LECO CHN 2000 analyser were used as standard procedure and instrumentation respectively. Oxygen was determined by difference while Sulphur was determined according to ASTM D4239-83 using LECO SC-432DR (Trace E16-2A). The water content of the liquid product was determined by Karl Fischer titration method according to ASTM E203 at the Galbraith labs.

3 Results and discussion

3.1 Feedstock characterization

The results of the characterization of the feedstock used in the pyrolysis experiments are presented in Table 1. The table contains the proximate (physical properties) and ultimate analyses results.

Table 1: Feedstock characterization

Property		*Base*	*Ogbono wood*	*Mango wood*	*Neem wood*	*Ogbono shell*	*Ogirisi wood*	*Tropical almond wood*
Physical	Moisture content (%)		6.27	4.83	6.83	7.70	6.42	7.62
	HHV MJ/kg)	ar	20.01	22.23	18.71	20.20	20.69	20.50
		db	21.34	23.35	20.08	21.88	22.10	22.19
		daf	21.61	23.60	20.35	22.10	22.60	22.40
	Ash (%)	ar	1.14	0.98	1.22	0.91	2.06	0.88
		db	1.22	1.03	1.32	0.99	2.21	0.96
Ultimate analysis	C (%)		45.94	46.39	45.86	47.62	46.00	45.86
	H (%)	Ar	6.11	6.27	6.36	6.34	6.50	6.36
		db	5.73	5.97	5.93	5.85	6.08	5.88
	N (%)		< 0.50	< 0.50	< 0.50	< 0.50	< 0.60	< 0.50
	O (%) (by difference)		44.64	45.19	45.34	44.03	44.04	45.34
	S (%)		<0.50	< 0.50	< 0.50	< 0.50	< 0.50	< 0.50
	O:C		0.97	0.97	0.99	0.92	0.96	0.99
	H:C		0.13	0.14	0.14	0.13	0.14	0.14

Note: ar = as received, db = dry basis, daf = dry and ash free

Table 1 shows the levels of moisture present in the samples at the time the experiments were carried out. There was varying moisture as expected, since wood samples have different cellular structure. It is obvious that moisture affects heating values of biomass samples (Demirbas, 2007), hence the variation in heating values of the samples 'on as received' basis. But on moisture fee (dry basis)', mango wood has the highest heating value of 23.35MJ/kg while Neem wood has the lowest heating value of approximately 20.1MJ/kg.

On an ash free basis, the lower heating value of mango wood appears to be highest even though its ash content is not lower than that of Tropical Almond wood. It has been shown that ash in biomass has a dominant effect on bio-oil yield and composition (Azeez *et al*., 2010; Brown, 2011). Removal of ash and extractives in pre-treatment steps prior to pyrolysis improves the quality of bio-oil (Das *et al.,* 2004). This implies that Tropical Almond wood with 0.88% ash content is a better option than the rest in terms of bio-oil yield and quality. But this does not agree with the result presented in Table 2, where Neem wood yielded 66 wt% of bio-oil followed by mango wood even though their ash contents are slightly higher than that of Tropical Almond wood. Since ash content is not the only factor determining the percentage bio-oil yield, there could be other conditions favouring the yield of bio-oil in one biomass than the others in this experiment.

The hydrogen to carbon ratio (H:C) and oxygen to carbon ratio (O:C) are good parameters to evaluate energy potential of biomass. It appears that all the biomass species are good feedstock for energy production by considering their H:C and O:C ratios with the later close to 1. The result of the composition analysis of the lignocelluloses is presented in Figure 2. Comparatively, all the biomass species are rich in cellulose and lignin. The percentage composition of cellulose is not less than 35%, while lignin is between 20 and 35%. The maximum value of hemicelluloses (18%) occurred in ogirisi wood, while the least (8%) occurred in ogbono shell. The biomass materials were not pre-analysed for extractives; hence the 'difference' could represent inorganic materials in form of extractives. The large value of this component is in agreement with Azeez *et al.* (2010) who asserted that tropical species are richer in extractives than European biomass species. The extractives are made up of phenolic compounds, terpenes, aliphatic acids, chinones and alcohols. High content of these components often results in low polyoses content in wood. These could be responsible for the chemicals present in the bio-oil as presented in Table 3.

Table 2: Pyrolysis experiment results

Parameter	*Sample*					
	Ogbono wood	*Mango wood*	*Neem wood*	*Ogbono shell*	*Ogirisi wood*	*Tropical almond wood*
Bio-oil yield (wt %)	60	61	66	58	57	53
Bio-char yield (wt %)	19	22	15	19	17	19
NCG (wt %) by difference	21	17	19	23	26	28

Table 3: Chemical components of the bio-oil (area %) on chromatograms

Compound	*% area by sample*					
	Ogbono wood	*Mango wood*	*Neem wood*	*Ogbono shell*	*Ogirisi wood*	*Tropical almond wood*
Acetic acid	23.18	24.06	27.7	29.58	30.68	22.99
Acetol	12.92	10.63	14.7	14.93	13.87	10.86
2,3-pentanedione	2.85	-	4.11	3.63	3.53	2.74
2,5-dimethyl-furan	2.35	-	2.44	2.48	2.81	2.56
3-methyl- 1,2-cyclopentanedione	3.08	3.48	3.39	3.29	3.9	3.49
Guaiacol	4.4	1.76	3.05	4.37	4.28	3.55
2-methoxy-4-methyl-phenol	4.25	-	1.84	4.01	2.66	3.12
2,6-dimethoxy-phenol	3.96	5.49	7.01	3.11	6.04	6.92
2-methoxy-4-(1-propenyl)-phenol	3.88	1.85	2.22	2.58	3.23	3.36
1,2,4-trimethoxybenzene	3.16	2.55	3.55	2.34	2.68	4.96
3',5'-dimethoxyacetophenone	-	2.68	2.10	-	2.29	2.40
Levoglucosan	17.2	12.92	7.48	15.55	3.65	12.16
2,6-dimethoxy-4-(2-propenyl)-phenol	3.52	8.03	4.9	1.52	4.18	5.51
4-hydroxy-3,5-dimethoxy-benzaldehyde	2.44	3.66	-	-	2.83	2.13

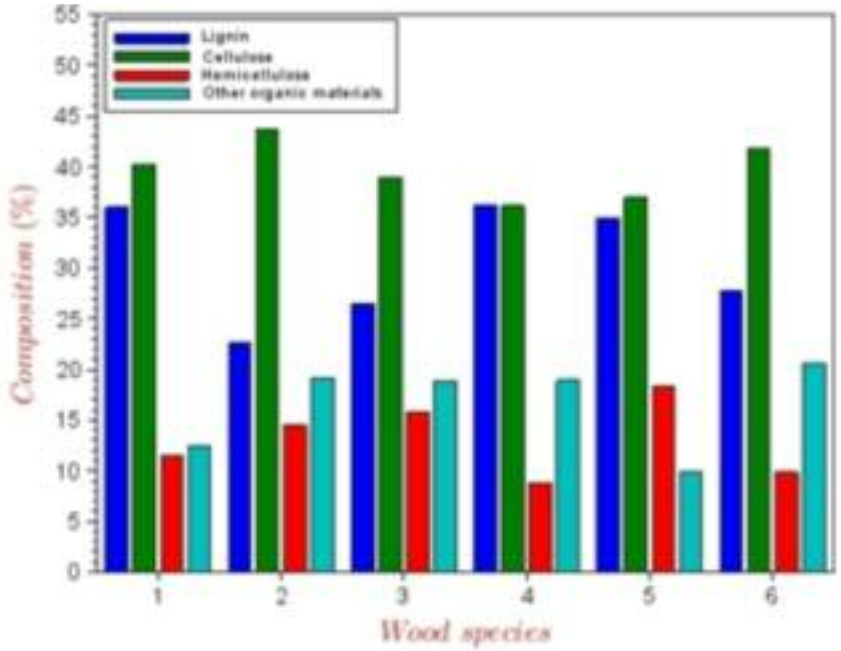

Figure 2: Structural carbohydrates and lignin composition

3.2 Pyrolysis experiments

Even though the experiments were carried out at different temperature, the operation temperature values were within the accepted range for maximum bio-oil production from fast pyrolysis experiments (Bayerbach *et al.,* 2006; Bayerbach *et al*., 2009, Sulaiman and Abdullah, 2011). The mass balance of the bio-oil production is presented in Table 2 and shows that the highest bio-oil yield of 66wt% was obtained from Neem wood, while the least yield occurred in Tropical Almond wood. These values are close to that obtained by Azeez *et al., (*2010) even though a fluidized bed reactor was used at 470°C. Meanwhile, the bio-oil % yield of all the samples is greater than those obtained by Mullen and Boateng (2008) in the pyrolysis of switchgrass, early bud and full flower alfalfa in a 2.5kg/hr fluidized bed reactor at 500°C.

However, the yields are lower than 75 – 80wt% bio-oil proposed by Bridgwater (1999) on fast pyrolysis of wood. Higher bio-oil yield may be obtained under improved reactor and operating conditions. As many factors affect the yield of bio-oil, it may be very difficult to specifically peg certain factors as responsible for the variation in the quantity obtained from these species. Since more than 50% by weight of materials pyrolyzed are converted to bio-oil, then the species might be good enough for commercial bio-oil production. Even though the water content of the bio-oils from fast pyrolysis of these biomass species is high, their carbon and hydrogen content are high such that the

Table 4: Some physical and chemical properties of the bio-oils

Bio-oil	*Density (g/cm^3)*	*pH*	*Viscosity @40°C (cp)*	*Water content (wt %)*	*Elementalanalysis (wt %)*				
					C	*H*	*O*	*N*	*S*
Ogbono wood	1.08	2.87	13.7	34.76	44.73	7.42	43.83	0.66	<0.05
Mango wood	1.10	3.31	10.5	33.41	38.39	7.78	47.97	0.90	<0.05
Neem wood	1.11	2.80	17.4	29.99	39.68	7.42	49.66	1.25	<0.05
Ogbono shell	1.05	2.88	5.7	36.82	37.83	7.96	41.93	0.70	<0.05
Ogirisi wood	1.06	3.50	12.2	37.10	35.01	8.05	43.36	0.69	<0.05
Tropical Almond wood	1.04	2.81	8.5	36.81	37.74	7.77	50.27	0.50	<0.05

fuels can combust well in boilers and engines. For high energy output the bio-oil from these species would need to undergo upgrading to improve their heating values.

3.3 Products characterization

a) Bio-oil

In order to achieve the desired quality of the bio-oils as sources of chemicals and fuel for power production, full characterization of the oils were carried out. Thus, Table 4 shows the elemental composition of the oils from the biomass samples. The table shows that the sulphur and nitrogen content of the oils were ≤0.05 and 1.5 respectively. This implies that the combustion of the oils will result in emission of little or no sulphur and nitrogen related pollutants. The values of oxygen content of the bio-oils in this work are close and similar to those obtained in the bio-oil of other woody biomass samples such as presented by (Dinesh *et al., 2006*; Adisak *et al.,* 2007; Uzun *et al.,* 2010) but slightly higher than those of Ingram *et al.(*2008). The presence of O_2 that is primarily responsible for the difference in the behaviour and properties of hydrocarbons and biomass liquid products such as bio-oils (Oasmaa and Czernik, 1999). In fact, it is rare to obtain bio-oil whose oxygen content is less than 30wt%. So, the values obtained in these tropical biomass samples are not out of place for a typical bio-oil. It is the presence of high oxygen and water content in the bio-oils, that the fuels are plagued by poor volatility, high viscosity (Table 4) and corrosiveness (Dinesh *et al.,* 2006; Oasmaa and Czernik, 1999). The elemental composition of the bio-oils resembles those of the parent feedstock from where they are derived and differ significantly from petroleum oils. The presence of O_2 and water in the biomass pyrolysis bio-oil may be responsible for the low pH values of the product as shown in Table 4. This agrees with the high value of acetic acid content of all the bio-oils shown in Table 3. The pH of heavy fuel oils is zero while that of bio-oil from wood pyrolysis can be as low as 2.5 (Dinesh *et al*., 2006), confirming the range of values (2.8 – 3.5) obtained in this work. Similarly, the density (gcm^{-3}) and/or the specific gravity of the bio-oils (Table 4) are slightly above 1 which are typical of pyrolysis liquids but are higher than those of heavy fuel oil. This implies

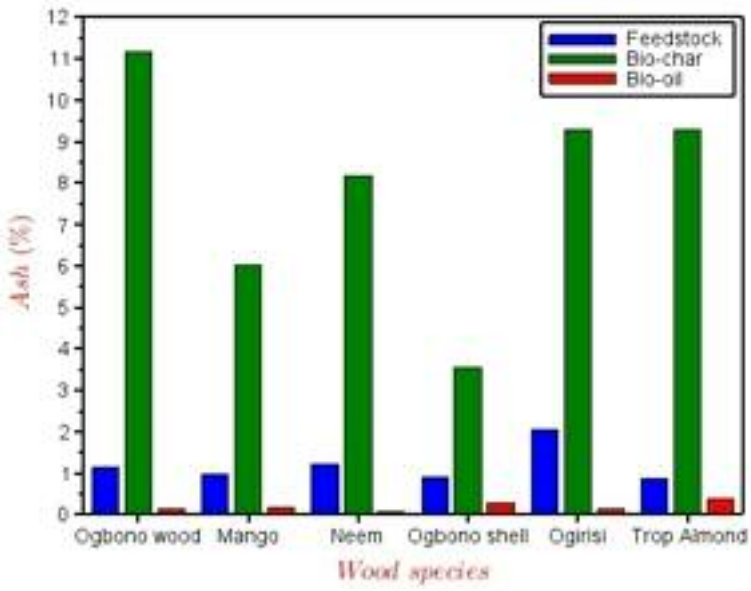

Figure 3: Ash content of feedstock and pyrolysis products

1: Ogbono wood, 2: Mango wood, 3: Neem wood, 4: Ogbono shell, 5: Ogirisi wood, 6:-Tropical Almond wood

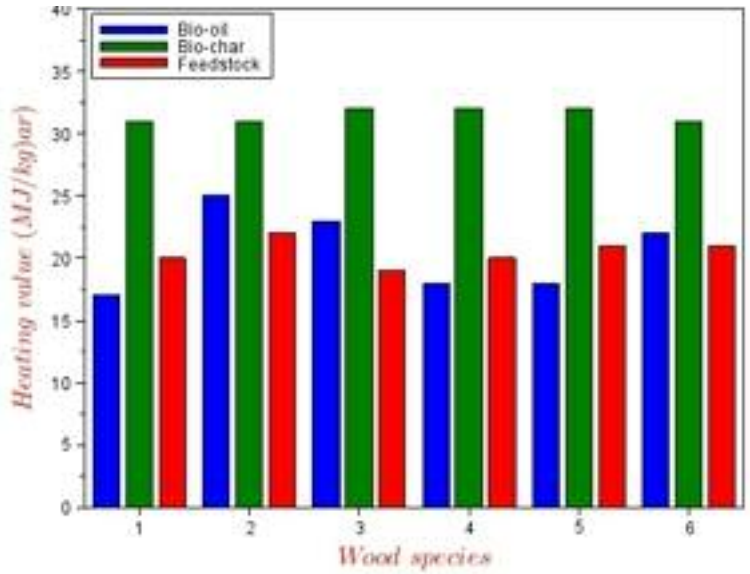

Figure 4: Heating value of feedstock and pyrolysis products

that the bio-oil from these tropical biomass samples can serve similar purposes which other non-tropical species have served.

The conversion of the biomass to bio-oil and char resulted in significant improvement in the quality of the products as fuel over the parent feedstock. Even though in Figure 3 the ash content of char increased over the values obtained for the raw feedstock, the heating values increased significantly (Figure 4), when compared with those for the feedstock. This implies increased energy value of the products (bio-oil, char and gas) vis-à-vis the raw feedstock.

GC/MS analysis result

The gas chromatography and mass spectrometry analysis of the bio-oils was carried out and Table 3 shows the composition by quantity (area %) of major chemical compounds in the bio-oils. It also shows the summary of some of the major chemical compounds and their relative abundance (% area) in the chromatographic analyses of the oils using GC/MS. The chemicals are similar to those identified by some researchers (Ingram *et al.,* 2008; Czernik and Bridgwater, 2004; Sipila *et al.,* 1998; Akwasi *et al.,* 2007). This shows that the biomasses and their bio-oil products can be sources of valuable chemicals such as phenols used for industrial purposes. Conversion to bio-oil and char through pyrolysis instead of direct combustion is value addition to the materials as sources of chemicals and energy.

b) Bio-char characterization

Only the heating values and the ash contents were determined as shown in Figures 3 and 4 respectively. All the char products show significant potential to be used as sources of thermal energy in combustion chambers of boilers and combustors. The pyrolysis conversion of the feedstock produces high energy density fuel (bio-char) whose higher heating values are close to those of coal. Generally, it implies that the bio-char from these samples can supplement the energy input of the pyrolysis reaction through product recycling and thus reduces the energy input. Even though the elemental analyses of these bio-char products were not carried out to identify the sulphur and nitrogen content, insignificance presence of these elements in the parent feedstock shows that these bio-char could serve as environmentally friendly fuel.

4. Conclusion

The feedstock and their pyrolysis products possess the properties required for applying the pyrolysis technology to the conversion of the feedstock and products to energy. The bio-oil products and char can be utilized in power generation by combustion in boilers and thermal plants. If upgraded, better fuel quality will be obtained from the bio-oil products. The results of the GC/MS analysis of the bio-oils show that these products can be sources of useful industrial chemicals where the focus lies on chemical production. The wastes resulting in the cultivation or use of the feedstock, in daily socio-economic activities of the tropical regions where they are largely produced, can be easily converted to useful energy through fast pyrolysis leading to improved lifestyle, better agricultural output and better environment. The use of these biomass species for energy and chemicals production through fast pyrolysis conversion is recommended.

Acknowledgement

This work was possible through the Fulbright Fellowship award b thy International Institute of Education (IIE) to Edmund Okoroigwe as Visiting Scholar to Michigan State

University, East Lansing and partly funded AgBioResearch at Michigan State University.

References

Adisak P, Titiloye J. O, and Bridgwater A. V. (2007). Fast Pyrolysis of Agricultural Residues from Cassava Plantation for Bio-oil production, *Asian J Energy and Environ* 8 (2): 496 – 502.

Akwasi B, Daugard D. E., Goldberg N. M, and Hicks K. B. (2007). Bench-Scale Fluidized Bed Pyrolysis of Switchgrass for Bio-oil Production, *Ind Eng. Chem Res*. (46) 1891 –1897.

Andreae M. O. (1991). In Global Biomass Burning: Atmospheric, Climatic and Biospheric Implications; Levine J.S., Ed.; MIT Press: Cambridge, MA pp 2-21.

Azeez A. M, Meier D, Odermatt J, and Willner T. (2010). Fast Pyrolysis of African and European Lignocellulosic Biomasses Using Py-GC/MS and Fluidized Bed Reactor, *Energy Fuels* 24: 2078–85: DOI: 10.1021/ef9012856.

Bayerbach R. and Meier DJ. Characterization of the water-insoluble fraction from fast pyrolysis liquids (pyrolytic lignin). Part IV: Structure elucidation of oligomeric molecules, *Anal. Appl. Pyrolysis* 2009, 85: 98– 107. In [Azeez *et al.,* 2010].

Bayerbach R, Nguyen V. D, Schurr U, and Meier D. J. (2006). Characterization of the water-insoluble fraction from fast pyrolysis liquids (pyrolytic lignin): Part III. Molar mass characteristics by SEC, MALDI-TOF-MS, LDI-TOF-MS, and Py-FIMS Anal. *Appl. Pyrolysis* 2006, 77(2) 95–101. In [Azeez *et al.,* 2010].

Bridgwater A. V. (1999). Principles and Practice of Biomass Fast Pyrolysis Processes for Liquids, *Anal Appl Pyrolysis* 51: 3-22.

Brown R. C. (Ed). (2011). Thermochemical processing of biomass. Conversion into fuels, chemical and power. Wiley publishers, 128 – 129.

Bui V. N, Toussaint G, Laurenti D, Mirodatos C, and Geantet C. (2009). Co-processing of pyrolysis bio oils and gas oil for new generation of bio-fuels: Hydrodeoxygenation of guaïacol and SRGO mixed feed, *Catalysis Today* 143(1-2): 172 – 178.

Czernik S. and Bridgwater AV. (2004). Overview of Applications of Biomass Fast Pyrolysis Oil Energy Fuels 2004; 18:590-8. In [Adisak *et al.,* 2007].

Das P, Ganesh A, and Wangikar P. (2004). Influence of pre-treatment for deashing of sugarcane bagasse on pyrolysis products. *Biomass Bioenergy* 27,445–457. In [Azeez *et al.,* 2010].

De Ramos P. L. E, Trugilho P. F, Napoli A, and Bianchi M. L. (2011). Characterization of residues from plant biomass for use in energy generation, Revista Cerne, 17 (2): 237 – 246.

Demirbas A. (2007). Effects of Moisture and Hydrogen Content on the Heating Value of Fuels**.** *Energy Sources, Part A: Recovery, Utilization, and Environmental Effects*; 29 (7). DOI**:** 10.1080/009083190957801.

Dinesh M, Pittman C.U Fr, and Steele P. H. (2006). Pyrolysis of wood/Biomass for Bio-oil: A critical Review, *Energy Fuels* 20: 848 – 889.

Ingram L, Dinesh M, Bricka M, Steele P, Strobel D, Croker D, Mitchell B, Mohammad J, Cantrell K, and Pittman C. U Jr. (2008). Pyrolysis of Wood and Bark in an Auger reactor: Physical properties and chemical Analysis of the produced bio-oils. *Energy Fuels* 22: 614 –625

Mullen A. C and Boateng A. A. (2008). Chemical Composition of Bio-oils Produced by Fast Pyrolysis of Two Energy Crops*, Energy and Fuels* 22: 2104 – 2109.

Oasmaa A, and Czernik S (1999). Fuel Oil Quality of Biomass Pyrolysis Oils State of the Art for the End Users. *Energy Fuels* 13:914 – 921. In [Adisak *et al.,* 2007].

Okoroigwe E, Zhenglong L, Stuecken T, Saffron C, and Onyegegbu S. (2012). Pyrolysis of *Gmelina arborea* Wood for Bio-oil/Bio-char Production: Physical and Chemical Characterization of Products. J Appl Sc. 12(4): 369 – 374.

Pantami S. A, Voncir N, Babaji G. A, and Mustapha S. (2010). Effect of Burning on Soil Chemical Properties in the Dry Sub-Humid Savanna Zone of Nigeria, *Researcher* 7: 78 – 83.

Roberts, G., Wooster, M. J., and Lagoudakis, E. (2009). Annual and diurnal African biomass burning temporal dynamics, Biogeosciences, 6, 849-866, doi: 10.5194/bg-6-849-2009.

Satyanarayan N, Vaibhav V. Goud P. K. Rout K. J, and Ajay K. D. (2010). Characterization of Canadian biomass for alternative renewable biofuel, *Renew Energy* 35(8), 1624–1631.

Senjobi B. A, Adeokun O. A, Dada O. A, and Ogunkunle A. O. (2007). Influence of Traditional Farming Practices on Soil Productive Potentials in Ago-Iwoye Enclave, Ogun State, Nigeria. *J Environ Ext*. 6: 64 – 70.

Sipila K; Kuopala E, Fagernas L, and Oasmaa A. (1998). Characterization of Biomass-Based flash Pyrolysis Oils, *Biomass Bioenergy* 14 (2) 103 – 113

Sivakumar G, Vail D. R., Xu J, Burner D. M, Lay J. O, Ge X, and Weathers P. J. (2010). Bioethanol and biodiesel: Alternative liquid fuels for future generations, *Eng. Life Sci.,* 10: 8–18. doi: 10.1002/elsc.200900061.

Sulaiman F, and Abdullah N. (2011). Optimum conditions for maximizing pyrolysis liquids of oil palm empty fruit bunches, *Energy* 36: 2352 –2359.

Tsamba A. J, Yang W, and Blasiak W. (2006). Pyrolysis Characteristics and Global Kinetics of Coconut and Cashew nut shells. *Fuel Proc Tech*. 87:523 –30.

Uzun B. B, Apaydin-Varol E, Ates F, Ozbay N, and Putun A.(2010). Synthetic Fuel Production from tea waste: characterization of bio-oil and bio-char, *Fuel* 89: 176 – 184.

Received 25 March 2014; revised 11 March 2015

Appendix A: Pyrolysis experiments photographs

Figure A1: Reactor in use

Figure A2: Char trap

Figure A3: Bio-oil condensers and containers

Figure A4: Bio-oil and bio-char

Figure A5: Combustibility test of NCG

Using participatory GIS to examine social perception towards proposed wind energy landscapes

Andrea Lombard
Department of Geography, University of South Africa

Abstract
Thirteen onshore wind farm projects, totalling approximately 700 wind turbines, are proposed for the West Coast Region (WCR) of the Western Cape Province in South Africa. Wind energy exploitation possesses the ability to transform what can be classified as natural landscapes into landscapes of power, making the type of landscape on which wind turbines are deployed a prominent factor in its social acceptance or rejection. This paper examines the landscape aesthetics and land use interference of proposed wind farms in the WCR of South Africa through determining if social acceptance or rejection of proposed wind farms is dependent on the residents and visitors scenic and land use valuation of the natural landscape. The results indicate that the visual intrusion of wind turbines is the impact that respondents are least concerned with contrasting with the findings of international literature and further reasons for this anomaly are interrogated against the background of South Africa's dire electricity needs. The paper concludes that visual impact assessments alone are not sufficient for evaluating landscapes and this paper recommends that participatory geographic information systems (PGIS) be used in addition to existing wind energy landscape assessments.

Keywords: wind energy landscapes, participatory GIS, South Africa

1. Introduction

The development of onshore wind energy is environmentally and socially controversial, with concerns stemming largely from the transformation of natural landscapes into landscapes of power (Pasqualetti, 2000). Landscape character is significant, i.e. what the landscape looks like and which qualities it possesses. This determines whether wind farm projects conform to the overall character of the landscape (Henningsson *et al*., 2013).

The West Coast Region (WCR) of South Africa is being targeted by wind energy developers because of the region's proven sustainable wind resources (Diab, 1995; Lombard, 2010). The region is renowned for its unique fisherman's culture, untouched natural landscapes that promote tranquillity and its small towns with their unpretentious atmosphere that offers a special quality of life for residents. Recent proposals for establishing a number of wind farm projects in the region are potentially threatening to the character of the WCR landscape. The aim of the research was to establish whether the social acceptance or rejection of proposed wind farms in the region is dependent on the residents and visitors scenic and land use valuation of the natural landscape. The overall objective is to critique wind farm visual and landscape impact assessment practice to determine if alternatives such as participatory geographic information systems (PGIS) would make a valuable contribution to this type of assessment. The paper first reviews existing scholarship on wind energy landscapes and assessment practices. Second, the research methods are reported and the study area – the WCR – is introduced. Third, the results are presented and discussed in detail. Last, the main findings are summarized and the paper concluded.

2. Background: Wind energy landscapes

The installation of wind turbines on natural landscapes is generally perceived to have a negative impact on the value of the landscape (Pasqualetti,

2000; Lothian, 2008). However, the valuation of the landscape differs between types of landscape, individuals as well as different wind energy projects. In some instances, the development of wind farm projects may even complement the character of the landscape. This paper investigates the impact of wind farms on landscapes in two manners, first the visual impact of wind turbines on landscapes and second the diversification of land use coupled with wind farm development.

2.1 Visual intrusion of wind turbines

The visual impacts of wind farms is undoubtedly the most controversial issue in wind farm development because wind turbines are accused of ruining the scenic value of landscapes (Pasqualetti, 2000; 2001). EWEA (2010) indicates:

> Wind turbines are man-made vertical structures with rotating blades, and thus have the potential of attracting people's attention. Typically wind farms with several wind turbines spread on the territory may become dominant points on the landscape.

The accusation does not hold everywhere as wind farms are not necessarily built where landscapes have scenic value. Some features in the design and siting of wind farms have been identified to minimize their potential visual impact (Hecklau, 2005; Stanton, 2005; Brusa and Lanfranconi 2006). Van de Wardt and Staats (1988) have made it clear that the type of landscape in which wind turbines are deployed is the most significant factor in visual landscape evaluations fully overshadowing all other visual and scenic factors of wind farms.

As stated by Wolsink (2012), the conception of 'visual impact' almost spontaneously classifies the impact on the landscape as negative. The visual impact is especially high in areas which lack any other form of human interference, for example natural, undisturbed landscapes free of any form of development (Katsaprakakis, 2012). Whether these turbine structures have positive or negative impacts on the aesthetic value of a landscape is a matter of individual opinion and the nature of the impacts is determined specifically by the type of surroundings (Wolsink, 2007). One of the main concerns in terms of bucolic landscapes is the influence of wind farm development on tourism in the area. While a tourist might see a landscape as a natural space with an aesthetic value and view it as a 'picture postcard', a farmer might see it as a 'production landscape' where the development of wind farms can lead to land use and income diversification.

2.2 Land use diversification

Land not only provides a material basis for the economy, it also gives us cultural meanings such as a 'sense of place and a sense of history' (Lobley and Winter, 2009: 7). Land and its use represent the core relationship between the natural environment and human activity. Wind farm development will change the use of land or diversify it to a certain extent. Manwell *et al*. (2002: 502) describes the relationship between land use and wind energy as one that is 'sometimes considered to be land intrusive rather than land intensive'.

This study mainly focuses on agricultural areas as wind farms are often developed on land used exclusively for agricultural purposes. It is advisable to develop wind farms on low-potential agricultural land, thereby supplementing farm income without adversely affecting agricultural production. The development of wind farms in agricultural landscapes can result in a multifunctional countryside, but if the potential wind farm areas surrounding farmland also have tourism value, conflict might arise. It is therefore cardinal that landscape assessment practice should be conducted properly.

2.3 Investigating landscape assessment practice

According to Wolsink (2012) the landscape assessment associated with wind power varies because of three factors which are:

1. the landscape impact varies widely among cases, as the character of the landscape is very different at different locations;
2. within each landscape there are many distinguishable elements that may be differently affected;
3. the valuation of the impact shows a wide variety among individuals: some can positively value landscape elements, whereas other individuals value the same element negatively.

Ideal landscape assessment practice should focus on landscape character, landscape value, landscape capacity and landscape sensitivity as a whole and not as homogenous entities. Unfortunately, landscape assessment practice focuses too often on the objectification of the landscape making use of only visual impact assessments. Current techniques of landscape assessment also rely almost solely on specialist perspectives without incorporating the indigenous knowledge of the local people at grassroots level. This study suggests a method first explored by Brown and Raymond (2007) as a way of integrating the local people into the spatial planning of wind energy landscape assessments.

3. Methods and study area

The case study area is part of the WCR in the Western Cape Province of South Africa. The whole WCR consists of six sub-regions of which this study involved parts of the Swartland and Bergrivier subregions and the whole West Coast Peninsula subregion portrayed in Figure 1. References to the WCR in this paper all imply the extent of the study

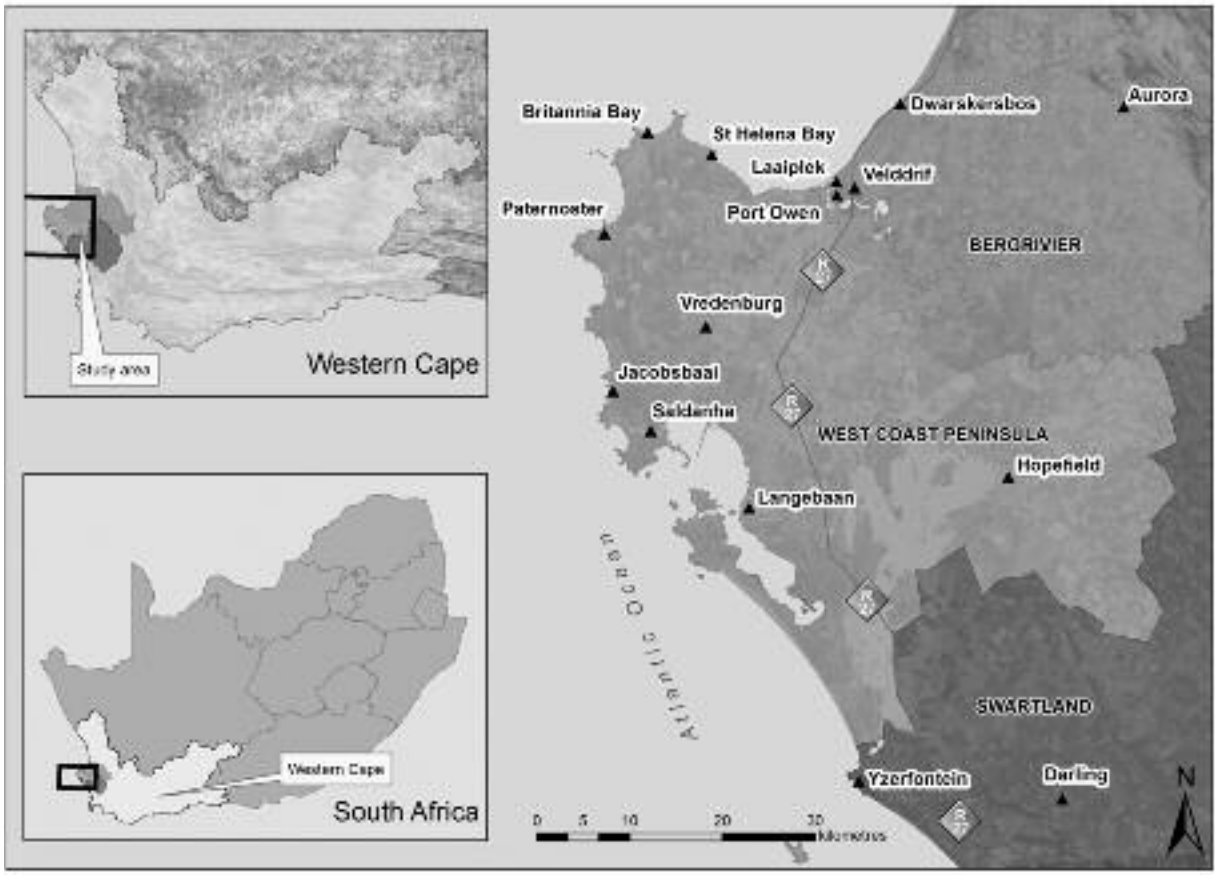

Figure 1: The study area within the West Coast region, Western Cape, South Africa
Source: Lombard, 2013

area described here and depicted in Figure 1, unless specified otherwise.

The three sub-regions spotlighted in the study boasts special contrasting landscape features ranging from beautiful and often deserted coastlines along the West Coast Peninsula and Bergrivier sub-regions to vineyards and wheat farms in the Swartland sub-region all of which appeal to the local residents and visiting tourists. The key economic sectors of the WCR are agriculture, fisheries, manufacturing, mining and tourism (West Coast District Municipality, 2012). This study area was selected because it is the focus of 13 proposals for wind farm projects which will incorporate approximately 700 wind turbines.

This empirical study made use of a questionnaire to elicit information from both residents of and visitors to the WCR. The questionnaire was also the main research instrument used in a broader study on the perceptions and attitudes of the residents of and visitors to the WCR concerning: (1) their place attachment and knowledge of the region; (2) the effects of wind turbines on the natural landscape and; (3) the anticipated influence of the proposed wind farm projects on the tourism industry (Lombard, 2013). This paper reports on the second component of the questionnaire concerning the perception of the proposed wind farm projects on the WCR natural landscape. A total of 410 questionnaires were distributed to both residents of and visitors to the WCR either in person, via post or by using a web-based questionnaire (Surveymonkey). Table 1 shows the number of questionnaires distributed among the two target groups as well as the various response rates.

The response rate of 36% for the 410 distributed questionnaires and the absence of a purposeful stratification of the sample limit generalizations from

Table 1: Questionnaire distribution and response rates

Respondent category	*Number via hand distribution*	*Response rate for hand distribution*	*Number via Internet distribution*	*Response rate for Internet distribution*	*Total distributed*	*Total response rate*
Residents (insiders)	150	55 (37%)	100	43 (43%)	250	98 (39%)
Visitors (outsiders)	50	15 (30%)	110	35 (32%)	160	50 (31%)
Totals	200	70 (35%)	210	78 (37%)	410	148 (36%)

this study. The conclusions drawn are applicable to the respondents and should not be interpreted as representing the views of the entire population of the WCR.

This study focused on the pre-construction phase of these projects and the low response rate can therefore be attributed to unfamiliarity with the proposed projects. A significant number of tourists also indicated that for them the WCR will always be a place to visit and therefore they are not interested in completing the questionnaire as they only frequent the region on a temporary basis.

Figure 2 shows that ninety-one per cent of the responding residents were 41 or older, including nearly half (47%) 61 or older. Most (more than three out of four) resident respondents live in the

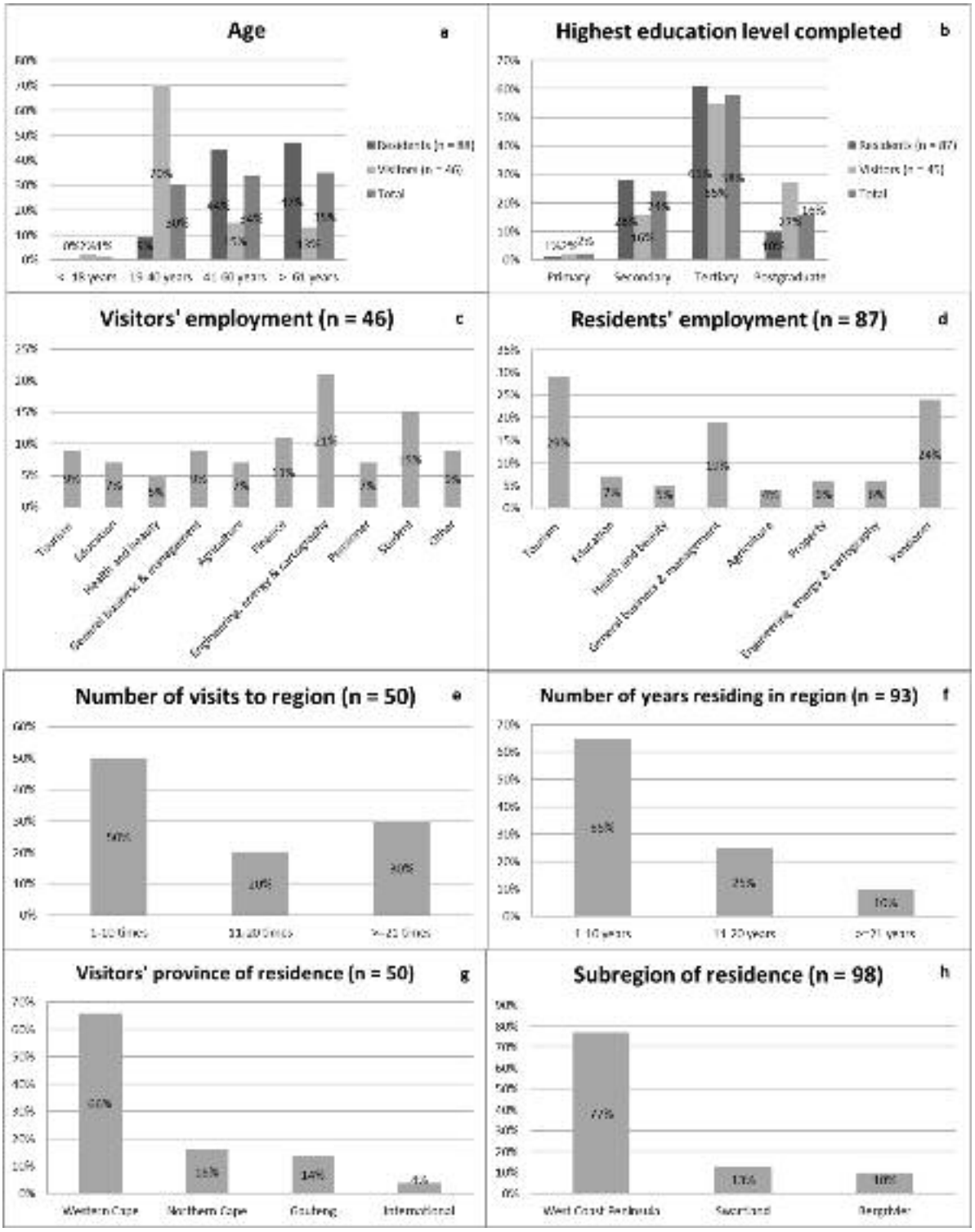

Figure 2: The demographical details of respondents to the survey
Source: Questionnaire survey 2012

West Coast Peninsula sub-region, where the coastal towns are popular retirement places. The major difference between the resident and visitors groups is their age distribution in that 70% of the visitors were in the 19-40 years cohort opposed to only 9% of the resident respondents. From the perspective of tourism planning for the region, the views of younger generations are important.

Most resident respondents (29%) are employed in the tourism industry, while engineering, energy and cartography represents the largest proportion (21%) of the visitors' employment. Twenty-four per cent of the residents are pensioners, while 15% of the visitors are students corresponding with the age distribution trend. The education levels attained by both groups of respondents are high, with more than 70% each having a tertiary or higher qualification. Sixty-five per cent of residents have lived between one and ten years in this region, whilst only 10% have lived in the WCR for more than 21 years. Half of the visitor respondent group indicated they have visited the WCR between one and ten times, whereas 30% have visited the region 21 times and more. The fact that eight of the 13 proposed windfarms are earmarked for the West Coast Peninsula probably accounts for the overwhelming (77%) representation of respondents from this sub-region. Very few international tourists participated in the survey as the WCR is mainly a domestic tourist destination. Most of the visitor respondents hailed from the Western Cape (77%), with Cape Town contributing 38%. With the WCR being only 85 km from Cape Town – and part of the pleasure periphery of Cape Town – it is not unexpected that most of the visitors reside there.

The questionnaire survey commenced with the researcher's attendance of public participation meetings where attendees were identified as prospective respondents. All members of the public were invited to these meetings by project developers, so that people from different population groups and socio-economic levels attended. The researcher went from door to door in different neighbourhoods in the 15 towns and villages to invite people who were available and willing to complete the questionnaire. An announcement about the survey was also published in the local newspaper, the *Weslander*, to which all sections of the community have access in an attempt to make the survey more representative. The surveying of insiders and outsiders of the region has contributed to the inclusiveness of the research. The first round of data collection relied on convenience sampling. When convenience sampling failed to secure an adequate number of respondents, a process of snowball sampling was employed. Snowball sampling involves 'using one contact to help you recruit another contact, which in turn, can put you in touch with someone else' (Valentine 1997: 116). Insider knowledge of residents to help identify potential respondents – family members, friends, colleagues and anyone willing to participate in the survey – was reverted. This proofed to be an effective sampling technique.

A section of the questionnaire focused on a map-based method of collecting data on landscape values associated with the WCR. This method of data collection is referred to as participatory geographic information systems (PGIS). PGIS is a process through which community members — that is people at grassroots level — become involved in spatial planning. PGIS has been touted as the 'democratization of GIS' (Dunn, 2007: 616). The printed versions of the questionnaires were accompanied by maps and coloured sticker dots with which respondents could indicate locational preferences, while the online version provided a map with a grid. The data analyses were performed with SPSS (frequencies and cross-tabulations) and ArcGIS (digitizing of PGIS data and creation of maps).

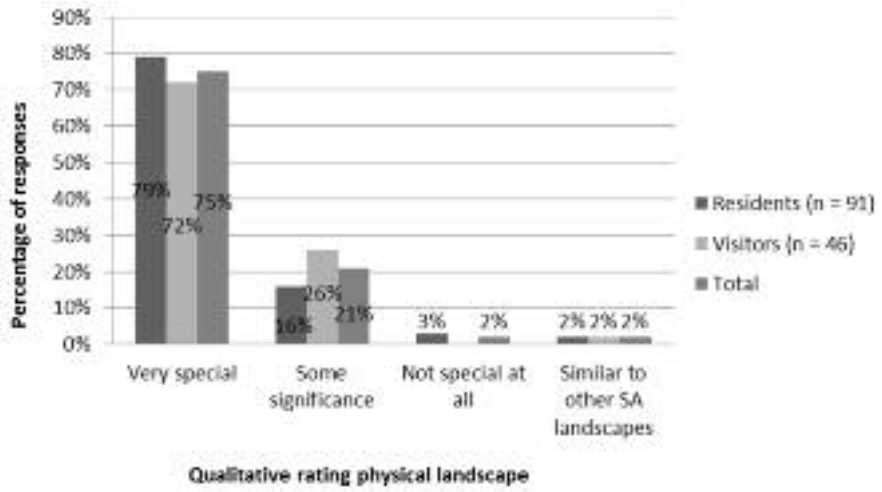

Figure 3: Nature of the physical landscape of the West Coast region
Source: Lombard, 2012

4. Results and discussion

The WCR is known for its simple, undeveloped and mostly natural landscapes. Potential disturbances of these fine and prized landscapes by wind farm developments may undoubtedly generate grave concern from various stakeholders in the WCR. Respondents were asked to indicate how special they consider the physical landscape of the WCR to be. Figure 3 displays their responses. The majority of residents and visitors regard the region's physical landscape as very special and they supported this by naming the fynbos vegetation, undisturbed coastlines, diversity and richness of floral species and the wide open and beautiful character of the landscape as features that make the landscape distinctive. Considering, among other factors, the special nature of the physical landscape, respondents were questioned on their support for or objection to proposed wind farm projects in the WCR.

The results indicated that 70% of both residents of and visitors to the WCR showed strong support for the development of wind farms in the region in accord with most international pre-impact surveys done on the social support of wind farm projects where only a minority is against the development of these projects. This section first explores respondents' reaction the visual impact of wind farms in the WCR, after which the focus shifts to land use diversification and landscape values associated with wind farms.

5.1 Visual impact of wind farms in the WCR

The natural landscapes of the WCR will experience scenic interference to a greater extent than in areas with developed landscapes. Respondents were presented with lists of both the advantages and disadvantages of wind energy as extracted from international literature which they had to rate on a Likert scale in accordance to how important they found the advantages to be and the degree of disturbance generated by the disadvantages. The disadvantages where weighed as not disturbing at all (-2), somewhat disturbing (-1), neutral (1), disturbing (2) and very disturbing (3). The total of each category was divided by the total respondents multiplied by 3 (n x 3) (as if all respondents indicated the disadvantage to be very disturbing) and expressed as an index value with 100 as the highest value. The advantages were weighed as unimportant (-2), low importance (-1), neutral (1), important (2) and very important (3). The total of each category was then divided by the total number of respondents multiplied by 3 (n x 3) (as if all respondents indicated the advantage to be very important) and expressed as an index value with 100 as the highest value. The results are given in Tables 2 and 3.

The drawback of wind turbines being perceived as ugly and so detracting from the scenic value of natural landscapes was appraised as the least disturbing liability which indicates that respondents have low levels of unease about the visual intrusion

Table 2: Respondents' weighted ratings of the disadvantages of wind energy (100 = very disturbing)

Disadvantages	*Residents (n = 98)*	*Visitors (n = 47)*	*Total*
Wind energy can be more expensive than other sources	36	22	31
Turbine blades can harm flying wildlife	25	20	28
Wind turbines may impair radio and television signals	28	17	24
Wind turbines might deter tourists from visiting certain areas	28	15	23
Wind energy potential varies seasonally and daily	22	22	24
Wind turbines may be noisy	25	3	16
Wind turbines are perceived as ugly and so detract from the scenic value of natural landscapes	9	12	2

Table 3: Respondents' weighted ratings of the advantages of wind energy (100 = very important)

Advantage of wind energy	Residents (n = 98)	Visitors (n = 47)	Total
Produces no atmospheric emissions	90	91	91
No air pollution	89	91	90
Increases electricity supply	86	87	86
Resource (wind) used to generate electricity is free	78	76	77
Land parcels used for wind turbine installations can still be used for farming	68	74	70
Conserves fossil fuels for future generations	65	66	65
Wind turbines are symbols of commitment to renewable energy	52	64	56
Produces economic gain for communities	46	72	55
Creates new employment opportunities	45	72	54
Increases tourism activities (as attractions)	5	24	5

of wind farms in the WCR. This result is unexpectedly positive as Wolsink (2007) and Pasqualetti (2011) both assert that the visual intrusion of wind farms is the most controversial issue surrounding their development.

Another way of exploring the attitude of respondents to the adverse scenic impacts of wind farms was to show them a collage of photographs. After being instructed to observe the photographs, they were asked if they wanted to change their earlier answers to the questions whether they would support the development of wind farms in the WCR. All the residents and visitors declared that they would not change their answers. The reasons provided were that wind turbines are aesthetically more pleasing than nuclear reactors; they do not have any deterring effect; and they look good in other countries. This indicates the very subjective nature of the scenic perception of wind turbines.

5.2 Wind farms and land use diversification in the WCR

Wind farms afford famers an economic opportunity to earn income through supplying land to developers. Table 3 shows that the advantage of using land parcels for farming after installation of wind turbines is considered cardinal for both visitors to and residents of the WCR.

Wind farm development can secure agricultural sustainability over the long run with economic security derived from renting portions of land to wind farm developers. According to Loubser (2011) of the Vredenburg Agricultural Society, wind farm development is a way to sustain the already struggling agricultural sector of the WCR.

A possible reason for the anomaly on the scenic impact of wind farms also present itself in Table 3. Since 2008, South Africa has experienced a severe electricity crisis (Inglesi, 2010; Clohessy, *et al.*, 2014) periodically suffering countrywide blackouts. The reserve margin – the excess of generation capacity over peak demand – is also contributing to the power crisis where this reserve has shrunk to about 8% against the international standard of at least 15% (Cary, 2012; *The Economist*, 2008). It is therefore not surprising that a rating of 86 was given to the possible increase in electricity supply.

Using scale-based approaches such as the above is sufficient, but can be strengthened by incorporating map-based approaches such as PGIS. The

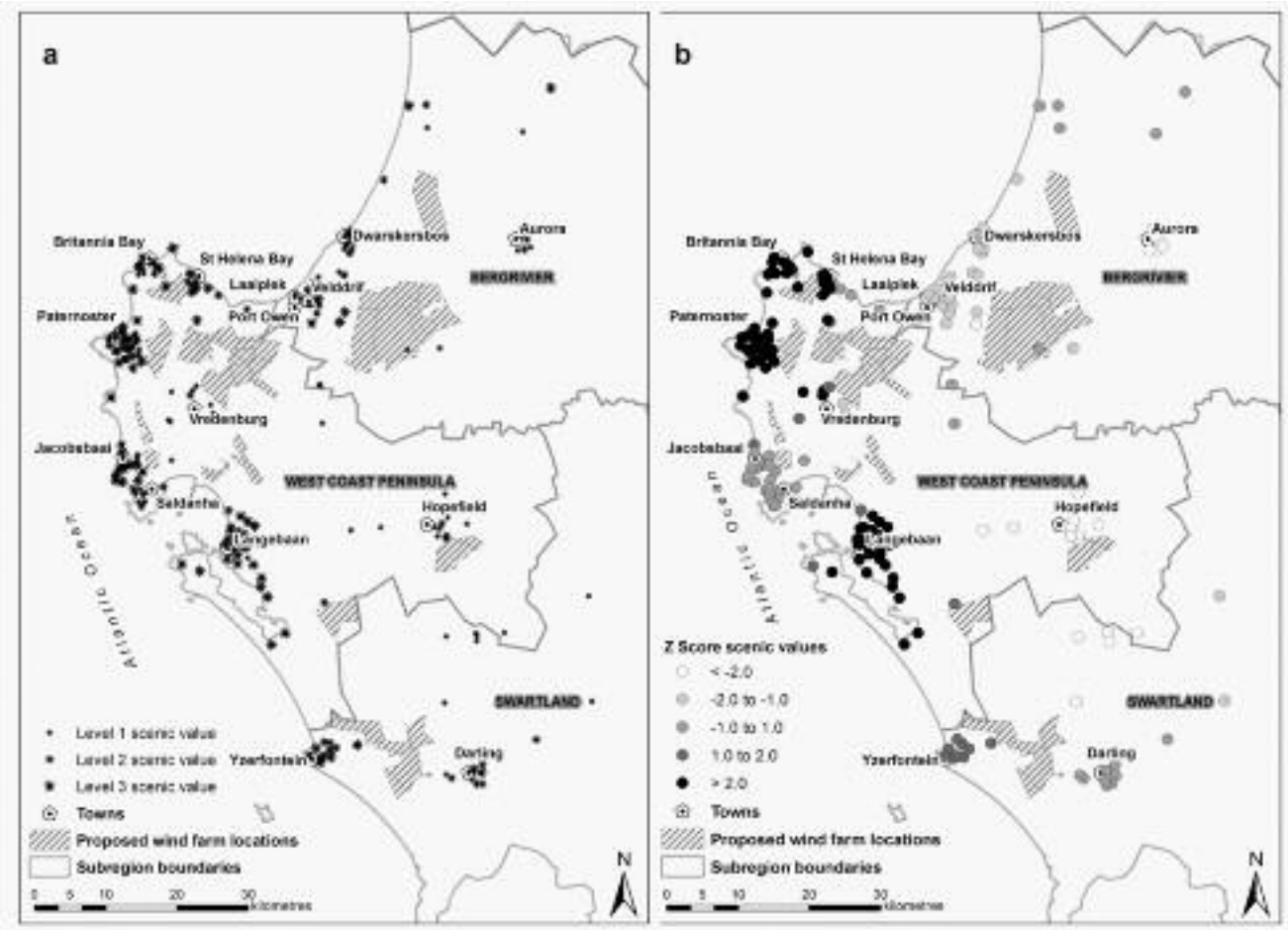

Figure 4: Scenic value of landscapes in the West Coast region: (a) Distribution of dots placed by respondents; (b) Hot Spot analysis results

Source: Lombard, 2012

PGIS exercise in this study was specifically focused on landscape values from a participatory planning perspective.

5.3 Wind farms and landscape values of the WCR

The PGIS exercise in the questionnaire required respondents to indicate on a map the landscape value of places they deem to possess scenic/aesthetic and economic value.

This is a descriptive mapping process of landscape valuation. The respondents had to rank the scenic and economic value of their chosen places on a scale of one to three with three being the most prominent (exceptional). The distribution of these values was analysed by evaluating the spatial clustering of values as a dimension of spatial analysis. According to Longley *et al.,* (2005: 316) 'spatial analysis can reveal things that might otherwise be invisible – it can make what is implicit explicit.' In this instance, spatial analysis is used to locate the areas where the highest concentrations of the two landscape values are found. To discern these patterns, a specific tool of spatial analysis was employed, namely Hot Spot analysis which 'identifies statistically significant spatial clusters of high values (hot spots) and low values (cold spots)' (ArcGIS Desktop, 2011). Figure 4a shows the distribution of places where the resident and visitor respondents consider the landscape to have scenic value. To make sense of this distribution, the results of the Hot Spot analysis are shown in Figure 4b.

Respondents indicated a total of 194 places with scenic value with 31% classified as level 1, 32% classified as level 2 and 37% classified as level 3. From the general distribution, it is evident that scenic value is predominantly associated with coastal areas. It is a cause for disquiet that some places of scenic value coincide with the proposed wind farm developments, for example, at St Helena Bay and Paternoster. Wind farm development in these two areas of clustered scenic value will have to be handled judiciously by wind farm developers. The second landscape attribute respondents were asked to map according from little to exceptional value which is the economic value of the WCR landscape. The chosen locations are portrayed in Figure 5a and the economic hot spots in Figure 5b.

The respondents identified 178 places with economic value with 26% classified as level 1, 34% as

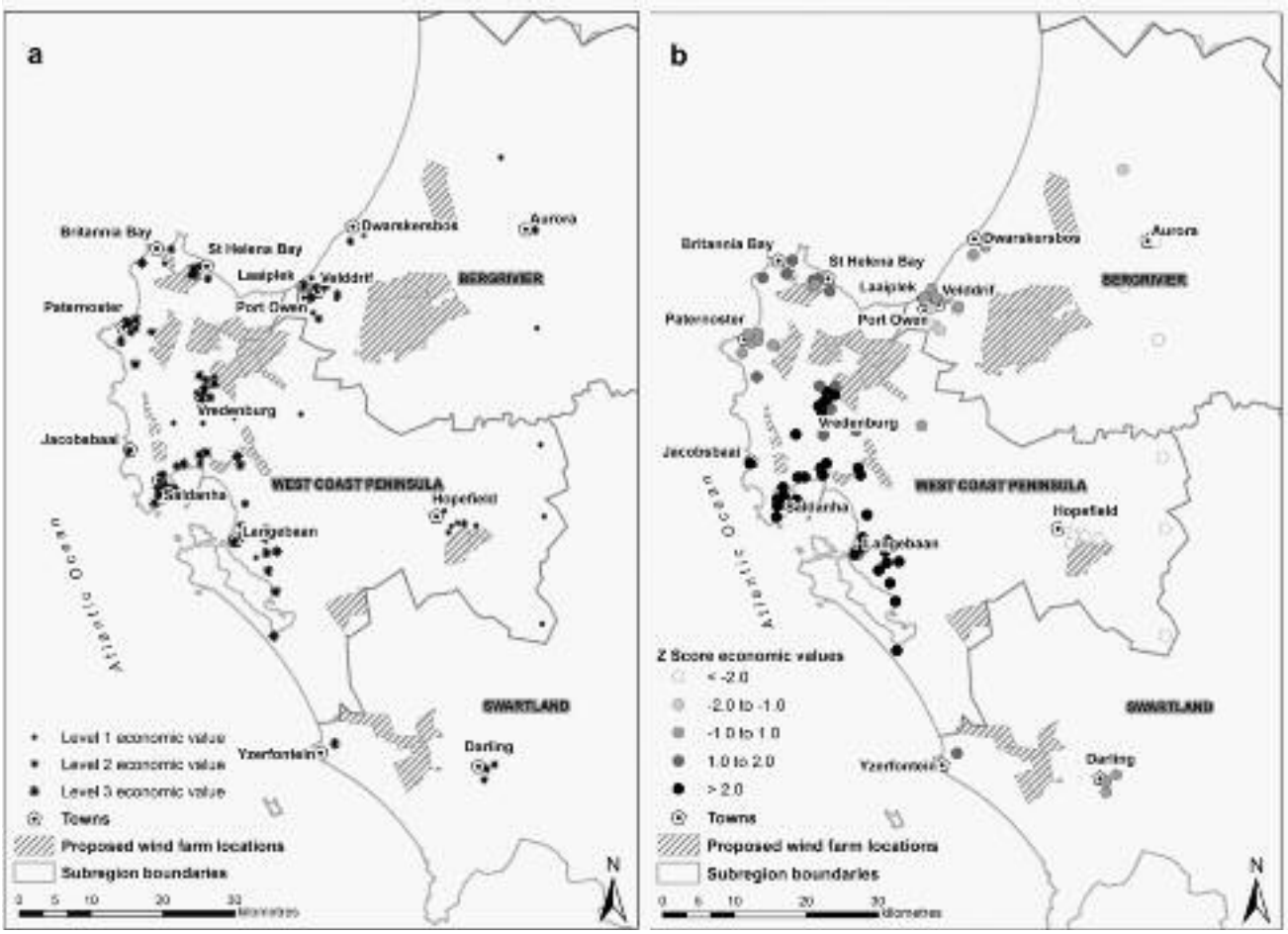

Figure 5: Economic value of landscapes in the West Coast region: (a) Distribution of dots placed by respondents; (b) Hot Spot analysis results

Source: Lombard, 2012

level 2 and 40% as level 3. The areas identified with the most prominent economic value occur in the West Coast Peninsula sub-region (78%) and are found in the Vredenburg, Saldanha and Langebaan areas according to the hot spot analysis. Vredenburg is the business centre of the WCR so that this economic hot spot is not surprising. The harbour industry and steel mill in the Saldanha area assign a high level of economic value to this area and Langebaan is a tourism hub of the WCR with various tourism-associated activities distinguishing the economy. Notable in Figure 5b is that the inland areas where mainly agriculture is practised are cold spots regarding economic value because agriculture exhibits a relatively low performance in comparison to the industries in the Langebaan, Saldanha and Vredenburg areas. The addition of wind farms to these agricultural areas may increase the associated economic value.

The research has shown that very few of the respondents are opposed to wind farm developments, provided that the development occurs in the appropriate places. Therefore, as a finale to the PGIS exercise, respondents were invited to indicate on a map where they believe appropriate locations for wind farms are (Figure 6a) as well as to map where wind farms should not be located (Figure 6b).

The distribution of places where the wind farms should be located clearly tends toward the interior of the region away from urban settlements. The inland locations are unfortunately not always endowed with exceptional prevailing wind resources like those closer to the coast (Diab, 1995). Some respondents indicated that wind farms should be located offshore, but no offshore wind farms have yet been proposed for South Africa. Figure 6a does, however, show that a number of these appropriate places coincide with the areas where wind farms have already been proposed. There are fewer points in the Paternoster, St Helena Bay and Britannia Bay areas compared to Figure 6b which indicates that the wind farms close to these two locations are the definite ones that deserve more attention from the developers. Locations close to the coast emerge as no-go areas with an emphasis on the areas surrounding St Helena Bay, Britannia Bay and Paternoster.

The community of Paternoster has formed a group 'NoWindfarmsPaternoster' to express their

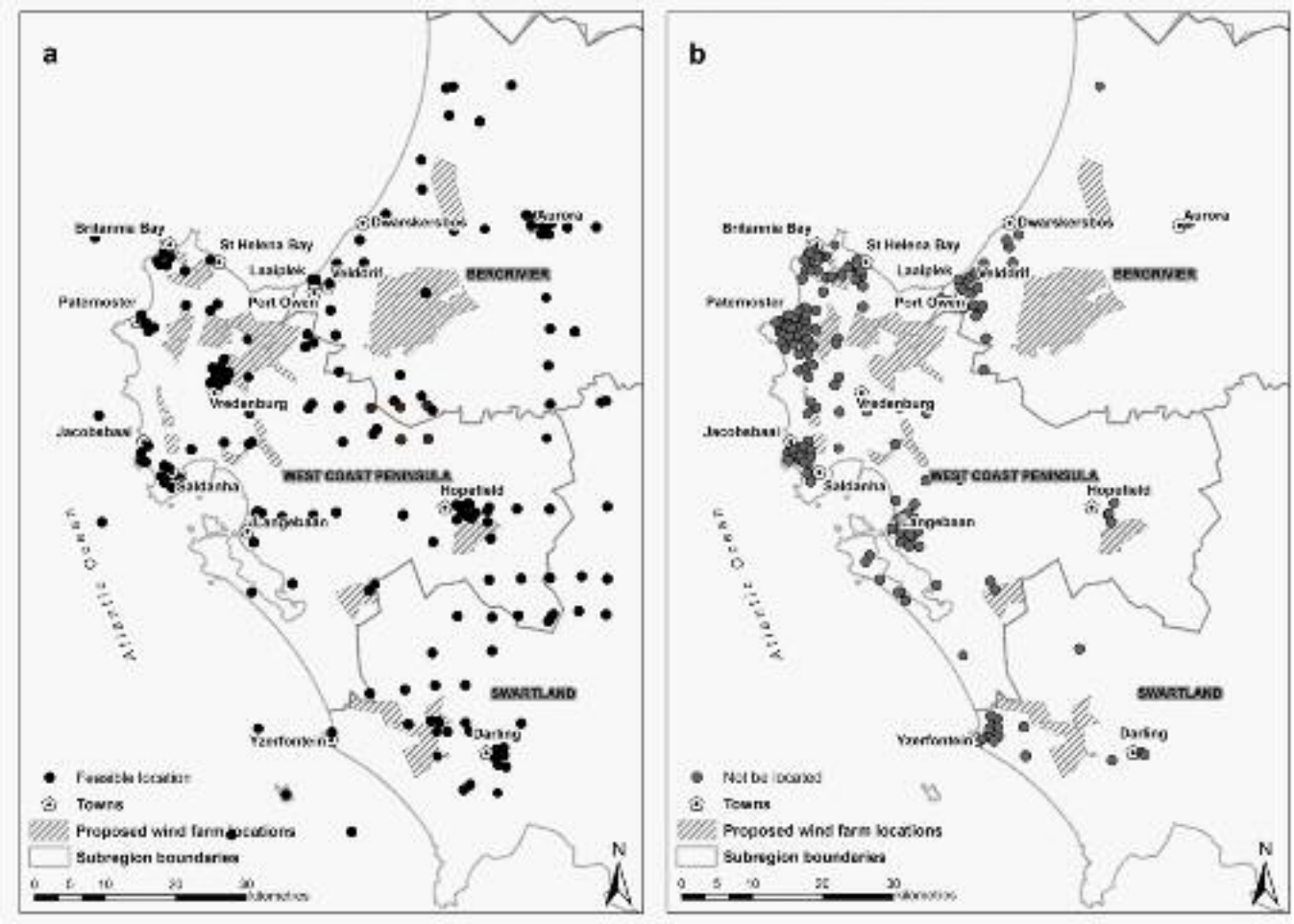

Figure 6: Respondents' view on the location of wind farms: (a) Where wind farms should be located; (b) Where wind farms should not be located

Source: Author 2012

discontent with the chosen locality of the proposed wind farm project in their immediate vicinity. During the group's meeting on 19 December 2011 their consternation became patently clear that the marginalized community of Paternoster had not been informed nor involved during the environmental impact assessment (EIA) process of the particular project. Only the literate members of the community have the opportunity to actively involve themselves in the proposed projects because the newspaper advertisements and information documents in the library are largely inaccessible to less literate citizens. The action group expressed the need for the developers and consultants to verbally and personally inform the marginalized groups about the meetings. PGIS also presents an opportunity for illiterates to take place in spatial planning processes. In St Helena Bay and Britannia Bay, residents believe that the wind farm project will benefit the community as a whole, although they do raise concerns, but to a lesser degree than the case with the Paternoster wind farm which has already been approved for construction. Heather-Clark (2011), of Environmental Resources Management (ERM), reiterated it during a meeting of the West Coast Business Chamber that there is no 'yes' or 'no' answer to whether wind energy is the solution for the WCR, but emphasized that exploration of the issues associated with the proposed developments must be done to establish the most appropriate locations from both developer and community perspectives. The positives of any location must exceed the negatives.

5. Conclusion

From the international literature it became evident that wind farm developments can influence the physical landscape mainly in two ways, namely impacting on the aesthetics of the landscape as well as diversifying the land use practiced. The visual intrusion is considered the most concerning impact of wind farm projects. However, the respondents of this study do not find the visual impact to be significantly concerning.

Seventy per cent of all respondents support the development of wind farms in the WCR in spite of regarding the landscape as very special. It became imperative throughout the study that a visual impact assessment is simply not enough to establish the impact of wind farms on natural landscapes, especially considering that the visual impact does not play a role in this region. Investigation of the sensitivity, value and character of the landscape can be enhanced using a participatory planning approach such as PGIS. This study mainly focused on landscape values to indicate the valuable contribution of a grassroots mapping exercise.

References

ArcGIS Desktop. (2011). *ArcGIS Desktop 10*. ArcGIS Inc. Online Help. Online. http://help.arcgis.com/en/arcgisdesktop/10.0/help/index.html#//005p00000010000000. (Accessed 10 June 2012).

Brown, G. and Raymond, C. (2007). The relationship between place attachment and landscape values: Toward mapping place attachment. *Applied Geography.* 27: 89-111.

Brusa, A. and Lanfranconi, C. (2006). Guidelines for realization of wind plants and their integration in the territory. Paper delivered at the EWEC 2006, Milano.

Cary, M. (2012). Energy efficiency and renewable energy resources. *Energize.* April, 3.

Clohessy, C.M., Brettenny, W., Sharp, G. and Vorster, F. (2014) Evaluation of noise levels of two micro-wind turbines using a randomised experiment. *Journal of Energy Southern Africa*. 25(1): 19-25.

Diab, R.D. (1995). *Wind atlas of South Africa*. Pretoria: Department of Mineral and Energy Affairs.

Dunn, C.E. (2007). Participatory GIS – a people's GIS? *Progress in Human Geography*. 31: 616-637.

European Wind Energy Association (EWEA). (2010). *Wind energy: The facts*. 2nd ed. London: Earthscan.

Heather-Clark, S. (2011). Wind energy: The good, the bad and the ugly. Paper delivered at meeting of the West Coast Business Chamber on 28 July, Saldanha.

Hecklau, J. (2005). Visual characteristics of wind turbines. Proceedings of the NWCC Technical Considerations in siting wind developments. Online. http://www.nationalwind.org/assets/siting/proceedings.pdf. (Accessed 2 September 2012).

Henningsson, M., Jönsson, S., Ryberg, J.B., Bluhm, G., Bolin, K., Bodén, B., Ek, K., Hammarlund, K., Hannukka, I., Johansson, C., Mels, S., Mels, T., Nilsson, M., Skärbäck, E., Söderholm, P., Waldo, A., Widerström, I. and Åkerman, N. (2013). The effects of wind power on human interests: A synthesis. Swedish Environmental Protection Agency, Report 6545. January 2013. Online. http://www.naturvardsverket.se/Documents/publikationer6400/978-91-620-6545-4.pdf. (Accessed 5 June 2013).

Inglesi, R. (2010). Aggregate electricity demand in South Africa: Conditional forecasts to 2030. *Applied Energy*. 87: 197-204.

Katsaprakakis, D.A. (2012). A review of the environmental and human impacts from wind parks: A case study for the Prefecture of Lasithi, Crete. *Renewable and Sustainable Energy Reviews*. 16: 2850-2863.

Lobley, M. and Winter, M. (2009). Introduction: Knowing the land. In Winter, M. and Lobley, M. (eds). *What is land for? The food, fuel and climate change debate*. 1-20. London: Earthscan.

Lombard, A. (2010). Feasibility of wind farms in the Western Cape. Honours research report. Stellenbosch: Stellenbosch University, Department of Geography and Environmental Studies.

Lombard, A. (2013). Wind energy landscapes, place attachment and tourism in the Route 27/West Coast region of South Africa. Master's thesis. Stellenbosch University, Department of Geography and

Environmental Studies, Stellenbosch.
Longley, P.A., Goodchild, M.F., Maguire, D.J. and Rhind, D.W. (2005). *Geographic information systems and science*. 2nd ed. Chicester: John Wiley & Sons, Ltd.
Lothian, A. (2008). Scenic perceptions of the Visual Effects of Wind Farms on South Australian Landscapes. *Geographical Research*. 46(2): 196-207.
Loubser, K. (2011). Boere versprei risiko met windplase. *Weslander*. 8 September: 17.
Manwell, J.F., McGowan, J.G. and Rogers, A.L. (2002). *Wind energy: Theory, design and application*. Chichester: Wiley.
Pasqualetti, M.J. (2000). Morality, space, and the power of wind energy landscapes. *Geographical Review*. 90: 381-394.
Pasqualetti, M.J. (2001). Living with wind power in a hostile landscape. In Pasqualetti, M.J., Gipe, P. and Righter, R.W. (eds). *Wind power in view: Energy landscapes in a crowded world*. 153-172. San Diego: Academic Press.
Pasqualetti, M.J. (2011). Social barriers to renewable energy landscapes. *The Geographical Review*. 101: 201-223.
Stanton, C. (2005). Visual impacts: UK and European perspectives. Proceedings of the NWCC Technical Considerations in siting wind developments. Online. http://www.nationalwind.org/assets/siting/proceedings.pdf. (Accessed 2 September 2012).
The Economist. (2008). The dark ages: South Africa's power crisis is having wider repercussions. Online. http://www.economist.com/node/10609230. (Accessed 30 May 2013).
Valentine G. (1997). 'Tell me about…': Using interviews as a research methodology. In Flowerdew R & Martin D (eds) Methods in human geography: A guide for students doing a research project, 110-126. Edinburgh Gate: Addison Wesley Longman.
Van de Wardt, J.W. and Staats, H. (1988). *Landschappen met windturbines*. Leiden: University of Leiden.
West Coast District Municipality. (2012). Integrated Development Plan 2012-2016 Online. http://westcoastdm.co.za/wp-content/uploads/2012/06/WCDM-IDP-2012-16-Final-Approved1.pdf. (Accessed 20 July 2012).
Wolsink, M. (2007). Planning of renewables schemes: Deliberative and fair decision-making on landscape issues instead of reproachful accusations of non-cooperation. *Energy Policy*. 35: 2692-2704.
Wolsink, M. (2012). Wind power: Basic challenge concerning social acceptance. In: Meyers, R.A., (Ed) *Encyclopaedia of Sustainability Science and Technology,* SpringerReference. 17: 12218-12254.

Received 21 May 2014; revised 17 March 2015

The optical design and performance of a concentrator photovoltaic module

Ross Dane Schultz

Ernest E van Dyk

Frederik J Vorster

Centre for Energy Research, Department of Physics, Nelson Mandela Metropolitan University, Port Elizabeth, South Africa

Abstract

Concentration photovoltaic (CPV) modules promise a more efficient, higher power output than traditional photovoltaic modules. This is achieved by concentrating sunlight onto a small 1 cm2 concentrator triple-junction (CTJ) InGaP/InGaAs/Ge cell by using high quality precision optics. In order to achieve high energy performance and reliability, well thought-out design decisions must be made in the development of a CPV module. This paper investigates the design of two CPV modules (Module I and II), which are based on the Sandia III Baseline Fresnel module. The investigation concentrated on the effect of the optimization of the optical design on the electrical performance characteristics of CTJ cells with good thermal dissipation. The best performance achieved by Module I was at 336 times operational concentration (Xo), which produced a Pmax of 10.29 W per cell, with cell and module efficiencies of 39% and 24%, respectively. In the development of the second module (Module II) pre-deployment criteria such as the CTJ cell and system components characteristics was used to eliminate faulty components from the system what was observed in Module I. Cell units that were optimized in Module II showed no form of degradation in their Current-Voltage (I-V) characteristics. The cell unit operating under optical misalignment showed a progressive degradation with long term operation in the field.

Keywords: concentrator photovoltaics, concentrated triple junction cells, efficiency, degradation.

1. Introduction

Concentrator photovoltaic (CPV) systems offer a cost effective alternative to flat plate photovoltaics (PV) to address the power challenge faced by nations (Hegedus & Luque, 2002; Cotal *et al*., 2009; Kost *et al.,* 2014).. A report by IMS Research states that advances in CPV technology could drive down costs by 16% annually, which will create an increase in installations globally from 2012's cumulative total of around 160 MW to 3 GW by 2016. Based on these figures, a projection of 0.14US$/kWh for 2015 was made (Kost *et al.,* 2014). This may be a cost effective technology to deploy to meet the 3 725 MW goal as set in the Integrated Resource Plan (IRP) (Chong & Siav, 2008).

This is achieved by replacing the standard flat-plate PV silicon cells with smaller, highly efficient III-V multi-junction cells (MJC) (Hegedus & Luque, 2002). The remainder of the module comprises of relatively cheap optical elements such as lenses and mirrors, which collect, concentrate and evenly distribute the direct incident solar flux onto the CTJ cell. These CPV systems are present today in South Africa and are operational at Touwsrivier and showcased at Megawatt Park by Soitec Solar. As from 25 March 2014, 22 MW of the planned 44 MW has been installed and operational at Touwsrivier (Chong & Siav, 2008).

This paper addresses some crucial design considerations needed to manufacture an operational, field-ready CPV module. The first module (Module I) was based on the Sandia III Baseline Fresnel module design (Hegedus & Luque, 2002), which utilizes a Fresnel lens as the primary concentrating optical element to concentrate incident light and a truncated reflector lens as the secondary optical element to distribute the concentrated light evenly

onto a concentrator triple-junction (CTJ) InGaP/InGaAs/Ge cell. Performance parameters were measured, and the findings obtained from Module I were used as an evolutionary step to improve the design of Module II. Module II was a new design using separate cell units, which were interconnected to form the module. This design facilitated experimentation and easy unit replacement, without decommissioning the entire module. The Module cell units that were tested under optimal design conditions showed no form of degradation after 228 sun-hours of operation under concentration, while degradation was seen in non-optimised units.

2. Theory

2.1. Concentrating sunlight

Concentration factor

In the CPV systems that were used in this study, parallel light rays from the direct normal solar irradiance (DNI) that are incident onto a primary optical element are concentrated on a secondary optical element. The secondary element distributes the intensity and spectral content of the concentrated light homogeneously across the area of the CPV receiver (CTJ) as illustrated in Figure1.

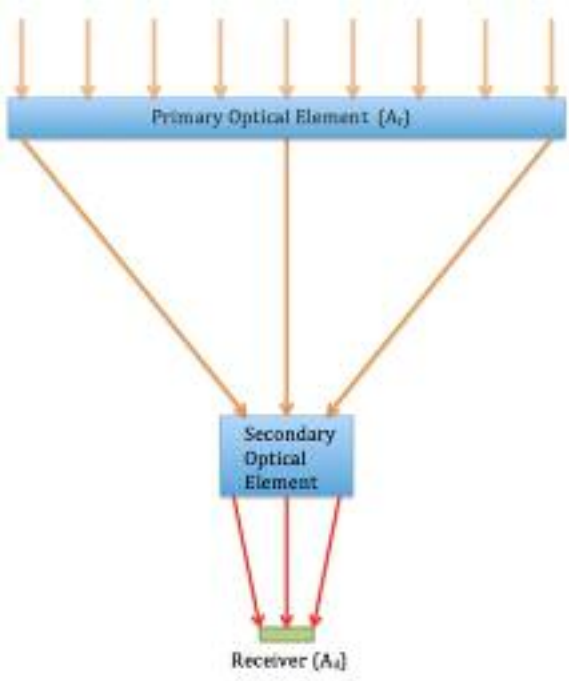

Figure 1: Schematic illustration showing the basic operation of a CPV module

The increased photon flux on the CTJ results in increased photocurrent density and hence, will lead to an increased power output from the CTJ (Kost *et al*., 2014; Chong & Siaw, 2008; Rumyantsevm *et al.,* 1997).

CPV systems are classified according to concentration ratio. The geometric concentration ratio (X_g) that is sometimes used is defined as:

$$X_g = \frac{A_r}{A_d} \quad (1)$$

Where A_r is the primary lens area and A_d is the MJC cell aperture area. This does not account for any optical, thermal and electrical losses. In this work we used the operational concentration (X_o), which takes the optical losses into account. X_o is the ratio of the concentrated irradiance in the device plane after optical losses (Ir_x) and the DNI non-concentrated irradiance (Ir_1) incident on the primary lens.

X_o is defined as:

$$X_o = \frac{Ir_x}{Ir_1} \quad (2)$$

Assuming that there is a linear relationship between the irradiance (Ir) and short circuit current of the CTJ cell ($_{Isc}$) under un-concentrated (Ir_1) as well as concentrated irradiance (Ir_x) Rumyantsevm *et al.,* 1997):

$$Ir = F.\ I_{sc} \quad (3)$$

Where the factor F relates the short circuit current (I_{sc1}) to irradiance. Using the linear relationship expressed in Equation 3, the expression for X_o in terms of the concentrated short circuit current (I_{scx}) as seen in Equation 2 may be rewritten as:

$$X_o = \frac{Isc_x}{Isc_1} \quad (4)$$

Equation 4 thus gives an operational concentration factor that takes into account optical and electrical interactions, misalignments and optical performance acting on the CTJ cell.

2.2. Short circuit current density

The short circuit current density J_{sc} produced by a CTJ cell is more complex than that from a single-junction cell as the sub-cells are series-connected. For a single cell, the current density is defined in Equation 5 as:

$$J_{sc} = \int S(\lambda).\Phi_{inc}(\lambda)d\lambda \quad (5)$$

where S is the spectral response and Φ_{inc} is the incident concentrated solar spectrum (Hegedus & Luque, 2002; Kost *et al*., 2014; Kinsey & Edmondson, 2009).

Since the device is series-connected, the overall current generation from the device will be limited to the lowest current generator. Equation 6 shows the current density generated from the CTJ cell under concentration (Hegedus & Luque, 2002):

$$J_{scx} = \mathrm{Min}[\int S(\lambda).\Phi_{inc}(\lambda)d\lambda\ ] \quad (6)$$

2.3. Open circuit voltage

The V_{oc} produced by a CTJ cell is the sum of the V_{oc} contribution for each sub-cell given in Equation 7 (Lorenzo, 1994):

$$V_{ocx} = \sum V_{oci} \quad (7)$$

where V_{ocx} is the open circuit voltage of the CTJ cell and V_{oci} is the individual V_{oc} of each sub-cell (Hegedus & Luque, 2002). The V_{oc} for an individual sub-cell is:

$$V_{oci} = \frac{nkT}{q} \ln\left(\frac{I_{scx}}{I_0}\right) \quad (8)$$

where k is Boltzmann's constant, T the temperature of the CTJ cell, q the elemental charge of an electron, n is the ideality factor and I_0 the saturation current for the semiconductor material. Since the same current passes through the sub-cell, each sub-cell will have the same concentration factor. Therefore, the most basic expression for the V_{ocx} for the CTJ device can be written as (Hegedus & Luque, 2002; Cotal *et al*., 2009):

$$V_{ocx} = V_{oc1} + \frac{nkT}{q} \ln(X_o) \quad (9)$$

where V_{oc1} is the V_{oc} of the CTJ cell at one-sun concentration and X_o is the operational concentration.

2.4. Power, fill factor and efficiency

Defining the power and efficiency is important as these features act as a tool to identify the performance of an H-CPV module.

2.4.1 Efficiency

The efficiency of a CTJ cell and HCPV module can be defined as:

- cell efficiency (η_c)

$$\eta_c = \frac{P_{out}}{P_{in}} \times 100 = \frac{V_{c(max)} I_{c(max)}}{X_o \, Ir_d A} \times 100 \quad (12)$$

where Ir_d is the direct normal irradiance and A is the area of the cell (Hegedus & Luque, 2002; Cotal *et al*., 2009).

- module efficiency (η_m).

$$\eta_m = \frac{P_{out}}{P_{in}} \times 100 = \frac{V_{m(max)} I_{m(max)}}{Ir_d A_m} \times 100 \quad (13)$$

where Ir_d is the direct normal irradiance and A_m is the area of the module (Ventre & Messenger, 2005; Vorster, 2001).

2.5. Sun-hours

The number of peak sun-hours is numerically identical to the average daily solar insolation for the location. Hence, the number of sun-hours available to a PV system is defined as the ratio of the total energy available for the monitoring period (typically a day) to 1 kW.m^{-2} as shown in Equation 14:

$$\text{Sunhours} = \sum_1^n t \times \frac{(Ir_n + Ir_{n+1})}{2 \times 1 kW.m^{-2}} \quad (14)$$

where $I\,r_n$ and $I\,r_{n+1}$ are the consecutive irradiance measurements for the monitoring period and t is the measurement time interval, measured in hours (Hegedus & Luque, 2002; Lorenzo, 1994).

2.6. CPV optical systems

One of the most important parts of the operation of CPV systems is the optical configuration and the precision and quality of the optical elements (Hegedus & Luque, 2002;; Rumyantsevm *et al.,* 1997; Schultz *et al.,* 2011; Xie *et al*., 2011). To achieve maximum energy yield, the optical elements need to transmit (in the case of refractive optics) or reflect (in the case of reflective optics) as much sunlight as possible in the wavelength range that is influenced by the quantum efficiency of the CTJ cell.

2.6.1. Primary Fresnel optics

A Fresnel lens is a light, thin, relatively flat lens used to concentrate incident sunlight by making use of concentric reflective or refractive facets known as Fresnel zones (Hegedus & Luque, 2002; Kwangsun Ryu (2006); Leutz & Rhodes, 2001). Refractive Fresnel lenses are usually made out of an acrylic, Poly(methyl methacrylate) (PMMA) or polycarbonate materials and are manufactured by compression moulding (Leutz & Rhodes, 2001). This allows for the manufacturing of single and parquet lenses in any shape or size.

2.6.2. Secondary optics

The main function of the secondary optical elements is to increase the acceptance angle to capture more concentrated and stray light from the primary optical element and to distribute the concentrated solar flux uniformly across the device's surface. Reflective secondary elements utilise mirrors in the form of highly reflective aluminium sheeting (Alanod material properties) with reflectance of 95% to reflect the concentrated incident solar light towards the cell's surface. Refractive secondary elements utilise specially shaped refractive material that refracts the light onto the cell's surface. The refractive secondary element is usually in optical contact with the cell's surface in order to transfer as much light as possible to the cell, reducing any loss that would result from spillage from the sides of the interface.

2.7. Multi-junction cells

Multi-junction cells offer a better absorption of photon energy from a wider spectral range than conventional PV cells do (Hegedus & Luque, 2002; Rumyantsevm *et al.,* 1997). The use of doped silicon as a semiconductor material only utilises a small fraction of the solar spectrum limited by the band gap of the material. To increase the performance and power output of a CPV cell, a multi-junction device is created to allow for more absorption from the solar spectrum. This is achieved by creating a device structure, which utilises vertically stacked multiple sub-cells connected in series (Vincenzo Fracastoro *et al.,* (2009). The sub-cells are made from materials that have quantum efficiency profiles that span the solar spectrum range from 300 nm to 1800 nm. This allows for a much larger portion of the solar spectrum to be absorbed, resulting in a higher performance (Hegedus & Luque, 2002; (Hegedus & Luque, 2002; Vincenzo Fracastoro *et al.,* (2009); Ventre & Messenger, 2005). Figure 2 shows the schematic of three material layers and their relative band gap energies in the multi-junction cell used in the study.

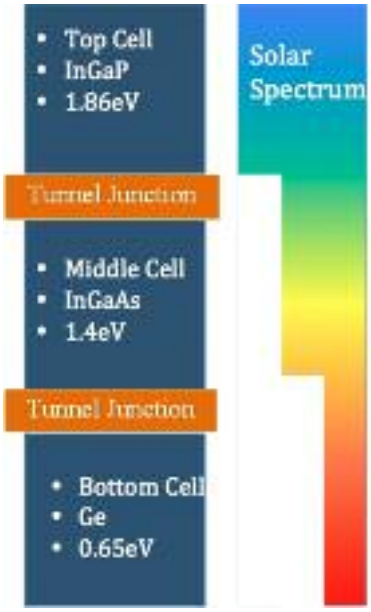

Figure 2: Schematic representation of the band gap energies of the materials used in a CTJ device

The cell assembly used in this study consists of a 1 cm^2 triple-junction InGaP/InGaAs/Ge semiconductor material, two bypass diodes and connection terminals mounted on a 6.78 cm^2 gold and ceramic base (Emcore datasheet). The InGaP/InGaAs/Ge active layers are monolithically integrated and lattice matched to the Ge substrate. The 3 p-n junctions are connected in series via tunnel junctions (Hegedus & Luque, 2002). Figure 3 shows a schematic diagram of the CTJ cell assembly used in the study.

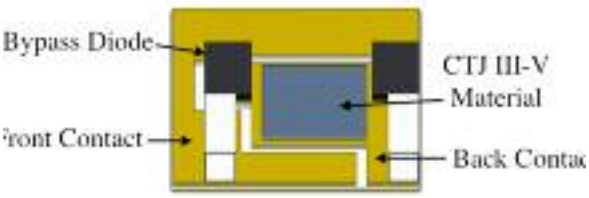

Figure 3: The schematic drawing of the CTJ receiver assembly cell used in the development of the prototype modules

Source: Vincenzo Fracastoro et al. (2009)

The CTJ cell consists of 3 p-n junctions with spectral responses ranging from 300 nm – 1800 nm. Bypass diodes allow for current to bypass the cell in the case of cell mismatch occurring in a CPV module.

3. CPV module design

An initial design was used to construct a prototype (Module I) and it was fully characterized with respect to the optics and electrical performance. The results obtained in this investigation were used to improve on the design of a second prototype (Module II), which was then constructed and evaluated.

3.1. Module I

Figure 4 shows (a) the schematic and (b) photograph of the experimental CPV module (Module I) developed in the study. As illustrated in Figure 4, the physical structure of the experimental CPV module was based on the Sandia III Baseline Fresnel Module (Xie *et al.,* 2011) because of its simplistic and compact design. The main structure of the experimental CPV module was made from aluminium, which supports a 2x4 Fresnel lens parquet array and 8 assembled CTJ cells attached to secondaries and heatsinks. Concentrating sunlight onto an area using a Fresnel lens without incorporating some form of secondary optical element will result in the formation of a non-uniform illumination intensity distribution across the CTJ's cell surface. This could result in the formation of hot spots, which may lead to low power production, cell damage and premature failure of the cell (Hegedus & Luque, 2002; Kwangsun et al., 2006; Leutz & Rhodes, 2001).

A truncated pyramid reflective secondary optical element was used for Module I. The secondary was constructed out of 4 pieces of highly polished mirrored aluminium sheeting (Alanod 95% (Leutz & Rhodes, 2001). forming the sides of the truncated pyramid with a square base. To determine the secondary element's dimensions, the focal length of the Fresnel lens and the general shape of the reflective secondary must be considered. The dimensions and angles for the reflective secondary were determined by using a ray-tracing program (IME

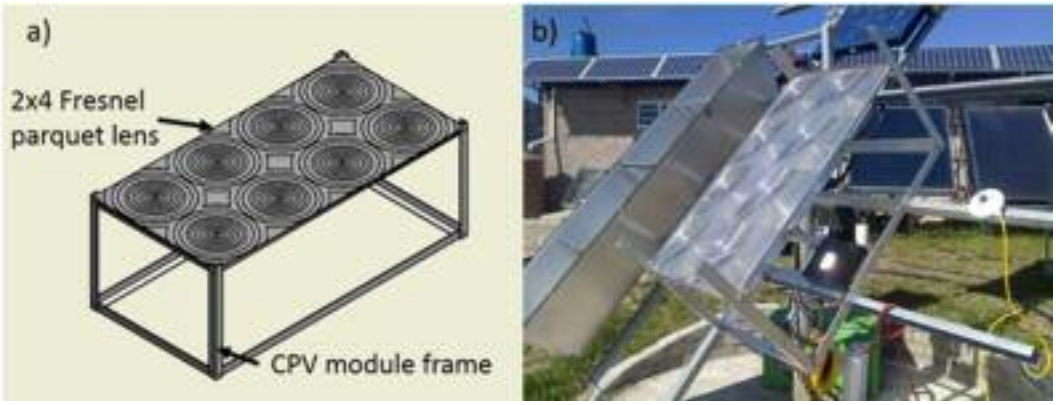

Figure 4: (a) A schematic and (b) photograph of the experimental Module I developed in the study

Raytrace software). A schematic diagram of the reflective truncated secondary used in Module I is shown in Figure 5.

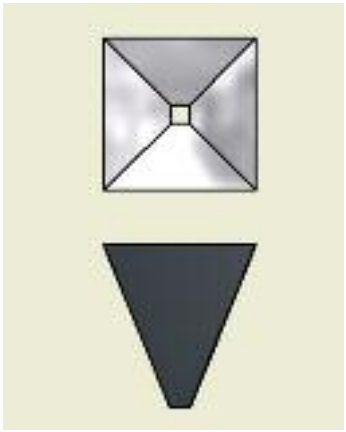

Figure 5: Schematic drawing of the reflective truncated secondary used in Module I

Using ray-tracing, a distance of 23.4 cm was found to be the optimal distance that allowed a 1 cm^2 area of the CTJ cell to be illuminated, while at the same time, showing minimal effect from lens aberrations.

3.2. Module II

To reduce the shortcomings observed in Module I, a new experimental CPV module (Module II) was designed. The new modular design comprised of a unit that contained a Fresnel lens, refractive secondary, heatsink and CTJ cell. These individual units were designed to eliminate the need to disassemble the whole module in the case of a single cell failure and to facilitate experimentation. Additionally, the size of the module is not restricted to the number of Fresnel lenses that are available in the parquet array.

Figure 6 shows the schematic diagram of each cell unit. The cell unit comprised of a single PMMA Fresnel lens, which acts as the primary optical element.

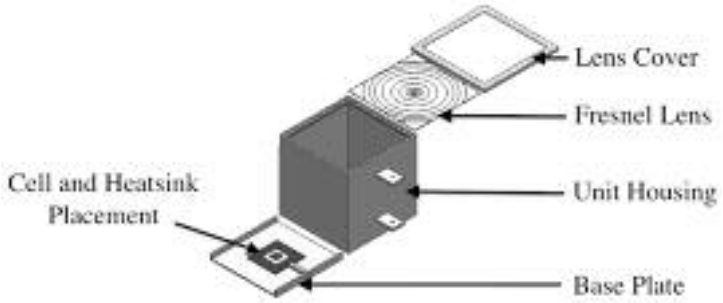

Figure 6: The schematic diagrams of a cell unit used in Module II

The use of a single lens reduced the effects of lens warp and deformation experienced by a larger parquet lens due to wind jarring and tracker movement (Leutz & Rhodes, 2001). Additionally, this is an easier and cheaper way to replace a single lens than a parquet lens, if damaged.

The box shaped housing of each unit was made from 0.6 mm galvanized steel that was folded to form a box. The box isolated the internal components of the CPV module from the environment. It also acted as a rigid platform for the mounting of the Fresnel lens and base plate. The housing has fixtures on the side of the box to allow for mounting to the module frame. A heatsink and the CTJ cell with refractive secondary are attached to the baseplate as shown in Figure 6.

Figure 7 shows a schematic drawing of the refractive secondary lens used in Module II. The lens consists of a piece of moulded glass, which is circular in shape with an optical aperture of 8.85 cm^2. The circular aperture is shaped down along the sides to form a tapered square with a cell aperture area of 1 cm^2 at the base. The refractive secondary is optically coupled to the cell, eliminating soiling of the cell from the environment and reducing the amount of maintenance needed. Figure 8 shows the schematic diagram of the improved CPV module, which comprised of an assembly of 8 of the cell units attached to a support frame.

The cell units were connected electrically in

Figure 7: Schematic diagram of the moulded refractive secondary

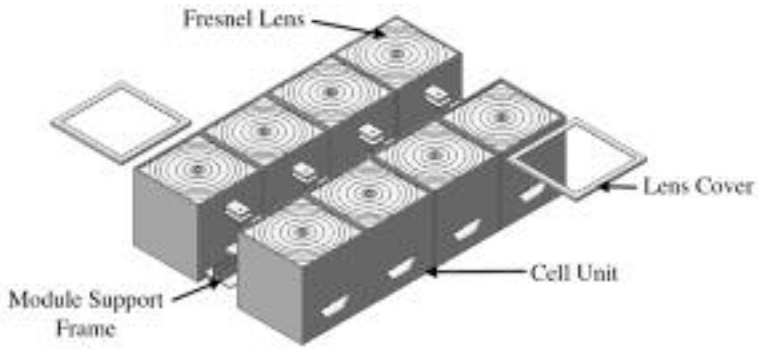

Figure 8: The schematic diagram of the improved CPV module (Module II) with its individual cell units

series for the time of operation. Table 1 shows the summary of the components and operational concentration factors for the two prototype modules.

4. Experimental procedure

4.1. Module I

On the completion of the design and fabrication of Module I, the electrical characteristics of the CTJ cells where determined, this included:

- An investigation of the effect of the variation in concentration on the performance of power conducted on a cell level. This was achieved by the variation of the Fresnel lens's focal length relative to the cell and obtaining corresponding I-V curves. The information extracted from the I-V measurements provided the current, power and efficiency of the CTJ cell. Plotting the concentration factor as defined in Equation 4 versus efficiency, the effect of concentration could be identified.
- An investigation of the effect of optical misalignment on the performance of an individual CTJ cell and a series connected 2 cell module. The investigation included the comparison of I-V measurements of an optically aligned cell unit to a cell unit where the reflective secondary was purposely misaligned. I-V measurements of a series-connected optically aligned cell units were compared to the later configuration where one of the cell unit's reflective secondary was purposely misaligned; and
- Long-term monitoring for individual CTJ cells. The monitoring included the comparison of I-V measurements taken weekly for 2 month period.

4.2. Module II

Based on the outcomes and shortfalls experienced in Module I, Module II was designed to improve the performance of CTJ cells under operation. The experiment performed with Module II included long-term monitoring of different cell units within Module II, operating under 2 specific optical conditions (modes). These are:

- An optimal configuration of the optics where the cell unit is optically aligned for optimal performance from the cell unit. This was conducted under operation with sufficient thermal management; and
- An intentional optical misalignment of both the primary and secondary optics of the cell unit. This was conducted under operation with sufficient thermal management.

I-V measurements of each cell unit were taken at periodic intervals of approximately 30 sun-hours for a duration of two and a half months with a total operation of 228 sun-hours. I-V measurements were normalized with respect to the short circuit current and open circuit voltage. This allowed for a visual representation of the decrease in performance (if any) of the cell unit over time.

5. Results

5.1. Module I

i) The effect of concentration

The results that follow show the effect of solar concentration on the performance of a CTJ cell. In

Table 1: A summary of the components and operational concentration factors for Module I and II

Parameter	*Module I*	*Module II*
Maximum X_o	336	225
Primary Optical Element	3M Fresnel Lens in a 2x4 parquet array	Basic PMMA single Fresnel lens
Secondary Optical Element	Reflective, aluminium, truncated pyramid	Refractive, low iron glass, moulded pyramid
CTJ Receiver	Emcore CTJ cell (InGaP/InGaAs/Ge)	Emcore CTJ cell (InGaP/InGaAs/Ge)

Figures 9 and 10, the one-sun and 336 X_o I-V characteristic curves for a CTJ cell are shown.

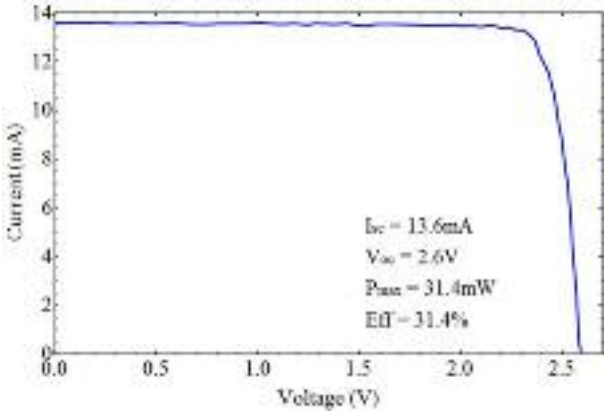

Figure 9: The normalized I-V curve with respect to irradiance and temperature of a CTJ cell at 1 X_o concentrations

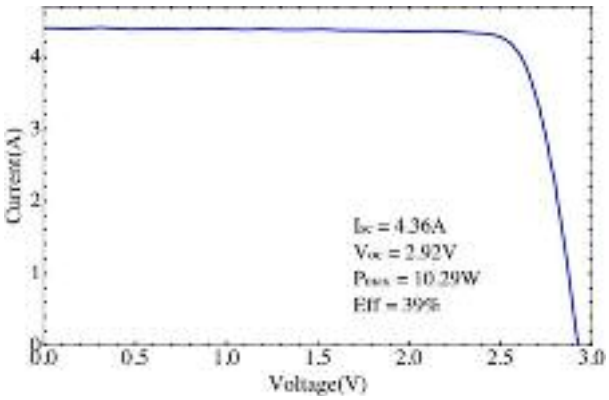

Figure 10: I-V curve of an operational CTJ cell at 336 X_o concentrations

The performance parameters at one-sun and under concentration, together with those at 124 X_o, are listed in Table 2.

Table 2: The effect of the increase operational concentration on I-V parameters of a CTJ cell

	1X_o concentration	*124 X_o concentration*	*336 X_o concentration*
Efficiency	31.4%	37.7%	39%
V_{oc}	2.58V	2.76V	2.92 V
I_{sc}	13.85mA	1.612A	4.36A
Power	31.4mW	3.62W	10.29W

Under concentration, as observed in Figures 9 and 10, the I_{sc} is increased by a factor of 336 X_o and the V_{oc} is increased from 2.58 V to 2.92 V. The increase in I_{sc} is due to the increase in incident irradiance on the 1 cm^2 CTJ device resulting from the concentration of sunlight by the optics. This is evident from Equation 5 as the I_{sc} and Φ_{inc} are directly related. Since the I_{sc} is directly proportional to the concentrated incident irradiance, it will increase linearly with concentration (Hegedus. & Luque, 2002; Cotal *et al.,* 2009; Chong & Siaw, 2008). The logarithmic increase observed in the V_{oc} is due the increased in I_{sc} with increasing irradiance (Cotal et al., 2009; Kinsey et al., 2009). The V_{oc} increases slowly (logarithmically) with increasing photo-current if dark current remains constant at the cell operating temperature. Hence, a CTJ cell at a concentration of 336 X_o will see an increase in V_{oc} of tens of kT/q at a constant operating temperature (refer Equation 9).

Hence, the quality of the optics to concentrate sunlight will affect the increase in the I_{sc} and V_{oc}. For Module I, the results showed an increase in the power output from 31 mW to 10.29 W, 343 times greater than at one-sun. The efficiency increases from 31 % to 39 %. Figure 11 shows the CTJ cell's efficiency as a function of increasing concentration.

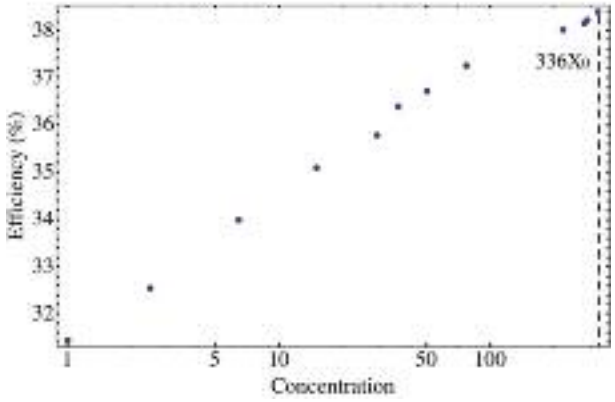

Figure 11: The increase in efficiency of a CTJ cell with the increase in concentration

From Figure 11, it is observed that the efficiency increases linearly with concentration. The increase in the efficiency is attributed to the combined effect of the increase in both the I_{sc} and V_{oc} due to concentration, with the latter being the primary contributor. From Equation 12, it can be approximated that the $I_{max} = X_o.I_{sc}$. Substituting for I_{max}, one can readily see that the X_o cancel and the only contributing factor to the increase in efficiency is the $V_{max.}$ As explained above, the V_{max} increases with the logarithmic increase in V_{oc}, due to the increase in I_{sc} with irradiance.

ii) Long-term measurements.

In order to assess the reliability and performance of Module I, the performance of single cells within the module were monitored over a 2 month period. Figure 12 shows the initial I-V characteristics, under concentration, of 2 individual cells in an optically aligned system before and after (shown with*) the 2-month operational period. Table 3 summarizes the parameters of the CTJ cells before and after an operational period.

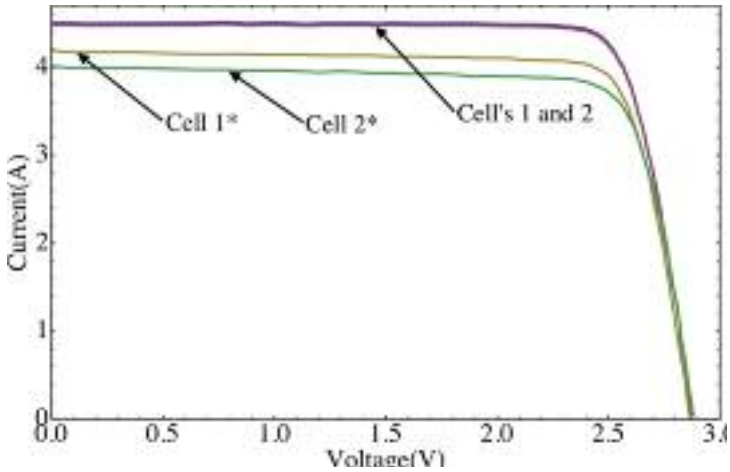

Figure 12: Graphs showing the CTJ cell I-V curves of Module I before and after a period of 2 months in operation

Table 3: The difference in the device parameters of 2 CTJ cells after 2 months of operation

Parameter	*Before*	*After*	*Before*	*After*
	Cell 1	*Cell 1**	*Cell 2*	*Cell 2**
Current (A)	4.43	4.21	4.43	4.05
Voltage (V)	2.82	2.92	2.82	2.88
Power (W)	10.02	9.10	10.02	8.98

As observed in Figure 12, the performance of cells 1 and 2 are identical at the start of the monitoring period. However, after 2 months of operation, there was a decrease in performance of both cells. The decrease observed in the performance parameters of both cells, I_{sc} and P_{max}, was attributed to possible soiling of the reflective secondary and/or cell damage. Upon removing the visible soiling from the reflective secondary and cell surfaces, the cause of the reduction of the performance parameters was established by comparing I-V characteristics measured at one-sun and at concentration before and after the monitoring period. Cell 1 showed no signs of any reduction in P_{max}, but cell 2 was reduced by 1.7 mW (6%) at one-sun. Figure 13 shows the I-V characteristics of cell 2 before and after the evaluation period.

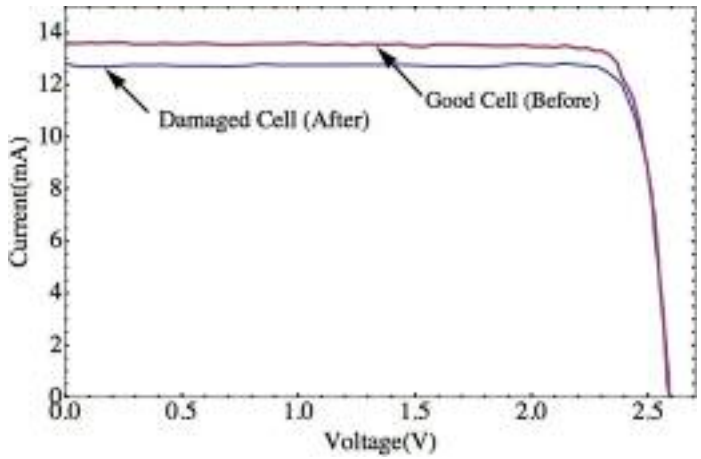

Figure 13: Graph showing the decrease in the I-V curve of cell 2 due to cell damage

The decrease in P_{max} observed for cell 1* as seen in Figure 12 must therefore be due to soiling of the optical system and cell itself. The Fresnel lens and the reflective secondary were, indeed, soiled, and the cell also had noticeable soiling. This leads to a decrease of almost 10% in power from the cell. Hence, it would be beneficial to the performance if one can eliminate the effect of soiling on the optics and cells. This will also contribute to low maintenance of the module.

The reduction in the performance parameters of cell 2 is due to the combination of soiling and noted cell damage. The cell damage may be due to deflects induced by unintentional misalignment in the optical system. The effect of the misalignment will result in the formation of non-uniformities or a localized, high intensity region. This region will thus cause that part of the CTJ cell to operate 'harder' than the rest of the cell. Depending on the degree of misalignment, the concentrated beam my create hotspots which may result in damage of the cell. This misalignment may in turn cause current mismatch within the cell that may induce material damage.

iii) Optical misalignment

Figure 14 shows the effect of optical misalignment on the I-V characteristics and power production of a CTJ cell. The difference in the I-V curves results from a shift of the intensity distribution from being symmetrical to being less symmetrical across the cell (Vorster, 2001).

Figure 15 shows the illumination distribution across the cell for the a) aligned and b) misaligned optical configuration. Although the magnitude of the maximum relative intensities is very similar, the photo-generated current produced is much less when the intensity distribution is less uniform. It appears that a less symmetrical distribution causes the shunt slope of the I-V curve to increase.

Efficiencies of 36.8 % and 35.2 % were achieved for the aligned and misaligned secondary setup, respectively. The decrease in V_{oc} observed from the misaligned setup is due to the logarithmic dependence of the output voltage on the effective concentration as a function of the I_{sc}. Hence, due to misalignment, the overall photon flux onto the CTJ receiver is much less, resulting in a decreased I_{sc} and V_{oc}. This would lead to a much lower P_{max} and thus a reduced efficiency (Schultz *et al.,* 2011; Luque & Sala, 1998).

The above result is made even more apparent when compared to that of a two-cell test series connected module with bypass diodes. Figure 16 shows

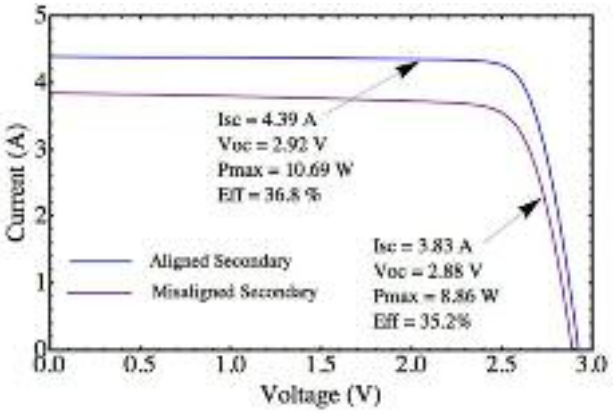

Figure 14: I-V characteristics of the effects of misalignment reflective secondary on a CTJ cell

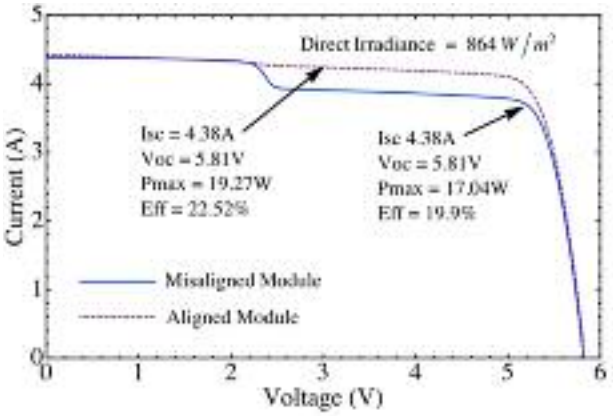

Figure 16: I-V characteristics of Module I showing the effect of misalignment on a 2-cell CPV module

the I-V characteristics of the test module under the best conditions and with intentional misalignment of one reflective secondary.

The effect of current bypassing the cell that produced the lowest short circuit current can be seen as a perturbation in the measured I-V curve indicated by the step. The current mismatch caused a 2.23 W loss, a 13.2 % decrease in the power production relative to the best-aligned module with no misalignment or mismatch. Although this decrease in performance in the 2 cell module does not appear to have a great effect to power production, on a larger modular scale, i.e. a 16 cell series connected module, optical misalignment may affect the performance greatly. Hence, the correlation between the optical alignment and performance of the cell shows that proper optical alignment is important for the optimal functioning of a CPV module.

5.2. Module II

To evaluate the performance of the improved CPV module, I-V characteristics before and after the 2.5 month operational period were compared with a total operation period of 228 sun-hours. Since the performance of the cells within the module were obtained at different irradiance and concentration values, the I-V curves were normalized with respect to I_{sc} and V_{oc} (I/I_{sc} and $V/V_{oc} = 1$).

i) Optimal operation mode of cell unit

Figure 17 shows the normalized I-V characteristics of one cell being operated under optimal conditions before and after the operational period.

It is noticed from the normalized curves that there is little deviation in the shape of the I-V curves from 4 to 228 sun-hours. The small deviation observed from the curve at 4 sun-hours may be attributed to the influence of the optical system, such as soiling of the refractive secondary. Although the operational mode for this cell was to have an optimal optical configuration, the optics may not optimal. There may be areas across the cell that have non-uniform illumination. This non-uniformity distribution of irradiance may cause the shunt slope of the I-V curve to increase due to the effect of localized photo-current mismatch which may

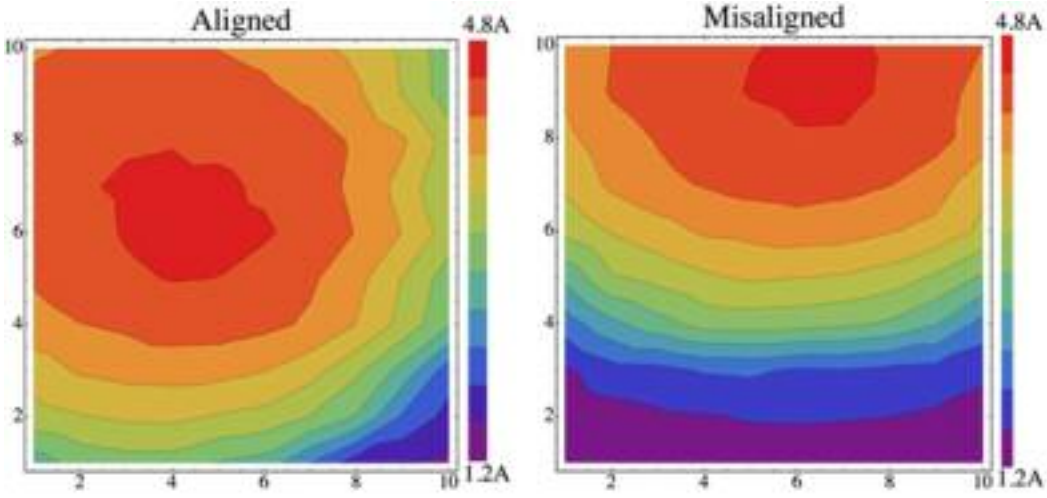

Figure 15: The illumination distribution across the cell for the a) aligned and b) misaligned optical configuration

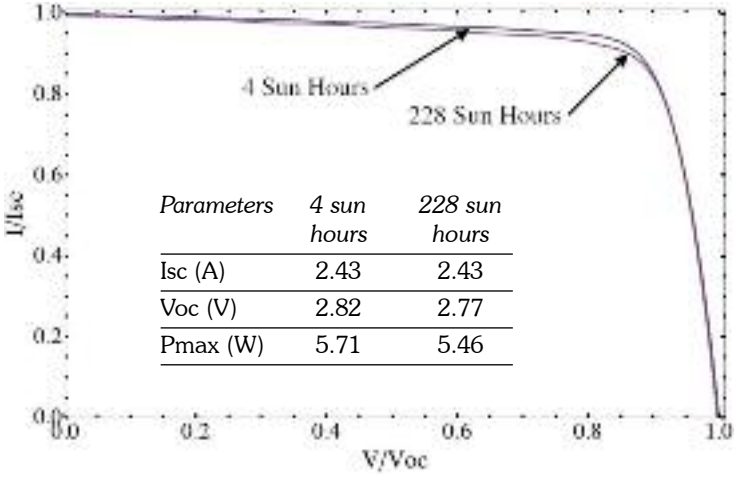

Parameters	*4 sun hours*	*228 sun hours*
Isc (A)	2.43	2.43
Voc (V)	2.82	2.77
Pmax (W)	5.71	5.46

Figure 17: I-V characteristics for a CTJ cell at different sun hours for the optimal unit set up

promote degradation. The table within the graph indicated that there is a small change in the normalized I_{sc} (to 850 $W.m^{-2}$.) This small variation can also be attributed to the optical illumination pattern. As a result of this illumination pattern, certain areas within the CTJ cell may experience a form of cell damage/ or the start of defects within device to occur.

However, a combination of good thermal dissipation and optical alignment has given the best operational module (Vincenzo Fracastoro *et al.,* 2009).

ii) Optical misalignment operation mode of cell unit

Figure 18 shows the normalized I-V characteristics of the optically misaligned cell mode before and after the operational period.

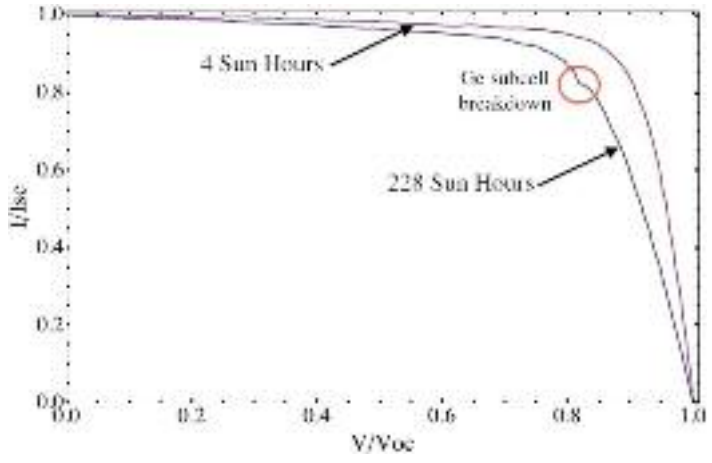

Figure 18: I-V characteristics for a CTJ cell at different sun hours for the optically misaligned unit set up

It is observed from Figure 18 that there is a difference in the shape of the final normalized I-V curve after 228 sun-hours when compared to the one after 4 sun-hours. The decrease in performance before and after the operation period for the misaligned cell is summarized within Figure 18. The optical misalignment may cause the formation or enhancement of defects within the CTJ cell. These defects act as recombination sites that may reduce the current production of the CTJ cell. Coupled with the variation in illumination intensity across the cell surface, there will be a resulting decrease in the shunt resistance.

Additionally, there is a noticeable change in the I-V characteristics with shift of the 'knee' or maximum power point. This observed shift is attributed to a decrease in shunt resistance, possibly caused by induced defects in the CTJ cell resulting from the non-uniform intensity distribution. This decrease will reduce the power production of the CTJ cell with increased irradiance exposure. The kink that is observed is possibly due to the breakdown of one of the sub-cells in the CTJ cell. Since the kink appears at a voltage of 2.42 V on the measured I-V curve after 228 sun-hours and the Ge has the smallest voltage contribution of 0.2 V (Hegedus. & Luque, 2002), it is prDoposed that the Ge sub-cell is undergoing breakdown. If the breakdown occurred in any other sub-cell, the kink would be seen at a $V < V_{max}$ because both the other sub-cells have voltages greater than 1 V. The direct cause of the sub-cell breakdown is not certain. All these effects lead to a power decrease of 13.2%.

It may, therefore, it can be deduced that a CTJ cell operating under some form of optical stress develops defects. It is proposed that these defects are induced from thermal stresses on the device caused by thermal gradients created within the CTJ cell by optical misalignment. Optical misalignment, even with a sufficient heatsink will generate temperature gradient regions within and between the subcell layers. These temperature gradients will have a negative effect on the performance of each sub-cell and CTJ cell.

6. Conclusion

The performance results obtained from Module I and II show that the best configuration for optimal CPV module performance must consist of good optical alignment, which produces a uniform intensity and irradiance pattern. This was confirmed by the I-V characteristics during the operational periods of both experimental modules. Coupled with a sufficient thermal dissipation system, the performance, reliability and longevity of a CTJ cell/ module will be increased significantly if optimally aligned.

However, a CTJ cell operating under optical misalignment showed a progressive decrease in power with prolonged operational exposure in both module systems. This decrease in performance was attributed to the possibility of induced or the enhancements of defects. These defects can act as recombination sites resulting in a lower current production.

In conclusion, to ensure the best design and to achieve the best performance from a CPV module, it is recommended that the characterisation of the whole optical system (the primary and secondary combined) be performed. This characterization will allow one to identify faulty optics so that they may be eliminated from the CPV system and allow for the best CPV modules to be deployed in the field for maximum energy yield. This is important at present as with recent developing technology of the multi-junction cell reaching 44.7% and 37% on a cell and module level, respectively, the power generation of the CPV system may be increased greatly. Additionally, this will allow for reliable systems to be deployed in South Africa to aid in meeting the goals set by government to have continuous uninterrupted power.

References

Alanod material properties, viewed 10 December 2010, http://www.alanod-solar.us/reflection-products.php

Chong K.K & Siaw F.L., (2008). Design and construction of non-imaging planar concentrator for concentrator photovoltaic system, *Renewable Energy,* 34, 1364-1370.

Cotal, C. Fetzer, J. Boisvert, G. Kinsey, R. King, P. Hebert, H. Yoon & N. Karam, (2009).*III*-V multijunction solar cells for concentrating photovoltaics, *Energy & Environmental Science*, 2, 174-192.

Emcore datasheet viewed 23 April 2010, http://www.emcore.com/terrestrial-photovoltaics/terrestrial_solar_cells_and_receivers/.

Hegedus, S. & Luque, A., (2002). Handbook of Photovoltaic Science and Engineering, Wiley.

IME Raytrace software, computer software, viewed 23 March 2010, from http://members.ozemail.com.au/~imesoft/.

Integrated Resource Plan for electricity 2010-2030, viewed 10 November 2014, http://www.energy.gov.za/IRP/irp%20files/IRP2010_2030_Final_Report_20110325.pdf.

Kinsey, G. & Edmondson, K., (2009). Spectral Response and Energy Output of Concentrator Multijunction Solar Cells, *Progress in Photovoltaics*, 17, 279-288.

Kost, C.; Mayer, J.; Thomsen, J.; Hartmann, N.; Senkpiel, C.; Philipps, S.; Nold, S.; Lude, S.; Saad, N.; Schmidt, J. & Schlegl, T. Levelized Cost of Electricity: PV and CPV in Comparison to Other Technologies EU PVSEC 2014, Amsterdam, 2014

Kwangsun Ryu, Jin-Geun Rhee, Kang-Min Park & Jeong Kim, (2006). Concept and design of modular Fresnel lenses for concentration solar PV system, *Solar Energy*, 80, 1580-1587.

Leutz R. & Rhodes, A. (2001). Nonimaging Fresnel Lenses: Design and performance of Solar Concentrators, Springer.

Luque, A. & Sala, G. (1998). Electric and thermal model for non-uniformly illuminated concentration cells, *Solar Energy Materials and Solar Cells*, 51, 269-290.

Lorenzo, E., (1994). Solar Electricity: Engineering of Photovoltaic Systems, Progensa.

Nrel data sheet, viewed 15 June 2012, http://science.gov.tm/projects/soltme/images/database/35_nrel.pdf

Rumyantsevm, V.D., Andreev, V.M. & Grilikhes, V.A., (1997). Photovoltaics Conversion of Concentrated Sunlight, Wiley.

Schultz, R.D., Vorster, F.J. & van Dyk, E.E., **(**2011**).** Performance of multi-junction cells due to illumination distribution across the cell surface, *Physica B.*

Soitec announces full commissioning of 22MWp on Touwsrivier solar plant in South Africa, viewed 15 July 2014, http://www.soitec.com/en/news/press-releases/soitec-announces-full-commissioning-of-22mwp-on-touwsrivier-solar-plant-in-south-africa-1456/.

Ventre, J. & Messenger, R.A., (2005). Photovoltaic Systems Engineering, CRC Press LLC.

Vincenzo Fracastoro, G., Zubi, G. & Bernal-Agustin, J. L, (2009). High concentration photovoltaic systems applying iii-v cells, *Renewable and Sustainable Energy Reviews,* 13:2645–2652.

Vorster, F.J. (2001). On the evaluation of a photovoltaic concentrator system, Master's thesis, department of Physics, Nelson Mandela Metropolitan University

Xie, W.T. Dai, Y.J., Wang, R.Z., & Sumathy, K. (2011). Concentrated solar energy applications using Fresnel lenses: A review, *Renewable and Sustainable Energy Reviews*, 15, 2588-2606.

Received 13 June 2013; revised 3 March 2015

Energy improvement in induction furnace using foaming slag with variation of carbon injection

Theodore Mwata Kipepe

Xiaowei Pan

Department of Extraction Metallurgy, University of Johannesburg, Johannesburg, South Africa

Abstract

Energy efficiency is nowadays one of the biggest concerns worldwide. It has become one of the critical matters to any country and industry particularly in South Africa. Because of the complexities and challenges found in industries and especially in foundry, many strategies have been established to measure and regulate more efficiently the energy. Many studies have been conducted in steelmaking process and electrical arc furnace using foaming slag to reduce energy consumption. As such, in this case study, the experiment will be conducted in a small foundry metal casting laboratory using an Induction Furnace (IF), which will reduce energy usage by using the foaming slag and as well pointing out the importance and the impact of carbon rate change on the foaming creation. After experiments all results show that the melting time can be reduced from 42min to 35 min, which is 20% time saving, the electrical energy consumption also has been reduced from 13.93kWh to 10kWh which is 39.3% saving. On the other hand, the foaming slag optimum height was reached at 1 cm. Therefore, a simple modelling has been designed and calculations have been made on heat transfer at the surface opening of the Induction Furnace and temperature loss has been reduced from 878°C to 870°C, with heat transfer loss reduced from 27.99kW to 26.38kW which was 6.10% of energy saving.

Keywords: energy efficiency, foaming slag, induction furnace, foundry metal casting

1. Introduction

For many years, trying to be energy efficient has become one of the first priorities all over the world. The energy efficiency goal is to reduce the amount of energy required to provide products and services (Wikipedia, 2014). The efficiency benefits can also be gained through environmental improvements.

More than ever, companies are facing increased competitive pressures to produce high quality products at equal or lower cost. With rising energy prices, companies are put under pressure to bring energy costs in line with standards of best practice. The efficiency is applied to all sectors so that they may be able to control and to use less energy by having a good result at the end of the process.

South Africa, for many years, is now facing very big challenges regarding energy consumption usage due to lower price of electricity which was a lack of motivation to save energy and has a negative effect of high energy usage (Rasmeni, 2014) (Figure 1). South African Industrial sectors (agriculture, mining, manufacturing and construction) are some of the biggest consumers of energy and use almost 45 to 49% of energy in South Africa (Davidson, 2006; Matlala, 2004). In the industrial sector, iron & steel use 29% of energy in the industrial sub-sector (Davidson, 2006). Therefore, in the iron & steel sector, foundries are the biggest consumers using different types of furnaces with the Induction Furnace known as the most efficient. Energy efficiency of any foundry largely rides on the efficiency of the melting process. Melting is the most energy-intensive operation in the metal casting industry with 55% of the total energy in the foundries (Incorporated, 2005) (Figure 2). The induction heating process has been considered as high productivity, repeatable quality, and green heating technology compared to other fuel-fired furnaces (Dang, 2012).

The aim of this paper is to increase the efficiency of the Induction Furnace (IF) by using a foaming slag layer as insulation material to reduce the heat

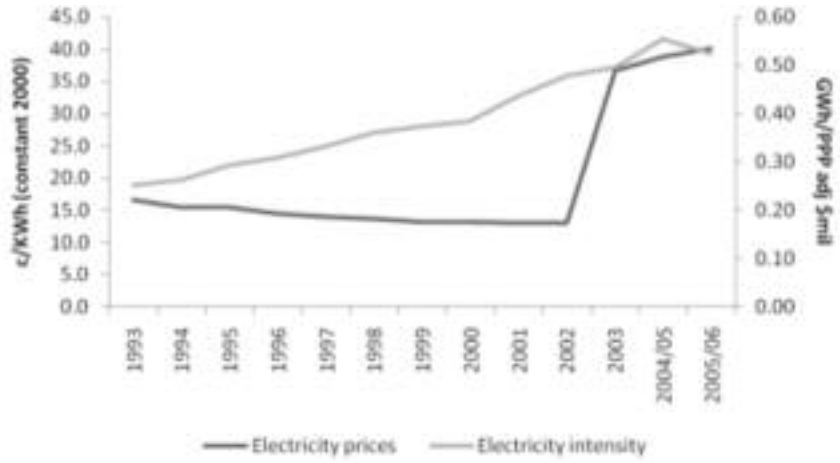

Figure 1: Electricity intensity and electricity prices in South Africa: 1993 to 2005

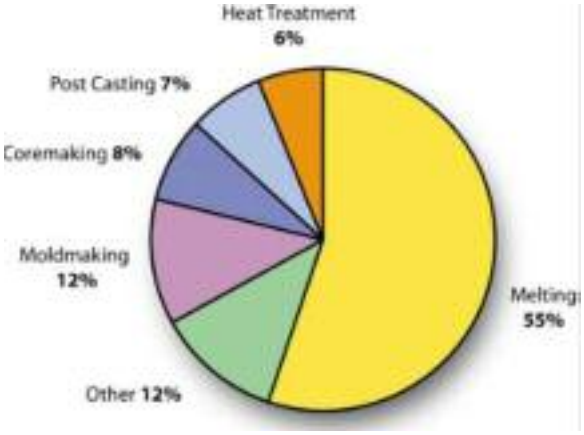

Figure 2: Melting operation as the most energy-intensive operation in metal casting industry

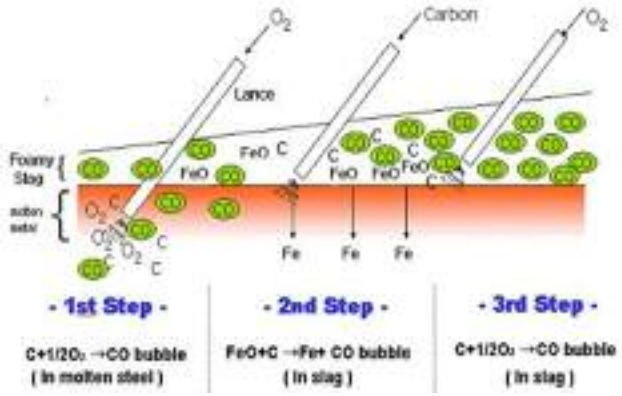

Figure 3: Mechanism of foaming slag creation

loss at the opening of the Induction Furnace (Figure 3). The importance of this paper is to show the value of the carbon rate change in the creation of the foaming slag and the impact that it plays during this process on the energy efficiency procedure. The use of the foaming slag will decrease the heat loss, which will increase the efficiency of the furnace. As such, a Heat Transfer calculation will be conducted at the opening of the Induction Furnace to measure the heat loss during the process and to show the relation between the foaming slag and the heat transfer at the furnace opening.

2. Experimental methods

2.1 Materials, apparatus and procedure

For this investigation, the materials used were slag particles, oxygen gas, pure carbon particles and cast-iron scraps (Figure 4). In this paper, the experimental processes were done using a small laboratory Induction Furnace of 5 kg, an electrical power

Figure 4: Cast-Iron scraps and carbon particles

station (Figure 5), some alumina lances used to inject gas, a pyrometer to measure the temperature and a thermometer.

Figure 5: Laboratory induction furnace and electrical power station

Figure 5 shows the schematic diagram of the experimental procedure, which consists of 4 main steps.

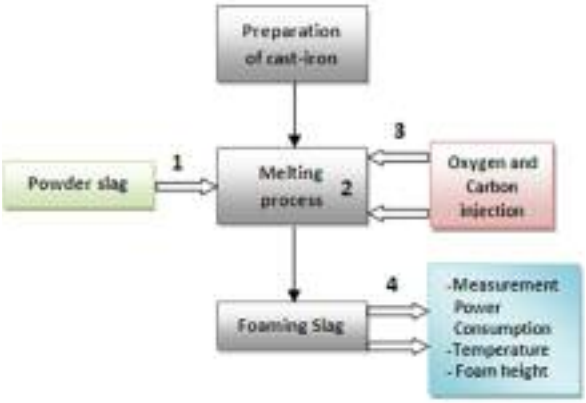

Figure 6: Schematic diagram of experiment procedure of foaming slag creation

Before any procedure, cast-iron scraps (5 kg) and the carbon particles in different weight of 21.27, 30, 35, 40, 45, and 55g were prepared. First step, the slag particles were poured into the crucible, followed by the cast-iron scrap reduced into small pieces and thereafter the laboratory's induction furnace was switched on.

At the temperature of 900°C when the cast-iron scraps are melting, the slag particles also melted and due to the difference of densities of the two melted elements, the slag has started floating and, at the same time, 100 ml of oxygen gas is injected

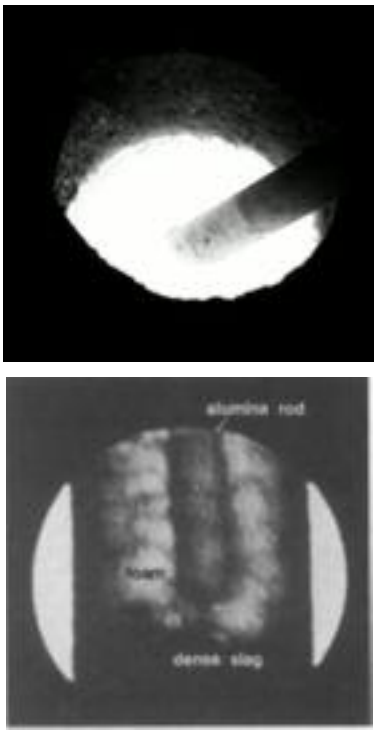

Figure 7: Overview of the measurement of height of the foaming slag using alumina rod

for 30 seconds into the molten. Thereafter, the carbon is now injected at 21.27g for the first experiment and the procedure went on and on until the last 55g of carbon was injected in the last experiment. The oxygen gas was injected for 30 seconds to ensure the reaction as shown in Figure 3 above. From the starting point until the measurement of the temperature on top of the foaming slag, the melting time and the power consumed were measured. The measurement of the height of the foaming slag was made by inserting an alumina rod into the molten and traces of the foaming slag left on the rod was allowing the reading of the height of the foam (Figure 7).

The melting process will be done using a pre-heated furnace for every experimental procedure due to the results obtained from the basic experimental procedure shown in Table 1.

3. Results and discussion

The results and discussion will give the influences of the carbon rate changes and its effect on parameters mentioned in Table 2.

3.1 Influences of foaming slag height

The carbon particles used in the melting process for

Table 1: Basic melting experimental processes for cold and pre-heated furnace

	Melting time (min)	*Electrical power) consumption (kWh*	*Temperature environment (°C)*	*Heat transfer rate (kW)*
Cast-iron cold furnace	49	16.98	22	156.8
Cast-iron pre-heat furnace	43	14.66	22	136.53

Table 2: Variations of parameters during the experimental procedure

	Oxygen (ml/sec)	*Carbon (gr)*	*Foam height (cm)*	*Melting time (min)*	*Electrical power consumption (kWh)*	*Temperature surface of foaming slag (°C)*	*Temperature of the molten (°C)*	*Heat transfer rate (kW)*	*Percentages (%)*
1	100	21.27	0.9	42	13.93	878	1275	32.62	38.21
2	100	30	0.9	39	13.85	878	1269	31.89	38.16
3	100	35	0.85	38	10.75	872	1263	30.23	37.20
4	100	40	1.0	35	10	865	1261	29.7	36.01
5	100	45	0.7	40	12.82	870	1271	29.3	36.86
6	100	55	0.6	41	14.34	877	1265	28	38.06

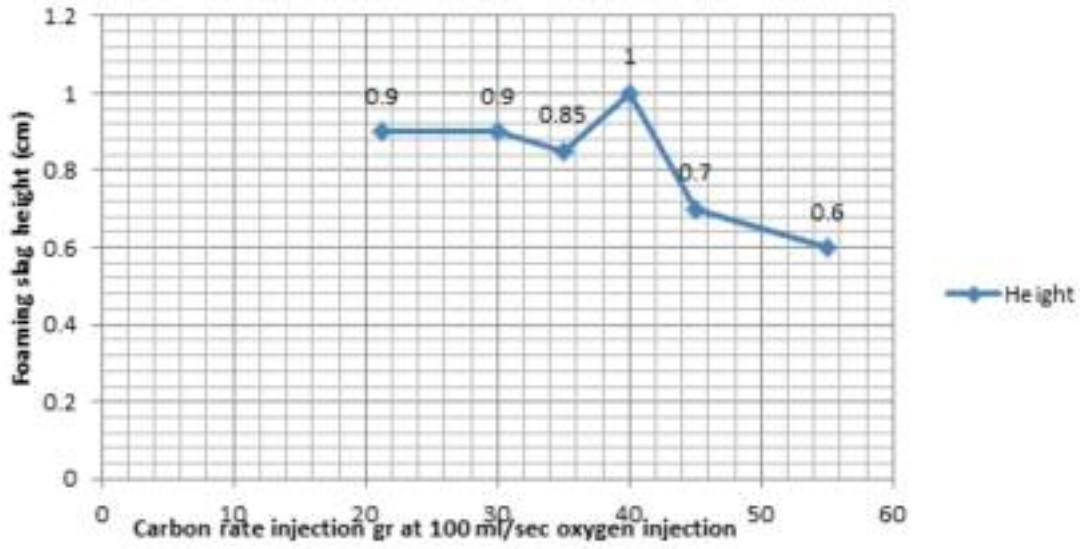

Figure 8: The effects of carbon rates variation on the foaming slag height

the foaming slag creation have been poured into the furnace at different rates from 21.27 to 55g. Figure 8 shows the variation of the height according to the carbon poured into the furnace; it also shows the height going up from 0.8 mm to 1cm for 40g of carbon poured. At 45g and 55g, the height started to decrease due to carbon particles which were now in excess and started destroying the foaming slag that was already made.

At the optimum, the temperature at the surface was 878°C, the melting time was 42 minutes and the optimum foaming slag height was 1cm, the electrical power consumption used was 13.93kWh.

At 40g of carbon poured in the molten, the reaction has reached the optimum and above this amount of carbon, the particles started destroying the bubbles because of the surface tension. A study conducted by Aminorroaya and Edris (2002) on the effect of foamy slag in electrical arc furnaces on electric energy consumption shows that the variation of carbon rate more than 9kg/min has no effect on slag foaming and increasing in electric energy consumption by increasing in melting time (Aminorroaya and Edris, 2002).

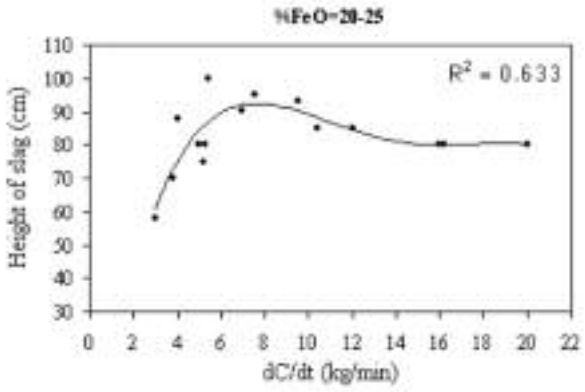

Figure 9: Variation of carbon injection rate with slag height

Source: Aminorroaya and Edris (2002)

3.2 Effect of melting time and temperature of the molten

The melting time and the temperature of the molten during this operation were also influenced by the carbon that was poured into the molten during the procedure. Figures 10 and 11 show that increasing the carbon in the molten until a certain point was contributing to the oxidation which was exothermic and increasing the heat means decreasing the melting time of the cast-iron in the crucible.

Figure 10 shows that at 21.27g the melting was 42 min and slightly increases for 1min at 43 min. But at 35g and 40g, the melting time starts decreas-

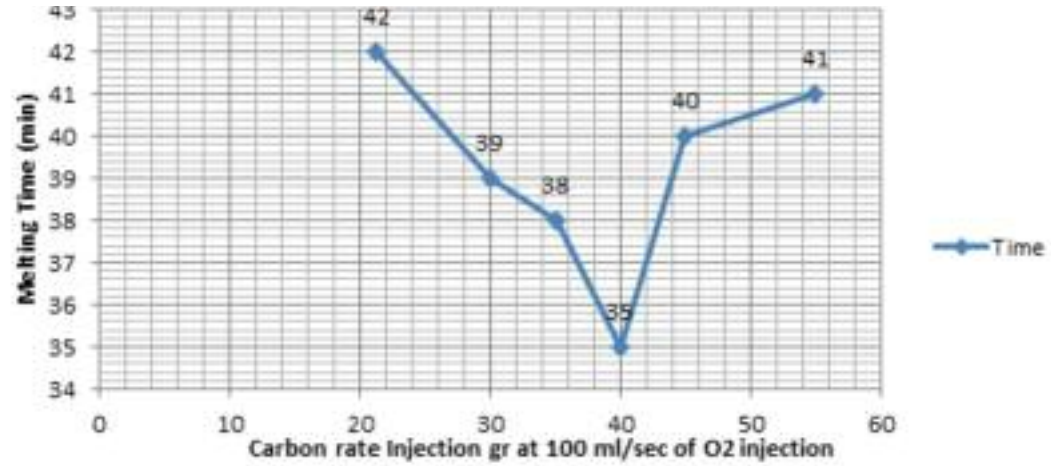

Figure 10: Influence of carbon rate on the melting time

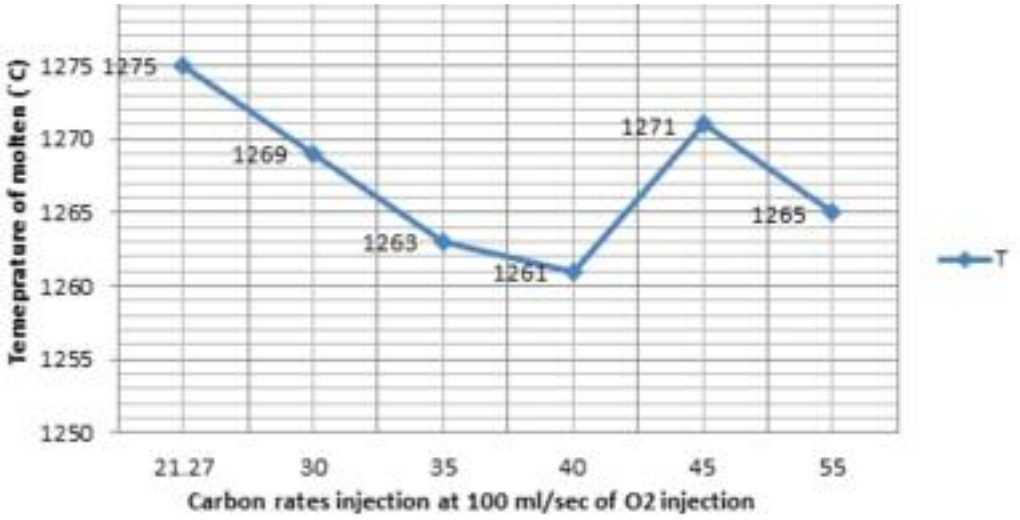

Figure 11: Influence of the carbon rate injection on the temperature of the melt

ing and the minima time was at 40g of carbon poured into the molten. From 45g until 55g, the melting time starts increasing again. During the melting process at 35g and 40g the oxygen gas injected at 100ml/sec has reacted until the major percentage of carbon injected was consumed due the reaction. But at 45 and 55g, the oxygen gas at 100ml/sec wasn't enough to oxidize all the carbon and that increases the time due the extra material added in the molten. But Figure 11 shows the relation between the temperature and the carbon rate injected in the molten from 21.27 to 40g, temperature was increasing due to the exothermic reaction which brought extra heat in the molten at 100ml/sec. But from 45 to 55g, heat was brought up and the rate of the oxygen could react with all the carbon particles poured in the molten. Ozturk and Fruehan have shown the impact of temperature on the foaming height. Foaming height on Figure 8 decreases with increasing the temperature (Fruehan, 1995). This shows the co-relation between the carbon and the temperature during the melting process.

3.3 Influence of electrical energy consumption

During the reading of electrical power, the carbon rate injection has shown some variation during the process. In fact, some other parameters have played an important role in the reduction of electrical energy consumption such as the basicity of the slag (Aminorroaya and Edris, 2002). Figure 12 shows the variation of the electrical power consumption. From 21.27g to 40g, the electrical energy went down and slightly started increasing from 40 to 55g.

Therefore, from 21.27g to 40g the room temperature was 23°C and from 40 to 55g room temperature was 9° less than normal. Room temperature also played a part on the heating process of the material, the time and eventually on the energy needed to heat the cast-iron. Figure 13 shows that the electrical energy consumption varies with the foaming slag height. If the foaming slag height increases, the electrical energy consumption decreases (Aminorroaya and Edris, 2002).

Aminorroaya and Edris (2002) have also stud-

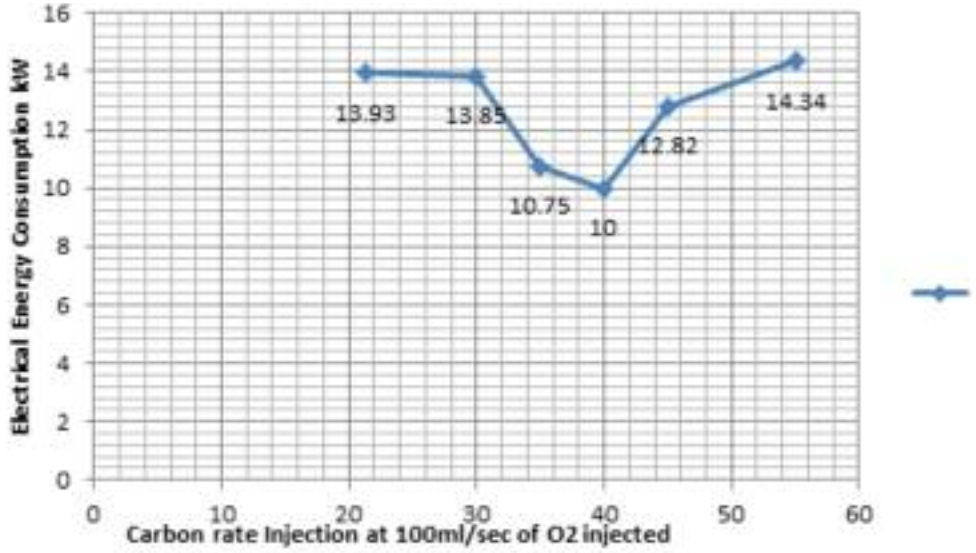

Figure 12: Influence of carbon rate injection on the electrical energy consumption kW

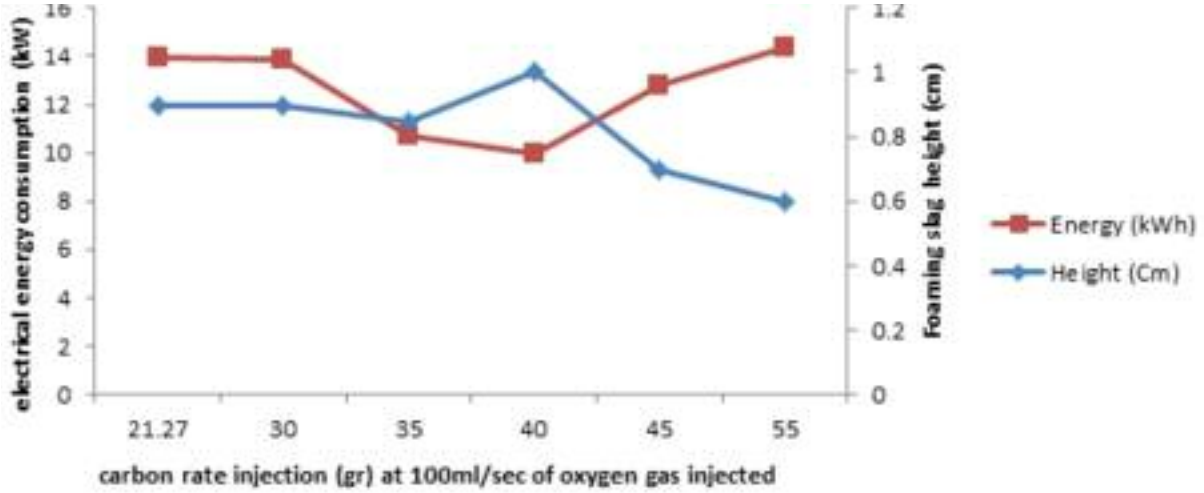

Figure 13: Relationship between the electrical energy consumption and the foaming slag height (cm)

ied and found the influence of the carbon rates on the electrical energy consumption and during their experience, electrical energy decreased with increasing carbon injection rate up to 9kg/min.

3.4 Influence of surface temperature of the foaming slag

The temperature determination on the surface of the foaming slag has all to do with the thickness of the foaming slag and the contribution of the carbon particles. The foam creation is one of the major elements during the process.

Figure 15 shows that from 21.27g to 40g the temperature decreases due to the carbon rate, which influences the foaming slag height, and increases the thickness of the foaming slag. Increasing the thickness means increasing the height which decreases the heat loss on top of the furnace (Figure 16). At 45g and 55g, the temperature starts increasing due to the fact that the foaming slag

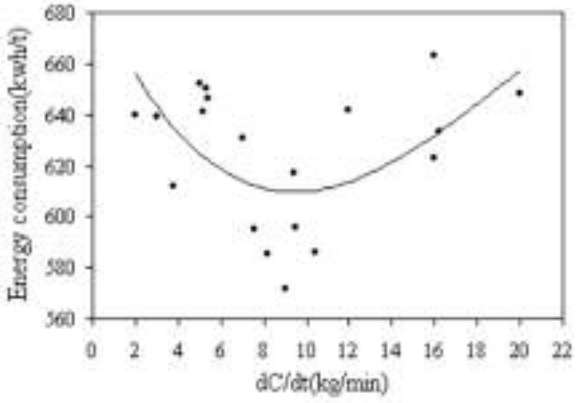

Figure 14: Variations of carbon injection rate with electrical energy consumption
Source: Aminorroaya and Edris (2002)

started to be destroyed due to the excess of carbon particles in the molten. The carbon particles reacted with the bubble and start destroying them and as

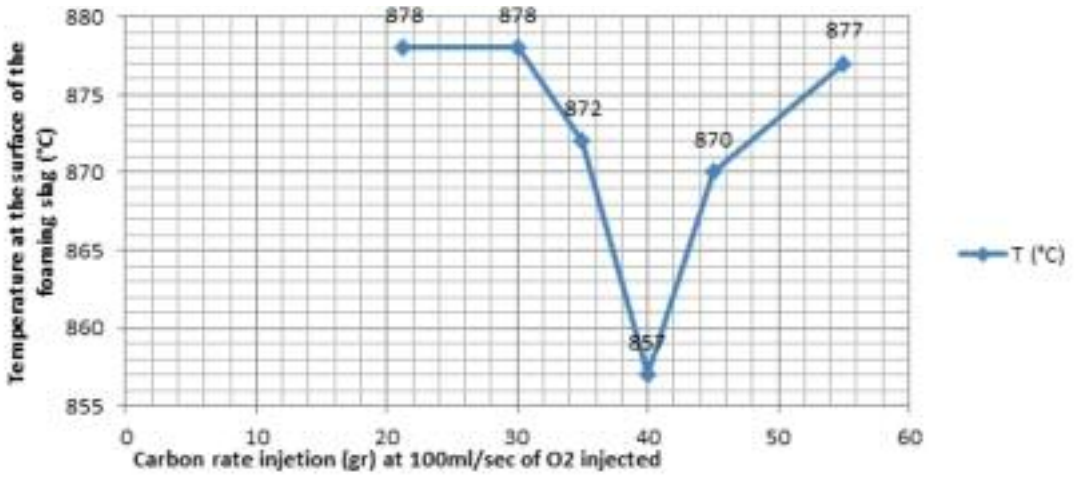

Figure 15: Influence of carbon rate injection (g) on the surface temperature of the foaming slag (°C)

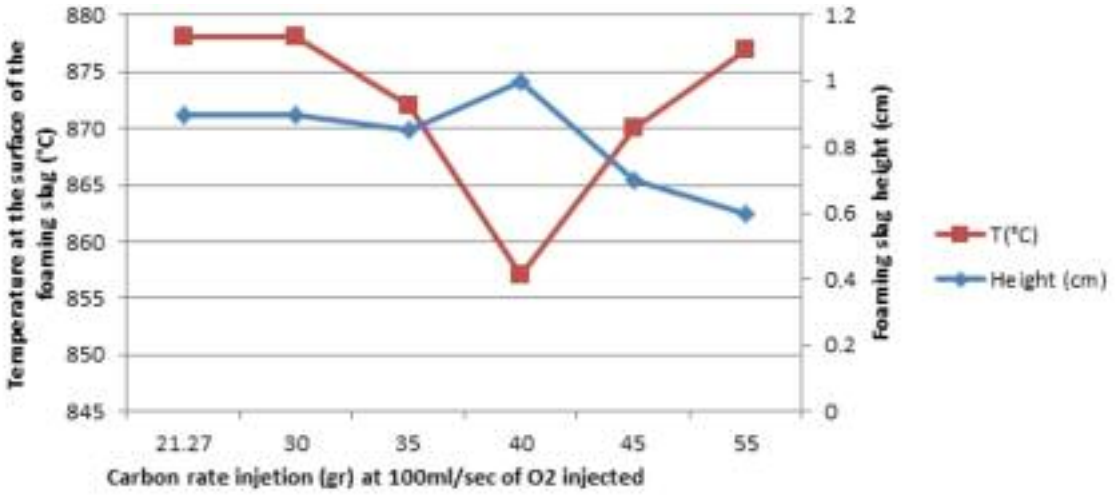

Figure 16: Relationship of temperature at the surface of the foaming slag with the foaming slag height at different carbon rate injection

such decreasing the foam height (Y. Zhang, 1995). The surface temperature of the foaming slag has also everything to do with the foaming height thickness.

3.5 Heat transfer calculation

The heat transfer in the induction furnace is located and comes from the metal to be heated. The thermal transfer is done to the wall and to the top or opening of the furnace. An Induction furnace is a made of a crucible in graphite, some coils cooled by water circulation (Mauricio V. Ferreira da Luz, 2010). Those coils are protected by an insulation material or refractory.

For a better understanding of the furnace, modelling should be done to see which part of the furnace might be influencing the calculation. The choice of the domain is very important because it shows and gives the kind of heat applied for. The aim is to find some domains which will influence and show which types are used: conduction, convection and radiation. Our focus will be on the thermal problems. Figure 17 gives us a sketch of the furnace and the possible heat and domain which needs to be measured.

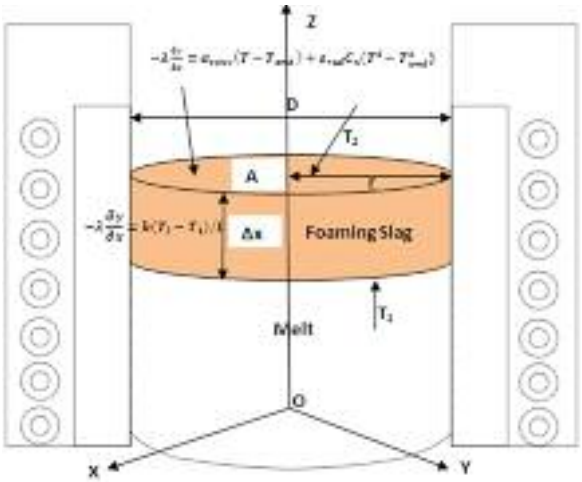

Figure 17: Sketch of the induction furnace

The calculus domain in our case will only be focused on the thermal problem, the inductor region will be considered as one single core and the

calculation will be done according to that.

The boundaries of the calculus domain are in fact the surface through that thermal transfer from the furnace parts to the surroundings.

At the surface of the furnace the domain will be given by and the heat transfer is a combination of convection and radiation:

$$-\lambda\, \partial y/\partial x = \alpha_{conv} (T-T_{amb}) + \varepsilon_{tot} C_s (T^4-T^4_{amb}) \quad [1]$$

Where, α_{conv} is the convection coefficient. ε_{tot} = 0.83 is the total emissivity and C_s = $5.67.10^{-8}$ W/m^2K^4 is Stephan constant, T is the surface temperature, T_{amb} is the temperature of surrounding environment. The coefficients α_{conv} and ε_{tot} could depend on temperature and ε_{tot} could depend in addition on surface quality.

If the heat transfer calculation in the inductor must be done, the convection heat transfer should be considered because of the exchange between the inductor and the cooling water that circulate through the coils and it given by:

$$-\lambda\, \partial y/\partial x = \alpha_{conv\,ind-cpu} (T-T_{med\,cpu}) \quad [2]$$

Where $\alpha_{conv\,ind-cpu}$ is the transmissivity between the inductor and cooling water whose medium temperature is $T_{med\,cpu}$ (Pasca, 2004). In this case the temperature of the molten, the surface temperature on top of the foaming slag has been considered in Table 2: At the Interface melt and foaming slag the heat transfer is made by conduction:

$$-\lambda\, \partial y/\partial x = kA (T_2-T_1)/L \quad [3]$$

Where k is the thermal conductivity, A is the surface of cylinder, L is the length of the layer.

During the calculation the ΔX changes according to the height of the foaming slag which influences the heat transfer operation.

The total heat transfer loss during the process on top of the furnace will be influence by the conduction, convection and radiation:

$$-\lambda\, \partial y/\partial x = \alpha_{conv} (T-T_{amb}) + \varepsilon_{tot} C_s (T^4-T^4_{amb}) + kA (T_2-T_1)/L \quad [4]$$

The influence of surface of the cylinder *A* in this case will be influenced by the height of the foaming slag and represented by *L*:

$$A=\pi (D^2/4) L=\pi r^2 L \quad [5]$$

$$A=\pi (D^2/4) L=3.14 \times 0.05^2 L \quad [6]$$

$$A=0.00785\ L \quad [7]$$

The measurement of the heat transfer will depend on the variation of the thickness of the foam. As such, the results will show the variation of the heat according to the foaming height. The calculation has been made according to the equation 4:

$$-\lambda\, \partial y/\partial x = 19.10 \times (878-23) + 0.83 \times 5.67.10^{-8} (878^4-23^4_{amb}) + 0.15 \times \pi \times 0.0025\ (1265-878)$$

$$-\lambda\, \partial y/\partial x = 27.99\ kW$$

All the results are shown on Table 2 which is the table of variations. The heat transfer calculation for the basic experiments without any kind of foam or insulation has been considered as such the calculation was given by the formula in equation 10. The conduction was considered as zero because the temperature at the interface was the same solid (molten) and the gas.

$$-\lambda\, \partial y/\partial x = 19.10 \times (1905-23) - 0.83 \times 5.67.10^{-8} (878^4-23^4_{amb}) + 0$$

$-\lambda\, \partial y/\partial x$ = 136.5 kW for cold furnace and;

$-\lambda\, \partial y/\partial x$ = 156.8 kW for preheated furnace.

During the carbon injection into the molten, the reactions below are exothermic because they increased the temperature into the furnace (N. Sahay, June 2014) (Pandey, 2003).

$$C + O_2 = CO_2 - 24.03\ Kcal/g\ mole\ (T<800^\circ C) \quad [8]$$

$$C + \tfrac{1}{2} O_2 = CO + 26.42\ Kcal/g\ mole\ (T>800^\circ C) \quad [9]$$

Figure 18 gives the variation of the heat loss compare to the height of the foaming; the figure shows that 1cm was the optimum height reached during the process. From 0.9cm the foaming height stays a little bit constant. When the height increases the heat loss decreases due to the thickness of the foam which reduces the heat loss.

4. Conclusion and summary

The importance of energy efficiency has been demonstrated during the experimental procedure. This paper illustrated the importance of the foaming slag during the melting process and the utility of the foaming slag during the heat loss. The results of the experiments and observations revealed that:

1. At 40g, the use of the foaming slag in the induction furnace has given a melting time saving of 5 minutes which is almost 17.15% of time.
2. The electric energy consumption has been saved from 13.93kW to 10kW at 39.3% of electricity energy. At 40g of carbon injected, the

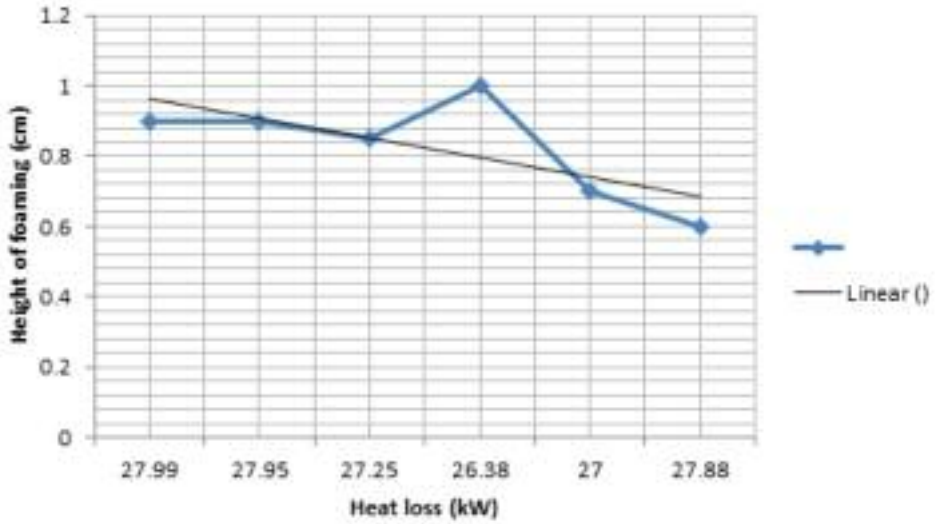

Figure 18: Relation of heat loss with height of foaming

foaming slag obtained its optimum at the height of 1 cm.

3. The foaming slag insulation has helped reduce the temperature radiation from 878°C to 870°C. The thickness of the foam creates a layer which could reduce the heat loss.
4. The heat transfer calculation during the parameters change shows a variation of the heat loss due to the height (Figure 18). The graph line goes down with the heat loss decreasing and that means if the height decreases the heat loss increases. The heat transfer loss during the calculation gives a variation of temperature from 27.99kW to 26.38kW, which give a saving of 6.10%.
5. Comparing the basic experimental heat loss (136.53kW) with the heat loss during the foaming slag (26.38kW) creation almost shows the importance of using foaming slag during the process because in this case, using foaming slag reduces the heat loss to 110,15kW which is almost 19.4% of the energy loss.
6. Usage of foaming slag in the induction furnace in this experiment shows that the foaming slag is theoretically and practically efficient but coming to the heat transfer a tremendous heat loss occurred due to the thickness of the foaming slag, which was very tiny and instead of reducing more heat radiation its reduces less.
7. The improvement of the induction furnace using carbon injection parameters in this research can be implemented to the actual furnaces and not only to the Lab situation.

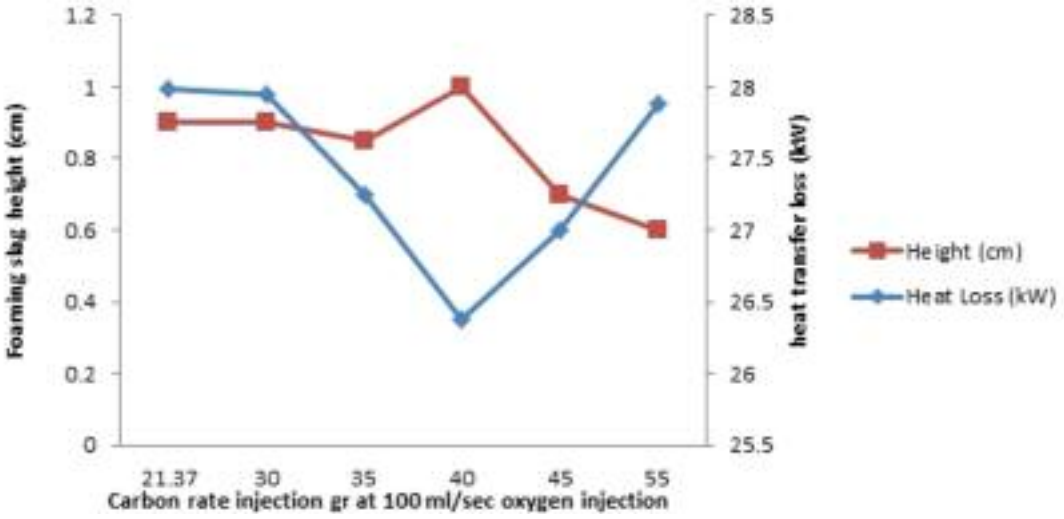

Figure 19: Comparison and variation of heat transfer (kW) and foaming slag height (cm) due to carbon rate injection at 100 ml/sec oxygen

Acknowledgments

The authors gratefully acknowledged the support of the University of Johannesburg's Foundry Laboratory of Doornfontein Campus for the realization of this project. Our thanks go to the Laboratory technician assistant, Mr. Gilbert. for his availability, time and assistance.

References

Agency, I. E. (2012). Worldwide engagement for sustainable energy strategies. Germany: International Energy Agency.

Aminorroaya, S and Edris, H. (2002). the effect of foamy slag in the electrical arc furnaces on the electric energy consumption. 7th European Electric Steelmaking Conference (pp. 2.447- 2.456). Venice: 7th European Electric Steelmaking Conference.

Dang, H.-S. P.-P. (2012). Optimization of the In-line induction Heating Process for Hot Forging in Terms of Saving Operating Energy. International Journal of precision engineering and manufacturing , 13 (1085), 1085-1093.

Fruehan, B. O. (1995). Effect of Temperarute on slag foaming. Metallurgical and Materials Transactions B, 26B, 1086- 1088.

Fruehan, B. O. (1995). Effect of temperature on slag foaming. Metallurgicall and Materials Transactions B, 26B, 1086.Fruehan, K. I. (1989). Study on the foaming of CaO-SiO2-FeO slags: Part 1. Faoming parameters and experimental results. Metallurgical Transaction B, 20B, 509- 511.

Incorporated, B. (2005). Advanced Melting Technologies: energy savings concepts and opportunities for the Metal Casting Industry. Columbia, MD: U.S Department of Energy Energy Efficiency and renewable Energy.

Matlala, T. (2004). Demand Side Management Implementation in South Africa.: Eskom.

Mauricio V. Ferreira da Luz, A. B. (2010). Modeling of a Crucible Induction Furnace Taking Into Account the Inter-laminar losses. Brazil: IEEE.

Mohamadi, A. E. (2011). A Collective approach towards green fourndries In South Africa-moving towards green foudnries in SA. Johannesburg: National Foundry Technology Network.

Sahay, A. B. (2014). Dealing with open fire in an underground coal mine vy ventilation control techniques. Journal of the Southern African Institute of Mining and Metallurgy , 114 (6), 447.

Ogunlade Davidson, H. W. (April 2006). Energy policies for sustainable development in South Africa. Cape-Town: Energy Research Centre, UCT.

Pandey, B. C. (2003). Laboratory study of channel gasification with stream-air blast in sub-bituminous coal from Pindra Raniganj coalfield. Minetech , 24 (6), 37-49.

Pasca, S. (2004). Particularities on numerical modeling of crucible induction furnace. Bucarest.

Wikipedia. (2014). Energy Efficiency. Wikipedia.

Y. Zhang, R. F. (1995). Effect of Carbonaceous Particles on Slag Foaming. Metallurgical and Materials Transactions B , 26B, 813.

Z.Z. Rasmeni, D. X. (2014). Analyse of energy efficiency and consumption in south african steel foundries. World Foundry Congress. Bilbao: World Foundry Congress.

Received 10 October 2014; revised 18 May 2015

Prediction of diesel engine performance, emissions and cylinder pressure obtained using Bioethanol-biodiesel-diesel fuel blends through an artificial neural network

Hasan Aydogan
Mechanical Engineering Department, Technology Faculty, Selcuk University, Konya, Turkey

Abstract
The changes in the performance, emission and combustion characteristics of bioethanol-safflower biodiesel and diesel fuel blends used in a common rail diesel engine were investigated in this experimental study. E20B20D60 (20% bioethanol, 20% biodiesel, 60% diesel fuel by volume), E30B20D50, E50B20D30 and diesel fuel (D) were used as fuel. Engine power, torque, brake specific fuel consumption, NOx and cylinder inner pressure values were measured during the experiment. With the help of the obtained experimental data, an artificial neural network was created in MATLAB 2013a software by using back-propagation algorithm. Using the experimental data, predictions were made in the created artificial neural network. As a result of the study, the correlation coefficient was found as 0.98. In conclusion, it was seen that artificial neural networks approach could be used for predicting performance and emission values in internal combustion engines.

Keywords: artificial neural networks, diesel engine, biodiesel fuel, bioethanol

1. Introduction

Today, diesel engines are widely used in transportation, industry and agricultural areas because of their high fuel efficiency and ease of operation (Demirbas, 2008). The demand for diesel engines has been continuing to increase worldwide as a result of expanding industrialization (Ma *et al.,* 2013). This is because diesel engines have certain advantages compared to spark ignition engines such as low fuel consumption, high engine torque and longevity (Park and Lee 2013).

The limited nature of oil resources has made the studies on alternative energy sources much more important in diesel engines, in which oil products are used as an energy source (Canakci *et al.,* 2006; Hazar, 2010; Hulwan and Joshi, 2011; Breda, 2011; Kannan *et al*., 2011; Fahd *et al.,* 2013). The use of renewable energy sources in internal combustion engines may also contribute to decreasing the increase in air pollution (Ghobadian *et al.,* 2009). Bioethanol and biodiesel are renewable energy sources (Mrad *et al.*, 2012).

Bioethanol is obtained through the fermentation of agricultural products containing sugar and starch such as sugar beet, sugar cane, corn, wheat and wood-like plants (Park *et al.,* 2012; Guido *et al.,* 2013). The use of bioethanol in diesel engines provides a decrease in the amount of particulate matter (PM) in exhaust emissions (Zhou *et al*., 2013; Hadi *et al*., 2009; Yilmaz and Sanchez, 2012). The decrease in PM (smoke) is related to the amount of oxygen contained in fuel blends (Shi *et al.,* 2005).

Biodiesel is a product which comes from the reaction of oils obtained from oilseed plants like canola, sunflower, soybean and safflower or from animal fats with a short-chain alcohol (methanol or ethanol) in the presence of a catalyst and can be used as fuel (Brunschwig *et al*., 2012; Acaroglu and Aydogan 2012). The biggest advantage of the use of biodiesel fuel is that it can be used without performing any modifications on the engine (Torrisi and Sabino, 2013; Aydogan *et al*., 2011, Adeyemo *et al.,* 2011).

Conducting performance experiments on engines using different operating conditions and different fuels requires cost and time. At this point, artificial neural networks (ANN) can be used in order to decrease costs and save time (Ghazikhani and Mirzaii, 2011). Different variables can be predicted by using the data obtained in previously conducted experiments. In recent years, the applicability of an artificial neural network method for internal combustion engines has gained considerable success (Sharkey *et al.,* 2000; Yilmaz and Bilgin 2013).

There are several studies conducted through the ANN approach. In a study, Uzun (2014) used the ANN approach to predict air mass flow in a diesel engine. Çay (2013) showed that ANN approach could be used for predicting performance values in

a gasoline engine. In their study, Ghazikhani and Mirzaii (2011) stated that correct predictions at a rate of 99% could be made in predicting the soot emissions of a diesel engine by using the ANN approach. Ghobadian *et al.* (2009) used ANN for predicting engine performance and exhaust emissions with the use of biodiesel obtained from waste oils.

In the present study, biodiesel and bioethanol obtained from safflower oil and diesel fuel blends were used in an engine with a common rail fuel system. The use of the ANN approach was examined using the measured values.

2. Experimental setup and procedure

Low-sulphur diesel fuel (Euro diesel) was purchased for the tests. Bioethanol produced from sugar beet was obtained from Konya Seker Inc. Safflower oil was used for producing biodiesel. Safflower oil was processed into biodiesel through transesterification. Three different fuel blends were prepared by using these fuels. The ratios of the fuel blends used in the experiments were determined based on the suggestions provided in previous studies. Density, kinematic viscosity and lower heating value (LHV) of the prepared fuel blends were measured. Fuel blends and their properties are presented in Table 1. The fuel blends were prepared right before the experiments in order to ensure homogeneity. Furthermore, the fuel in the tank was mixed using a mixer in order to prevent phase separation.

A water-cooled, turbocharged diesel engine with an intercooler and a common rail fuel system was used in the study. The schematic diagram of the experimental setup used in the study is presented in Figure 1. All the experiments were conducted without performing any modifications on the engine. The technical specifications of the test engine are presented in Table 2. An AVL GH13P/AG04 cylinder pressure sensor and AVL 365C Crank angle encoder were installed on the test engine. Afterwards, the test engine was connected to a hydraulic dynamometer. Fuel consumption was measured by using a Dikomsan™ JS-B model electronic scale. A digital chronometer was used in order to determine the fuel consumption per unit time. An Orifice™ plate and differential pressure manometer was used to measure the air consumption of the engine. Exhaust temperatures were measured using a K-type thermocouple. A Bosch BEA 350 gas analyser and Bosch RTM 430 smoke meter were used to measure the exhaust emissions. The specifications of the exhaust measuring devices and the calculated uncertainty values are presented in Table 3. All the tests were conducted at full-throttle opening. Before starting the tests, the engine was operated until it reached a stable condition. Afterwards, the experiments were started. Engine speed, engine power, engine torque, fuel consumption and exhaust emission values were recorded during the experiment. During the measurement of the in-cylinder gas pressure, the pressure values

Table 1: Some properties of the test fuels

Fuel property	*D*	*E20B20D60*	*E30B20D50*	*E50B20D30*	*Measurement method*
Bioethanol content (%)	0	20	30	50	
Biodiesel content (%)	0	20	20	20	
Diesel Fuel content (%)	100	60	50	30	
Density (kg/m^3) at 15 °C	826.7	839.2	835.1	825.1	ASTM D4052
Kinematic Viscosity (mm^2/s) at 40 °C	2.8221	2.4645	2.4853	2.0139	ASTM D445
Lower heating value (Mj/kg)	47.521	39.322	38.966	34.131	ASTM D240

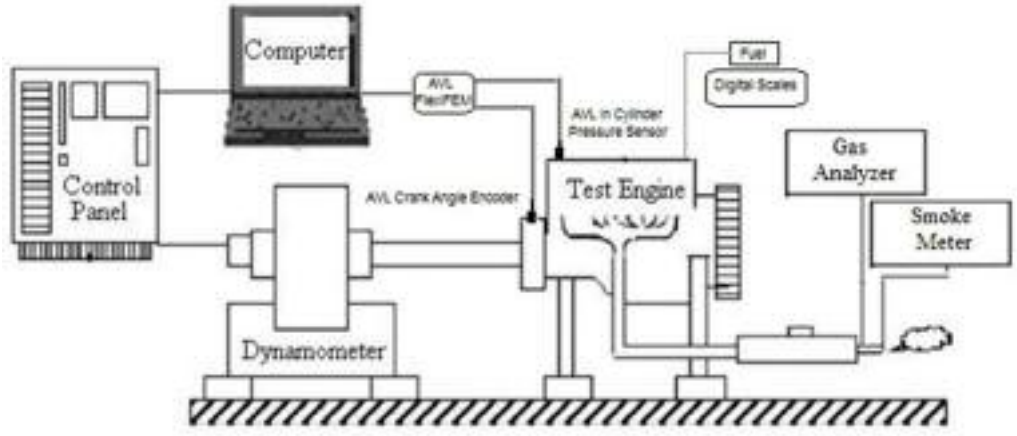

Figure 1: The schematic diagram of the experimental setup

were recorded at each 0.5 degree of the crankshaft through 120 cycles and the mean values were calculated. The relative humidity, ambient temperature and pressure of the test room were measured using a hygrometer, a thermometer and a barometer, respectively. The fuel pump, fuel pipes and the fuel filter were emptied at each fuel change. All the experiments were repeated three times and the means of the obtained values were calculated.

Table 2: Specifications of the test engine

Engine type	Water-cooled, four stroke, turbo charged, intercooler, common rail fuel system
Number of cylinders	4
Cylinder volume	1910 cm^3
Bore and stroke	82 x 90.4 (mm)
Compression ratio	18.5/1
Maximum torque	200 Nm@1750 rpm
Maximum power	77 kW@4000 rpm
Number of holes in nozzle	4
Size of nozzle	0.132 mm

3. Experimental results

The variation of engine power depending on engine speed is presented in Figure 2. As it can be seen in Figure 2, the power curves are similar in shape. As a result of the tests, it was seen that the highest engine power was obtained at 3000 rpm with all types of fuels. At this engine speed, engine power was measured as 46.3 kW with the use of D fuel, 44 kW with the use of E20B20D60 and E30B20D50 fuels and 39.75 kW with the use of E50B20D30 fuel. Engine power showed a decrease as the percentage of the bioethanol in the fuel blends increased. The engine power obtained through the use of fuel blends was found to be approximately 15% lower compared to diesel fuel. The major reason for the decrease in engine power is the difference between the heating values of the fuels. As it can be seen in Table 1, LHV values of the fuels decreased as the ratio of bioethanol in the blend increased.

When we examine the engine torque values given in Figure 3, we can see that a similar curve was formed with all types of fuels. The highest torque values were observed at 2000 rpm. Engine torque values showed a decrease as the ratio of the bioethanol in the fuel blend increased. At 2000 rpm, engine torque was measured as 185.59 Nm with D fuel, 175 Nm with E20B20D60 fuel, 170 Nm with E30B20D50 fuel and 153 Nm with E50B20D30 fuel. When we look at the lowest value, it is seen that there was an approximately 18% decrease compared to D fuel.

The brake specific fuel consumption (BSFC) values presented in Figure 4 shows that the lowest value was obtained within the range of 2000-3000 rpm. Engine torque and engine power also reached the highest values at this speed range. As shown in Figure 4, BSFC values increased as the ratio of bioethanol in the fuel blend increased. At 2500 rpm, the lowest BSFC value was 225 g/kWh with the use of D fuel, while the highest BSFC value was 267 g/kWh with the use of E50B20D30 fuel. This value is 18% higher compared to the BSFC value obtained with the use of D fuel. The amount of fuel used by the engine shows an increase as the heating value of the fuel decreases (Stone 1999; Zhu *et al.,* 2010; Armas *et al*., 2011, Soloiu *et al.,* 2013).

The most important problem in diesel engines is the NOx emissions (Morisugi and Ohno 1996, Hsieh et al. 2002, Armas et al. 2011, Agarwal and Dhar 2013). The high temperatures reached during the combustion in the cylinder combines the oxygen with the nitrogen in the air to form NOx (SAE 2001). Humidity has a large in□uence on NOx emissions (Pilusa et al. 2013). Therefore, in this study, humidity in the air was continuously measured. The humidity correction factor for NOx was calculated as stated by the Society of Automotive Engineers (Qi *et al*., 2011). The variation of NOx emissions at different engine speeds is presented in Figurer 5. NOx concentration first showed an increase depending on engine speed. However, it started to decrease after reaching the maximum torque speed. Maximum NOx values were measured as 1488 ppm with the use of E50B20D30 fuel at 2500 rpm. This value was approximately 32% higher compared to the value obtained with D fuel. Bioethanol contains 34% oxygen 14. Furthermore, its low cetane number compared to that of diesel

Table 3: Technical details of the emissions measuring equipment

Equipment	*Method*	*Measurement*	*Upper limit*	*Accuracy*	*Uncertainty*
Bosch BEA 350	Non-dispersive infrared	CO	10.00 vol.%	0.001 vol.%	0.002 vol.%
	Non-dispersive infrared	CO_2	18.00 vol.%	0.001 vol.%	0.150 vol.%
	Non-dispersive infrared	HC	9999 ppm vol.	1 ppm vol.	2 ppm vol.
	Electro-chemical transmitter	NO	5000 ppm vol.	1 ppm vol.	21 ppm vol.
Bosch RTM 430	Photodiode receiver	Smoke opacity	100%	0.1%	0.8%

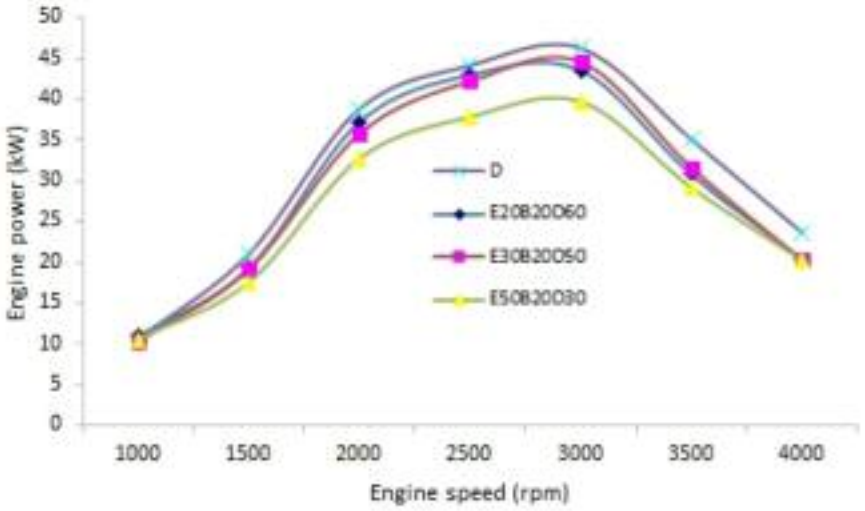

Figure 2: Variation of engine power depending on engine speed

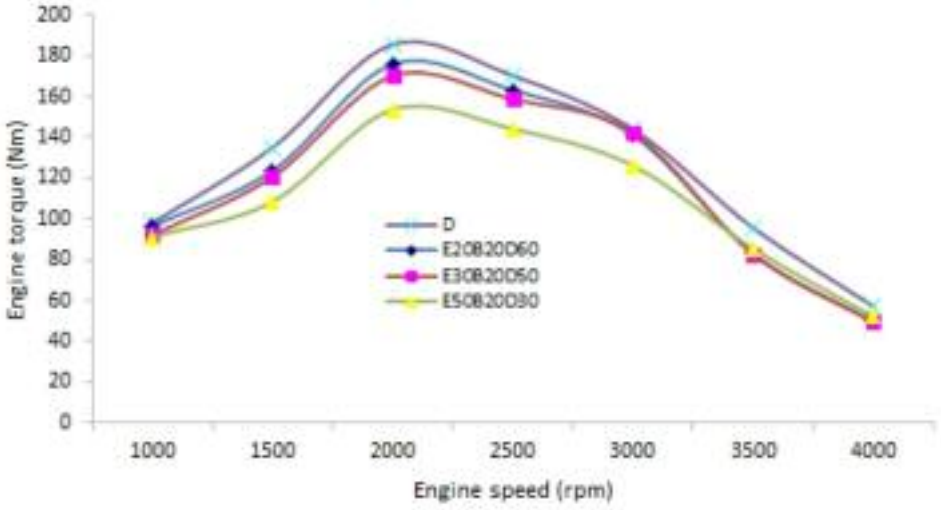

Figure 3: Variation of engine torque depending on engine speed

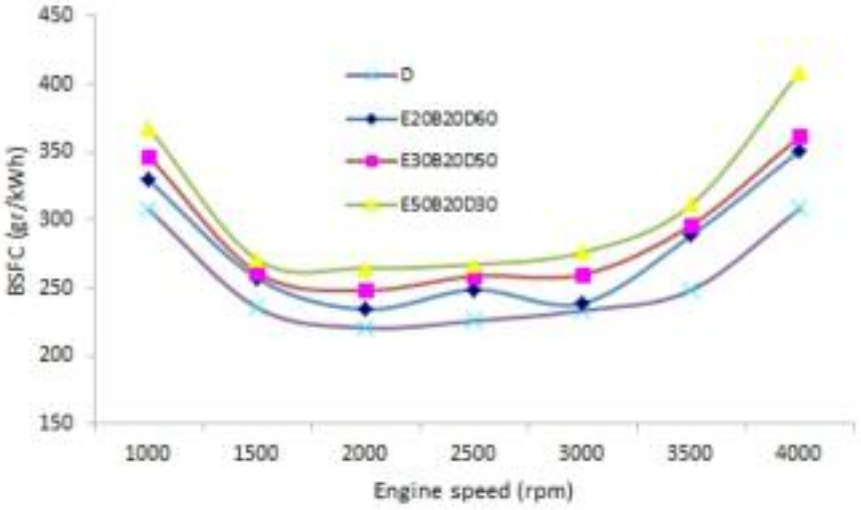

Figure 4: Variation of BSFC values depending on engine speed

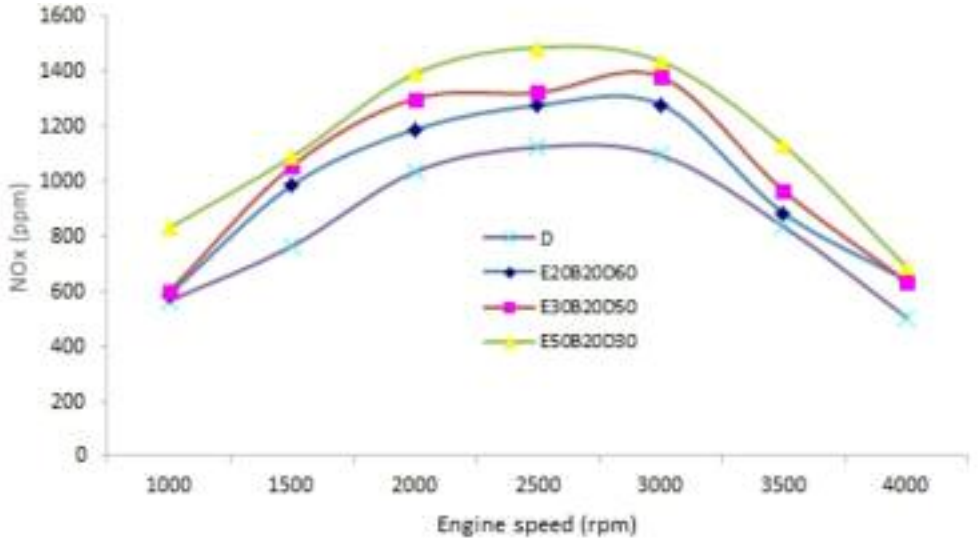

Figure 5: Variation of NOx values depending on engine speed

fuel increases the peak temperature in the cylinder (Amiri *et al*., 2011). For this reason, the concentration of NOx emissions increased with the use of all types of test fuels containing bioethanol.

4. Artificial neural networks

The concept of ANN is a calculation model which emerged as an inspiration of the working principle of the biological neural system. ANN is a method which has appeared as the result of the studies on modelling the learning ability of the neurons in the human brain and which has effective abilities for numerical optimization applications (Sefriti *et al.,* 2002). ANN structure is generally composed of factors such as processing components, structural distribution of the neural network and learning rules. ANN is composed through the organization of processing components in totally or partly connected ordered layers (Ioanaş, 2002; Balti *et al.,* 2013). These layers are composed of input, hidden and output layers and a desired number of processing components is used in each one (Figure 6). The processing components in the input layer receive the information from the outside world and deliver it to the middle layer (Hafaifa *et al.,* 2013; Singh *et al.,* 2013). In some networks, no information processing occurs in this layer. The middle layer, i.e. the hidden layer processes the information received from the input layer and transfers it to the output layer. There may be more than one middle layer in a network. The processing components in the output layer process the information received from the middle layer for the input set submitted from the input layer of the network (Uzun, 2014).

In the present study, an ANN model was developed by using the data obtained from the conducted experimental studies. Training sets were created by randomly selecting the 70% of the data obtained in the experimental study. The remaining 30% data was used for testing purposes. Firstly, a normalizing

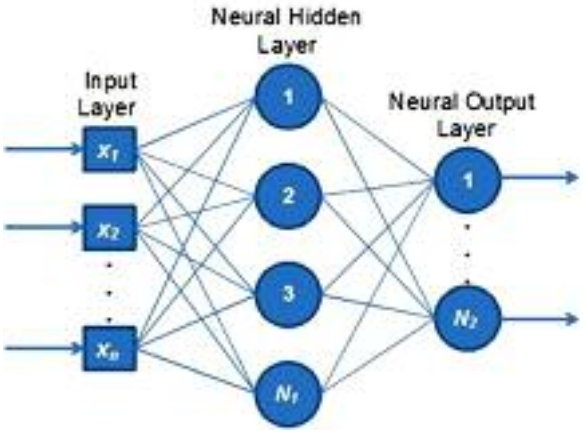

Figure 6: Artificial neural networks

process was conducted in order to enable the use of the data within the ANN structure. Thus, all the data obtained a value between 0-1. The formula used for the normalizing process is presented below (Aydogan *et al.,* 2011, Ismaila *et al.,* 2012):

$$X_N = 0.8x\left[\frac{X_R - X_{min}}{X_{max} - X_{min}}\right] + 0.1 \qquad (1)$$

X_N = *normalized data*
X_R = *data to be normalized*
X_{min} = *data with the smallest value*
X_{max} = *data with the biggest value*

MATLAB 2013a software was used for the ANN study. Back propagation (BP) algorithm, Levenberg-Marquardt Back propagation (TRAINLM), Gradient descent with momentum and adaptive learning rate back propagation (TRAINGDX) training functions were used for the ANN structure. Logsig was preferred as the transfer function. The ANN structure used in the study is presented in Figure 7. One input layer, one hidden layer and one

output layer were used in the ANN. While the engine speed and the fuel type of the test engine constituted the input values, torque, power, SFC, NOx and maximum cylinder inner pressure (Pmax) values constituted the output values. The performance of the ANN is directly affected by variables such as the number of the neurons in the hidden layer and the number of hidden layers. The configuration that yielded the best correlation coefficients were tried to be created by forming different ANN configurations. The number of the neurons in the hidden layer was selected as 6, 7, 8, 9, 10, 15, 20 and 50 and the ANN application was repeated. As the result of the study, it was found that the best correlation values were obtained through using TRAINLM training function, logsig transfer function and 20 neurons in the hidden layer (Table 1). The formula of the logsig transfer function is presented below. Mean squared error (MSE) was used for the performance index of the TrainLM algorithm and its formula is given below (Aydogan et al., 2011):

$$\text{logsig}(n) = \left(\frac{1}{1+e^{-n}}\right) \quad (2)$$

$$MSE = \frac{1}{n}\sum_{i=1}^{n}(y_i - y_i)^2 \quad (3)$$

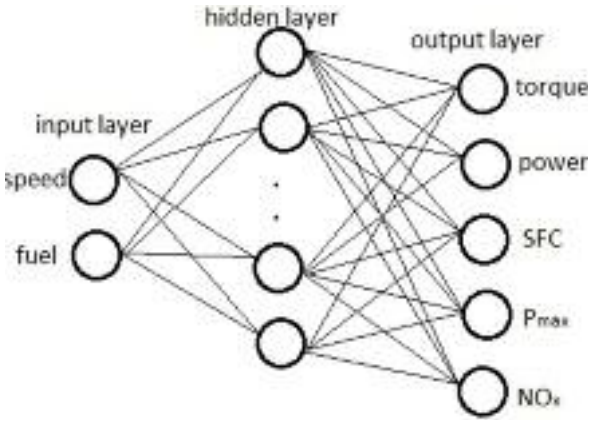

Figure 7: Architecture of the NN model

where, y_i is predicted value of i^{th} pattern, y_k is the target value of the i^{th} pattern and n is the number of patterns. R values of training, validation and test data of the ANN created in the study are presented in Figure 8.

Engine power, engine torque, BSFC, NOx and Pmax values, both experimental and predicted through ANN, are graphically presented in Figure 9. When the Figure. is examined, it can be seen that the predicted values and experimental values are close to one another. The closeness of the values

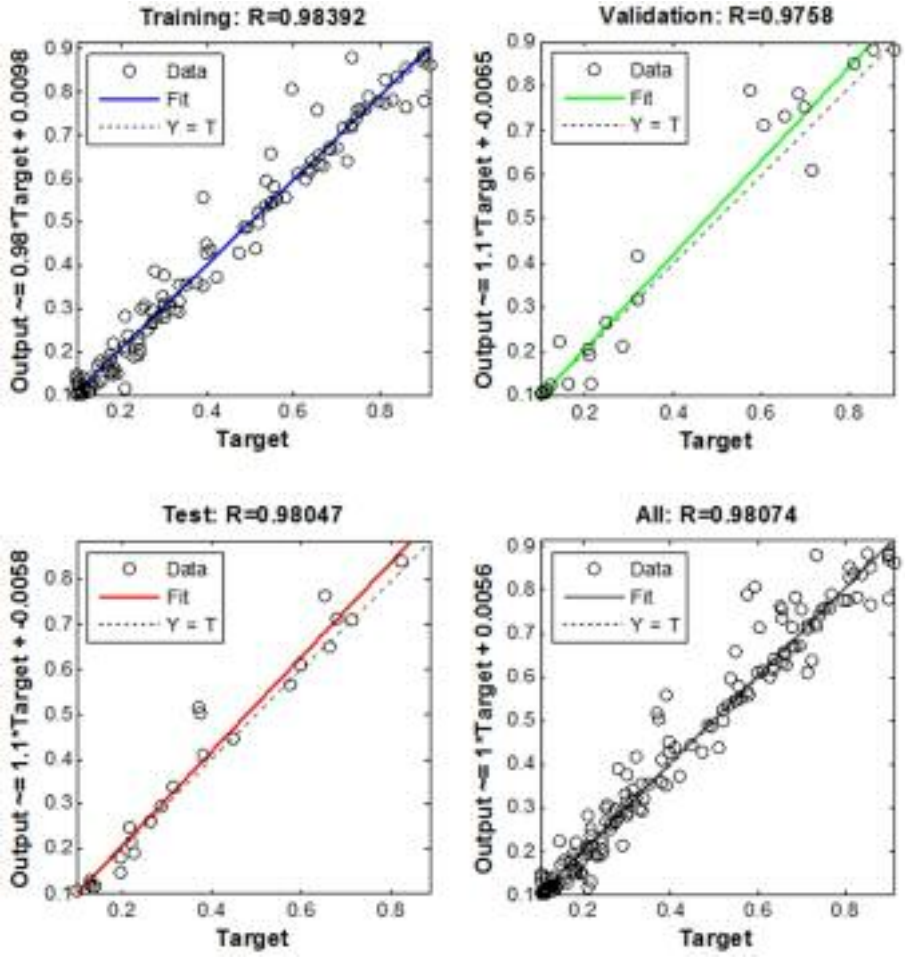

Figure 8: R values of training, validation and test data

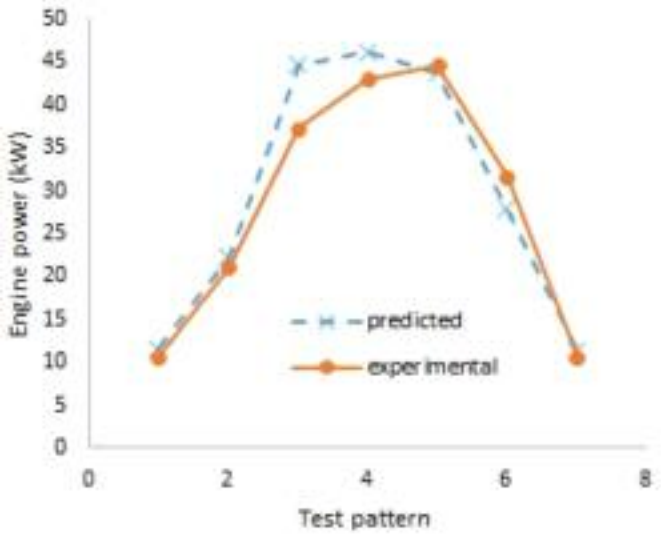

(a)

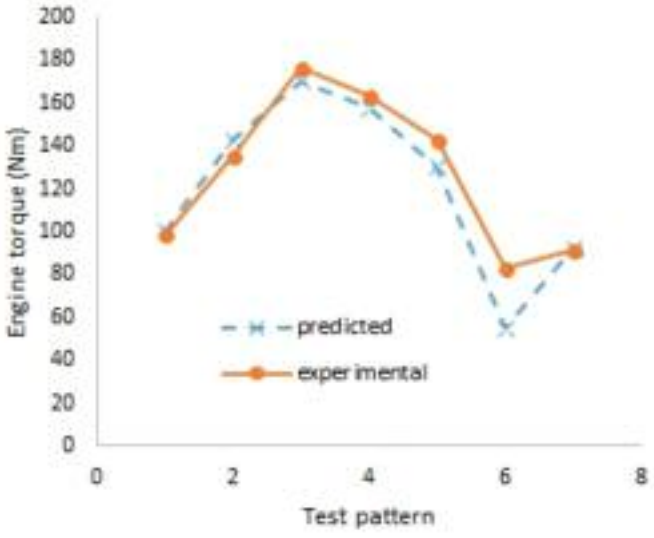

(b)

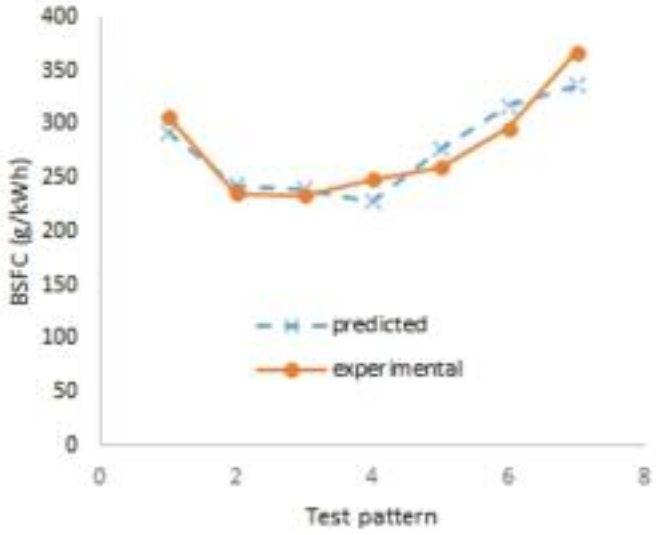

(c)

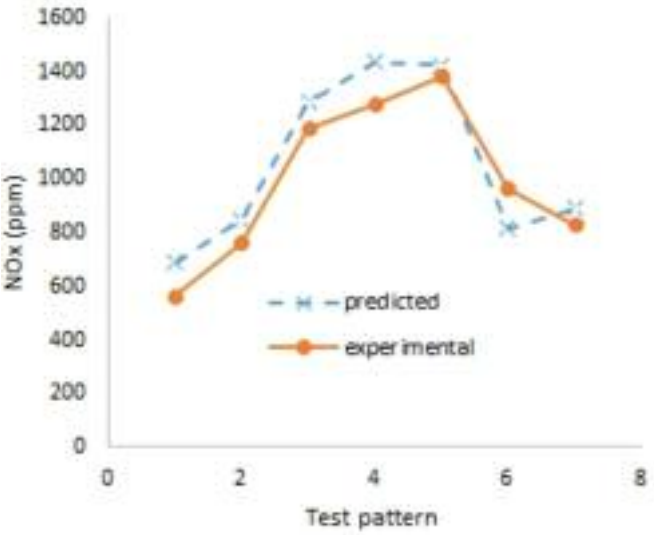

(d)

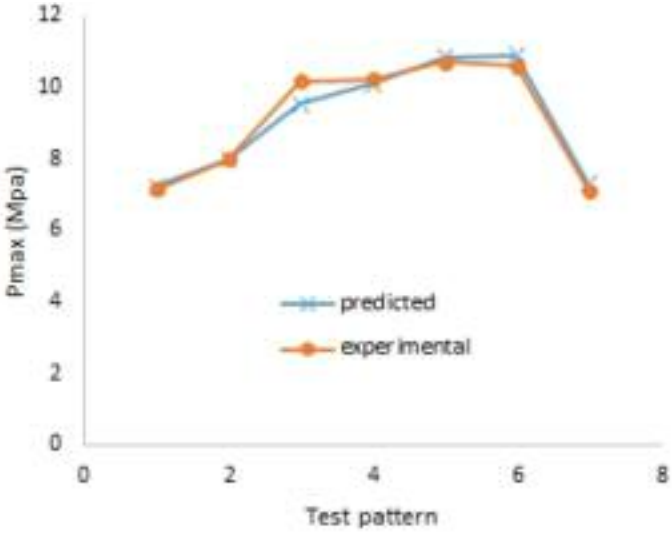

(e)

Figure 9: Comparisons of experimental results and the ANN predictions for (a) engine power, (b) Engine Torque, (c) BSFC (d) NOx (e) Pmax for various test patterns

Table 4: Training and testing results

Hidden layer neurons	*Training function*	*Transfer function*	*MSE*	*R^2 (ALL)*	*R^2 (Training)*	*R^2 (Testing)*
6	TRAINLM	LOGSIG	0,001573	0,9671	0,9577	0,9911
7	TRAINLM	LOGSIG	0,002476	0,9756	0,9734	0,9979
8	TRAINLM	LOGSIG	0,006305	0,9844	0,9916	0,9892
9	TRAINLM	LOGSIG	0,007409	0,9608	0,9970	0,7111
10	TRAINLM	LOGSIG	0,00475	0,9178	0,9597	0,6370
15	TRAINLM	LOGSIG	0,001802	0,9811	0,9779	0,9992
20	TRAINLM	LOGSIG	0,001558	0,9807	0,9839	0,9805
6	TRAINGDX	LOGSIG	0,063115	0,7065	0,7072	0,9248
7	TRAINGDX	LOGSIG	0,035614	0,7165	0,7213	0,7210
8	TRAINGDX	LOGSIG	0,085569	0,5191	0,5150	0,5332
9	TRAINGDX	LOGSIG	0,033121	0,8399	0,8477	0,8600
10	TRAINGDX	LOGSIG	0,010719	0,9554	0,9596	0,9724
15	TRAINGDX	LOGSIG	0,043304	0,8050	0,7890	0,9426
20	TRAINGDX	LOGSIG	0,027462	0,7439	0,7283	0,7688

shows that the created ANN structure was successful. The correlation coefficient found around 0.98 also supports this claim.

5. Conclusions

The changes in performance, emission and ignition characteristics that occurred through the use of bioethanol-safflower biodiesel and diesel fuel blends in a diesel engine with a common rail fuel system were investigated in the present study. An ANN approach was applied by using the data obtained in the experimental studies. Torque, power, SFC, Pmax and NOx values in a diesel engine were tried to be predicted though ANN. ANN training was performed by randomly selecting the 70% of the data obtained in the experimental study. The remaining 30% was used for testing purposes. Values that were substantially close to the experimental values were predicted through the ANN application. In conclusion, it was seen that ANNs could be used for predicting performance and emission values in internal combustion engines. In this way, it would be possible to conduct time and cost efficient studies instead of long experimental ones.

Acknowledgements

This study was supported by the Selcuk University Scientific Research Projects Centre.

References

Acaroglu, M. and Aydogan, H. (2012). Biofuels energy sources and future of biofuels energy in Turkey. *Biomass & Bioenergy,* 36:69-76.

Adeyemo O, Wise R, and Brent A, (2011). The impacts of biodiesel feedstock production systems in South Africa: An application of a Partial Equilibrium Model to the Eastern Cape Social Accounting Matrix, *Journal of Energy in Southern Africa,* 22(1);1-11.

Agarwal, A.K. and Dhar, A. (2013). Experimental investigations of performance, emission and combustion characteristics of Karanja oil blends fuelled DICI engine. *Renewable Energy,* 52:283-291.

Amiri, S., Mehrnia, M.R., Barzegari, D., and Yazdani, A. (2011). An artificial neural network for prediction of gas holdup in bubble columns with oily solutions. *Neural Computing and Applications,* 20:487-494.

Armas, O., Martínez-Martínez, S., and Mata, C. (2011). Effect of an ethanol–biodiesel–diesel blend on a common rail injection system. *Fuel Processing Technology,* 92:2145-2153.

Aydogan, H., Altun, A.A., and Ozcelik, A.E. (2011). Performance Analysis of a Turbocharged Diesel Engine Using Biodiesel with Back Propagation Artificial Neural Network. *Energy Education Science and Technology Part A.,* 28:459-468.

Aydogan, H., Ozcelik, A.E., and Acaroglu, M. (2011). The Effect of Peanut Oil Methyl Ester on the Performance and Emissions of a Diesel Engine with a Pump Injection Fuel System. *Energy Education Science and Technology Part A,* 28:189-200.

Balti, A., Sayadi, M., and Fnaiech F. (2013). Fingerprint Verification Based on Back Propagation Neural Network. *Control Engineering and Applied Informatics,* 15(3):53-60.

Breda, K. (2011). In□uence of biodiesel on engine combustion and emission characteristics. *Applied Energy,* 88:1803-1812.

Brunschwig, C., Moussavou, W., and Blin, J. (2012). Use of bioethanol for biodiesel production. *Progress in Energy and Combustion Science,* 38:283-301.

Canakci, M., Erdil, A., and Arcaklioglu, E. (2006). Performance and exhaust emissions of a biodiesel engine. *Applied Energy,* 83:594-605.

Cay, Y. (2013). Prediction of a gasoline engine perform-

ance with artificial neural network. *Fuel,* 111:324-331.

Demirbas, A. (2008). Biofuels sources, biofuel policy, biofuel economy and global biofuel projections. *Energy Conversion and Management,* 49:2106-2116.

Ma, Y., Zhu, M., and Zhang, D. (2013). The effect of a homogeneous combustion catalyst on exhaust emissions from a single cylinder diesel engine. *Applied Energy,* 102:556-562.

Fahd M.E.A., Wenming, Y., Lee, P.S., Chou, S.K., and Yap, C.R. (2013). Experimental investigation of the performance and emission characteristics of direct injection diesel engine by water emulsion diesel under varying engine load condition. *Applied Energy,* 102:1042-1049.

Ghazikhani, M., and Mirzaii, I. (2011). Soot emission prediction of a waste-gated turbo-charged DI diesel engine using artificial neural network. *Neural Computing and Applications,* 20:303-308.

Ghobadian, B., Rahimi, H., Nikbakht, A.M., Najafi, G., and Yusaf, T.F. (2009). Diesel engine performance and exhaust emission analysis using waste cooking biodiesel fuel with an artificial neural network. *Renewable Energy,* 34:976-982.

Guido, C., Beatrice. C., and Napolitano, P. (2013). Application of bioethanol/RME/diesel blend in a Euro5 automotive diesel engine: Potentiality of closed loop combustion control technology. *Applied Energy,* 102:13-23.

Hadi, R., Barat, G., Talal, Y., Gholamhasan, N., and Mahdi, K. (2009). Diesterol: an environment friendly IC engine fuel. *Renewable Energy,* 34:335-342.

Hafaifa, A., Djeddi, A.Z., and Daoudi A. (2013). Fault detection and isolation in industrial control valve based on artificial neural networks diagnosis. *Control Engineering and Applied Informatics,* 15(3):61-69.

Hazar, H. (2010). Cotton methyl ester usage in a diesel engine equipped with insulated combustion chamber. *Applied Energy,* 87:134-140.

Hsieh, W.D., Chen, R.H., Wu, T.L., and Lin, T.H. (2002). Engine performance and pollutant emission of an SI engine using ethanol–gasoline blended fuels. *Atmospheric Environment,* 36:403-410.

Hulwan, D.B., and Joshi, S.V. (2011). Performance, emission and combustion characteristic of a multicylinder DI diesel engine running on diesel-ethanol–biodiesel blends of high ethanol content. *Applied Energy,* 88:5042-5055.

Ioanaş, G.L. (2002). Modelling, Identification and Prediction of Inherent quasi-stationary Pressure Dynamics of a Common-Rail System using Neuro-Fuzzy Structures with Local Linear ARX models. *Control Engineering and Applied Informatics,* 14(3):61-70.

Ismaila, H.M., Nga, H.K., Quecka, C.W., and Ganb, S. (2012). Artificial neural networks modelling of engine-out responses for a light-duty diesel engine fuelled with biodiesel blends. *Applied Energy,* 92:769-777.

Park, S.H., and Lee, C.S. (2013). Combustion performance and emission reduction characteristics of automotive DME engine system. *Progress in Energy and Combustion Science,* 39:147-168.

Kannan, G.R., Karvembu, R., and Anand, R. (2011). Effect of metal based additive on performance emission and combustion characteristics of diesel engine fuelled with biodiesel. *Applied Energy,* 88:3694-3703.

Morisugi, H., Ohno, E. (1996). NOx Reduction Effects of the Policy to Reduce Diesel Automobiles and its Influence on Price Change. *Transport, Land-Use and the Environment Transportation Research, Economics and Policy*, 171-190.

Mrad, N., Varuvel, E.G., Tazerout, M., and Aloui, F. (2012). Effects of biofuel from fish oil industrial residue – Diesel blends in diesel engine. *Energy,* 44:955-963.

Park, S.H., Cha, J., and Lee, C.S. (2012). Impact of biodiesel in bioethanol blended diesel on the engine performance and emissions characteristics in compression ignition engine. *Applied Energy,* 99:334-343.

Pilusa T.J., Huberts R., and Muzenda E. (2013). Emissions analysis from combustion of eco-fuel briquettes for domestic applications. *Journal of Energy in Southern Africa,* 24 (4): 30-36.

Qi, D.H., Chen, H., Geng, L.M., and Bian, Y.Z. (2011). Effect of diethyl ether and ethanol additives on the combustion and emission characteristics of biodiesel-diesel blended fuel engine. *Renewable Energy,* 36:1252-1258.

SAE (2001). *SAE handbook,* MI Vol. 1, Warrendale, SAE: 1304-1306.

Sefriti, S., Boumhidi, J., Naoual, R., and Boumhidi, I. (2002). Adaptive Neural Network Sliding Mode Control for Electrically-Driven Robot Manipulators. *Control Engineering and Applied Informatics,* 14(4):27-32.

Sharkey, A.J.C., Chandroth, G.O., and Sharkey, N.E., (2000) A Multi-Net System for the Fault Diagnosis of a Diesel Engine. *Neural Computing and Applications,* 9:152-160.

Shi, X., Yu, Y., He, H., Shuai, S., Wang, J., and Li, R. (2005). Emission characteristics using methyl soyate–ethanol–diesel fuel blends on a diesel engine. *Fuel,* 84:1543–1549.

Singh, A.K., Tyagi, B., Kumar, V. (2013). Application of Neural Network based Control Strategies to Binary Distillation Column. *Control Engineering and Applied Informatics,* 15(4):47-57.

Soloiu, V., Duggan, M., Harp, S., Vlcek, B., and Williams, D. (2013). PFI (port fuel injection) of n-butanol and direct injection of biodiesel to attain LTC (low-temperature combustion) for low-emissions idling in a compression engine. *Energy,* 52:143-154.

Stone, R. (1999). *Introduction to internal combustion engines.* 3rd Ed. New York: Macmillan.

Torrisi, N.M., and Sabino, M. (2013). Biodiesel production control using PNN and Coriolis flowmeter. *Neural Computing and Applications,* 23:1275-1282.

Uzun, A. (2014). Air mass flow estimation of diesel engines using neural network. *Fuel,* 117:833-838.

Yilmaz, N., and Sanchez, T.M. (2012). Analysis of operating a diesel engine on biodiesel-ethanol and

biodiesel-methanol blends. *Energy,* 46:126-129.
Yilmaz, S., and Bilgin, M.Z. (2013). Modelling and simulation of injection control system on a four-stroke type diesel engine development platform using artificial neural networks. *Neural Computing and Applications,* 22:1713-1725.
Zhou, J.H., Cheung, C.S., and Leung, C.W. (2013). Combustion, performance and emissions of ULSD, PME and B50 fuelled multi-cylinder diesel engine with naturally aspirated hydrogen. *International Journal of Hydrogen Energy,* 34: 14837–14848.
Zhu, L., Cheung, C.S., Zhang, W.G., and Huang, Z. (2010). Emissions characteristics of a diesel engine operating on biodiesel and biodiesel blended with ethanol and methanol. *Science of the Total Environment,* 408: 914-921.

Received 12 April 2014; revised 14 April 2015

Exhaust gas treatment for reducing cold start emissions of a motorcycle engine fuelled with gasoline-ethanol blends

A Samuel Raja

A Valan Arasu

Department of Mechanical Engineering, Thiagarajar College of Engineering, Madurai, Tamilnadu, India

Abstract

In countries like India, transportation by a two wheeled motorcycle is very common owing to affordable cost, easy handling and traffic congestion. Most of these bikes use single cylinder air cooled four-stroke spark ignition (SI) engines of displacement volume ranging from 100 cm^3 to 250 cm^3. CO and HC emissions from such engines when started after a minimum stop-time of 12 hours or more (cold-start emissions) are higher than warmed-up emissions. In the present study, a 150 cm^3 single cylinder air cooled SI engine was tested for cold start emissions and exhaust gas temperature. Different gasoline-ethanol blends (E0 to E20) were used as fuel expecting better oxidation of HC and CO emissions with additional oxygen present in ethanol. The effect of glow plug assisted exhaust gas ignition (EGI) and use of catalytic converter on cold start emissions were studied separately using the same blends. Results show that with gasoline-ethanol blends, cold start CO and HC emissions were less than that with neat gasoline. And at an ambient temperature of 30±1°C, highest emission reductions were observed with E10. EGI without a catalytic converter had no significant effect on emissions except increasing the exhaust gas temperature. The catalytic converter was found to be active only after 120 seconds in converting cold start CO, HC and NO_x. Use of a catalytic converter proves to be a better option than EGI in controlling cold start emissions with neat gasoline or gasoline-ethanol blends.

Keywords: cold start, gasoline-ethanol blends, exhaust gas ignition, glow plug

1. Introduction

Emissions from an internal combustion engine, started after a minimum halt time of 12 hours or more, are known as cold start emissions (Favez *et al.,* 2009). Carbon monoxide (CO) and unburnt hydrocarbon (HC) are emitted in larger quantities during the first few minutes of a spark ignition (SI) engine with cold start because of the inactive or less active catalytic converter (Iliyas *et al.,* 2007). The catalytic conversion is more effective only after the catalyst reaches its light-off temperature which is above 150°C (Singer *et al.,* 1999). The time period required for the catalyst to reach its light-off temperature is referred to as cold-start period or unstable engine running period. In water cooled engines, stable engine operation is achieved at coolant temperature of about 70°C and it may take 6 to 7 minutes of the engine running after cold start (Botsaris *et al.,* 2003). In air cooled SI engines, stable engine operation is achieved earlier than water cooled SI engines due to higher exhaust temperatures resulting from less effective cooling by air. The test engine in the current work is a single cylinder air cooled engine and hence cold start emissions and exhaust temperature have been recorded for the first four minutes after a cold start.

Generally, engine-out emissions are controlled in any one or two or all of the three techniques namely fuel modification, engine modification and exhaust gas treatment. Fuel modification (gasoline-ethanol blends) and exhaust gas treatment (exhaust gas ignition and catalytic converter) are attempted in the current work. Considering fuel modification for SI engines, gasoline-ethanol blends have been reported as a suitable alternate fuel for neat gasoline by various researchers (Pourkhesalian *et al.,* 2010; Bayraktar, 2005; Eyidogan *et al.,* 2010) all over the world. The two factors that make gasoline-ethanol blends suitable for S.I. Engines are the presence of an oxygen atom in the fuel structure of ethanol and a higher octane number of ethanol

than that of gasoline. According to different researchers (Balki *et al.,* 2012; Masum *et al.,* 2013; Canakci *et al.,* 2013), the optimum blend may contain 5 percent ethanol to 20 percent ethanol. This variation is due to difference in the experimented parameters such as compression ratio, ignition timing, engine load and speed. In the current work, no modification was made in the compression ratio and ignition timing. Ethanol was blended with gasoline in 5, 10, 15 and 20 percent by volume and the blend is correspondingly named E5, E10, E15 and E20. The RVP (Reid Vapour Pressure) of ethanol is 17 kPa, far lower than 53.7 kPa for gasoline. But their mixture does not have an RVP value linearly proportional to the volume fraction. A volume fraction of 5 to 10% ethanol can achieve the maximal RVP and thus facilitate cold-start (Thring, 1983). On account of higher latent heat of vaporization of ethanol, poor cold start performance has been observed with such blends when used in a water cooled engine (Turner *et al.,* 2011; Clairotte et al., 2013). But with electronic fuel injection, the optimum percentage of ethanol in the blend for least cold-start emissions is reported to be at least 20 but not exceeding 30 (Chen *et al.,* 2011). It is also reported that E10 blend results in higher acetaldehyde and ethanol emissions compared to neat gasoline (Poulopoulos & Philippopolous, 2003).

In order to overcome the poor vaporization effect of ethanol, modifications in the engine such as heated intake air or/and heated intake fuel system have been attempted (Spegar *et al.,* 2012; Sales & Sodré, 2012; Raja & Arasu, 2014). This modification has not only reduced cold-start CO and HC but also has increased exhaust gas temperature which enables the catalytic converter (if used) to reach its light-off temperature quicker.

Among various exhaust gas treatment techniques for SI engines, use of a catalytic converter is popular owing to its ability to convert the harmful CO,HC and NO_x emissions into CO_2, H_2O, O_2 and N_2 in stable engine running conditions (Twigg, 2007). The substrate used in a catalytic converter can be ceramic or metallic. At low speeds, conversion of HC emissions is higher with a ceramic substrate whereas a metallic substrate behaves better at higher engine speeds and higher exhaust temperatures. But the substrate type has a less significant effect on CO or NO_x conversion (Santos & Costa, 2008). Among the various metals, Platinum (Pt), Palladium (Pd) and Rhodium (Rh) have been found to remain metallic and not to form volatile metallic oxides. Due to this reason, currently Pt or Pd is used for conversion of CO and HC emissions and Rh is used for conversion of NO_x emissions (Twigg, 2006) in the present day catalytic converters. In the current work, a catalytic converter of metallic substrate loaded with Pd and Rh catalysts in the ratio of 37:3 g/ft^3 has been used.

To increase the catalyst surface temperature quickly to its light-off temperature, glow plugs installed at the front and at the middle of converter have been used to heat the metal substrate and hence the catalyst (Horng & Chou, 2004). The results show that CO oxidation was higher with heating at inlet and at catalyst temperature of 180°C.

Though adequate literature is available on the effect of gasoline-ethanol blends in water cooled engines, only a few references (Leong *et al.,* 2002; Yang *et al.,* 2005) are available for air cooled engines. Moreover, the effect of EGI or the effect of a catalytic converter in such engines fuelled with gasoline-ethanol blends, on cold-start emissions has not been addressed. The aim of the present work is to fill this gap and hence it focuses on the experimental study on the effect of EGI or use of a catalytic converter on cold-start emissions of an air cooled motorcycle engine fuelled with gasoline-ethanol blends.

2. Experimental set-up and procedure

A single cylinder air cooled motorcycle SI engine with specifications shown in Table.1 was used to conduct experiments which were conducted in three phases. In the first phase, cold start emissions and exhaust temperature were recorded for neat gasoline and gasoline ethanol blends without a catalytic converter and without exhaust gas ignition. These experiments were carried out to study the effect of gasoline-ethanol blends alone in the cold start emissions. In the second phase, experiments were done with the same fuels with exhaust gas ignition (EGI) using a glow plug. The glow plug was mounted after the exhaust port. The objective of this phase is to study the effect of EGI alone on cold start emissions. As a considerable percentage of two wheelers (manufactured before 2010) are still running on roads without a catalytic converter, these two sets of experiments were performed to study the effect of gasoline-ethanol blends and EGI on motorcycle engines equipped with no catalytic converter. To meet the stringent emission norms, from 2010 onwards, a 4-stroke motorcycle S.I. Engine is fitted with a catalytic converter. Hence, third phase of experiments was completed with the same fuel blends with a catalytic converter and without EGI to study the effect and behaviour of a catalytic converter alone on cold start emissions.

The exhaust pipe of the test engine was modified to accommodate a catalytic converter, glow plug, thermocouples and an exhaust gas sampling probe at the required locations and their positions are indicated in Figure.1. A time interval of 12 hours was given between each experiment to ensure a cold start. An idling speed of 1400 ± 50 rpm was maintained in all experiments. The fuel blends were prepared just before starting the exper-

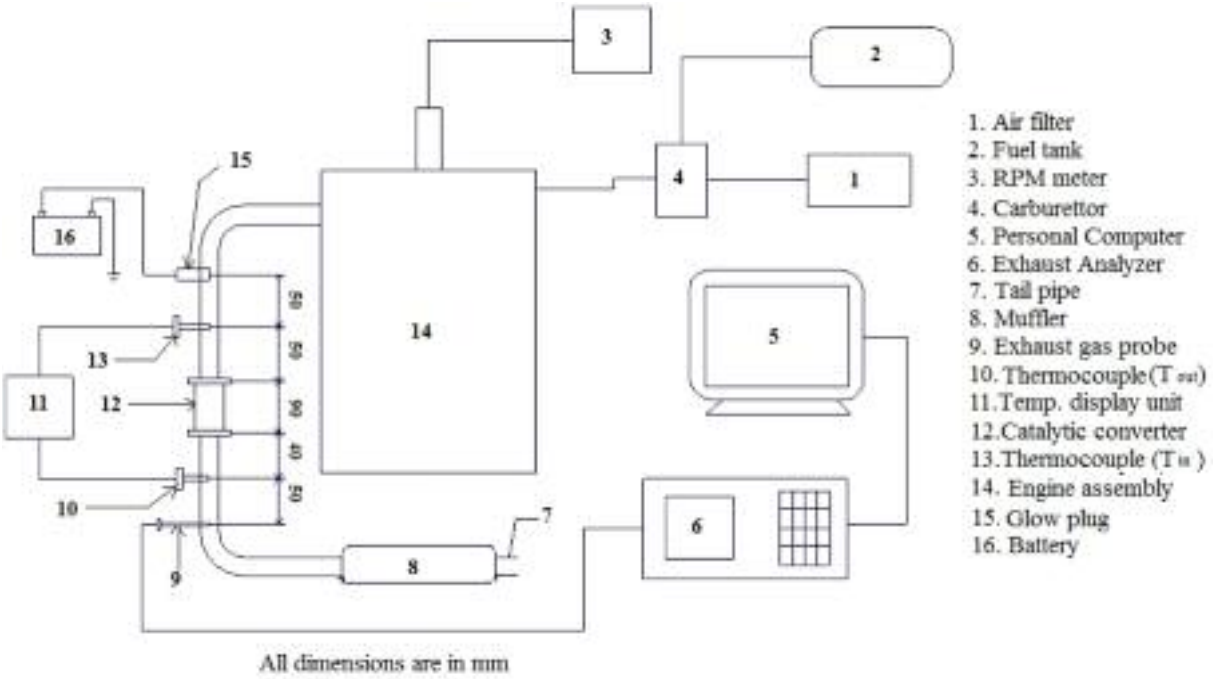

Figure 1: Experimental set-up

Table 1: Engine specifications

Engine Type	Four-stroke, air cooled, single cylinder, SI Engine
Bore x Stroke	58 mm x 56.4 mm
Maximum power	11 kW @ 8500 rpm
Maximum Torque	12.76 Nm @ 6500 rpm
Compression ratio	9.5:1
Fuel supply system	Constant Vacuum carburettor
Fuel	unleaded gasoline + anhydrous ethanol
Idling speed	1400 ± 50 rpm
Valve timing	Intake opens 12.1° CA before TDC
	Intake closes 55.5° CA after BDC
	Exhaust opens 36.5° CA before BDC
	Exhaust closes 14.1° CA after TDC
Ignition timing	9.1° CA before TDC

Table 2: Fuel properties

Property	*Gasoline*	*Ethanol*
Formula (liquid)	C_8H_{18}	C_2H_6O
Molecular weight (kg / kmol)	114.15	46.07
Density (kg/m^3)	765	785
Heat of vaporization (kJ/kg)	305	840
Specific heat (kJ/kg K) Liquid	2.4	1.7
Specific heat (kJ/kg K) Vapour	2.5	1.93
Lower Heating Value (kJ/kg)	44,000	26,900
Stoichiometric air–fuel ratio by mass	14.6	9.00
Research Octane Number	92	108.6
Motor Octane Number	85	89.7
Enthalpy of formation (MJ/kmol) Liquid	259.28	224.10
Enthalpy of formation (MJ/kmol) Gas	277.0	234.6

iment to ensure that the fuel mixture was homogenous and no water was formed by reaction of ethanol with water vapour in the atmosphere. Properties of neat gasoline and neat ethanol are given in Table 2.

As the multiple attempts to start the engine affected the cold start emissions considerably, adequate care was taken to start the engine in the first attempt using the starter motor. Emissions were recorded for every two seconds for 4 minutes from the engine start by 5-gas analyser with specifications shown in Table 3 and the values were stored in a personal computer interfaced with an exhaust gas analyser. In the third phase of experiments, a new catalytic converter with specifications shown in Table 4 was used. Exhaust gas temperatures before and after the catalytic converter were measured using K-type thermocouples.

Table 3: Exhaust gas analyser specifications

Gas	*Range(by volume)*	*Accuracy*	*Resolution*
CO	0 to 10%	± 0.06 %	0.01 %
HC	0 to 10000 ppm	± 12 ppm	1ppm
CO_2	0 to 20%	± 0.5 %	0.1 %
O_2	0 to 25%	± 0.1 %	0.01 %
NO_x	0 to 2000 ppm	± 5 ppm	1 ppm

Table 4: Catalytic converter specifications

Composition	JM665/40/0:37:3
Catalyst loading	40 g / ft^3
Platinum	0 g / ft^3
Palladium	37 g / ft^3
Rhodium	3 g / ft^3
Size (diameter x length)	33 x 60 mm
Number of cells/ square inch (cpsi)	100

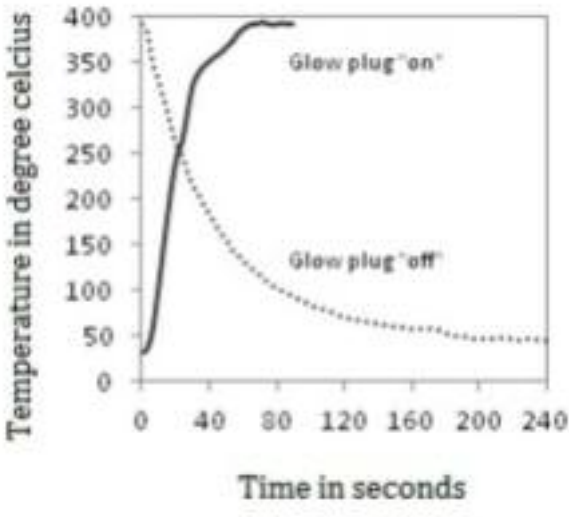

Figure 2: Glow plug surface temperature
Source: Raja & Arasu (2014)

An extra 12V, 80 Ah battery was used as power source to energize the glow plug for the exhaust gas ignition. The voltage and amperage for the glow plug were 11.9 V and 4.65 A respectively. To understand the characteristics of the glow plug, it was energized continuously by battery and its surface temperature was measured in still air condition after installing the glow plug in the exhaust pipe. At about 60 seconds, it reached the highest temperature (390°C) and remained constant. At this point of time, power supply was cut and the surface temperature was measured. At about 200 seconds, it reached almost a constant value of 50°C. The variation of glow plug surface temperature with time during on and off conditions is shown in Figure 2 (Raja & Arasu, 2014).

3. Results and discussion

3a) Phase 1 experiments – no modifications to the exhaust system

The variations of exhaust emissions (CO, HC, CO_2, O_2 and NO_x) and exhaust temperature with time in seconds are shown in Figure 3. It illustrates the sole effect of gasoline ethanol blends on cold start emissions in the absence of EGI and a catalytic converter. On comparison with neat gasoline, all blends showed reduction in CO, HC, NO_x emissions and exhaust temperature. But there was an increase in O_2 and CO_2 emissions. The reduction in CO and HC emissions is due to the excess oxygen present in ethanol structure and this is confirmed by the increase in CO_2 and O_2 emissions. The reason for reduction in exhaust gas temperature is the higher latent heat of vaporization of blends compared to that of neat gasoline. Normally, NO_x emissions are formed due to both oxygen availability and higher combustion temperature. Here, a drop in combustion temperature (inferred from exhaust temperature) plays a dominant role for reduction in NO_x emissions though oxygen content is in excess. Despite the fact that NO_x emissions are reported to be insignificant during cold-starts of gasoline and diesel fuelled engines (Weilenmann *et al.*, 2005), its variation with ethanol percentage in the blend is presented here to understand the effect of fuel, EGI and the catalytic converter.

CO and HC emissions generally decrease with higher oxygen content and higher combustion temperature. With gasoline-ethanol blends, oxygen percentage in the exhaust is increased and combustion temperature is decreased. Therefore, the factor which reduces CO emissions with E5 and E10 is higher oxygen availability and the factor which increases CO emissions with E15 and E20 is lower combustion temperature. The same reasoning holds good for the increase in HC emissions with E20 compared to that of E5, E10 and E15. To confirm these observations, experiments were conduct-

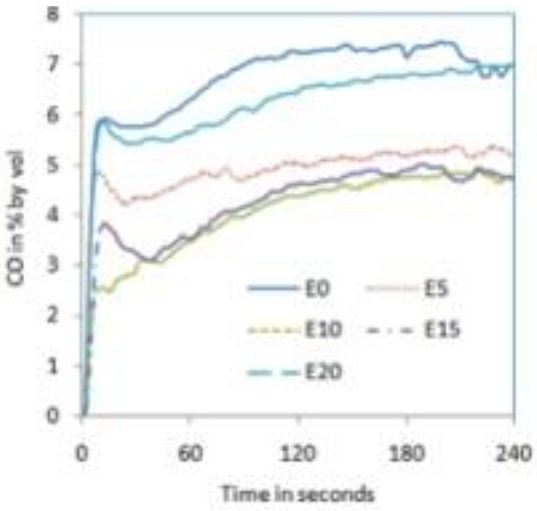

Figure 3a: Variation of CO with time

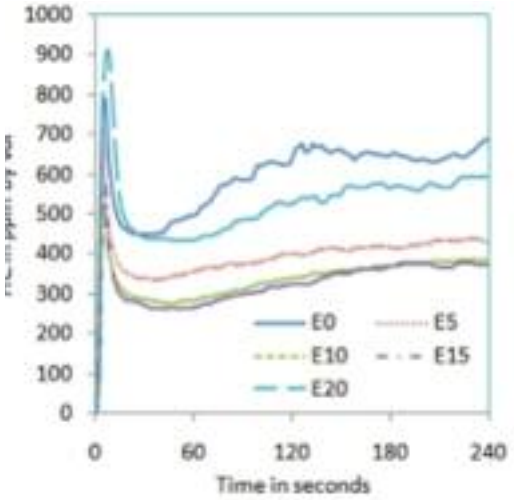

Figure 3b: Variation of HC with time

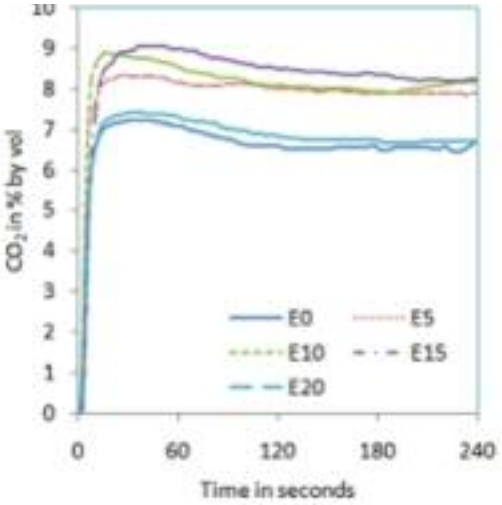

Figure 3c: Variation of CO_2 with time

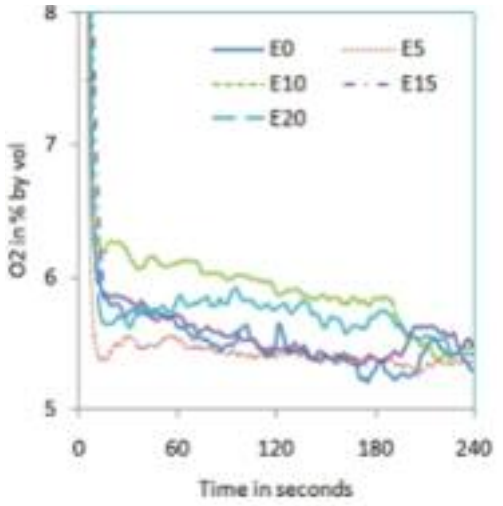

Figure 3d: Variation of O_2 with time

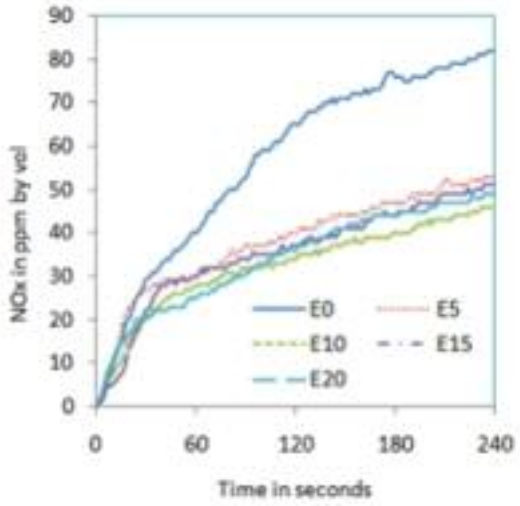

Figure 3e: Variation of NO_x with time

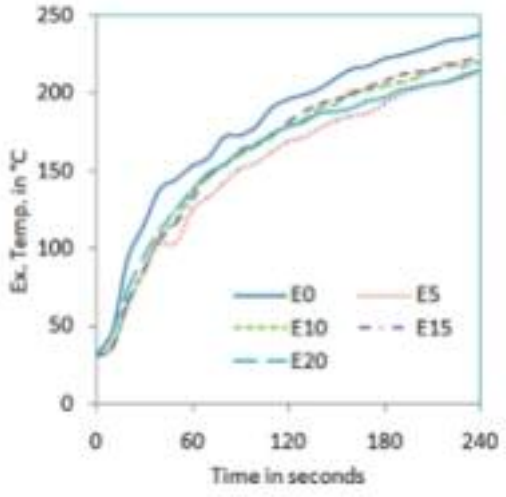

Figure 3f: Variation of Ex. Temp with time

Figure 3: Cold start emissions and exhaust temperature of phase 1 experiments

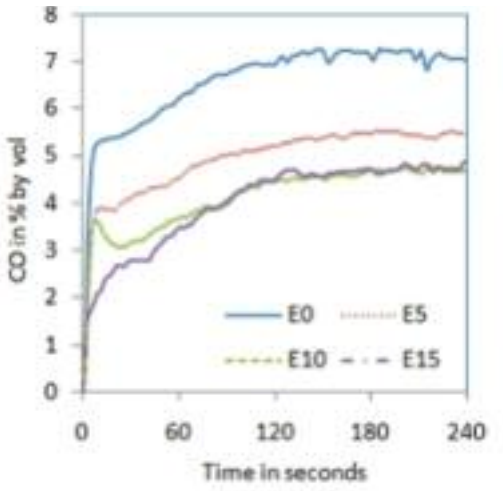

Figure 4a: Variation of CO with time

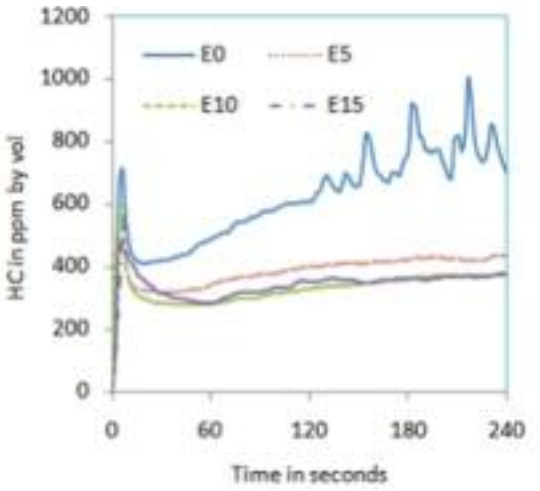

Figure 4b: Variation of HC with time

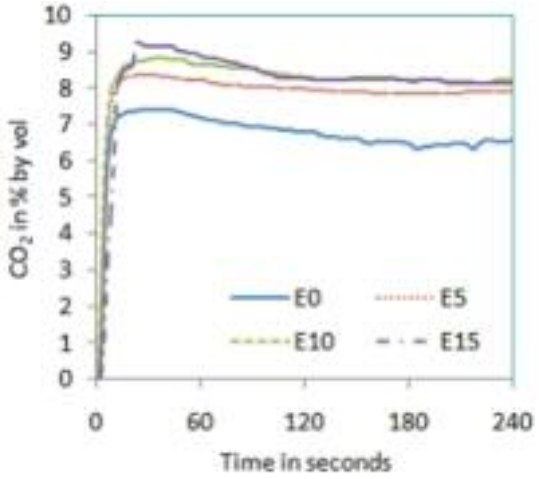

Figure 4c: Variation of CO_2 with time

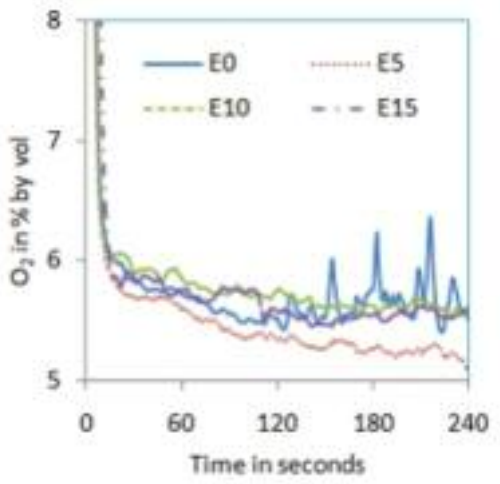

Figure 4d: Variation of O_2 with time

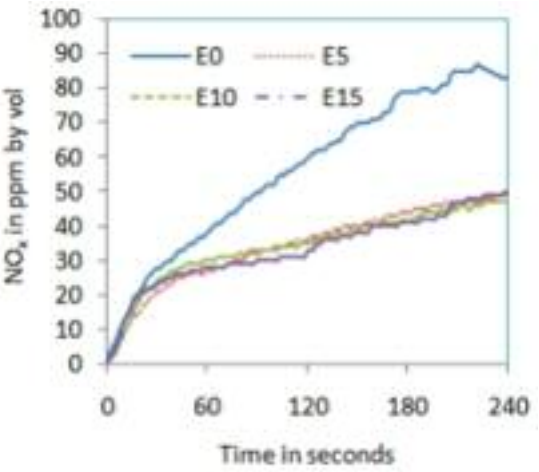

Figure 4e: Variation of NO_x with time

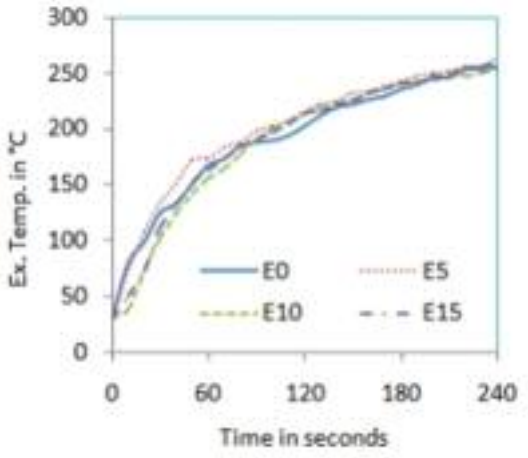

Figure 4f: Variation of Ex. Temp with time

Figure 4: Cold start emissions and exhaust temperature of phase-2 experiments

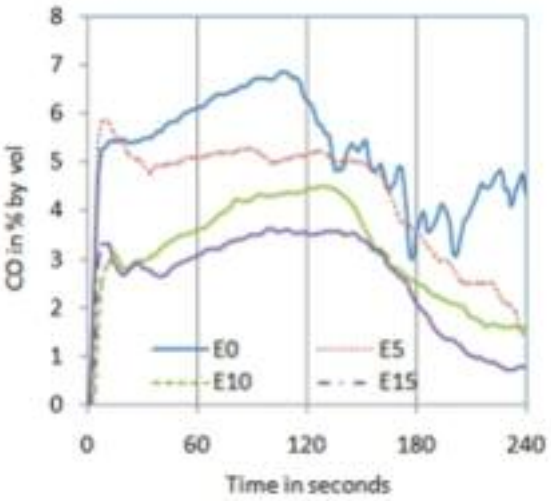

Figure 5a: Variation of CO with time

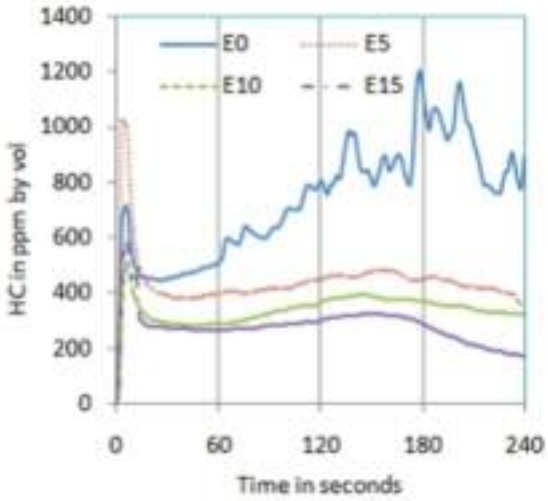

Figure 5b: Variation of HC with time

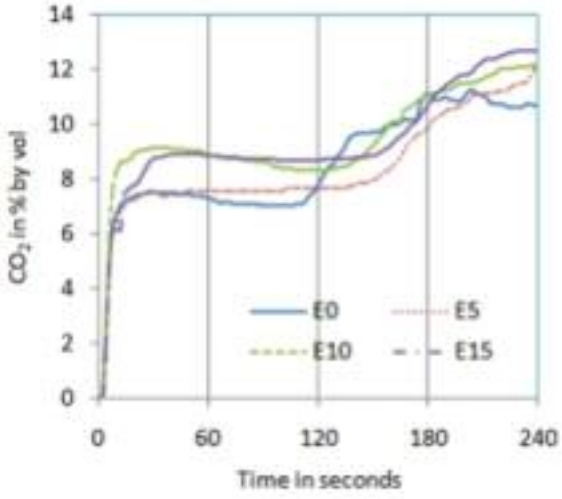

Figure 5c: Variation of CO_2 with time

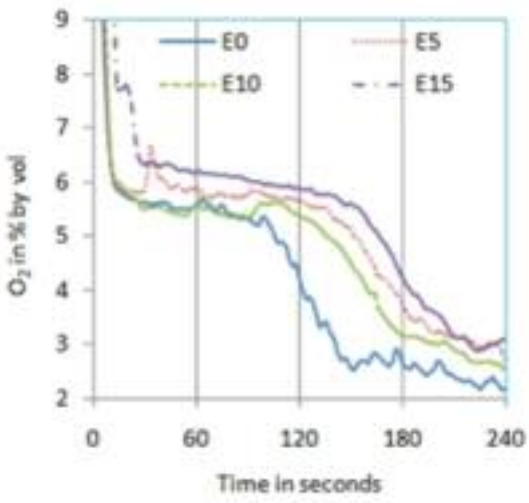

Figure 5d: Variation of O_2 with time

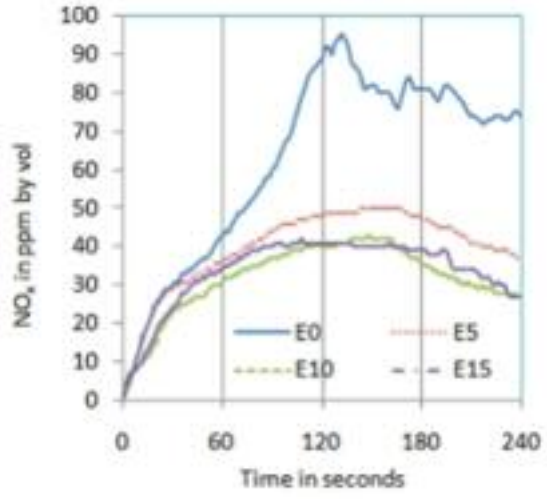

Figure 5e: Variation of NO_x with time

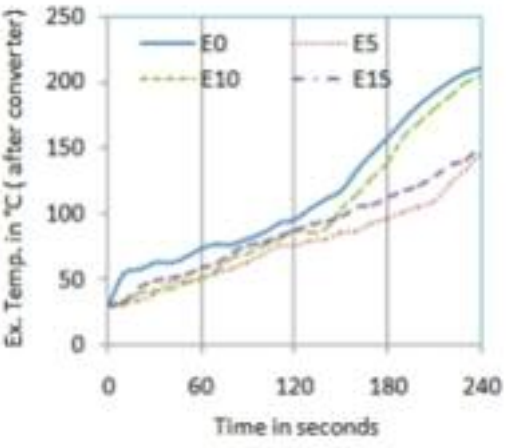

Figure 5f: Variation of Ex. Temp (after converter) with time

Figure 5: Cold start emissions and exhaust temperature of phase-3 experiments

ed with E25 which led to very high amounts of CO and HC emissions. The magnitudes were about 50 -75% higher (not shown in this paper) than those measured using neat gasoline and moreover unstable engine operation was noticed. This may be attributed to flame quenching and misfiring during combustion of E25 blend-air mixture. Hence, results are presented up to E20 in this paper. Taking average of CO and HC emissions for 4-minutes, highest reduction in CO (40%) was observed with E10 and highest reduction in HC (44.8%) was observed with E15, as shown in Figures 6 and 7 respectively.

3b) Phase 2 experiments – Impact of EGI

As E5, E10 and E15 showed better results compared to E20, these three blends were considered in the second and third phase of experiments. The first phase of experiments was repeated with EGI in the second phase for E0, E5, E10 and E15. Figure 4 shows the effect of gasoline ethanol blends and EGI on cold start emissions in the absence of a catalytic converter.

All emissions and exhaust gas temperature were almost similar for E10 and E15 with EGI. Comparing the 4-min average CO emissions for different blends to that of neat gasoline, highest CO reduction of 39% was observed for E15 and highest HC reduction of 46.5% was observed for E10 as shown in Figures 6 and 7 respectively. These reductions in CO and HC emissions reflect in the increase in CO_2 and decrease in O_2 as is shown in Figures.4c and 4d respectively. The decrease in CO and HC is due to the partial combustion with the support of EGI. NO_x emissions reduced with all blends in the same pattern as that without EGI which indicates that the effect of EGI is not predominant. The drop in exhaust gas temperature observed in the first phase of experiments is overcome with EGI in the second phase. Exhaust gas temperature of all blends was almost the same as that with neat gasoline as shown in Figure 4f.

Comparing reductions in CO and HC emissions without EGI, a marginal improvement has been observed with EGI for almost all blends. The only positive change noticed was increase in exhaust temperature, which may help reduction of cold start HC and CO emissions by shortening the light off period of catalytic converter, if used.

3c) Phase 3 Experiments – Catalytic convertor installed

In order to understand the behaviour of a catalytic converter with gasoline-ethanol blends during the cold start period, a third phase of experiments was conducted and the results are shown in Figure.5. For all blends, CO emissions started to decrease after about 130 seconds whereas this cut-off time was about 105 seconds for neat gasoline. The delay in the activation of the catalysts is due to the lower exhaust gas temperatures with blends compared to neat gasoline. However, the highest percentage reduction in 4-min average CO and HC observed were 49.8 and 62.5 respectively for E15, as shown in Figures.6 and.7 respectively. No positive effect was noticed in HC emissions for neat gasoline which reveal that the light off period for HC is longer than that for CO (Heywood, 1998). But with the blends, a slight reduction in HC was noticed after 150 seconds. The sudden increase in CO_2 and sudden decrease in O_2 at about 120 seconds confirm the action of the catalytic converter on CO and HC emissions. The decrease in NO_x after about 120 seconds further ascertains the redox nature of the catalysts used. The oxidation of CO and HC to CO_2 are exothermic reactions and the heat released increases exhaust gas temperature. The increase in the slope of the after–converter temperature curve at about 140 seconds (with E10 blend) confirms this effect and is shown in Figure 5f.

3d) Consolidated comparison of 4-minute average CO and HC emissions

The percentage reduction in 4-minute average CO and HC emissions compared to that of neat gasoline in each of these three phases are presented in Figures.6 and.7 respectively. (1 – without EGI and without catalytic converter, 2 – with EGI and without catalytic converter, 3 – without EGI and with catalytic converter).

4. Conclusion

Experiments were conducted in three phases on an air cooled four-stroke motorcycle S.I engine to (1) study the effect of gasoline-ethanol blends; (2) study the effect of exhaust gas ignition; and (3) study the effect of a catalytic converter on cold start emissions.

The impact of gasoline-ethanol blends alone ranging between E5 to E20 on cold-start emissions was studied in first phase experiments. E10 showed highest CO reduction (40%) and E15 showed highest HC reduction (44.8%). The same experiments were repeated with exhaust gas ignition (EGI) in the second phase to study the combined effect of gasoline-ethanol blends and EGI. Highest CO reduction of 39% was observed for E15 and highest HC reduction of 46.5% was observed for E10. From these two phases of experiments, it is concluded that gasoline-ethanol blends play a more important role in controlling cold start HC and CO emissions than the glow plug assisted exhaust gas ignition.

The combined effect of impact of a catalytic converter and gasoline-ethanol blends on cold-start emissions was studied through a third phase of experiments. It was found that a catalytic converter starts functioning after the light off period of 130 seconds or more for gasoline-ethanol blends where-

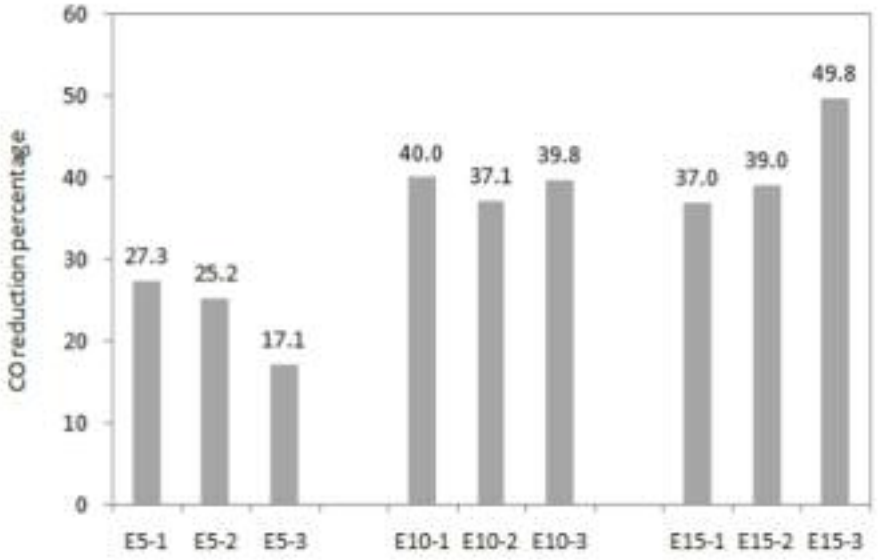

Figure 6: CO reduction percentage

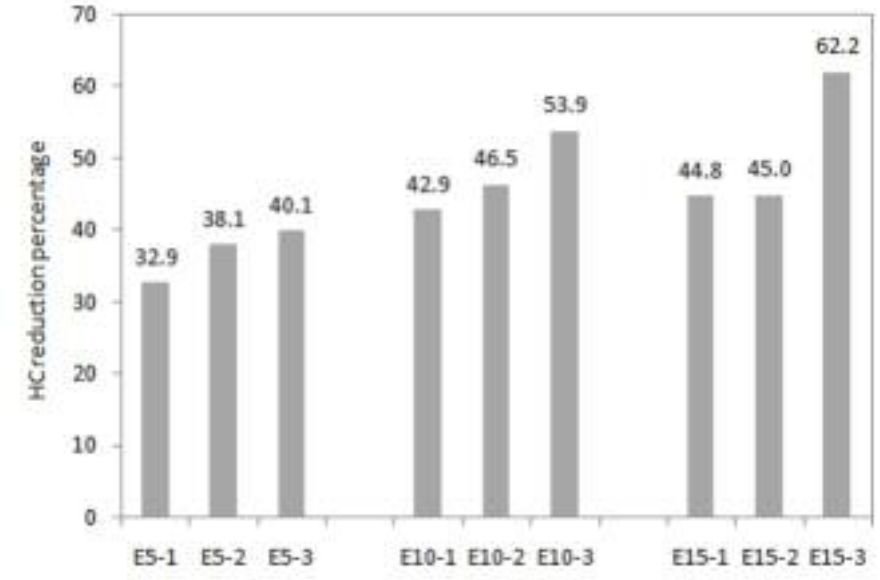

Figure 7: HC reduction percentage

as this light-off period was about 105 seconds for neat gasoline. However, the 4-min average CO and HC emissions decreased for all blends. The highest percentage reduction in CO and HC were observed to be 49.8 and 62.5 respectively for E15.

As most of the motorcycle engines manufactured before 2010 in India are running without a catalytic converter, use of E10/E15 blend and/or use of a catalytic converter are recommended for reducing cold start emissions.

References

Balki, MK., Sayin, C., and Canakci, M., (2012). The effect of different alcohol fuels on the performance, emission and combustion characteristics of a gasoline engine, *Fuel*, 115, pp. 901-906.

Bayraktar, H., (2005). Experimental and theoretical investigation of using gasoline-ethanol blends in spark-ignition engines, *Renewable Energy*, 30, pp. 1733-1747.

Botsaris, P.N., Bechrakis, D., and Sparis, P.D., (2003). An estimation of three-way catalyst performance using artificial neural networks during cold start, *Applied Catalysis A: General*, 243, pp. 285-292.

Canakci, M., Ozsezen, AN., Alptekin, E., and Eyidogan, M., (2013). Impact of alcohol-gasoline fuel blends on the exhaust emission of an SI engine, *Renewable Energy*, 52, pp. 111-117.

Chen, R.H., Chiang, L.B., Chen, C.N., and Lin, T.H., (2011). Cold-start emissions of an SI engine using ethanol-gasoline blended fuel, *Applied Thermal Engineering*, 31, pp. 1463-1467.

Clairotte, M., Adam, TW., Zardini, A.A., Manfredi, U., Martini, G., Krasenbrink, A., Vicet, A., Tournié, E., and Astorga, C., (2013). Effects of low temperature

on the cold start gaseous emissions from light duty vehicles fuelled by ethanol-blended gasoline, *Applied Energy,* 102, pp. 44-54.

Eyidogan, M., Ozsezen, A.N., Canakci, M., and Turkcan, A., (2010). Impact of alcohol-gasoline fuel blends on the performance and combustion characteristics of an SI engine, *Fuel,* 89, pp. 2713-2720.

Favez, J.Y., Weilenmann, M., and Stilli, J., (2009). Cold start extra emissions as a function of engine stop time: Evolution over the last 10 years, *Atmospheric Environment,* 43, pp. 996-1007.

Heywood, J.B., (1998). Internal Combustion Engine Fundamentals, McGraw-Hill Publications, New York, USA.

Horng, RF., and Chou, H.M., (2004). 'Effect of input energy on the emission of a motorcycle engine with an electrically heated catalyst in cold-start conditions', *Applied Thermal Engineering*, 24, pp. 2017-2028.

Iliyas, A., Zahedi-Niaki, M.H., Eic´, M., and Kaliaguine, S., (2007). Control of hydrocarbon cold-start emissions: A search for potential adsorbents, *Microporous and Mesoporous Materials*, 102, pp. 171-177.

Leong, S.T., Muttamara, S., and Laortanakul, P., (2002). Influence of benzene emission from motorcycles on Bangkok air quality, *Atmospheric Environment*, 36, pp. 651–661.

Masum, B.M., Masjuki, H.H., Kalam, M.A., Fattah, I.M.R., Palash, S.M., and Abedin, MJ., (2013). Effect of ethanol-gasoline blend on NOx emission in SI engine, *Renewable and Sustainable Energy Reviews*, 24, pp. 209-222.

Poulopoulos, S.G., and Philippopolous, C.J., (2003). The effect of adding oxygenated compounds to gasoline on automotive exhaust emissions', *Eng. Gas Turbine power*, 125, pp. 344-350.

Pourkhesalian, AM., Shamekhi, A.H., and Salimi, F., (2010). Alternative fuel and gasoline in an SI engine: A comparative study of performance and emissions characteristics, *Fuel*, 89, pp. 1056-1063.

Raja, A.S., and Arasu, A.V., (2014). Control of cold start hydrocarbon emissions of motor bike engine by gasoline-ethanol blends and intake air heating, *Journal of Mechanical Science and Technology*, 28, (4), pp. 1567-1573.

Sales, L.C.M., and Sodré, J.S., (2012). Cold start emissions of an ethanol-fuelled engine with heated intake air and fuel, *Fuel*, 95, pp. 122-125.

Santos, H., and Costa, M., (2008). Evaluation of the conversion efficiency of ceramic and metallic three way catalytic converters*, Energy Conversion and Management*, 49, pp. 291-300.

Singer, B.C., Kirchstetter, T.W., Harley, R.A., Kendall, G.R., and Hesson, J.M., (1999). A Fuel-Based Approach to Estimating Motor Vehicle Cold-Start Emissions, *J. Air & Waste Manage. Assoc.,* 49, pp. 125-135.

Spegar, T.D., Burke, D., and Lavan, L., (2012). Delphi's Heated Injector Technology: The Efficient Solution for Fast Ethanol Cold Starts and Reduced Emissions, SAE Technical paper 2012-01-0418.

Thring, R.H., (1983), Alternative fuel for spark-ignition engines', SAE Paper 831685.

Turner, D., Xu, H., Cracknell, R.F., Natarajan, V., Chen, X., (2011), Combustion performance of bio-ethanol at various blend ratios in a gasoline direct injection engine, *Fuel*, 90, pp. 1999-2006.

Twigg, M.V., (2006). Roles of catalytic oxidation in control of vehicle exhaust emissions, *Catalysis Today*, 117, pp. 407-418.

Twigg, M.V., (2007). Progress and future challenges in controlling automotive exhaust gas emissions, *Applied Catalysis B: Environmental,* 70, pp. 2-15.

Weilenmann, M., Soltic, P., Saxer, C., Forss, A.M., and Heeb, N., (2005). Regulated and non-regulated diesel and gasoline cold start emissions at different temperatures, *Atmospheric Environment*, 39, pp. 2433-2441.

Yang, H.H., Hsieh, LT., Liu, H.C., Mi, H.H., (2005). Polycyclic aromatic hydrocarbon emissions from motorcycles, *Atmospheric Environment*, 39, pp. 17–25.

Received 18 August 2014; revised 23 March 2015

Building power control and comfort management using genetic programming and fuzzy logic

Safdar Ali

DoHyeun Kim
School of Computer Engineering, Jeju National University, Jeju, Republic of Korea

Abstract
In the last couple of years, energy management in the building environment has been a topic of interest to the research community. A number of renowned methods exist in the literature for energy management in buildings, but the trade-off between occupants comfort level and energy consumption is still a major challenge and needs more attention. In this paper, we propose a power control model for comfort and energy saving, using a fuzzy controller and genetic programming (GP). Our focus is to increase the occupants' comfort index and to minimize the energy consumption simultaneously. First, we implemented a Genetic Algorithm (GA) to optimize the environmental parameters. Second, we control the environment using fuzzy logic and third, we predict the consumed power using GP. The environmental and comfort parameters considered are temperature, illumination and air quality. At the end of the work we compare the power consumption results with and without prediction. The results confirmed the effectiveness of the proposed technique in getting the solution for the above mentioned problem.

Keywords: energy management in buildings; genetic programming; comfort index; energy saving; fuzzy logic; genetic algorithm

1. Introduction

Energy conservation and the user comfort index are two significant design objectives in the future building sector. The reason is that, in the energy consumption sectors, buildings is one of the main stakeholders of energy consumption. The energy consumption increases day by day while its sources of generations are less and expensive as well. On the other side occupants of a building want to consume less energy without compromising the comfort index. This requirement of minimum energy consumption without compromising users comfort index is a challenging task to the research community. This leads to the trade-off between energy consumption and occupants comfort index (Owen, 2009). To address this trade-off, an efficient and effective control system is required to maintain both energy consumption and occupants' comfort index in a building environment.

The fundamental three parameters which control occupant's quality of lives in a building environment are thermal comfort, visual comfort and air quality (Wang *et al.*, 2010; Dounis and Caraiscos, 2009; Peeters *et al.*, 2009). Temperature indicates the thermal comfort of the occupants in a building environment. The auxiliary heating and cooling system is applied to preserve the temperature in a comfortable area of the building. The illumination level is used to indicate the visual comfort of the occupants in building environment (Wang *et al.*, 2010). The electrical lighting system is used to manage the visual comfort. CO_2 concentration is used as an index to measure the air quality in the building environment (Emmerich and Perily, 2001). The ventilation system is utilized to keep a low CO_2 concentration. The combination of these three parameters can serve as an occupant's comfort index in buildings and will be used to evaluate it.

The research community has been presented with many approaches in the area of energy savings and some valuable energy management systems have been devised. Approaches based on conventional control systems have been introduced in previous works. Designers used Proportional Integral Derivative Controllers in order to overcome the overshoot of temperature (Levemore, 1992). Other conventional controllers proposed in the literature were optimal control (Bernard *et al.*, 1982) and adaptive control (Curtis *et al.*, 1996). There are some drawbacks of these approaches, such as they need a model of the building, they are not user friendly and there are many difficulties in monitoring and controlling the parameters caused by nonlinear features.

Other proposed methods in this connection are predictive control methods (Kusiak *et al*., 2010; Siroky *et al.,* 2011), where predictive control with weather predictions has been applied to heating, ventilating and air-conditioning systems. Previously we have proposed a predictive control model for building energy management (Safdar and DoHyeun, 2013; Safdar and DoHyeun, 2015). A multi-agent control system with information fusion has been proposed by (Wang *et al.,* 2012). They proposed an indoor energy and comfort management model based on information fusion using ordered weighted averaging (OWA) aggregation. They achieve a high level of comfort with minimum power consumption. Perceived comfort in office buildings is strongly influenced by several personal, social and building factors. The relationship between these factors are complex, so to get a better understanding of the relationships between these factors, a proposal has been presented by Bluyssen *et al. (*2011). A method presented by Marino *et al*., (2012) proposed singular comfort classification indices suitable for both a single environment and whole buildings. The methodology allows evaluation of both energy consumption and polluting impacts and takes into account the comfort conditions of the indoor environment and outdoor climate.

Genetic Algorithm (GA) has been applied for energy management in many ways, e.g. GA proposed for heating, ventilation and air-conditioning (HVAC) control problems (Huang and Lam, 1997). This technique is also applied to the control problems of energy systems consisting of fuel cells, thermal storage, and heat pumps (Obara and Kudo, 2003). (Wright *et al.,* 2002) applied GA to analyse multi-objective (building energy cost and occupant thermal discomfort) problems to classify the optimal pay-off characteristics. Hongwei *et al*. (2006) applied GA to mixed integer and nonlinear programming problems in an energy plant in Beijing, and made a comprehensive economic analysis by changing the economic and environmental legislative contexts. (Montazeri *et al.,* 2006) proposed an application of GA for the optimization of the control parameters in parallel to hybrid electric vehicles (HEV). The optimization problem was formulated for an electric assistant control strategy (EACS) in order to meet the minimum fuel consumption and emissions, while maintaining the vehicle performance requirements.

Azadeh and Tarverdian, (2007) proposed an integrated algorithm based on GA, simulated-on GA, time series and DOE (ANOVA and DMLT) to forecast electricity energy consumption. A technique which demonstrated the application of GP to learn occupancy behavioural rules that predict the presence and absence of an occupant in a single-person office was presented by (Yu, 2010). An optimum scheduling approach of a cold water supply system in an intelligent building has been presented by (Ming and Qing-chang, 2010).

The combination of GA and Artificial Neural Network (ANN) to estimate and predict electricity demand using stochastic procedures has been presented by Azadeh *et al.* (2007). Optimal control approaches of variable air-volume and air-conditioning systems were proposed by Mossolly *et al.* (2009). The control approaches included a base control approach of a fixed temperature set point and two advanced approaches for ensuring comfort and Indoor Air Quality (IAQ). The optimization problem for each control approach was formulated based on the cost of energy consumption and constrained by system and thermal space transient models. They used GA to solve the problem of optimization. Supervisory control for hybrid solar vehicles proposed by Sorrentino *et al.* (2010), and some initial tests have been performed on the road. An optimal design method for the energy system of a single building has been implemented for the first time by establishing an optimal design technique for a distributed energy system (Kayo and Ooka, 2009).

In this work, we proposed a power control model for users' comfort index and energy saving using fuzzy logic, GP and GA (Holland, 1975). Our proposed technique addressed both energy savings and occupants comfort index. GA assimilates, in its fitness function, the indoor occupants' comfort index and the corresponding energy consumption. A range of user set parameters (temperature, illumination, air quality) which constitute occupants' comfort index in building (Wang et al., 2010) are selected and then optimized using GA according to the user's comfort index. The error difference of optimal parameters and real environmental parameters is then fed to the fuzzy controller. The output of the fuzzy controller is the minimum required power according to the user's comfort index. A software based coordinator agent takes the required power (fuzzy controllers output) and available power from the switching control unit as input. It then adjusts the input power of the building on the basis of available power and required power. The adjusted power is then compared with the required power to get the actual consumed power (measured power). The measured power is then used as input to the GP to get the predicted power for the building.

2. Proposed power control model for energy management

2.1 System diagram of the proposed power control model

Figure 1 shows the system diagram of the proposed energy management system for building environment using fuzzy controllers, GP and GA. In Figure

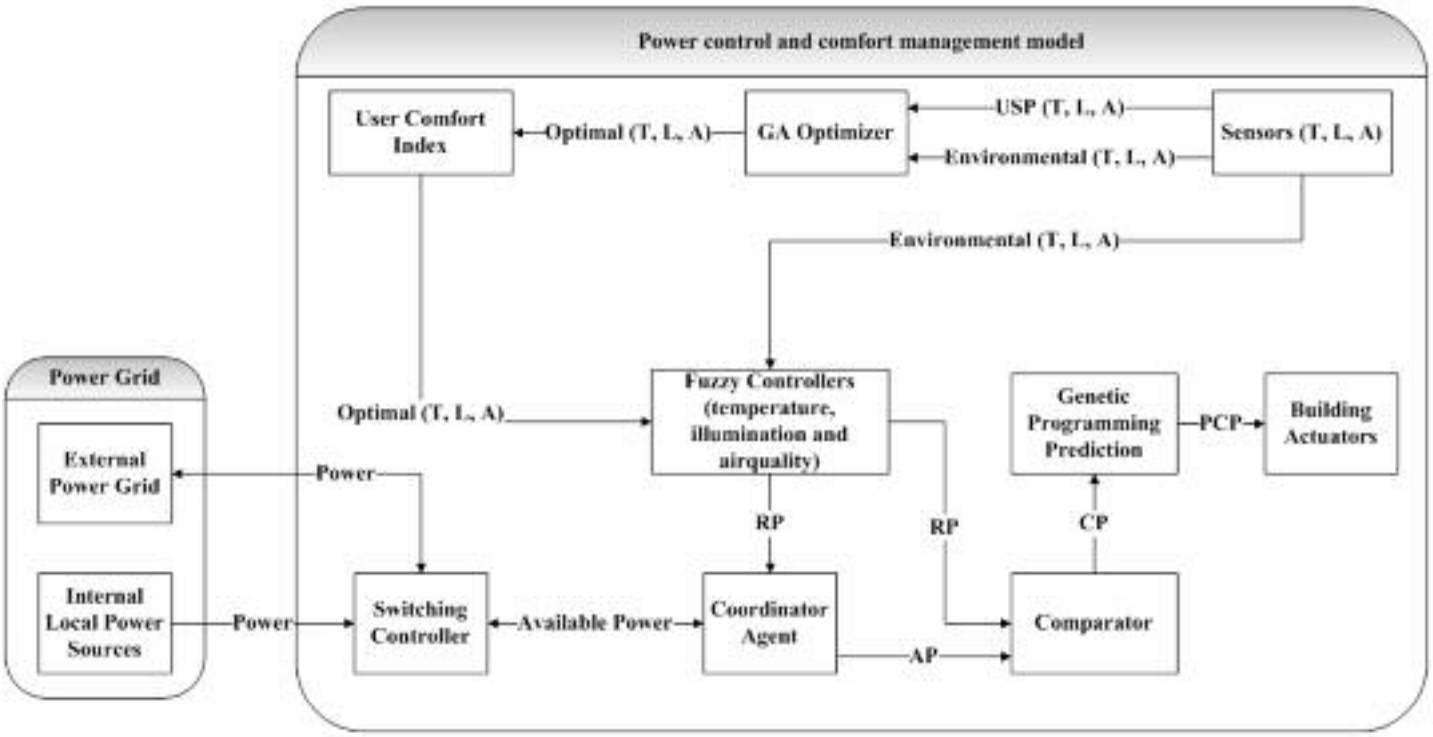

Figure 1: System diagram of proposed power control model

1, USP means User Set Points/Parameters, AP means Adjusted Power, CP means Consumed Power, RP means Required Power, PCP means Predicted Consumed Power, T, L and A means Temperature, Illumination and Air quality respectively.

Environmental and user set parameters are inputted to the GA optimizer to get optimal parameters. Then optimal parameters were used to calculate the occupant's comfort index with respect to the user set points. The coordinator agent adjusted the power according to the user comfort index, using the required power in conjunction with available source power from the power grid or local energy sources. The coordinator agent performs the function of coordination between the three controllers on the basis of required power of the building and available power to provide a maximum comfort index according to the user requirements, while keeping energy consumption as low as possible.

2.1.1. Optimization using GA

GA steps for parameter optimization and comfort index are:

1. Initial random population
2. Calculate fitness function for user comfort using equation (1)
3. Select best individuals using one of the three selection criteria (Rank, Roulette wheel or Tournament selection), we used rank based selection
4. Perform 'one point' crossover of the selected individuals
5. After crossover, we get offspring
6. Calculate user comfort index for the offspring using equation (1)
7. Combine populations of step (3) and (5)
8. If mutation criteria meet, then perform mutation
9. Repeat above eight steps until required numbers of iterations have been performed
10. After arrival of termination criteria select best fitting chromosome.

These parameters were selected after running the algorithm for λ times to get optimal results. The GA stops either when the maximum number of generation's Ω is met, or no significant change is observed in the fitness for μ (few successive) generations. The maximum population size selected is 100. The conventional single point crossover is performed with the probability of 0.9 and mutation rate of 0.1. GA parameters (population size, crossover rate and mutation rate) have been set after running GA for δ times. The experiments were performed using a Latitude D620 laptop with a 2.0GHz processor and 2GB of RAM. The C # 2008 was used for the simulation. When the GA evaluation process finishes, the best fitting chromosome is selected to get optimal parameters and comfort index.

2.1.2. Comfort index

The comfort index can be calculated by using equation (1) (Safdar, DoHyeun, 2013)

$$Comfort = \beta_1 [1-(err_T/T_{setpoint})^2] + \beta_2 [1-(err_L/L_{setpoint})^2] + \beta_3 [1-(err_A/A_{setpoint})^2] \quad (1)$$

Where '*comfort*' is the overall comfort level of the user and is ranged between [0, 1], β_1, β_2 and β_3 are the user defined factors which solve any possible conflict between the three comfort factors (temperature, illumination and air quality). Their values fall in the range [0, 1]. Also $\beta_1 + \beta_2 + \beta_3 = 1$ which means that at any time addition of these values should not exceed '1' so that value of comfort is scaled down to in between [0,1]. err_T is the error difference between environmental parameter (temperature in this case) and actual sensor temperature. err_L is the error difference between environmental parameter (illumination in this case) and actual sensor illumination. err_A is the error difference between environmental parameter (air quality in this case) and actual sensor air quality. $T_{setpoint}$, $L_{setpoint}$ and $A_{setpoint}$ are the user set parameters of temperature, illumination and air quality.

2.1.3. Fuzzy logic controller

The concept of Fuzzy Logic (FL) was introduced by Zadeh, (1968), a professor at the University of California at Berkley.

The real parameters, optimal parameters and rate-of-change in these parameters are passed as input to the fuzzy controller. The fuzzy controllers produce the results based on the membership functions. The output of the fuzzy controller(s) is the required power to control temperature, illumination and air quality inside the building. This required power is input to the coordinator agent.

The input to the fuzzy controller for temperature is the error difference between optimal parameters of GA and real environmental parameters along with the rate of change of temperature. For efficient control, both error difference err_T and change in error $cerr_T$ (difference between current and previous error) is used. The input/output membership functions for the temperature controller are shown in Figure 2. Table 1 shows the fuzzy controller rules for temperature control. It is a 7 x 7 matrix. Each entry in Table 1 is the error difference err_T and change in error $cerr_T$. The required power is the power to fulfil the user requirements inside the building.

The input to the fuzzy controller for illumination is the error difference between optimal parameter of GA and real environmental illumination parameter. The input membership/output membership functions for illumination are shown in Figure 3. The input membership function is for the error err_L, which is the only input error. In equations (2, 3 and 4) λ_T, λ_L, and λ_A are the temperature, illumination and air quality increment relationship with consumed power P in per unit time K respectively. θ is the weight factor to balance the relationship. The value of θ can be between [0, 1] and d is the basic operation power of ventilator.

$$\lambda_T = \theta * P_T / K \quad (2)$$

$$\lambda_L = \theta * P_L / K \quad (3)$$

$$\lambda_A = \theta * P_A / K * d \quad (4)$$

Table 2 shows fuzzy controller rules for illumination control. Here 'HS', 'MS' and 'BS' means High Small, Medium Small and Basic Small respectively. 'OK' means no change, 'SH' and 'H' means Small High and High respectively. 'OLittle', 'OMS', 'OBS', 'OOK', 'OSH' and 'OH' means Output Little, Output Medium Small, Output Basic Small, Output OK, Output Small High and Output High.

The input to the fuzzy controller for air quality is the error difference between optimized air quality parameter of GA and the real environmental air quality parameter. The input/output membership functions for air quality are shown in Figure 4. The input membership function is for the error err_A which is the only input to the air quality fuzzy controller. Table 3 shows the fuzzy controller rules for air quality control. Here 'LH' means Little High, 'MH' means Medium High, 'OL' means Output High, 'OLH' means Output Little High.

2.1.4. Coordinator agent

The coordinator agent takes the required building power from the fuzzy controller, according to the comfort index and available power from the switching controller, as input. It adjusted the building power on the basis of available power and required power for the comfort index. The adjusted building power is compared with the required power to get the actual consumed power. The actual consumed power is given to the actuators for usage. The measured power is then passed to the GP and predicted power for the building is determined.

In equations 5, 6 and 7, parameters G_1, G_2 *and* G_3 are small optional values for compensating the power losses in distribution. These parameters range between [0,1]. $P\ (K)$ is the required power, which is the sum of power demands from temperature, illumination and air quality. $P_{available}\ (K)$ is the total energy source (outside grid-power or internal local power source). $P_{max\_power}\ (K)$ is the maximum input power either from the power grid or from the local micro sources to the building. K, is the sample time variable.

$$P_T\ (K+1) = P_T\ (K) + G_1 \quad (5)$$

$$P_L\ (K+1) = P_L\ (K) + G_2 \quad (6)$$

$$P_A\ (K+1) = P_A\ (K) + G_3 \quad (7)$$

$$P_T(K) + P_L(K) + P_A(K) = P_{required}(K) \quad (8)$$

$$P_{available}(K) <= P_{max\_power} \quad (9)$$

2.1.5. Genetic programming

GP is an evolutionary approach based on the concept of natural evaluation (Koza, 1992). It searches computer programs that perform a user-defined function. It is a specialized version of GA where each individual is a computer program. It is a machine learning approach used to optimize a large set of individual's population. GP evolves computer programs which are conventionally stored in the memory as a tree like constructions.

Table 2: Fuzzy controller rules for illumination control

Error	HS	MS	BS	OK	SH	H
Required power	OLittle	OMS	OBS	OOK	OSH	OH

Table 3: Fuzzy controller rules for air quality control

Error	Little	OK	LH	MH	HIGH
Required power	OFF	ON	OL	OLH	OHIGH

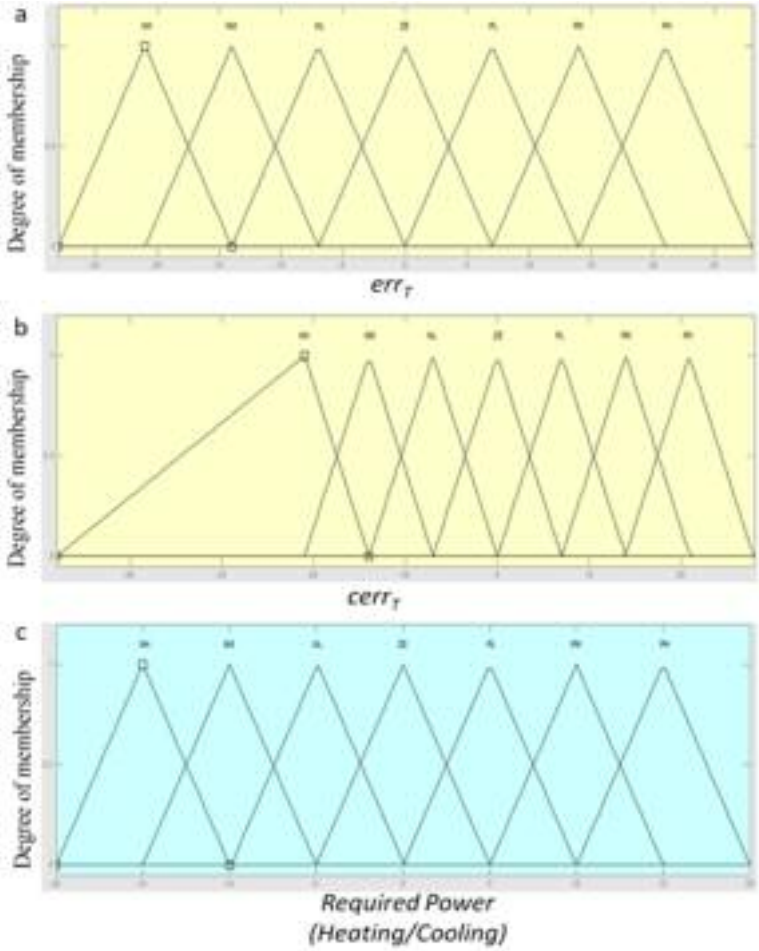

Figure 2: Input/output membership functions for temperature: (a) Input membership function of err_T, (b) Input membership function of $cerr_T$, (c) Output membership function

Table 1: Fuzzy controller rules for temperature control

Required Power		err_T						
		NH	*NM*	*NL*	*ZE*	*PL*	*PM*	*PH*
$cerr_T$	NH	NH	NL	PL	PH	PH	PH	PH
	NM	NH	NM	ZE	PM	PM	PH	PH
	NL	NH	NM	NL	PL	PM	PH	PH
	ZE	NH	NM	NL	ZE	PL	PM	PH
	PL	NH	NH	NM	NL	PL	PM	PH
	PM	NH	NH	NM	NM	ZE	PM	PH
	PH	NH	NH	NH	NH	NL	PL	PH

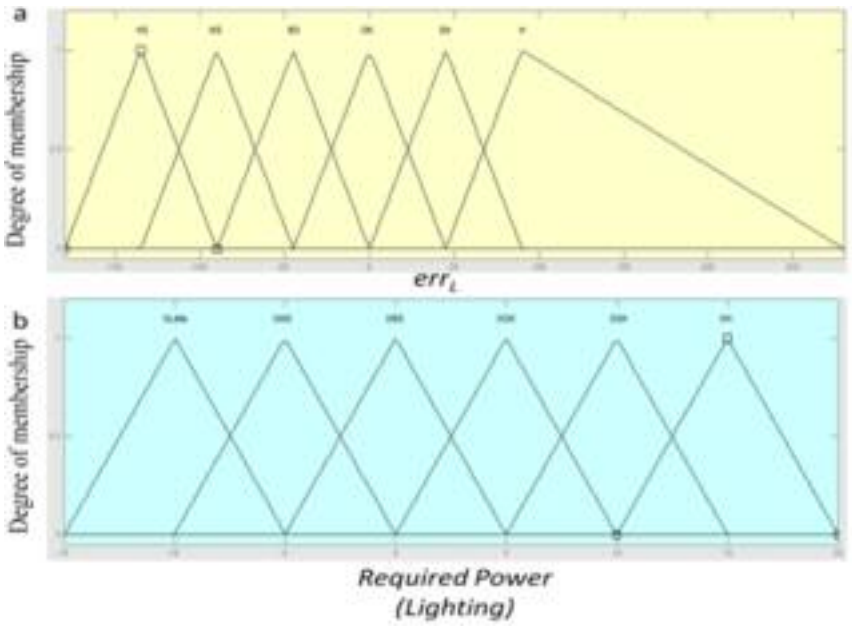

Figure 3: Input/output membership functions for illumination: (a) Input membership function of err_L (b) Output membership function

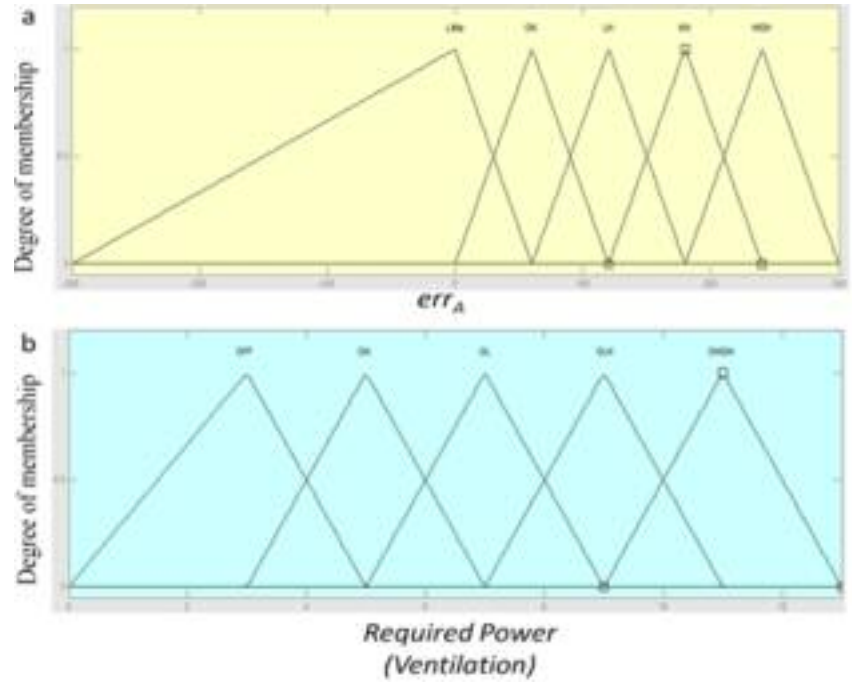

Figure 4: Input/output membership functions for air quality. (a) Input membership function of err_A (b) Output membership function

2.1.6 Switching controller

The switching controller manages the available power sources. When the external power sources are unable to provide enough power to the building or its price is high, it switches to the internal power sources.

2.1.7. Building actuators

Building actuators are the devices which use the energy inside the building. That is, AC (cooling), heater (heating), refrigerator (cooling) and oven (heating). The sensors provide temperature, illumination and air quality information.

3. Simulation and results discussion

Matlab/Simulink was used for input/output membership functions construction. The simulation was carried out in C# 2008. User preference set points ranges are $T_{setpoint}$ = 66, 78 K, $L_{setpoint}$ = 720, 880 lux and $A_{setpoint}$ = 700, 880 ppm.

Figure 5 shows the comparisons of power consumption. From the results of Figure 5a, it is evident, that in case of power consumption for temperature, the system with prediction method consumed less power as compared to the non-predicted system. This is due to the fact that the predicted method makes use of previous information and

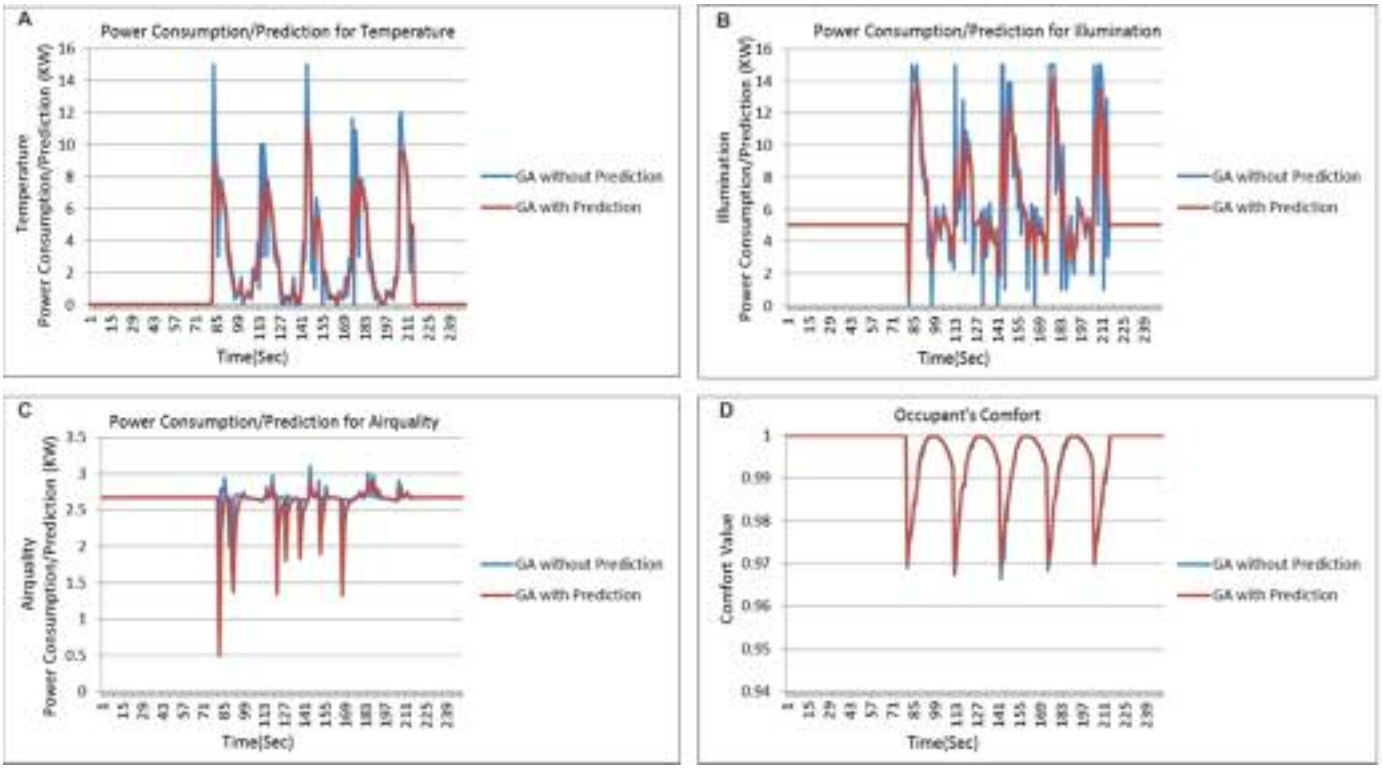

Figure 5: Comparison of power consumption and comfort index in case of GA based prediction system and GA based without prediction system

consumed power accordingly. So when environmental disturbance occurs, the predicted method consumes less power. Lower power consumption is guaranteed by the decision of the coordinator agent on the basis of required power and available power in accordance with comfort index.

Similarly for illumination as shown in Figure 5b, the predicted based method confirmed to consume less power as compared to the without-prediction method. Figure 5c shows the results for the air quality control. Here, once again, predicted based system consumed less power as compared to its counterpart without-prediction.

Figure 5d shows the results of user comfort index in case of prediction based system and non-predicted based system. With prediction based estimated power usage, user comfort index is the same as that of without prediction based system. Although in the prediction based system less power is consumed as compared to that of non-predicted system, but maintained its required comfort level. The first power disturbance occurs at 82sec. At that time, the comfort level of the prediction based system goes down to almost 0.97 similar to that of non-predicted based system. The prediction based system recovers soon similar to that of its counterpart and immediately provides the same comfort level as compared to non-prediction. During environmental disturbance, the prediction based system recovered soon, similar to its counterpart and without compromising the comfort index.

4. Conclusion

In this study, we presented a power control model for comfort and energy saving in a building environment using fuzzy logic, GP and GA. We addressed both the energy efficiency and user comfort level. User set points are considered in deciding the comfort level. The focus of our study is to increase occupants comfort index and minimize energy consumption simultaneously. To achieve this, GA was implemented to optimize the environmental parameters with respect to the user set points and comfort index. Secondly, we applied fuzzy logic to control the environment and thirdly, we predict the consumed power using GP. The parameters we considered are temperature, illumination and air quality. We compared the power consumption results with and without prediction.

The results proved the effectiveness of the proposed technique in acquiring the solution for the problem. The proposed prediction method for building energy management produces overall exactly the same comfort level as compared to without prediction method. The main benefit of our proposed predicted approach is that it consumed less power when compared to its counterpart technique where no prediction is applied while maintaining the same required comfort level of the occupants. Using a prediction based system for users comfort index and energy savings, the building environment can be made user friendly. Our proposed approach for comfortable and energy saving system can be

incorporated with SCADA software of buildings for practical applications.

References

Azadeh, A., and Tarverdian, S. (2007). Integration of genetic algorithm, computer simulation and design of experiments for forecasting electrical energy consumption, *Energy Policy* 35(10): 5229-5241.

Azadeh, A., Ghaderi, S. F., Tarverdian, S., and Saberi, M. (2007). Integration of artificial neural networks and genetic algorithm to predict electrical energy consumption. *Applied Mathematics and Computation,* 186(12): 1731-1741.

Bernard, C., Guerrier, B., and Rasset-Louerant, M. M. (1982). Optimal building energy management, Part II: Control. ASME *Journal of Solar Energy Engineering* 114(1): 13-22.

Bluyssen, P. M., Aries, M., and Dommelen, P. V. (2011). Comfort of workers in office buildings: The European HOPE project, *Building and Environment* 46(1): 280-288.

Curtis, P. S., Shavit, G., and Kreider, K. (1996). Neural networks applied to buildings—a tutorial and case studies in prediction and adaptive control: *ASHRAE Transactions* 102(1): 732-737.

Dounis, A. I., Caraiscos, C. (2009). Advanced control systems engineering for energy and comfort management in a building environment – A review, *Renewable and Sustainable Energy Reviews* 13(6-7): 1246-1261.

Emmerich, S. J., and Persily, A. K. (2001). State-of-the-art review of CO2 demand controlled ventilation technology and application. National Institute of Standards and Technology: Technology Administration, US. Department of Commerce, 1-43.

Huang, W., and Lam, H. N. (1997). Using genetic algorithms to optimize controller parameters for HVAC systems, *Energy and Buildings* 26(3): 277-282.

Hongwei, Li., Nalimi, R., and Haldi, P. A. (2006). Thermal-economic optimization of a distributed multi-generation energy system: A case study of Beijing: *Applied Thermal Engineering* 26(7): 709-719.

Holland, J.H. (1975). Adaptation in natural and artificial systems Ann Arbor, MI: The University of Michigan Press.

Koza, J. (1992). On the Programming of Computers by Means of Natural Selection, MIT Press.

Kusiak, A., Li, M., and Zhang, Z. (2010). A data-driven approach for steam load prediction in buildings, *Applied Energy* 87(3): 925-933.

Kayo, G., and Ooka, R. (2009),.Application Multi-Objective genetic algorithm for optimal design method of distributed energy system, Eleventh International IBPSA Conference Glasgow, Scotland, 167-172.

Levermore, G. J. (1992). Building Energy Management Systems, An Application to Heating, Natural Ventilation, Lighting and Occupant Satisfaction, London. E & FN SPON.

Marino, C., Nucara, A., and Pietrafesa, M. (2012). Proposal of comfort classification indexes suitable for both single environments and whole buildings, *Building and Environmen*t 57: 58-67.

Montazeri-Gh, M., Poursamad, A., and Ghalichi, B. (2006). Application of genetic algorithm for optimization of control strategy in parallel hybrid electric vehicles, *Journal of the Franklin Institute* 343(4-5): 420- 435.

Ming-hai, L., and Qing-chang, R. (2010), Optimization for the Chilled Water System of HVAC Systems in an Intelligent Building. Computational and Information Sciences (ICCIS), International Conference, 889-891.

Mossolly, M., Ghali, K., and Ghaddar, N. (2009). Optimal control strategy for a multi-zone air conditioning system using a genetic algorithm, *Energy*, 34(1): 58-66.

Owen, M. S. (2009). ASHRAE Handbook – Fundamentals (I-P Edition). American Society of Heating, Refrigerating and Air-Conditioning Engineers: Inc 2009.

Obara, S., and Kudo, K. (2003),.Multiple-purpose operational planning of fuel cell and heat pump compound system using genetic algorithm: Transaction of the Society of Heating, Air-Conditioning and Sanitary Engineers of Japan 91: 65- 76.

Peeters, L., Dear, R. D., Hensen, J., and Dhaeseleer, W. (2009). Thermal comfort in residential buildings: Comfort values and scales for building energy simulation, *Applied Energy,* 86(5): 772-780.

Safdar, A., and DoHyeun, K. (2013). Effective and Comfortable Power Control Model Using Kalman Filter for Building Energy Management. *Journal of Wireless Personal Communication,* 73(4): 1439-1453.

Safdar, A., and DoHyeun, K. (2015). Optimized power control methodology using genetic algorithm. *Journal of Wireless Personal Communication,* http://dx.doi.org/10.1007/s11277-015-2405-3.

Siroky, J., Oldewurtel, F., Cigler, J., and Privara, S. (2011). Experimental analysis of model predictive control for an energy efficient building heating system, *Applied Energy* 88(9): 3079-3087.

Sorrentino, M., Arsie, I., Di-Martino, R., and Rizzo, G. (2010). On the Use of Genetic Algorithm to Optimize the On-board Energy Management of a Hybrid Solar Vehicle, IFP International Conference – Advances in Hybrid Powertrains, 133-143.

Wang, Z., Yang, R., and Wang, L. (2010). Multi-agent control system with intelligent optimization for smart and energy-efficient buildings. The 36th Annual Conference of the IEEE Industrial Electronics Society, Phoenix, AZ, 1144-1149.

Wang, Z., Yang, R., and Wang, L. (2010). Multi-agent intelligent controller design for smart and sustainable buildings. IEEE International Systems Conference, San Diego, 277-282.

Wang, Z., Wang, L., Dounis, A. I., and Yang, R. (2012). Multi-agent control system with information fusion based control model for smart buildings, *Applied Energy* 99: 247-254.

Wright, J. I., Loosemore, H. A., and Farmani, R. (2002).

Optimization of building thermal design and control by multi-criterion genetic algorithm. *Energy and Buildings* 34(9): 959-972.
Yu, T. (2010). Modeling Occupancy Behavior for the Energy Efficiency and Occupants Comfort Management in Intelligent Buildings. Machine Learning and Applications (ICMLA), Ninth International Conference, 726-731.
Zadeh, L. A. (1968). Fuzzy Algorithms: Information and Control: 12: 94-102.

Received 10 February 2014; revised 8 May 2015

Differential power algorithm based maximum power point tracking for a standalone solar PV system

Dinesh K Sharma

Ghanshyam Purohit

School of Engineering, Sir Padampat Singhania University, Udaipur, India

Abstract

We report on an improved maximum power point tracking (MPPT) system based on a differential power algorithm. In the proposed algorithm, which is a modified form of a perturb and observe (P&O) algorithm, differential powers, as well as voltages at different time, are compared. The proposed algorithm has been implemented with a highly efficient boost converter, in which duty cycle of a switch is varied in such a way, that the power reaches a maximum at any instant of the day, irrespective of the environmental conditions. The improved MPPT is able to reduce the number of oscillations and tracking time significantly before reaching the maximum power point (MPP). The simulated I-V and P-V characteristic curves (individual and combined) of a solar PV module were generated in MATLAB.

Keywords: solar PV system, MPPT, efficiency, control algorithm, boost converter

1. Introduction

Generation of power from renewable energy sources is an important way to reduce carbon footprints in our environment. Low efficiency and high cost are the main factors which impedes the global utilization of renewable energy resources for generation of electrical power. Power generation, using solar PV (Koutroulis *et al.,* 2001), is not popular (especially in developing countries) due to the higher cost and lower efficiency (D'Souza *et al.,* 2005) of solar PV modules. The efficiency of a solar PV system can be maximized using a maximum power point tracker (MPPT). The MPPT is a power electronic circuit of an efficient DC-DC converter, which is controlled by an algorithm. The function of the control algorithm is to minimize the deviations (Hua and, Lin, 2003) from a maximum power point so that the maximum possible power can be extracted from the PV module(s) under varying atmospheric conditions (Subudhi, and Pradhan, 2013)] with minimum possible wastage of power. Various MPPT techniques and control algorithms (Esram and Chapman, 2007; Hohm and Ropp, 2003; de Brito *et al.,* 2013; Moacyr *et al.,* 2007; Thounthong, *et al.,* 2013) have been studied.

2. Standalone solar PV system modelling

Modelling of a standalone PV system is the basic requirement for obtaining the characteristic curve on which MPP is to be tracked. A standalone solar PV system (Amin et al., 2009; Xiao and Dunford, 2004) consists of a PV module, load, power electronic converters (DC-DC conversion or DC-AC conversion), charge controller (Xiao and Dunford, 2004) (to avoid undercharge and overcharge conditions of the battery) with battery (for storage) and Maximum Power Point Tracker (MPPT). The function of control algorithm is to decrease or increase the duty cycle of the switch (Subudhi and Pradhan, 2013; Koutroulis and Blaabjerg, 2012) power switch of DC-DC converter (Salam *et al.,* 2010) by means of Pulse Width Modulation (PWM) in order to track the maximum power points on the characteristic curves of the PV module. Figure 1 represents a typical standalone solar PV system.

For implementing the proposed algorithm, it is required to model a solar PV system with maximum power points on the I-V and P-V characteristic curve of the PV module. The following section describes the electrical equivalent circuit and associated equation for the modelling of a solar PV module and to finally obtain the characteristic curves.

3

a) Electrical equivalent circuit of a solar PV module

An electrical equivalent circuit of a solar PV cell is shown in Figure 2. The circuit consists of a current

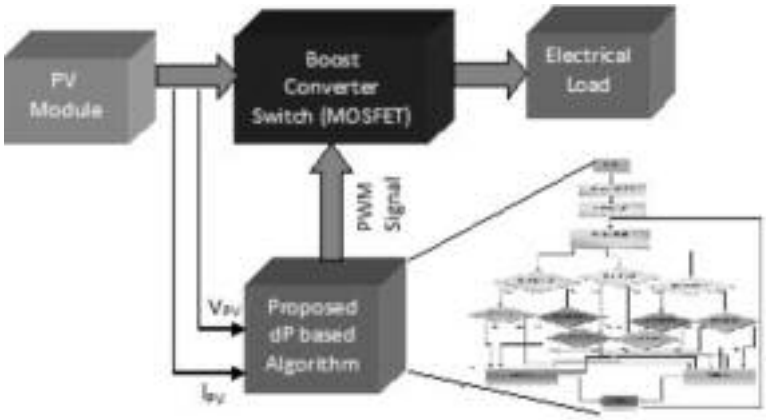

Figure 1: Standalone Solar PV system with dP based algorithm

source connected with a diode in parallel and two resistors R_{SH} in parallel and R_S in series. The current produced by solar cell is given by equation (1).

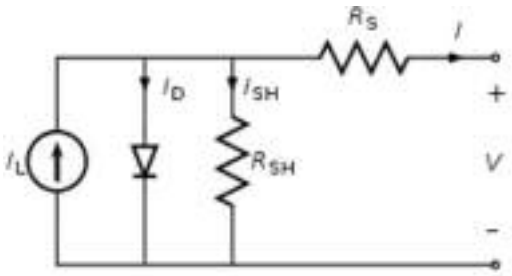

Figure 2: Electrical equivalent of solar PV module

From the equivalent circuit it is evident that the current produced by the solar cell is equal to that produced by the current source, minus that which flows through the diode, minus that which flows through the shunt resistor (using Kirchhoff's current law) (Weidong *et al.,* 2013:

$$I = I_L - I_0 \left[\exp\left(\frac{qV + IR_S}{nkT} \right) - 1 \right] - \frac{V + IR_S}{R_{SH}} \quad (1)$$

where,
I_L = light generated current
I_0 = reverse saturation current q = charge of electron
V = voltage across output terminals R_S = series resistance
R_{SH} = shunt resistance
n = ideality factor of diode k = Boltzmann's constant
T = room temperature

b) Simulated results of I-V and P-V characteristics of PV module

We obtained the simulated results for the I-V and P-V Characteristic curves of a PV module using MATLAB. The thick portion on these curves is due to continuous overlapping of different curves. The following I-V characteristic curves have been obtained by adjusting the series resistance (R_S=0.340000) and parallel resistance (R_P=164.585828) of a two diode model (Femia *et al.,* 2005) of a solar PV cell.

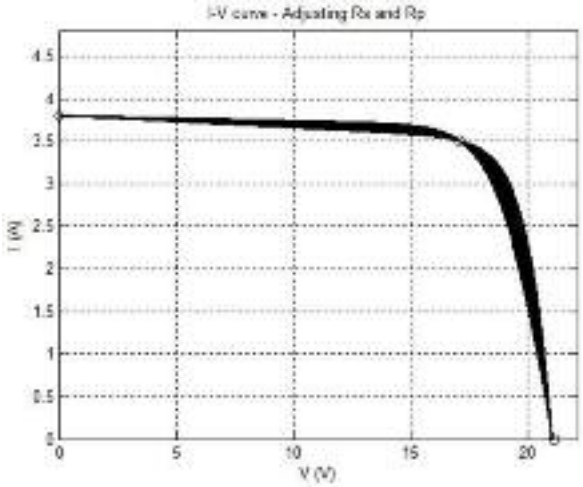

Figure 3: I-V characteristic curve of PV module

The following P-V characteristic curve was obtained in MATLAB by adjusting the peak power (Pmax= 59.85 W). This curve is the superposition of several curves, closely spaced in order to obtain its present form. This curve shows the shifting of maximum power point (MPP) for various solar irradiation levels. By adjusting the peak power, global MPP is obtained by different local MPPs on the P-V characteristic curves.

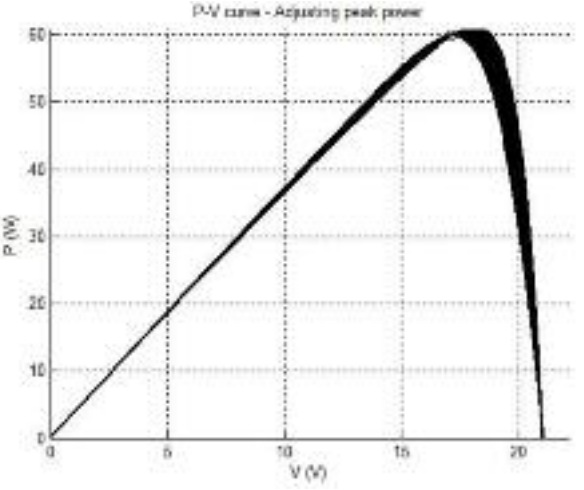

Figure 4: P-V characteristic curve of PV module

The following characteristic curve (I-V and P-V in one plot) has been obtained by superimposing the I-V and P-V at various values of voltage, current and power (in varying insolation) as shown in Figure 5.

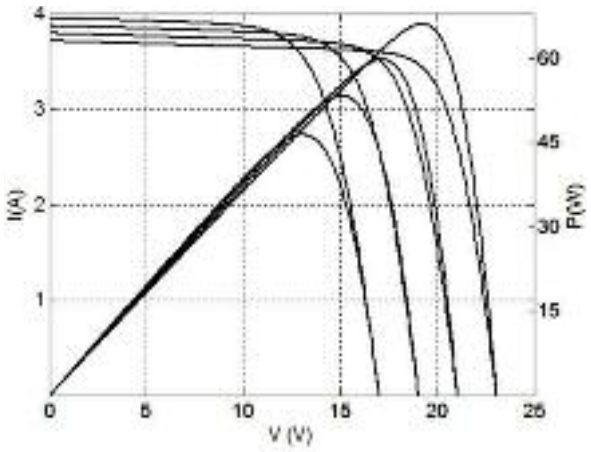

Figure 5: I-V and P-V characteristic curve of PV module in one plot

4. Boost converter

A boost converter is required to vary the output voltage (as shown in characteristic curves) of the solar PV systems in order to obtain the MPP. The boost converter is a highly efficient power electronic converter which only raises voltage. The control algorithm is used to control the duty cycle of the switch of the boost converter. The duty cycle of the boost converter is formulated by:

$$D = \frac{T_{ON}}{(T_{ON} + T_{OFF})}$$

where,

T_{ON} = On period of switch of boost converter T_{OFF} = Off period of switch of boost converter

The output voltage is related with the duty cycle of the boost converter as following:

$$V_{out} = \frac{V_{in}}{(1 - D)}$$

where,

V_{in} = input voltage to the boost converter, V_{out} = output voltage from the boost converter

D = duty cycle of the switch of boost converter.

The control algorithm is used to calculate the duty cycle (on and off time) of the switch of the boost converter. The proposed algorithm (based upon the difference of consecutive power and voltage levels) has been implemented to control the duty cycle of the switch of the boost converter.

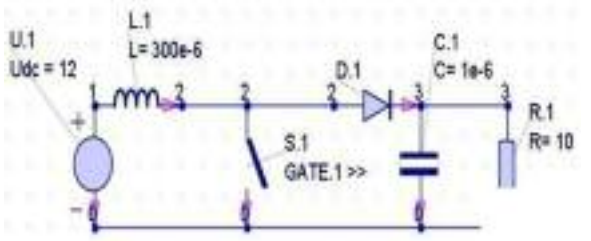

Figure 6: Boost converter circuit

The boost converter circuit is described as follows:

1. DC voltage source (V_{dc} = 12 V), which is used for energizing the circuit
2. Inductor (L = 300e^{-6} H), which is used for storing and releasing the electrical energy
3. Power electronic switch, which is used for keeping ON and OFF of the switch
4. PN junction diode, which is used for blocking the reverse flow of current from load to source.
5. Capacitor (C = 1e-6 F) is used as voltage filter.

The results have been taken from Gecko Circuits simulation software (GeckoCIRCUITS). The results for various parameters [i.e. input voltage (u1), output voltage (u2), switch voltage (uS), inductor current (I_L), capacitor current (I_C)] are obtained in Gecko Circuits and shown in Figure 7.The variation in output voltage (u2) along with the constant input voltage (u1) has been shown in Figure 7(a). This figure shows that the output voltage increases from 0 V to 16 V (peak value) after 170 e^{-6} sec. from the beginning. It further reduces from peak value to 8.5 V in the next 340 e^{-6} sec. Consequently, this waveform stabilizes at 408 e^{-6} sec. This waveform has been constant and almost overlapping with the input voltage.

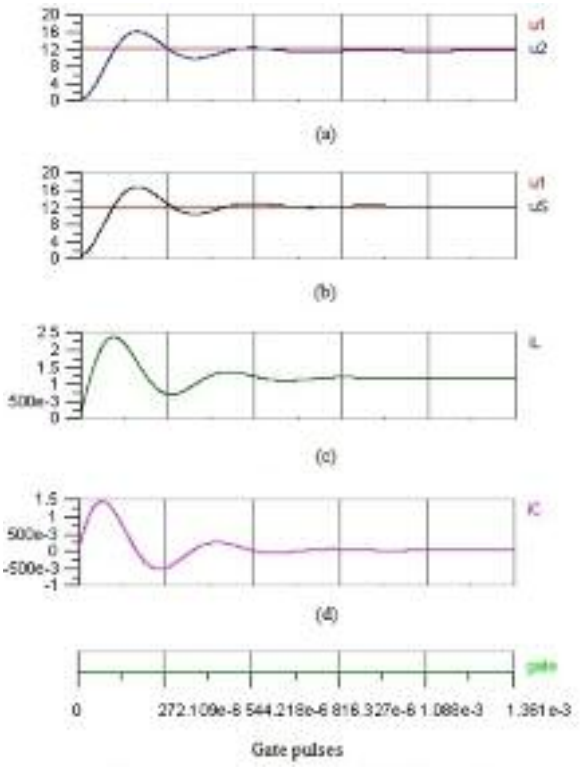

Figure 7: Simulation results of boost converter

In Figure 7(b), the waveform of switch voltage (uS) is almost the same as that of output voltage (u2) with some oscillation before stabilization. Figure 7(c) represents the variation in inductor current (I_L). In this figure, I_L reaches to the peak value

of 2.75 A in 136 e^{-6} sec. Further, I_L goes down to the bottom value of 0.75 A at 280 e^{-6} sec. Subsequently, it goes up to the value of 1.25 A at 415 e^{-6} sec. Then after some minor oscillations, it stabilizes with the value of 1.15 A at 860 e^{-6}.

The variation of capacitor current (I_C) is depicted in Figure 7(d). The I_C increases from 0 A to the peak value of 1.5 A in 68 e^{-6} sec. Then it reduces slowly and reaches to the bottom value of -500 e^{-3} sec at 250 e^{-6} sec. Subsequently I_C further goes up from this value to 0.25 A at 410 e^{-6} sec. After some minor oscillations, I_C stabilizes at 0.9 e^{-3} sec. Sequence of gate pulses is represented in Figure 7.

5. Differential power (dP) algorithm

The control algorithm proposed in this paper is based upon the simple and widely used Perturb and Observe (P&O) algorithm (Amrouche *et al.,* 2007; Villalva *et al*., 2009; Mohammed *et al.,* 2012). In the proposed algorithm, the perturbation and observation steps are increased in order to closely track the maximum power point with minimum possible oscillations around the operating point on the characteristic curve of the solar PV module. In this algorithm, the different values of power are compared with each other at different instance of time. The presented algorithm is based upon the difference of old and new power values. Therefore, this algorithm may be called as differential power (dP) based algorithm.

In this algorithm, the difference of three consecutive power levels, as given in equations (1), (2) are calculated. Then the voltage differences of the corresponding power levels are calculated. Consequently, the voltage of the converter is increased and decreased accordingly. Due to this, the duty cycle (thereby pulse width) of the power switch is also modulated in order to efficiently track the MPPs.

$$dP = P(n) - P(n-1) \quad (1)$$

$$dP' = P(n-1) - P(n-2) \quad (2)$$

$$dP'' = P(n-2) - P(n-3) \quad (2)$$

After comparing the differential power, from equations (1), (2) and (3), the corresponding voltages are also compared. Consequently, the duty cycle of the switch of the boost converter is modulated as shown in the dP algorithm (Figure 9). The main advantage of this method is that it works on the basis of calculation of power difference in consecutive instants throughout the day. Due to this, it provides the direct determination of maximum power from a solar PV system. The implementation circuit and simulation results are presented in the next section.

6. Results and discussion

The proposed algorithm has been implemented in Gecko Circuits as shown in the following circuit diagram in Figure 8. The simulation results of the MPPT with proposed algorithm are in Figure 8(a) and shows that the output voltage stabilizes rapidly, within a fraction of a second in comparison to the input PV voltage and inductor current (I_L) which both stabilize at 4.975 seconds. In Figure 8(b), the voltage across the switch (sg.1) is also stabilized after 4.975 seconds. At the same time, the PV voltage (filter i.e. across C2) and PV current (filter i.e. through C2) decreases and increases respectively that follow the law of conservation of energy.

The results shown in Figures 8(a) and 8(b) indicate that the proposed algorithm is not only able to effectively reduce the stabilizing time (tracking time) of output (load) voltage but it also able to reduce the ripples and oscillations in the output. The result shows that the proposed method is able to track the MPP with a reduced number of oscillations and thereby higher stability of the solar PV system. At the same time, the efficiency of the solar PV system is increased due to lower amount of oscillations and the performance of the overall solar power system has been upgraded. The main disadvantage of this algorithm is that it has increased complexity.

7. Conclusion

In this paper, a differential power algorithm is presented and consequently implemented to control the operation of the boost converter. By the efficient control of the boost converter, the output power from the solar PV power generating system has been significantly increased for an optimal efficiency. The simulation results for characterization of the PV module (i.e. I-V and P-V characteristics) are presented. The simulation results of the realized circuit with the proposed algorithm are also presented, which shows the stable operating point for maximized constant output power from a solar PV system.

References

Amin, N.; Lam Zi Yi; and Sopian, K., (2009). Microcontroller based smart charge controller for standalone solar photovoltaic power systems, Photovoltaic Specialists Conference (PVSC), 2009 34th IEEE, Vol., No., pp.001094, 001097, 7-12 June 2009.

Amrouche, B. Belhamel, M. and. Guessoum A., (2007). Artificial intelligence based P&O MPPT method for photovoltaic systems, Revue des Energies Renouvelables ICRESD-07 Tlemcen (2007) 11– 16.

de Brito, M.A.G.; Galotto, L.; Sampaio, L.P.; de Azevedo e Melo, G.; and Canesin, C.A., (2013). Evaluation of the Main MPPT Techniques for Photovoltaic Applications, *IEEE Transactions on, Industrial*

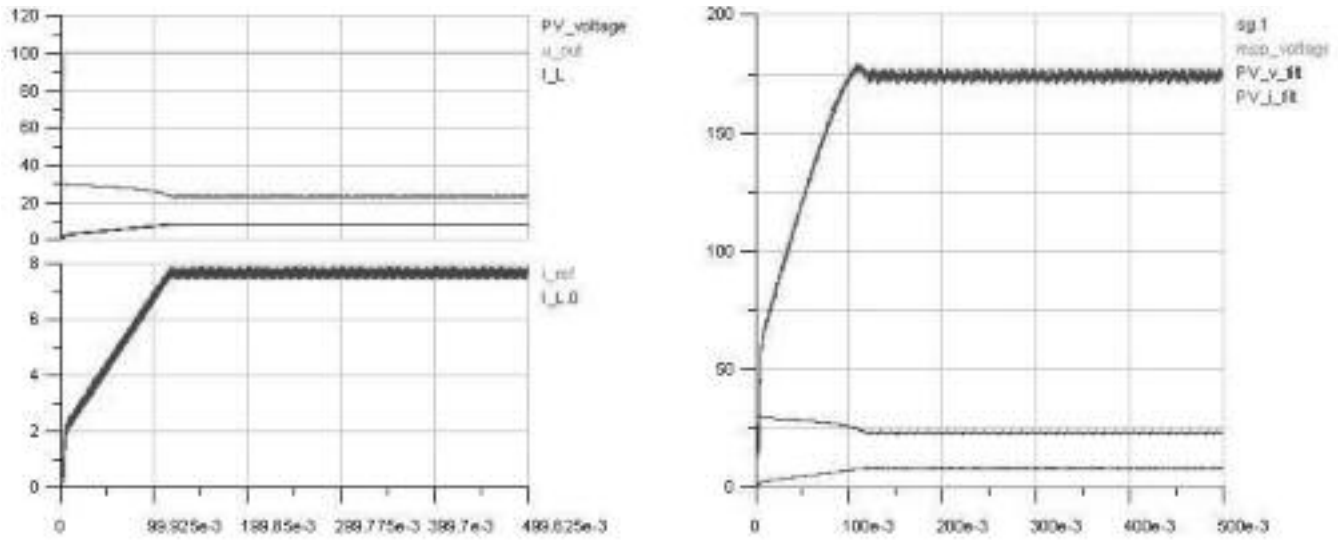

(a) (b)

Figure 8: Simulation results for variation of voltage and currents of solar PV system with proposed algorithm

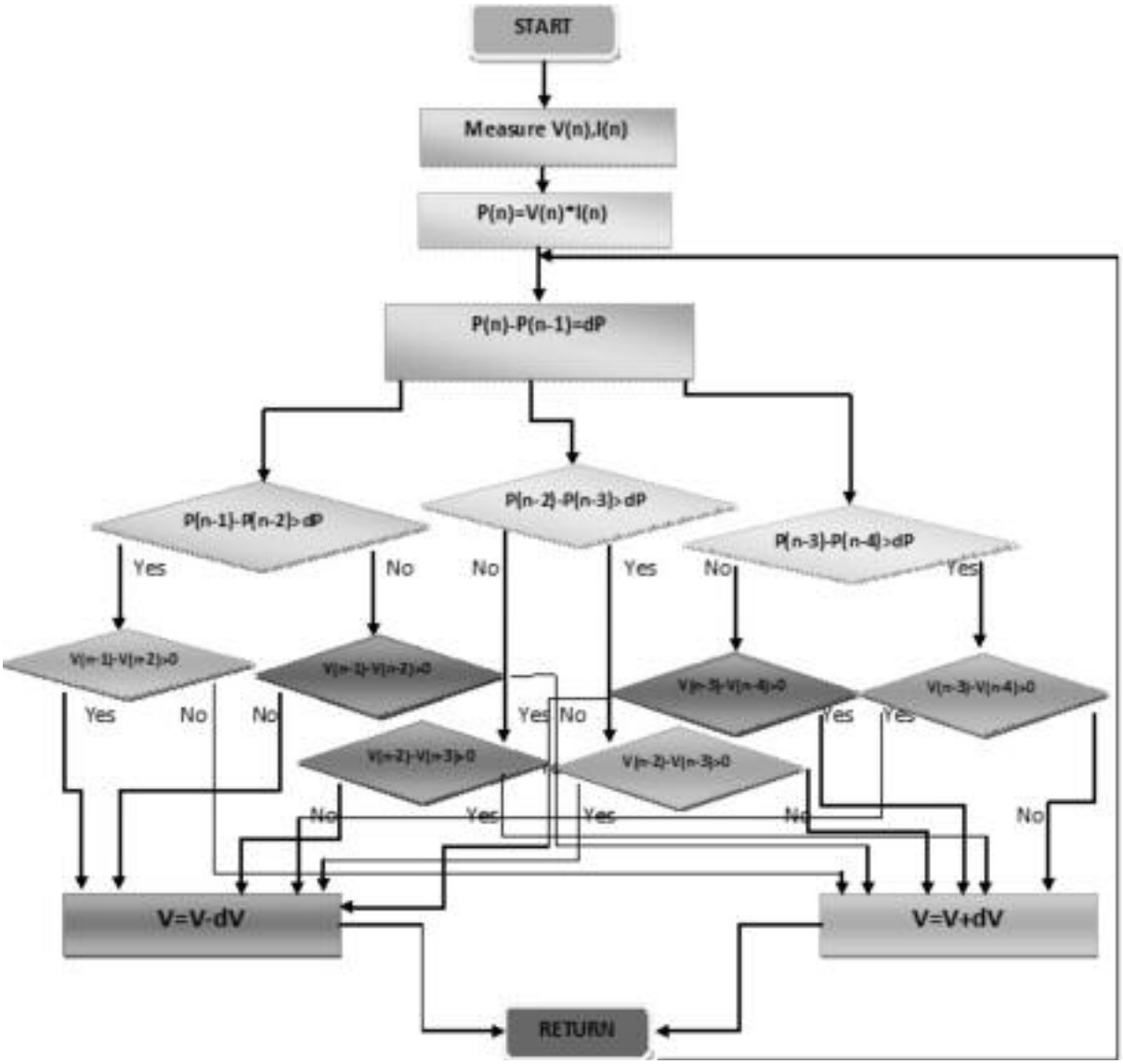

Figure 9: Differential power (dP) algorithm

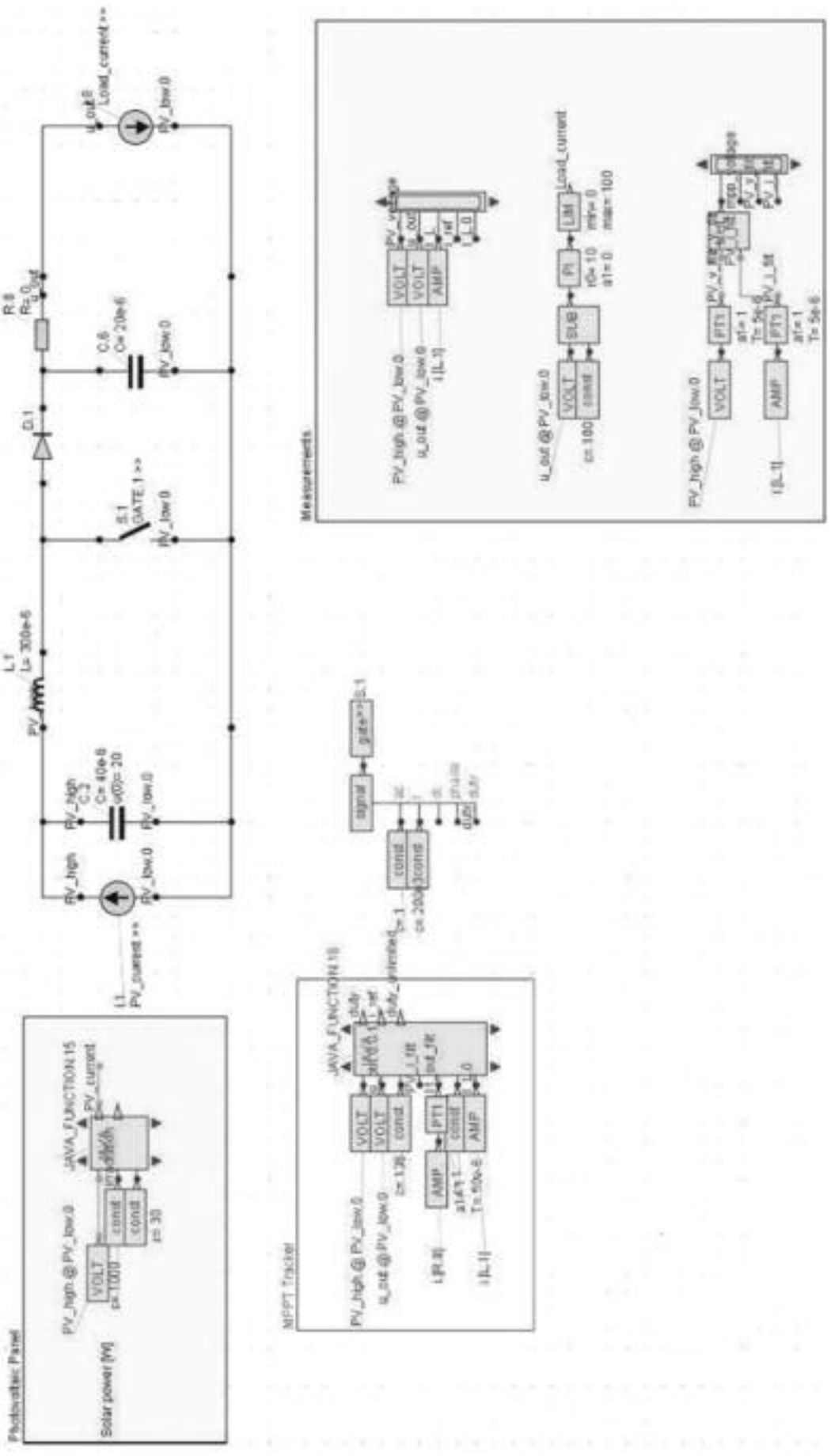

Figure 10: Circuit implementation of dP algorithm based MPPT

Electronics, Volume: 60, Issue: 3, pp.1156 – 1167 March 2013.

D'Souza, N.S.; Lopes, L. A C; and Liu, X. (2005). An Intelligent Maximum Power Point Tracker Using Peak Current Control, Power Electronics Specialists Conference, 2005. PESC '05. IEEE 36th, Vol., No. pp.172, 16-16 June 2005.

Elgendy, M.A., Zahawi, B. and Atkinson D.J. (2012). Assessment of Perturb and Observe MPPT Algorithm Implementation Techniques for PV Pumping Applications, *IEEE Transactions on Sustainable Energy*, Vol. 3, no. 1, January 2012.

Esram, T., and Chapman P.L., (2007). Comparison of Photovoltaic Array Maximum

Power Point Tracking Techniques, IEEE, *Transactions on Energy Conversion*, Vol. 22, No.2, June, 2007.

Femia, N., Petrone, G., Spagnuolo, G., and Vitelli, M., (2005). Optimization of perturb and observe maximum power point tracking method. *IEEE Transactions on Power Electronics,* 20, 963–973.

GeckoCIRCUITS. Power Electronic Simulation Software.

Green, M.A. (1992). Solar Cells – Operating Principles, Technology and System Application, University of NSW, Kensington, Australia.

Hohm, D.P., and Ropp, M.E., (2013). Comparative study of maximum power point tracking algorithms, *Prog. Photovolt: Res. Appl.,* Vol. 11, pp. 47–62, 2003.

Hua, C., and Lin, J., (2003). An on-line MPPT algorithm for rapidly changing illuminations of solar arrays, *Renew Energy* 28, 1129–1142.

Koutroulis, E., Kalaitzakis, K., and Voulgaris, N.C., (2001). Development of a microcontroller-based. Photovoltaic maximum power point tracking control system. *IEEE Trans. Power Electron*, 16, 46–54.

Koutroulis, E., and Blaabjerg, F., (2012). A New Technique for Tracking the Global Maximum Power Point of PV Arrays Operating Under Partial-Shading Conditions, Photovoltaics, *IEEE Journal,* Vol.2, no.2, pp.184,190, April 2012.

Moacyr A. G. de B, Junior L.G., Sampaio L.P., Guilherme A. e Melo, G. A., and Canesin C.A., (2007). 'Main Maximum Power Point Tracking (MPPT) strategies intended for Photovoltaics, *IEEE Transactions on Energy Conversion*, Vol.22, No.2, June 2007.

Salam, Z.; Ishaque, K.; and Taheri, H.,(2010). An improved two-diode photovoltaic (PV) model for PV system, 2010 Joint International Conference on Power Electronics, Drives and Energy Systems (PEDES) & 2010 Power India, Vol., No., pp.1-5, 20-23 Dec. 2010.

Subudhi, B., and Pradhan, R., (2013). A Comparative Study on Maximum Power Point Tracking Techniques for Photovoltaic Power Systems, Sustainable Energy, *IEEE Transactions*, Vol. 4, No.1, pp.89 – 98, Jan. 2013.

Thounthong, P.; Luksanasakul, A.; Koseeyaporn, P.; and Davat, B., (2013). Intelligent Model-Based Control of a Standalone Photovoltaic/Fuel Cell Power Plant With Supercapacitor Energy Storage, *IEEE Transactions on Sustainable Energy,* Vol. 4, No.1, pp.240,249, Jan. 2013.

Villalva, M.G., Gazoli, J.R., and Filho, E.R. (2009). Analysis and simulation of the P&O MPPT algorithm using a linearized PV array model', Industrial Electronics, 2009. IECON '09. 35th Annual Conference of IEEE.

Weidong Xiao; Edwin, F.F.; Spagnuolo, G.; and Jatskevich, J. (2013). Efficient Approaches for Modelling and Simulating Photovoltaic Power Systems', Photovoltaics, *IEEE Journal*, page(s): 500 – 508 Volume: 3, Issue: 1, Jan. 2013

Xiao, W., and Dunford, W.G., (2004). A modified adaptive hill climbing MPPT method for photovoltaic power systems. Proceedings of 35th Annual IEEE Power Electronics. Specialists Conference, Aachen, Germany. pp. 1957–1963.

Received 22 August 2014; revised 24 February 2015

Thermodynamic analysis of a direct expansion solar assisted heat pump water heater

Masoud Yousefi

Misagh Moradali

Mechanical Engineering Department, South Tehran Branch, Islamic Azad University, Tehran, Iran

Abstract

In this paper, the thermodynamic performance of a direct expansion solar assisted heat pump (DX-SAHP), which is used to heat domestic water from 20 °C to 45 °C, is theoretically investigated. The system includes a 3m^2 single-cover flat plate solar collector, 0.150m^3 water tank and 70m tube immersed in the water tank as a condenser. The effect of various parameters such as radiation on the collector surface, compressor speed and the ambient temperature on the coefficient of performance (COP) are calculated. Results show that obtained COP is considerably more than that of a conventional heat pump water heater when radiation on the collector is high. Also, increasing collector area and reducing compressor speed enhance COP. The same occurs when the ambient temperature increases. For instance, at an ambient temperature of 15 °C and 450 w/m^2 irradiation on collector surface, the calculated COP was 6.37.

Keywords: solar, solar boosted, heat pump, water heater

Nomenclature

A_c Collector area (m^2)
A_{coil} Coil area (m^2)
cp_w Water specific heat ($\frac{J}{kg\ k}$)
F' Collector efficiency factor
g Acceleration due to gravity ($\frac{m}{s^2}$)
H Coil convective heat transfer coefficient ($\frac{w}{m^2\ k}$)
h Enthalpy ($\frac{J}{Kg}$)
K_w Water conductive heat transfer ($\frac{w}{m^2\ k}$)
I Solar irradiance ($\frac{w}{m^2}$)
L Condenser length (m)
$\dot{m}$ Refrigerant mass flow rate ($\frac{kg}{s}$)
m_w Water mass (Kg)
N Compressor speed (RPM)
Q_e Heat flow rate (w)
$Ra = g\ \beta\ \Delta T\ {}^{L^3}/_{\nu\lambda}$ Rayleigh number
VD Compressor displacement volume (m^3)
Ta Ambient temperature (°c)
Tp Plate temperature (°c)
Tr Refrigerant temperature (°c)
Tw Water temperature (°c)
U_{LC} Collector heat loss coefficient ($\frac{w}{m^2\ k}$)
Vw Wind velocity ($\frac{m}{s}$)
W Compressor power consumption (w)

Greek symbols

α Absorptivity
β Thermal expansion coefficient ($\frac{1}{k}$)
σ Steffan-Boltzman constant
θ Collector slope
εc Glass emittance factor
εp Plate emittance factor
ηv Compressor volumetric efficiency
ν Dynamic viscosity ($\frac{m^2}{s}$)
λ Thermal diffusivity ($\frac{m^2}{s}$)
v Refrigerant specific volume ($\frac{m^3}{kg}$)

1. Introduction

Due to growing energy demand and depletion of fossil fuel resources, the application of renewable energy resources has attracted a lot of interest. Among different renewable energy sources, solar energy is one of the best alternatives which is readily available in many parts of the world. Consequently, research and developments have been conducted to expand application of solar energy. Solar assisted heat pump is one these applications. The idea of combining conventional heat pumps and solar systems has taken many interests. As is well known, the COP of heat pumps improves by increasing the evaporator temperature. On the other hand, solar collectors work better if the plate

(absorber) temperature decreases. As a result, both systems operate better in comparison with working separately.

Grozable *et al.,* (2005) investigated the effect of using different refrigerants on the COP of a DX-SAHP. Using R22 and R134a instead of R12 decreased COP 2 to 4%. Replacement of R410a, R407C and R404a with R12 reduced COP 15 to 20%.

Kuang *et al.,* (2006) reported the results of analysis of a multi-functional DX-SAHP which offered space heating during winter and water heating the whole year. The system employed a 10.5 m^2 solar collector and variable speed compressor and could supply 0.200 to 1 m^3 hot water a day at 50 °C. The daily average heat pump COP was calculated between 2.6 to 3.3 for space heating only mode, while it varied from 2.1 to 2.7 for water heating only mode.

Guoying *et al.,* (2006) simulated the operating performance of a DX-SAHP for water heating. The system used a specially designed solar collector with spiral-finned tubes, which contributed to heat transfer from the air to the tubes. The effect of different parameters was analysed and the authors recommended using a variable speed compressor due to the wide range of operating conditions, namely, variable solar radiation.

Dickci et al., (2008) investigated experimentally a DX-SAHP which is used to heat a 60 m^2 residential building. The average COP of the system was 3.08 and the overall exergy loss was obtained to be 3.845 kW.

Chatuverdi et al., (2009) proposed to use two stage compressors for producing high temperature hot water in the range of 60-90 °C. Calculated COP was higher than that of a single-stage DX-SAHP.

Liu Keling *et al.,* (2009) presented a mathematical model and reported the results for the performance of a DX-SAHP where the compressor's power was supplied by photovoltaic panels. The system worked in the weather conditions of Tibet and had a variable frequency compressor. They found that in a sunny summer day, COP of the system reached to 6.01 and the average electric efficiency, thermal efficiency and overall efficiency were 0.135, 0.47 and 0.625, respectively.

Chow *et al.,* (2010) examined a DX-SAHP and simulated the long term performance of a model with typical meteorological data (TMY) for Hong Kong. The average yearly COP of the system was reported as 6.46. Results showed this system works better in summer where the COP reaches 10.

Dott, *et al*., (2012) simulated different combinations of solar heat pumps. An analytical study has been done on a solar assisted heat pump with carbon dioxide as the refrigerant (Raisul Islam and Sumathy, 2013). Recent research based on a life cycle cost analysis showed that DX-SAHP systems are economical as well as energy conserving compared to the conventional electrical water heaters (Chaturvedi, *et al*., 2014).

It is the aim of this paper to investigate the effect of operating parameters on the performance of a DX-SAHP used for water heating. Following an introduction of the system analysed, mathematical description of the system governing equations is presented and the effect of different contributing parameters in a sample system was analysed.

2. System description

Among different combinations, direct expansion solar assisted heat pumps (DX-SAHP) and indirect expansion solar assisted heat pumps (IX-SAHP) are the two more applicable systems. In an IX-SAHP, a fluid like water is heated in the solar system and then, in a heat exchanger, the process of heat transfer takes place between the heat pump evaporator and hot fluid to raise evaporator temperature. Figure 1 presents a schematic of IX-SAHP.

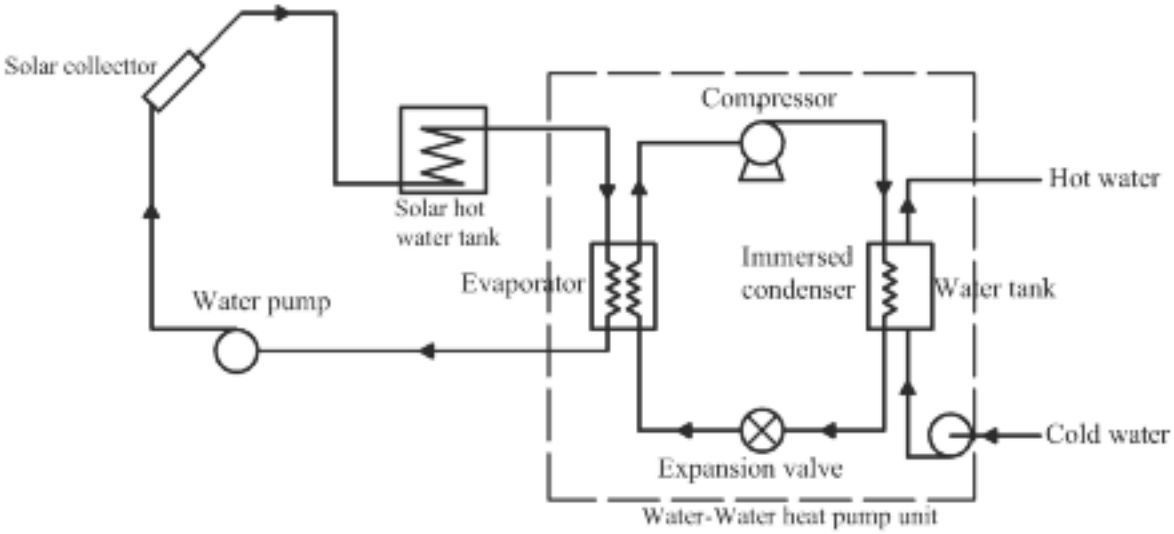

Figure 1: A schematic diagram of IX- SAHP

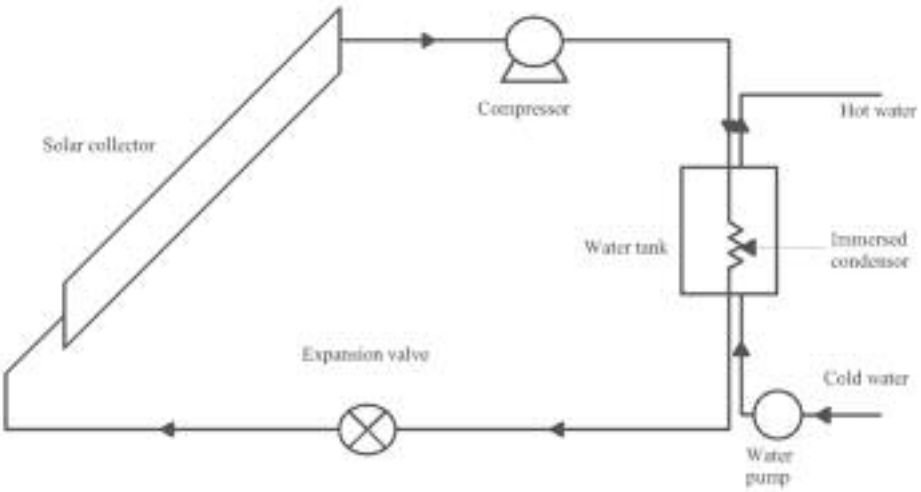

Figure 2: A schematic diagram of DX- SAHP

In a direct expansion solar assisted heat pump (DX-SAHP), solar collector tubes contain a refrigerant so it serves as the evaporator of system. Evaporation of refrigerant takes place by solar radiation and causes a decrease in plate temperature. Reduction of required components and risk of corrosion in the collector are two main advantages of this coupling. Figure 2 presents a schematic diagram of a DX-SAHP.

3. Mathematical model

A mathematical model is developed to predict the performance of a DX-SAHP. Except the water tank, quasi-steady modelling is used to model all components.

3.1 Solar collector

The solar energy collected by the collector/evaporator per unit area, Q_c, and the radiation heat transfer coefficient for one-cover solar collector, U_{LC}, are calculated as shown below (Duffie and Beckman, 2006):

$$Q_c = A_c(\alpha I - U_{LC}(t_p - t_a)) \quad (1)$$

$$Q_c = A_c F'(\alpha I - U_{LC}(t_p - t_a)) \quad (2)$$

$$U_{LC} = \left[\frac{1}{\frac{c}{t_p}\times\left(\frac{t_p - t_a}{1+f}\right)} + \frac{1}{h_w}\right]^{-1} + \left(\frac{\sigma(t_p + t_a)(t_p^2 + t_a^2)}{\frac{1}{\varepsilon_p + 0.0059\, h_w}} - 1\right) + \frac{1+f+0.133\,\varepsilon_p}{\varepsilon_c} \quad (3)$$

where:

$$f = (1 + 0.089\, h_w - 0.1166\, h_w \varepsilon_p)\times(1.07866) \quad (3\text{-a})$$

$$c = 520 \times (1 - 0.000051 \times \theta^2) \quad (3\text{-b})$$

$$e = 0.43 \times \left(1 - \frac{100}{t_p + 273}\right) \quad (3\text{-c})$$

Plate emittance factor (εp) and glass emittance factor (εc) are assumed to be 0.95 and 0.88, respectively. h_w is the convective heat loss coefficient and is equal to:

$$h_w = 2.8 + 3\, V_w \quad (4)$$

The energy balance equation in the collector/evaporator yields:

$$Q_e = \dot{m}(h_2 - h_1) \quad (5)$$

3.2 Compressor

The refrigerant mass flow rate is calculated by the following equation:

$$\dot{m} = \frac{\eta_v \, VD \, N}{60 \, v} \quad (6)$$

The compressor power consumption is found by the energy balance equation:

$$w = \dot{m}(h_3 - h_2) \quad (7)$$

3.3 Condenser

The energy balance equation in condenser is expressed as:

$$Q_c = \dot{m}(h_4 - h_3) \quad (8)$$

The heat transfer coefficient of an immersed condenser can be calculated as shown below (Ji et al., 2010):

$$H = 0.685\ (Ra)^{0.235}\ \frac{k_w}{L} \qquad (9)$$

The heating capacity of the condenser is found by coil heat transfer coefficient:

$$Q_c = H\ A_{coil}\ (T_c - T_w) \qquad (10)$$

Water tank temperature variation can be found from:

$$Q_c = m_w\ cp_w\ \frac{dt_w}{dt} \qquad (11)$$

3.4 Expansion valve

The expansion valve process is assumed to be isentropic. So:

$$h_1 = h_4 \qquad (12)$$

The heat pump coefficient of performance is obtained from:

$$COP = \frac{Q_h}{w} = \frac{h_4 - h_3}{h_3 - h_2} \qquad (13)$$

All above equations are solved by MATLAB based on a flowchart shown in Figure 3. All thermodynamic properties are found by equations presented for R134a (Ji et al., 2010).

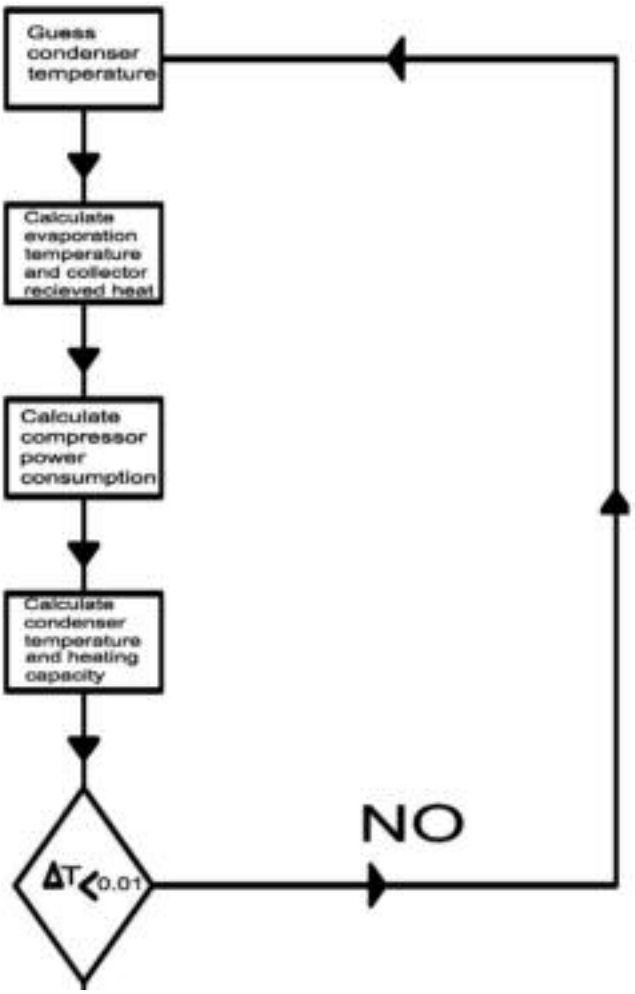

Figure 3: Calculation flow chart

4. System configuration

The above equations were solved for a system which is similar to some other previous experimental setups. Details of this system are described in Table 1.

Table 1: System configuration

Collector	One-cover flat plate collector F' =0.9, εC = 0.88, ερ = 0.95, θ = 35.5
Compressor	Reciprocating, VD= 24.1 cm^3 , ηv = 0.9, N= 1400 (rev/min)
Condenser	70m copper tube, Inner tube diameter = 8 mm, Outer tube diameter=12.5 mm

5. Results and discussions

Figure 4 shows the effect of solar irradiance and the average tank temperature on the performance of the system at 15°C ambient temperature and a wind velocity of 3 m/s. COP of the system increases when the received irradiance increases. In addition, reduction of water tank temperature results in increasing COP. The measured COP, when received radiation on the titled surface was 450 w/m^2, were calculated as 6.37, 5.16 and 4.28 at an average tank temperature of 20°C, 32.5°C and 45°C, respectively. At average water tank temperatures of 20°C, 32.5°C and 45°C and 950 w/m^2 radiation, the calculated COP were found to be 8.39°C, 6.62°C and 5.41°C, respectively.

Figure 5 shows system performance variation with ambient temperature. COP of the system boosts when the ambient temperature increases. The effect increases with increasing received irradiance.

At an ambient temperature of 10°C, and radiation values of 500, 700 and 900 w/m^2, COP was calculated as 6.52, 7.35 and 8.02, while at 20°C ambient and same received solar irradiance, calculated COP was 6.69, 7.55 and 8.25, respectively.

The variation of heat pump compressor power consumption with the received solar irradiance is presented in Figure 6. At 15°C ambient temperature and 450 w/m^2 solar irradiance, DX-SAHP power consumption was approximately 223.3, 347 and 347 W and at 950 w/m^2. These would change to 295, 378 and 468 W if the water tank temperature is taken as 20, 32.5 and 45, respectively.

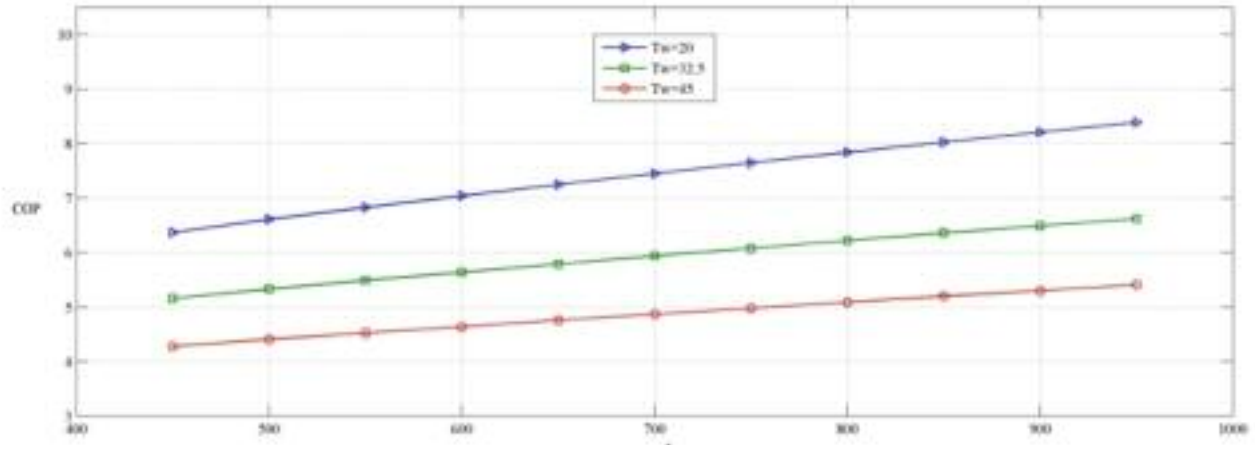

Figure 4: Variation of COP with solar irradiance

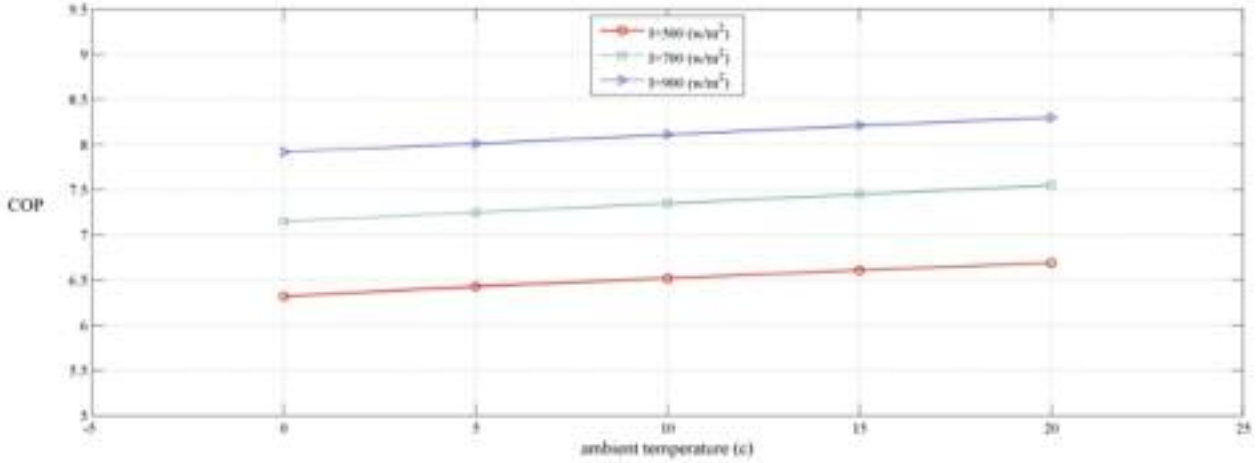

Figure 5: The effect of ambient temperature on COP

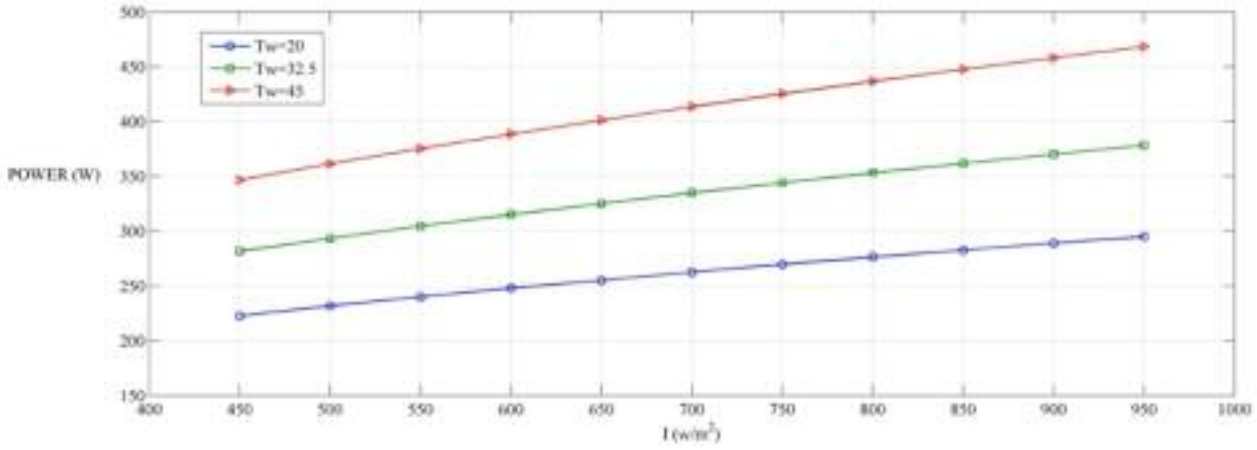

Figure 6: SAHP compressor power consumption

Figure 7 presents the effect of variation of compressor speed on the system at 15°C ambient temperature. Increasing compressor speed from 1100 rev/min to 1700 rev/min results in a reduction of coefficient of performance from 11 to 7 at 950 w/m^2 and from 7.64 to 6.72 at 450 w/m^2 when water tank temperature is 20 °C.

Figure 8 shows the improvement in the DX-SAHP coefficient of performance with increasing collector area. At 15°C ambient temperature and 20°C water tank temperature with 450 w/m^2 solar irradiance, calculated COP were 6.74 and 9.8 for collector area of 3.5 and 5 m^2, respectively.

Time required to heat 0.150 m^3 water is shown in Figures 9 to 11 in steady-state conditions when ambient temperature is assumed to be 15°C, compressor speed taken as 1400 rev/min with constant received solar irradiance. According to the calcula-

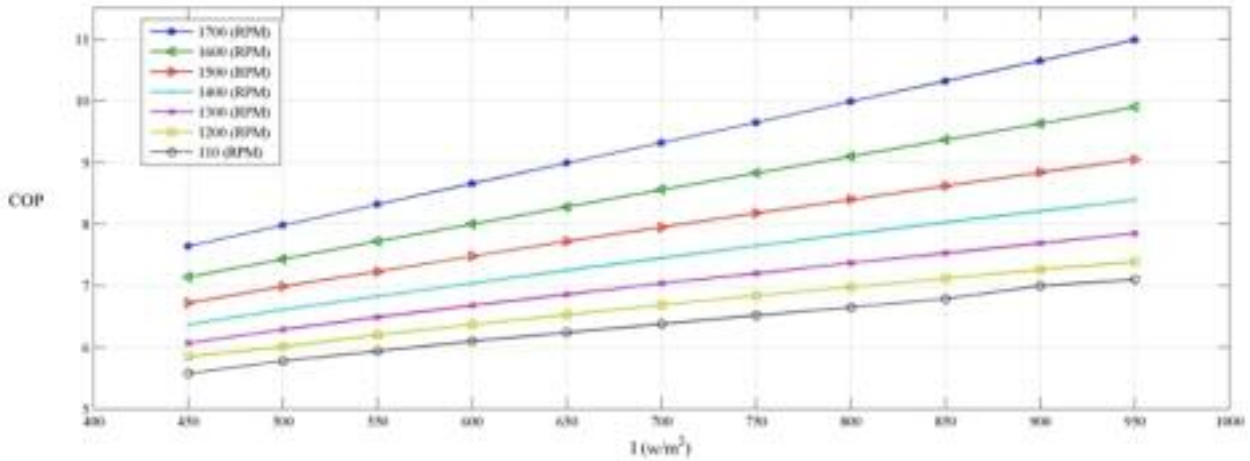

Figure 7: Effect of compressor speed on the performance of SAHP

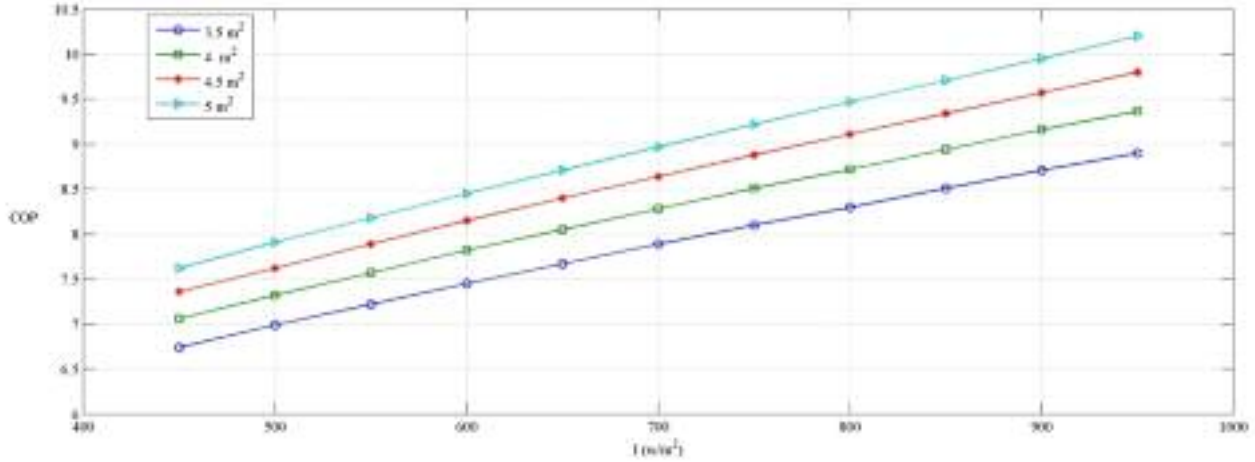

Figure 8: The effect of collector area on the performance

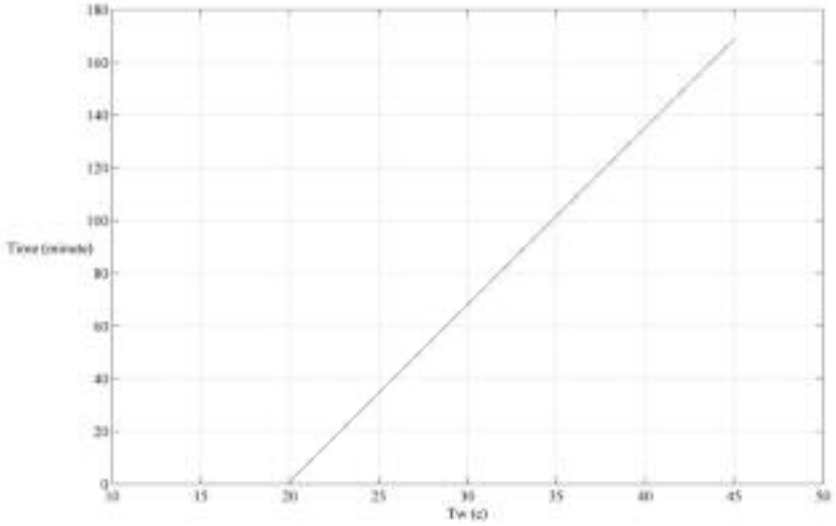

Figure 9: Variation of water tank temperature with time in 500 w/m²

tion at 500, 700 and 900 w/m^2 irradiation, the heating process takes 169, 132 and 112 minutes, respectively.

6. Conclusion

The results of simulation and thermodynamic analysis of a solar assisted heat pump water heater with a 0.150 m^3 water tank was presented. Effective parameters on the performance of the system was investigated which included solar irradiance, ambient temperature, compressor speed and solar collector area. According to the results, increasing solar irradiance and ambient temperature, reducing water tank temperature and compressor speed, all

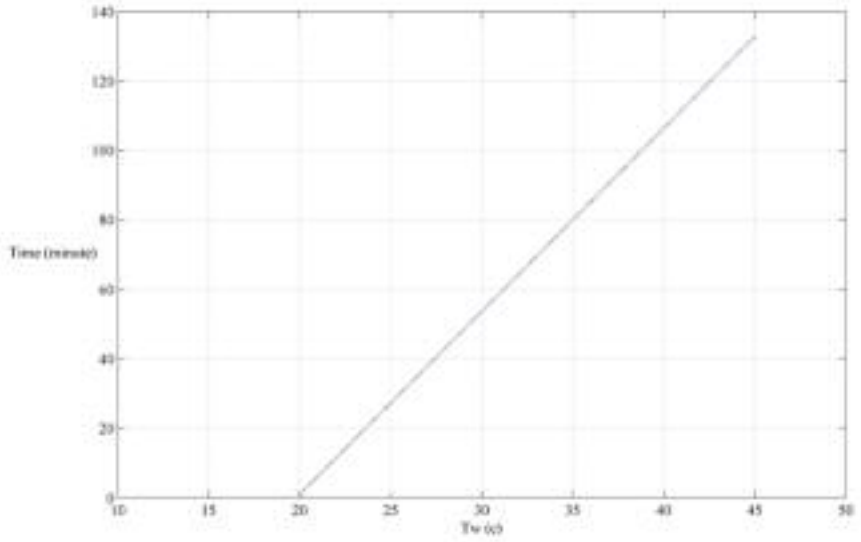

Figure 10: Variation of water tank temperature with time in 700 w/m^2

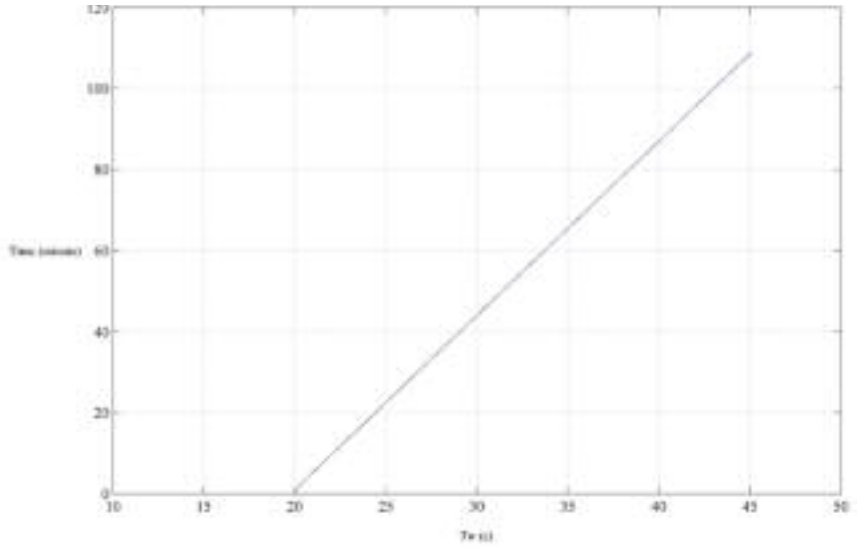

Figure 11: Variation of water tank temperature with time in 900 w/m^2

enhance the coefficient of performance. System COP was found to be 6.37 and 8.39 at solar irradiance values of 450 and 950 w/m^2, Table 1 Fuzzy controller rules for temperature controlrespectively. This is higher in comparison with that of a conventional heat pump water heater.

Acknowledgements

The authors would like to acknowledge the financial support of the Islamic Azad University, South Tehran Branch.

References

Chaturvedi, S.K., *et al.* (2009). Two-stage direct expansion solar-assisted heat pumps for high temperature application. *Applied Thermal Engineering*, 29: 2093-2099.

Chaturvedia, S.K., Gagranib, V.D. and Abdel-Salam, T.M. (2014). Solar-assisted heat pump – A sustainable system for low-temperature water heating applications. *Energy Conversion and Management.* 77: 550-557.

Chow, T.T., *et al.* (2010). Modelling and application of direct-expansion solar-assisted heat pump for water heating in subtropical Hong Kong. *Applied Energy*. 87: 643-649.

Cleland, A.C. (1994). Polynomial curve-fits for refrigerant thermodynamic properties: extension to include R134a. *International Journal of Refrigeration*. 17: 245-249.

Dikci, A., and Akbulut, A. (2008). Performance characteristics and energy-exergy analysis of solar assisted heat pump. *Building and Environment*. 43: 1961-1967.

Dott, R., Genkinger, A., and Afjei, T. (2012). System evaluation of combined solar and heat pump systems. *Energy Procedia*, 30: 562-570.

Duffie, J.A., and Beckman, W.A. (2006). Solar engineering of thermal processes. Third edition. John Wiley and Sons Inc.

Gorozabel, F.B., *et al.* (2005). Analysis of direct expan-

sion solar assisted heat pump using different refrigerant. *Energy Conversion and Management*. 46: 2614-2624

Guoying Xu, Xiaosong Zhang, Shiming Deng. (2006). A simulation study on the operating performance of a solar-air source heat pump water heater. *Applied Thermal Engineering*. 26: 1257-1265

Ji, J., *et al.* (2010). Performance analysis of an air source heat pump using an immersed condenser. *Frontiers of Energy and Power Engineering*. 4: 234-245.

Keling, L., *et al.* (2009). Performance study of a photovoltaic solar assisted heat pump with variable-frequency compressor- A case study in Tibet. *Renewable Energy*. 34: 2680-2687.

Kuang, Y.H., and Wang, R.Z. (2006). Performance of multi-functional direct-expansion solar assisted heat pump. *Solar Energy*. 80: 795-803.

Received 11 May 2014; revised 27 April 2015

Coherence and time-frequency analysis of impulse voltage and current measurements

Jelena Dikun
Electrical Engineering Department, Klaipeda University, Klaipeda, Lithuania

Emel Onal
Electrical Engineering Department, Istanbul Technical University, Maslak, Istanbul, Turkey

Abstract
The aim of this paper is to point out the advantages of the use of the time-frequency analysis in the digital processing of waveforms recorded in high voltage impulse tests. Impulse voltage tests are essential to inspect and test insulation integrity of high voltage apparatus. On the other hand, generated impulse currents are used for different test applications such as investigation of high current effects, electromagnetic interference (EMI) testing, etc. Obtained voltage and current waveforms usually have some sort of interferences originated from the different sources. These interferences have to be removed from the original impulse data in order to evaluate the waveform characteristics precisely. When the interference level is high enough, it might not be possible to distinguish signal parameters from the recorded data. Conventional filtering methods cannot be useful for some interference like white noise. In that case, time-frequency filtering methods might be necessary. In this study, the wavelet analysis, which is a powerful time-frequency signal processing tool, is used to recognize the noise of impulse current and voltage data. Thus, the noise sources can be determined by short time Fourier Transform, and a coherence approach is used to determine the bandwidth of noises.

Keywords: impulse voltage, impulse current, overshoot waveform, short-time fourier transform

1. Introduction

An impulse voltage test on high-voltage equipment is a useful application to evaluate the insulation integrity and to identify the ability to withstand over-voltages encountered during operation. The measured waveforms in practice may contain oscillations and overshoots due to the inclusion of different noise sources. One of the major challenges of impulse voltage and current measurements is the existence of the noise that affects the precise identification of impulse parameters. The measurement of lightning impulses with superimposed overshoot or oscillation has been the subject of extensive studies in the last few years in light of results of an important study (IEC 60060-1, 1995; IEEE Standard 4, 1995) with regard to the relationship of the effective peak voltage and the overshoot frequency.

The main findings of the study are the test voltage equation for the determination of the effective peak voltage. The evaluation of the overshoot and the test voltage from an output waveform is performed with the residual filtering method. Basically, the evaluation of the high voltage impulse signals consists of the evaluation of the peak amplitude (U_{max}) and three time parameters (T_1: Front time, T_2: Time to half value for full impulse and T_c: Cut-off time). When the level of disturbance in signals is low, computation of these parameters is also quite simple, but when the disturbance level rises, they become much more difficult.

In terms of frequency contents, there are three kinds of disturbance: Oscillation on the test circuit, electromagnetic disturbance and digitizer noise. The results show that those three disturbance types have different frequency characteristics (Angrisani, *et al*., 1998). The oscillations due to the test circuit have a frequency above 500kHz, the electromagnetic disturbance usually is characterized by frequencies in the range of several hundreds of kilohertz (more than 500kHz) up to a few megahertz

(less than 10MHz) and the digitizer noise that comes from digitizers used in high voltage test halls, and these frequencies are clearly above 10MHz.

Taking this information into account, the standard states that the evaluation of the high voltage impulse parameters, must be based on the low voltage part of the wave that is really applied to the equipment under test. This means that only the oscillations due to the presence of capacities in the test circuit can be considered. So, all of the disturbances having frequencies above 500 kHz, can be removed from the low voltage part before evaluation of the impulse parameters. For this reason, it is very important to know the sources and eliminate the noises (Garnacho *et al.,* 1997).

In this study, short time Fourier transform is applied to voltage and current measurements in order to define the noise effects on the signals and the coherence relationship between the voltage and current signals. They are used to determine frequencies of low pass filter characteristics. Hence, the frequency range of a band pass filter is found by means of a threshold among the high correlated frequencies components.

2. Time-frequency analysis

In this section, a mathematical background to be used in this application is focused on the Short-Time Fourier Transform (STFT) techniques and coherence analysis, which is presented as cross spectral property between two signals (Harris, 1978).

2.1. Short-time Fourier Transform

The signal to be transformed is multiplied by a window function which is defined for a short time period. Then it is represented by the integral form of the classical Fourier transform by sliding the window function along the time axis. In the application, there are a large number of so many window types, however, one of the most popular one is 'Hanning Type windowing'. The shape of this window function is shown as a Gaussian function at around the zero value. In this manner, Short-Time Fourier Transform of a given signal x(t) is described as below:

$$STFT\{x(n)\} = X(\tau,\omega) = \int_{-\infty}^{\infty} x(t)\,\omega(t-\tau)\,e^{-j\omega t}\,dt \quad (1)$$

For discrete case, STFT of discrete time domain signal x[n] is given by the following equality

$$STFT\{x[n]\} = X(m,\omega) = \sum_{n=-\infty}^{\infty} x[n]\,\omega[n-m]\,e^{-j\omega n} \quad (2)$$

2.2. Coherence and threshold value

The coherence between two time domain signals x(t) and y(t) is defined as similarity degree in the frequency domain. Hence it can be shown as a real-valued function as below:

$$C_{xy} = \frac{|G_{xy}|^2}{G_{xx}G_{yy}} \quad (3)$$

Where, G_{xy} is the cross-spectral density between x and y. And also, G_{xx} and G_{yy} are the auto-spectral densities of x and y respectively. The magnitude of the spectral density is denoted as $|G|$. The numerical values of the coherence will always take place between zero and unit. Namely it is given by

$$0 \le C_{xy} \le 1$$
$$Threshold > (C_{xy})_{max}/2 = 0.5 \quad (4)$$

An accepted threshold can be considered as a value greater than 0.5 in coherence variation. It can be chosen as 0.6.

3. Measurement system and data

The lightning impulse voltages used in this study are produced by a 1 MV, 50 kJ, Marx type impulse generator. The voltages are measured by means of a capacitive divider and a HIAS 743 digital oscilloscope with 12 bit real vertical resolution at 120 Mega sample / sec. All measurements of the experimental study are given in IEC standard. This paper is a study of the breakdown strength signal analysis of Sulphur hexafluoride (SF_6) with negative impulse voltage. Due to its exceptional insulating and arc-extinguishing properties, Sulphur hexafluoride gas has been widely employed as insulation of high voltage power apparatus. The experimental set-up is seen at Figure 1.

Signals are carried using a sphere-plane electrode with a sphere diameter of 10 mm and electrode gap spacing of 5 cm. The sphere electrode is connected to high voltage while the plane electrode is earthed. Electrodes are mounted in a pressure vessel of 120 mm diameter and 600 mm length.

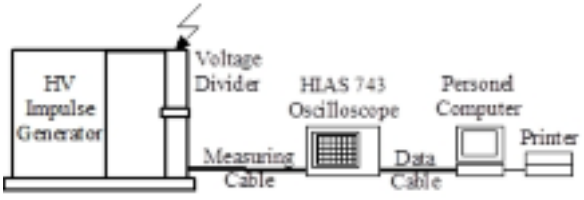

Figure 1: Experimental set-up

Figures 2 and 3 show the front chopping impulse voltage and impulse current signals, respectively. It is difficult to establish the traceability of the test results and compare them with those of other

high-voltage (HV) testing laboratories. In view of such information, the standard states that the evaluation of the HV impulse parameters must be based on the lightning high voltage image of the wave that was actually applied to the equipment under test. This means that only the oscillations due to the presence of capacitances in the test circuit must be considered. All of the disturbances with frequencies above 500 kHz must be removed from the lightning voltage waveform prior to the evaluation of the impulse parameters (Simon *et al.,* 2006; Li and Rungis, 2003; Gamacho *et al*,, 2002; Lewin *et al*, 2008).

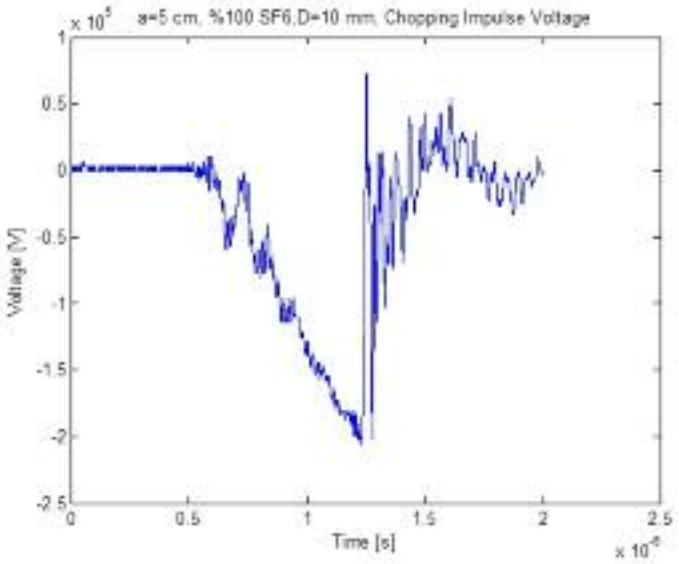

Figure 2: Negative chopping impulse voltage

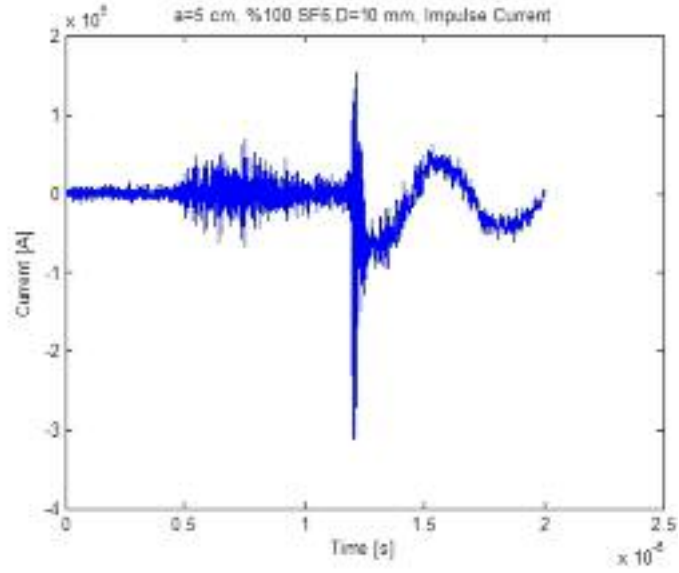

Figure 3: Negative impulse current

The overshoot can be eliminated or reduced by improving the electric circuit. As seen in Figure 4, the spectrum of the waveform and the expected frequency content of the disturbances are used to determine whether a given frequency component corresponds to a disturbance that should be removed or not. For this reason, the test circuit includes components that may have a large capacitance. Due to the large dimensions of the equipment under test and the components of the test circuit, there is also a significant amount of stray capacitance between components and the test site. The closed loop formed by the test circuit also includes some inductances. Many researchers focused on the disturbances caused by the combination of a high rate of rise of impulses in the stray capacitances and inductances that are present in the circuit. The measuring circuit, as well as the high-voltage generator, should produce or cause oscillations and overshoots as few as possible. Oscillations can only be accepted if it is certain that they are produced by the device under test in connection with the high-voltage generator. In some cases, oscillations come from a generator and measuring device. It is necessary to ensure that they are generated in the measuring system, e.g. in the low voltage arm of the divider.

Generator and measurement circuits are located on high voltage and low voltage area of the laboratory, respectively. Chopped impulse voltage is obtained by adjusting the spherical gaps to sparkover at desired time of the signal. Because the chopping time is dependent on the spherical electrode spacing and the amplitude of voltage, it is necessary to reduce the electrode gap to obtain a wave chopped near to the front, as a result, the ionization causing breakdown and the formation of space charges occurs in a shorter time. Electromagnetic interferences radiated from a high voltage impulse generator are mainly caused by the discharges occurring in air gaps, which are used to switching on the impulse generator (Onal *et al.*, 2008; Rungis and Li, 1999; Gockenbach *et al.,* 2001; Altay and. Kalenderli, 2012).

The effect of these interferences with increases of the applied voltage decreases with the secession of the generator. To reduce the interference to a satisfactory level, shielding shall be provided for both to the spark gaps and the electronic circuit. The removal of noise with low frequency is difficult comparing with the removal of noise with high frequency. Removal of high frequency noise from data is simple.

4. Time-frequency and coherence analysis

For this study, sampling frequency is 10^9 Hz. As shown in Figure 4, the maximum frequencies are between 0.8 and 1.4 μs. This time range refers to the front of chopping signal. It starts corona discharge in this area before breakdown. For this signal, the characteristic values taken from oscilloscope according to IEC, max voltage are $U_p = 164.1$ kV, $T_1 = 0.468$ μs.

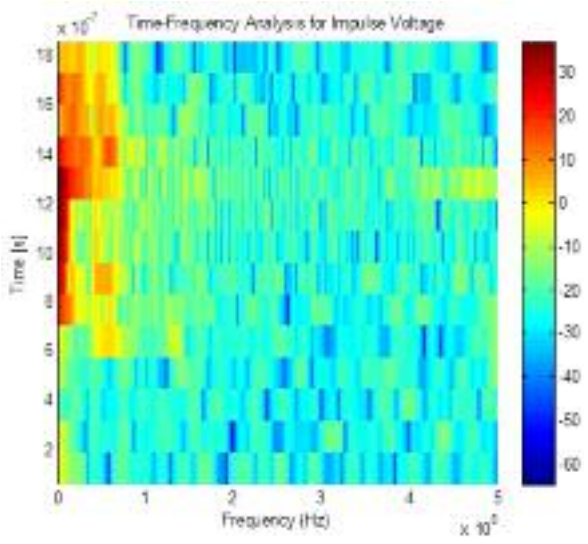

Figure 4: Time-frequency analysis for chopping impulse voltage

For impulse current as seen in Figure 5, there is a breakdown approximately at 1.2 μs. This time is nominal value for standard impulse voltage. There is a common frequency area at 1.2 μs up to 500 MHz. This is a breakdown process. As seen in the Figure 4, maximum frequencies are nearly 10 MHz

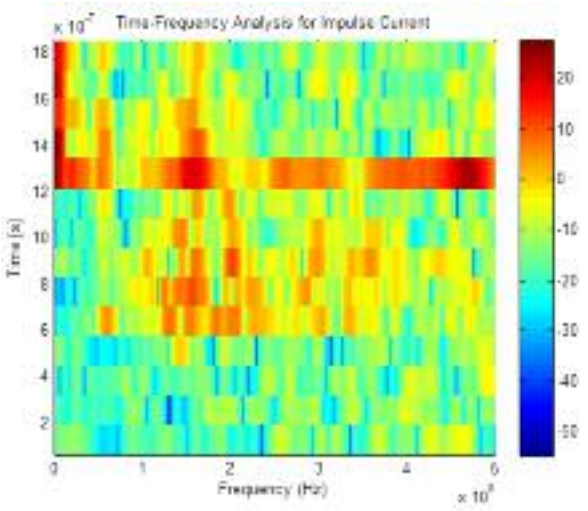

on the crest of the impulse voltage signal.

Figure 5: Time-frequency analysis for impulse current

In this study, coherence analysis is applied to extract the common properties between impulse voltage and current measurements. In this way, highly correlated frequency components between (50-150 MHz) can be determined as frequency characteristics of the corona phenomena comparing with threshold of 0.6.

5. Conclusions and discussions

The electromagnetic interferences in a circuit and the digital recorder quantization noise have been ascertained to the basic causes for error. Stray inductances formed in connection points can cause electromagnetic interference within the frequency of 50 MHz.

The main problem in an impulse generator circuit is the undesired inductive effect that causes ripples in the output waveform and forms an obstacle for a shorter duration of the pulse. This effect is mainly reduced by making relatively short connections between the components and using bus-bars as connection units, rather than wiring. For our electrode system, the peak of frequency of distortions which has above 10 MHz belongs to the digitizers. However as in many practical situations, a transient electromagnetic interference can enter the measuring circuit at the divider low-voltage arm, or penetrate through the coaxial cable sheath and the digital recorder enclosure.

Ideally, all these devices shall be protected by a perfect electromagnetic shield, but in reality shielding, they may effectively mask the measured signal spectrum at a much lower frequency than the limit imposed by the digitizer quantization noise. There are different sources of high frequency interferences on an impulse waveform: stray capacitances and inductances of elements in the generating and measuring circuits; circulation currents or induced currents and voltages on the measuring cable shield or all of the connection as ground and high voltage connections; signals penetrating into the recording instrument via power supply or coming from electromagnetic radiation can cause high frequency undesired signals.

High voltage switching operations and discharge phenomena in the gas gap cause electromagnetic transients. These transients radiate high electromagnetic fields of high frequency and cause interference to sensitive electronic equipment as oscilloscope, voltmeter and PC. Interference of the switch increases with the applied voltage to gap space and decreases with the distance from the source (Custodio et al., 2000). As shown in Figure 6, the peaks of between 50 and 150 MHz are common for voltage and current. Moreover, from the beginning up to breakdown, there are signals having the frequency range of 100-200 MHz. These signals can be the partial discharge phenomena. The reason for these situations can be disturbing depending on electrode system. This caused more distortion peaks due to the corona phenomena before the breakdown. It can be said that corona begins around the sphere electrode. Removing high frequency oscillations is also necessary for detecting overshoot and determining its amplitude and duration. For example, it can be used as digital filter to eliminate between around 50 and 150 MHz distortions for our system. The duration of chopping time is important in terms of the verification of the chopped impulse voltage on high-voltage power transformers. In practical applications, this duration

must be known to simulate the impulse spark over between arc horns and it should be correctly adjusted to the range of 2-6 □s. Having these features can be useful both in terms of the calculation of the circuit parameters and the filter design.

Acknowledgment

The authors show their gratitude to Prof. Dr. Serhat Seker from Istanbul Technical University in Turkey, and Prof. Stefan Tenbohlen from IEH Stuttgart University in Germany.

References

Angrisani L., Daponte, P., Dias, C., and Vale A., (1998). Advanced Processing Techniques of High- Voltage Impulse Test Signals' *IEEE Trans. on Instrumentation and Measurement*, Vol. 47, No. 2, April 1998.

Altay, O. and Kalenderli O. (2012). Interference Removal on Impulse Voltage and current measurements with wavelet analysis – 2012 International Conference on High Voltage Engineering *and Application*, Shanghai, China, September, 17-20, 2012.

Custodio D. and Almeida do Vale A. (2000). High Performance Digital Processing of High Voltage Impulses based on Time-Frequency Analysis,' *10th Mediterranean Electrotechnical Conference* Melecon, pp. 766-769, Vol. 2.

Garnacho, F. *et al.* Evaluation Procedures for Lightning Impulse Parameters in case of Waveforms with Oscillations and/or Overshoot' *IEEE Trans. On Power Delivery*, Vol. 12, No. 2, pp. 640 – 649, 1997.

Gamacho, F, *et al.* (2002). Evaluation of lightning impulse voltages based on experimental results, *Electra*, No. 204, pp. 31 – 38.

Gockenbach E., Hackemack K., and .Werle P. (2011). A contribution to the evaluation of lightning impulses with oscillations or overshoot near the peak – *Intern. Symposium on High Voltage Engineering*, Bangalore, Paper No. 7-3.

Harris F. (1978). On the Use of Windows for the Harmonic Analysis with the Dicrete Fourier Transform in Proceedings of the IEEE, Vol. 66, No.1, pp. 51-83, January 1978.

IEC 60060-1 (1989). High Voltage Test Techniques – Part 1: General Definitions and Test requirements, *Int. Electrotech. Comm*.

IEEE Standard 4 (1995). Standard Techniques for High Voltage Testing.

Lewin P.L., Tran T.N., Swaffield D.J., and. Hällström J.K. (2008). Zero-Phase Filtering for Lightning Impulse Evaluation: A k-factor Filter for the Revision of IEC60060-1 and -2 – *IEEE Trans. on Power Delivery*, Vol. 23, No. 1, January 2008.

Li Y. and Rungis J. (2003). Evaluation of parameters of lightning impulses with overshoot,' *13th Int. Symp. High Voltage Engineering*, Delft, Netherlands, Aug. 25 – 29, 2003.

Onal, E., Kalenderli O., and .Seker S. (2008). , Multi-Resolution Wavelet Analysis for Chopped Impulse Voltage Measurements and Feature Extraction – *IEEE Trans on Dielectrics and Insulations*, July 2008.

Rungis J. and Li Y. (1999). Precision digital filters for high voltage impulse measurement systems, *IEEE Trans. Power Del.*, Vol. 14, No. 4, pp. 1213–1220, October 1999.

Simon P. Garnacho F., Berlijn S.M., and Gockenbach E. (2006). Determining the test voltage factor function for the evaluation of lightning impulses with oscillations and/or an overshoot, *IEEE Trans. Power Del.*, Vol. 21, No. 2, pp. 560–566, April, 2006.

Received 11 May 2013; revised 26 March 2015

The determination of short circuits and grounding faults in electric power systems using time-frequency analysis

Vedat Esen
Vocational High School, Department of Electricity, İstanbul Arel University, Istanbul, Turkey

Bulent Oral
Department of Electrical & Electronics Engineering, Faculty of the Technology, Marmara University, Istanbul, Turkey

Tahir Cetin Akinci
Department of Electrical & Electronics Engineering, Engineering Faculty, Kirklareli University Kirklareli, Turkey

Abstract
In order to ensure that electrical energy reaches consumers uninterrupted, researchers constantly try to improve power transmission lines. To realize this improvement, probable faults should be analysed through every known method, and new methods should also be implemented. In this study, firstly, the Keban power transmission line located in the Eastern Anatolia region of Turkey was modelled. After that, probable short circuit scenarios were applied on the model, and the short circuit faults in the scenarios were analysed by using the Fourier analysis. The Fourier analysis is a mathematical method that is used as an effective way to determine the sudden changes in the frequency and time band. The study was successful in determining phase and grounding faults through the analyses of the scenarios using Fourier analysis. The fact that the mathematical method was applied on the probable scenarios on a physical model increases the importance of the study.

Keywords: Fourier analysis, short circuits in electrical power systems, modelling electrical power systems, time-frequency analysis

1. Introduction

Today, the production, transmission and distribution of electrical energy are performed firstly by planning the processes through computer programs, evaluating certain risk factors by performing various analyses, performing an economical analysis and lastly by the application of the plans (IAEA, 1995). With the improvements in computer technology, these analyses and mathematical modelling processes have become inevitable. Many factors that previously had to be neglected in the process, from the production of energy to its distribution to end users, can now be calculated and the analysis of those evasive probable shortcomings can be performed in the planning phase (Paska, 2007; Billinton *et al.,* 1997; Chanda and Bhattschsrjee, 1994).

Two of the most important types of faults in electrical power systems to come to mind are short circuits and probable grounding faults. Short circuiting is presently one of the most prevalent faults in electrical power systems (Yuhai *et al.,* 2007). These faults may occur between the phases as well as between the phases and the ground (Hambley, 2011). Short circuits can be classified as three phase short circuit faults, arc faults and grounding faults. The faults may occur for various reasons. These faults can be analysed through conventional methods as well as modern sign processing methods (Akinci *et al.,* 2013). Sign processing methods provide successful results through the analysis of the fault in the frequency domain.

The only valid standard for short circuit studies in the world is IEC 60609 (Kasikci, 2002). Improvements in computer systems provide us with the opportunity to perform modelling processes in

these studies, and enable us to get results in a much shorter time with highly realistic simulations.

The Matlab-Simulink © software, which was used for the simulations in this study, has also been conducted using many similar studies. There are many studies on short circuit faults performed through various simulation techniques in the literature, as well as many other studies where simulation programs were used (Kankaratug *et al.,* 2011; Faig *et al.,* 2010; Pamuk, 2011; Aygen *et al.,* 1995; Gopalakrishnan *et al.,* 2000; Miroshnik, 2000; Maslo and Vnoucek, 2009; Ekici *et al.,* 2009; Serrican *et al.,* 2010; Ekiz and Tumay; Závodný, 2005; Evrenosoglu, 2005; Tekin, 2006).

In recent years, the evaluation of short circuit effects in power systems through the static synchronized serial compensator method (Kankaratug *et al.,* 2011), the evaluation of short circuits in electrical systems which include wind generators (Tekin, 2006), the evaluation of short circuits in the Van city electric power transmission line (Dogruer, 2007), and the computer modelling of the Tedas block substation – stadium distribution system in Adapazarı (Acar, 2008) have been performed. In this study, the Keban power transmission line was modelled and the faults occurring as a result of the probable short circuiting scenarios were analysed by using the Short Time Fourier Transformation. At the end of the analysis, the characteristic properties of phase-ground and phase-phase faults were determined using the Short Time Fourier Transform (STFT) method.

2. Types of short circuits

Short circuit currents can be calculated based on the impedance the circuit represents. This impedance, in turn, can be calculated by summing up the various resistances and the reactance in the power source and the error line loop. Mathematically, this short circuit impedance is calculated through (Z_{SC}) Equation (1). In this calculation, ΣR is the sum of the serial resistances and ΣX is the sum of the serial reactance (Schneider Electric, 2005).

$$Z_{sc} = \sqrt{\left(\sum R\right)^2 + \left(\sum X\right)^2} \qquad (1)$$

The calculation of short circuit currents is based on Ohm's Law. The mathematical expression is given in Equation (2). In this expression, I_{SC} is the short circuit current in the three phase short circuit (Schneider Electric, 2005). V_n is the uncharged nominal network voltage and 3-5% higher than the voltage on the terminals.

$$I_{SC} = \frac{V_n}{\sqrt{3} \times Z_{SC}} \qquad (2)$$

Different types of short circuits can be seen in electrical systems. Short circuits can be classified under four titles as three phase short circuits, two phase short circuits, the phase – neutral short circuits and the phase – ground short circuits. Three phase short circuits are symmetric faults since currents of equal amplitudes flow through the phases in these faults. Phase-ground, two phase and two phase-ground short circuits are classified as asymmetrical faults (Smeets and Lathouwers, 2010).

Three phase short circuits are the most common ones in electrical systems. However, it is also the heaviest form of short circuiting, and the electrical systems have to be sized according to the greatest short circuit currents, which are three phase symmetrical short circuit currents, with respect to their endurance. On the other hand, important short circuit accidents are seen in phase - neutral and phase – ground short circuits. It is also possible for there to be a short circuit between the neutral-ground-conductors or two conductors on the same phase.

Three phase short circuit is a symmetrical fault on which the determination of the opening capacity of the current overflow protection device and the establishment of thermal endurance are based (Kasikci, 2002). The short circuit current flowing through the given circuit was defined as I_{SC3}, and the formula pertaining to the short circuit current was given in Equation (3).

$$I_{SC3} = \frac{V_{LL}}{\sqrt{3} \times Z_{SC}} \qquad (3)$$

In Eq. (3), I_{SC3} represents the three phase short circuit current, V_{LL} represents the voltage between the phases and Z_{SC} represents the impedance.

In this type of short circuiting, the fault occurs between the two phases providing the voltage between phases (V_{LL}). The short circuit current (I_{SC2}) in a two phase short circuit fault is lower than that of a three phase fault (Short Circuits Analysis, 2013). The formula for the calculation of the two phase short circuit current is given in Eq (4).

$$I_{SC2} = \frac{V_{LL}}{2 \times Z_{SC}} = \frac{\sqrt{3}\, I_{SC3}}{2} = 0.86\, I_{SC3} \qquad (4)$$

The phase-neutral short circuit is a fault caused by the contact between the phase and the neutral (Short Circuits Analysis, 2013). The model for phase-neutral short circuits is and the formula, with the short circuit current on this line defined as I_{SC1}, was given in Eq. (5).

$$I_{SC1} = \frac{V_{LL}}{\sqrt{3} \times \left(Z_{SC} + Z_{LN}\right)} \qquad (5)$$

In some special cases of the phase-neutral faults, the zero component impedance of the source is lower than Z_{sc}. This can be seen in the star-cross connected transformers or the secondary generators (operating in power outages). Therefore, the short circuit current in a phase-neutral short circuit can be greater than that of a three phase fault (Short Circuits Analysis, 2013).

In a phase-ground short circuit, a component impedance of zero occurs in motion. The short circuit current in a phase-ground fault is expressed as I_{sc0} and its mathematical expression is given in Eq. (6).

$$I_{sc0} = \frac{V_{ll}}{\sqrt{3} \times (Z_{sc} + Z_0)} \quad (6)$$

3. Modelling the Keban transmission line and the simulation of short circuiting

Modelling or simulation are the terms used in the systematic evaluation and design of an existing system. Mathematical modelling is an efficient and economical way of better understanding, analysing and designing systems (Unal, 1996).

In modelling, the model should be mathematically calculable and detailed enough to allow for the same results obtained from the real system, and the results should reflect the reality. In a study about the performance of a system, first, a model of the system should be constructed. A model should be similar to a real system; it should be a simplified example of the ideal state of a system. The modelling of electrical systems is especially important, since it allows for future faults to be predicted and calculated and the precautions to be taken (Patel *et al.*, 2002).

In this context, the model used in this study was designed as an exact model of the Keban line using 2009 TEİAS data for the parameters on the transmission line under ideal conditions.

Transmission systems are the systems which encompass everything between the production plants and the distribution systems, and in which the transmission of electrical energy at the levels of High Voltage (HV) and Very High Voltage (VHV) are performed. In Turkey, the transmission system voltage level is standardized as 380 kV and 154 kV (TEIAS, 2011).

The length of the 380 kV lines in Turkey is approximately 14 420 km and their carrying capacity is approximately 1000 MW. Even though relay stations are sufficient, transmission system insufficiency and problems persist in certain areas. As a result of the new dams built in Turkey in order to meet the energy need and the disruptions in the power transmission lines after the 1999 Marmara earthquake, after 2006, the transmission lines in the country are constantly being renewed through the new budget and new programs implemented, and they are improved with new lines, new transformer groups, or adding new thermal plants to the networks. These improvements and renewals constantly cause changes in power transmission and distribution lines. According to data from TEIAS, the production capacity of present plants in 2010 was 222,533 GWh, while this number is expected to be 255,362 GWh in 2012 when the new plants which already had their licenses and began construction start to operate. Additionally, a 4 000 MW additional consumption need every year necessitates the present system to be altered every year and new plants to be added to the system. This renewal and improvement continue without any interruption with the added effect of industrialization and urbanization.

In this study, the 380 kV Keban power transmission line was realistically modelled using the 2009 TEIAS data. The modelling was performed using the Matlab-Simulink© software. Keban Transmission Line Matlab Simulink Modelling is shown in Figure 1.

4. Modelling with system parameters

The load distribution of power systems in Turkey is done and controlled by the National Dispatching Centre. These institutions are responsible for the maintenance, work and load distribution of the interconnected system elements in their regions (TEIAS; EMO, 2007; Donmez, 2008). The map showing Dispatching Centre regions is given in Figure 2 (TEIS).

In the load dispatching map given in Figure 2, regions can be seen to have integrations with the neighbouring countries besides the integrations among them. In this study, the South-eastern Anatolia Power system in the Electrical Power Network of Turkey was evaluated, and the 380 kV/1,530 MVA Keban transmission line was modelled. The data from the Turkey Electric Transmission Corporation (Donmez, 2008) was used in the model. The load values and other parameters of the selected line reflect the properties of the interconnected network, which was updated in 2009. The line schematics of the model are shown in Figure 3.

In Figure 3, the model of the line on the Keban transmission line was constructed. The schematics of the faults are given in Figure 4. Here, the point (1) identifies the first data collection point, and (2) denominates the second. The second point is also the point of fault where short circuiting occurs.

In Figure 4, the data collection system pertaining to the Keban power transmission line is shown schematically. The explanations of the scenarios on the model are given in Table 1.

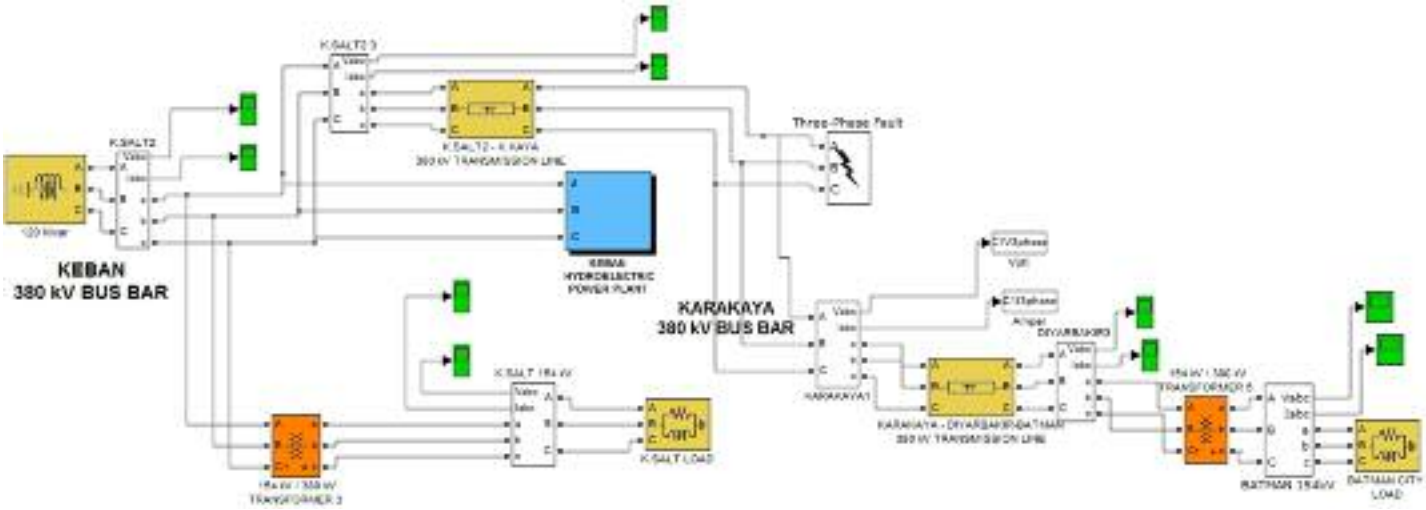

Figure 1: Keban transmission line Matlab Simulink modelling
(TEIAS)

Figure 2: Inter-regional integration plan on the Turkey electrical network
(TEIAS)

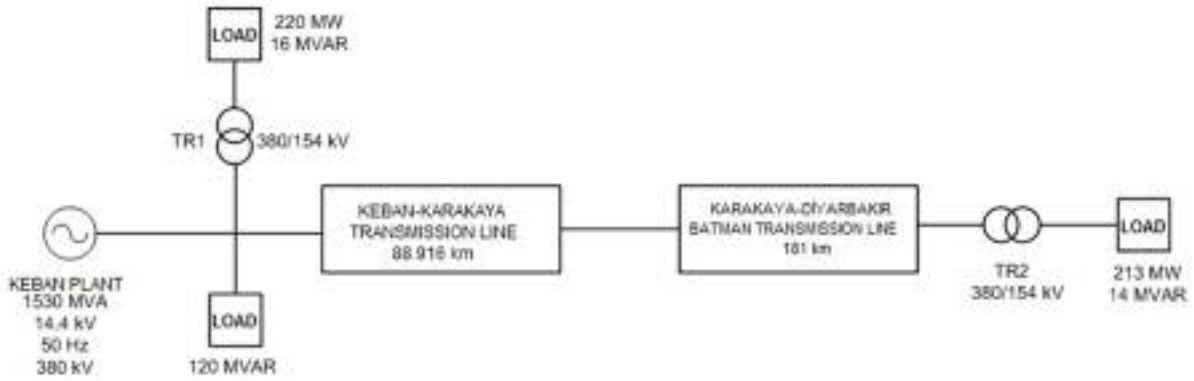

Figure 3: Keban power transmission line plan

Figure 4: Keban power transmission line data collection plan

Table 1: Short circuit scenarios are created on the model

Case 1	R Phase – Ground Short Circuit
Case 2	R – S Phase – Ground Short Circuit
Case 3	R – S – T Phase – Ground Short Circuit
Case 4	R – S Phase Short Circuit (Two Phase)
Case 5	R – S – T Phase Short Circuit (Three Phase)

In Table 1, five basic scenarios were taken and the type of fault each scenario represents was shown. These scenarios include Phase-Ground or Phase-Phase short circuits. Figure 5 shows that Matlab Simulink models created faults in Table 1, and the time-frequency analysis method was used for these failures. Figure 5 shows the Current-Time and Voltage-Time graphs for an R phase-ground fault formed on a point on the line. The timing for the short circuit event starts at the 1st second and continues until the 1.3rd second. The short time short circuit event, the current and the voltage to time graphs are given in Figures 10, 11 and 12, respectively.

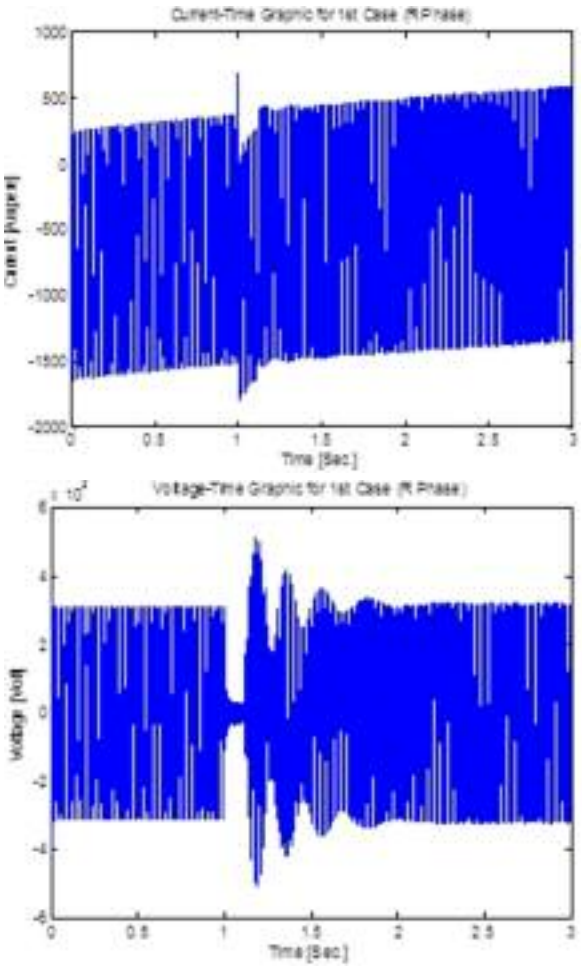

Figure 5: R phase-ground short circuit current-time and voltage-time graphic

The current-time graph of the second case is given in Figure 6. It can be clearly seen here that the second case graphs are different from the graphs of the first fault point. Here, the 1st fault point is closer to the generator point of the Keban plant and at the beginning of the transmission line. The second data collection point (2nd point) is on the line between the 89 km transmission line and the 181 km transmission lines. The 2nd point is where the fault is simulated to occur. It has also been used in the data collection as a measurement point. This transmission line is shown in Figure 3, and the line schematics are the occurrence point for the faults as shown in Figure 4. Fault scenarios were formed based on the line schematics in Figure 4.

In Figure 7, the r Phase-Ground short circuit (Case 1) of the data gathered from the 2nd point is

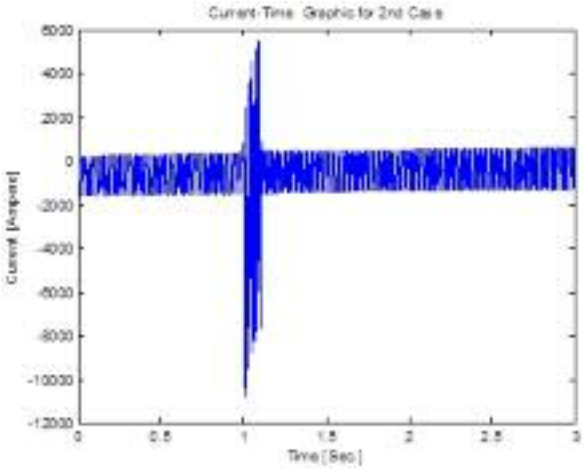

Figure 6: Current-time graphic for Case 2

given. The graph shows, the formation of an R phase-ground short circuit after the 1st second can be clearly seen. This graphic is a current-time graphic and very different from the voltage-time graphic. This difference is caused by the 2nd data point located between two transmission lines. Similarly, the voltage-time graphic of the Case 5 is given in Figure 8.

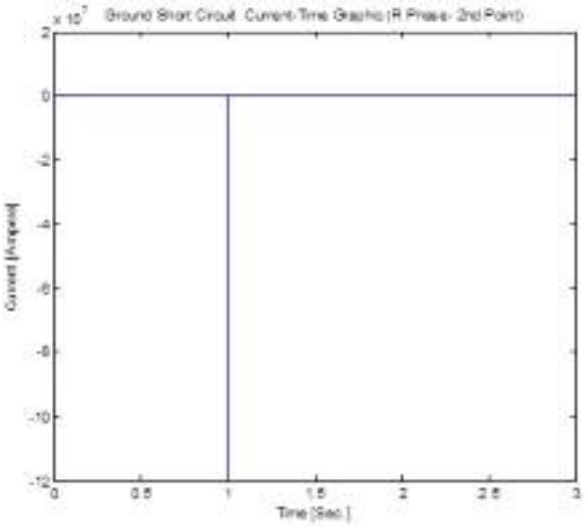

Figure 7: R phase – ground short circuit current-time graphic (R phase- 2nd point)

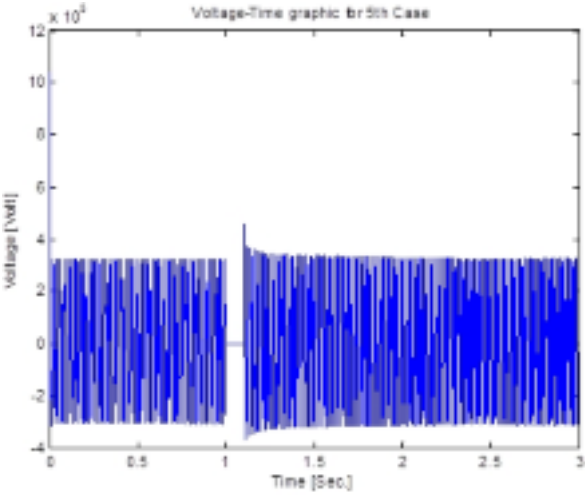

Figure 8: Voltage-time graphic for the Case 5

5. Mathematical methods

In this section, the mathematical methods used in the analysis of short circuit events in the electrical power systems are mentioned. The Time-Frequency analysis method was used in the analysis.

6. The time-frequency analysis method

Spectral analysis methods (Time-frequency analysis) are Fourier Transformation (FT) based approaches, and this study used mostly the Short Time Fourier Transformation (STFT) approach. The STFT approach is an alternative method based on the classic Fourier Transformation used in the analysis of dynamic data (Vaseghi, 1996; Akinci *et al.*, 2009; Onal and Dikun, 2013).

$$S_{yy}(f) = \frac{1}{N}\left|X(m\Delta f)Y(m\Delta f)\right| \quad (7)$$

7. Short time Fourier transformation and the spectrogram

Let us assume $x(t)$ is a stationary sign to determine STFT. This sign is framed in a fixed $g(t)$ dimension cantered on τ time. In this case, the STFT is of the sign (Akinci *et al.*, 2009; Onal and Dikun, 2013; Seker and Akinci, 2012).

$$STFT\{x(t)\} \equiv X(\tau, f) = \int_{-\infty}^{+\infty} x(t)g(t-\tau)exp[-j2\pi ft]\,dt \quad (8)$$

The equation of the sign can be identified on the time-frequency (t, f) plane with a two dimensional function. The analysis depends on the chosen window size $g(t)$. After the window $g(t)$ is chosen, the resolution of the STFT is fixed throughout the time-frequency plane. In a disjoint case it is identified with Eq. (9).

$$STFT\{x(n)\} \equiv X(m, f) = \sum_{n=-\infty}^{+\infty} x(n)g(n-m)e^{-j\omega n} \quad (9)$$

The amplitude changes on the time-frequency plane for the Fourier transformation windowed for the $x(t)$ signal in the time identification region is observed through the equality below:

$$S\{x(t)\} = \left|X(\tau, f)\right|^2 \quad (10)$$

In this context, the $S\{.\}$value is called the spectrogram of the $x(t)$ signal.

8. The spectral analysis of the short circuit fault

In this section, the analysis of the data obtained from the Keban energy transmission line model through the short circuit fault was performed with the Fourier method (Time-Frequency analysis). Analyses for every scenario or case were performed in the study.

In Figure 9, as a result of a phase-ground short circuit, high frequency components begin to form after the 1st second. Although the fundamental frequency of the system is 50 Hz, frequencies as high as almost 3 kHz occur.

Figure 10 demonstrates the time frequency analysis output of the current short circuit for the R phase of Case 2. As seen in the analysis, the high frequency components are only seen at the moment of the short circuit fault, and current flows through the circuit with the system frequency, which is about the fundamental frequency 50 Hz, in other time

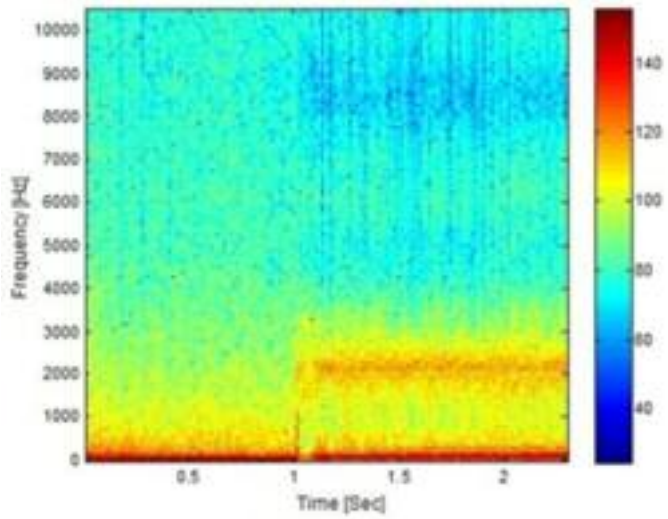

Figure 9: Voltage spectrum of the R phase ground short-circuit failure

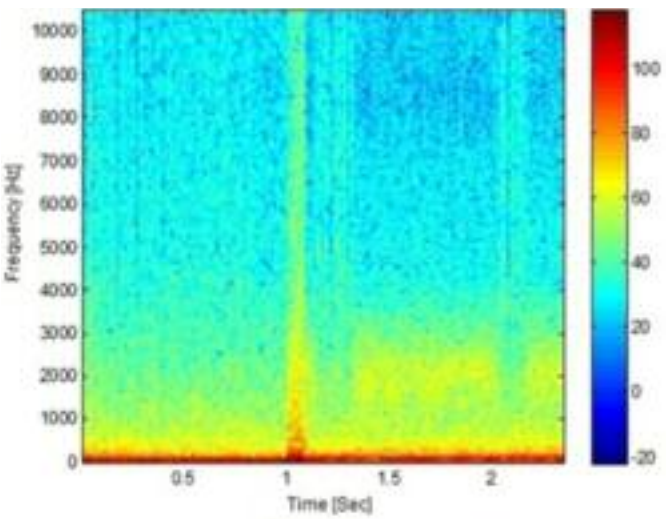

Figure 10: Short circuit analysis of the R phase for Case 2

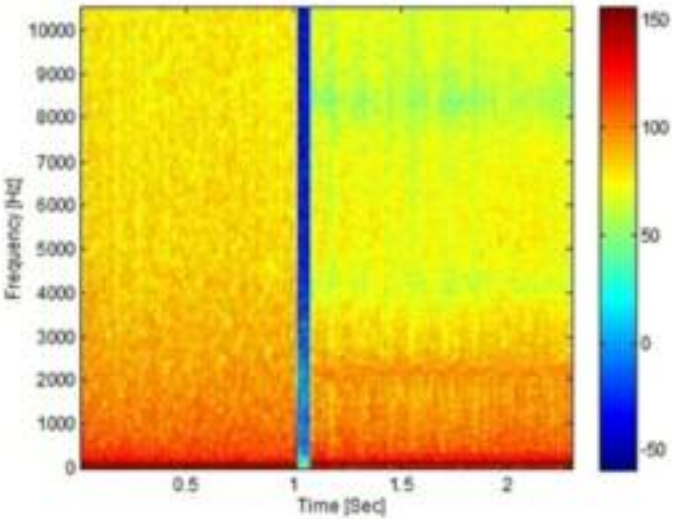

Figure 11: 1st case Short circuit analysis of the R phase at the 2nd point

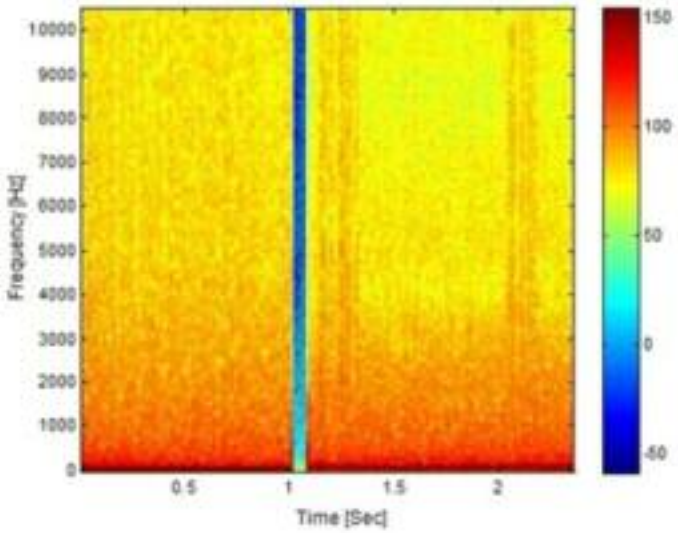

Figure 12: Time-frequency analysis of Case 2 – 2nd fault point

regions. A similar case can be seen in Figures 11 and 12.

In Figure 13, the time frequency spectrum of a three phase short circuit on the 2nd point was given. As seen on the spectrum, voltage is not induced on the system at the moment when the short circuit fault occurs, and the system returns to its nominal values as soon as the fault ends.

While a similar problem is encountered on the system, especially in the case of short circuit faults between two transmission lines, it can be seen at the 1st measurement point that the current draws on the system in cases of fault. This can be interpreted as the system feeding other loads. The Keban power transmission line was examined exclusively in this study, and the interpretations on system characteristics are made based on this system. The results of time-frequency analyses may be different in different systems.

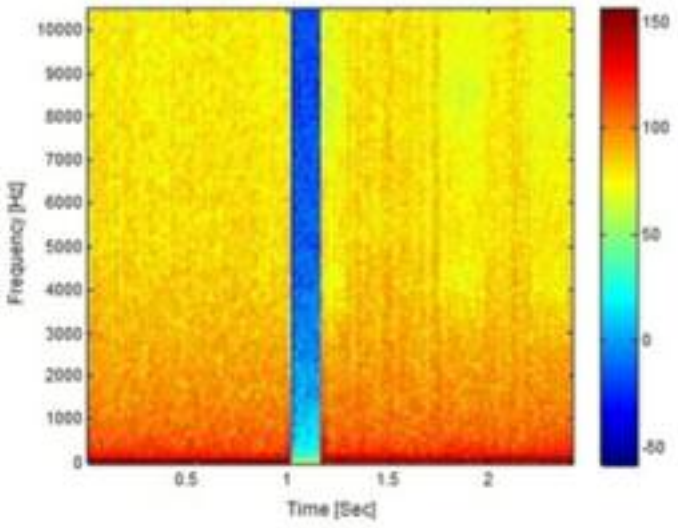

Figure 13: Time-frequency analysis of the Case 5 – 2nd point

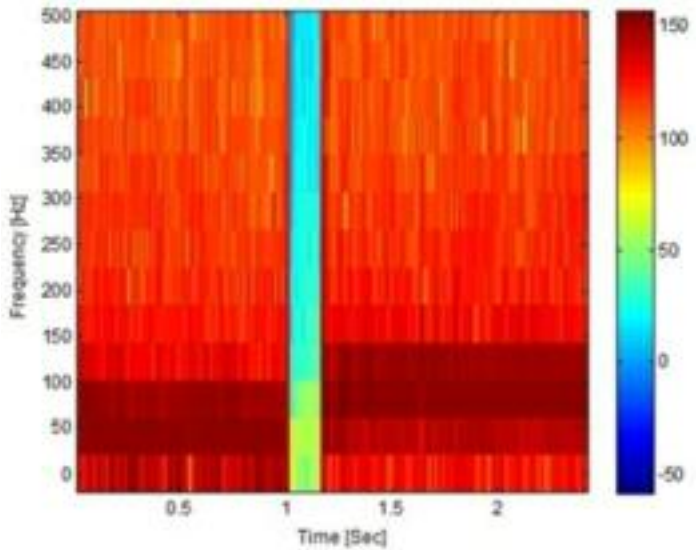

Figure 14: Three phase short circuit fault for 2nd fault point

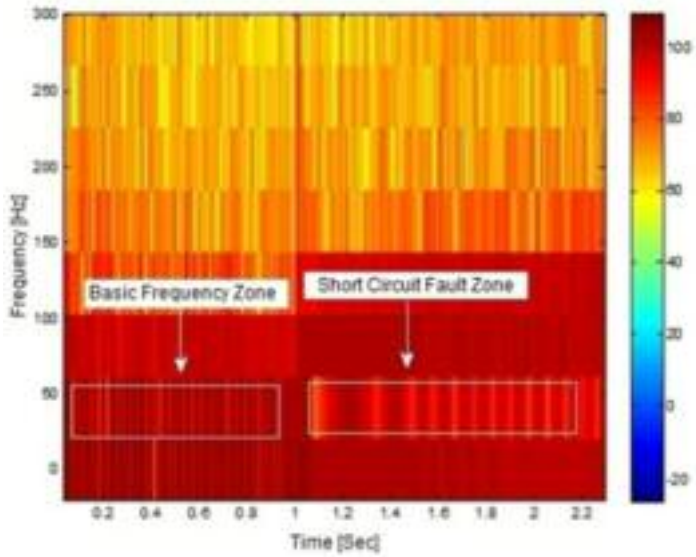

Figure 15: Analysis of short-circuit fault zones

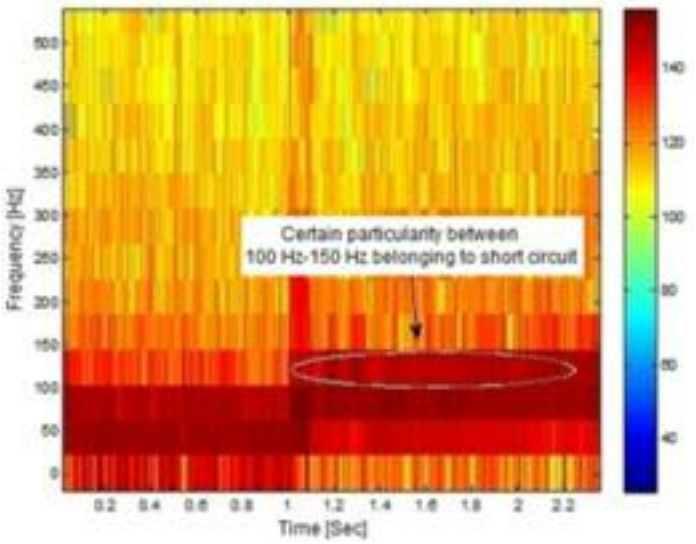

Figure 16: Short-circuit faults feature extraction

9. Conclusion

In this study, a line on the Keban power transmission line in the Eastern Anatolia Region in Turkey was modelled using real parameters, and the short circuit scenarios were generated over this model. In addition, the data was analysed using the Time-frequency spectrum. It was observed that the findings were consistent with the graphics derived from the Matlab-Simulink modelling. In the study, a short circuit fault was generated on one point over the line and the measurements were taken from two points. The important findings related to the measurements of the short circuit fault spectrums are listed below.

The graphic regarding the three phase short circuit fault, namely the fifth condition on the second fault point, is presented in Figure 14. This graphic can also be interpreted as a graphic demonstrating that there was no voltage transmission during the short circuit between the 1.0 and 1.3 seconds. A column can be observed at approximately 0 Hz, which can also be seen in the colour bar between the 1.0 and 1.3 seconds.

Another important finding of this study was that 50 Hz, which can be seen in Figure 15, is clearly the fundamental frequency area. The short circuit fault area, which is the fundamental frequency area, can be clearly observed in the same frequency area with different distributions after the short circuit. In addition, the short circuit fault area can also be seen clearly between the frequencies of 100 Hz and 150 Hz with its high amplitude.

In Figure 16, it can be observed that frequency components higher than the fundamental frequency of 50 Hz are formed immediately after the short circuit fault. This analysis can be regarded as one of the most important findings of the current study. The high frequency area became evident on all frequencies (50-500 Hz), particularly during the period between the 1.0 and 1.3 seconds. Its distinct characteristics were observed on different frequency components after the mentioned period.

Finally, another important finding of the present study was that the results of the Fourier analysis, which occur during short circuits, differ according to the type of fault, the length of the line or loading (Onal and Dikun, 2013; Seker and Akinci, 2012). In case of conducting characteristic investigations on the line, it can be suggested that the Time-Frequency analysis yields effective results and is an efficient method for determining the characteristics of a system. Regarding the region, where the present study was conducted, it was observed that the high frequencies occurred as a result of the fault in 100-150 Hz frequency components after the short circuit fault and that frequencies above 500 Hz occurred during the fault.

Further studies can investigate the sensitivity of systems to short circuit fault by using the methods of artificial intelligence.

Abbreviations

Z_{SC} Short circuit impedance
I_{SC} Short circuit current
ΣR Sum of serial resistances
ΣX Sum of serial reactance
V_n Uncharged nominal network voltage
V_{LL} Voltage between phases

References

Acar O. (2008). Modelling on Computer Environment of Adapazarı Tedaş Ada Transformer-stadium Dispatching System. Master's Thesis, Sakarya University, Sakarya, Turkey.

Akinci T.C., Ekren N., Seker S., and Yildirim S. (2013). Continuous Wavelet Transform for Ferroresonance Phenomena in Electric Power Systems, I*nternational Journal of Electrical Power & Energy Systems*-Elsevier, 44:403-409.

Akinci, T.C., Seker S., and Ekren N. (2009). Feature Extraction for Ferroresonance Phenomena in Electric Power System, International Conference on Modeling and Simulation (IASTED) MS'09, Alberta, Canada, July 2009.

Aygen Z.E., Batman M.A., and Tarkan N. (1995). Short Circuit Analysis up to Probability with Monte Carlo Method in Electrical Energy Systems. Electrical Engineering 6th International Congress, pp.41–44, September 11–17, 1995.

Billinton R, Salvaderi L, McCalley JD, Chao H, Seitz Th, Allan R. N, Odom J, and Fallon C, (1997). Reliability issues in today's electric power utility environment. *IEEE Transac Power Systems*, 124: No. 4.

Chanda R.S., and Bhattacharjee P.K. (1994). Application of computer software in transmission expansion planning using variable load structure. *Electric Power Syst Res*, 31:13–20.

Dogruer V. (2007). Short Circuit Fault Analysis via Matlab Simulink and Van's Energy Transmission Line Examination as a Pattern. Master's Thesis, Yuzuncu Yil University, Van, Turkey.

Donmez F. (2008). Computer Supported Analysis of System Fall Appearing after Calamity in Electrical Meshwork. Master's Thesis, Marmara University, Istanbul, Turkey.

Ekici S., Yildirim S., and Poyraz M, A. (2009). Pattern Recognition Application to Keep Distance. *Gazi University Faculty of Engineering Architecture Periodical*, 24:51–61.

Ekiz A., and Tumay M. Modelling Harmonics Appearing in Factories by being used Matlab/Simulink. Electrical- Electronics- Computer Engineering 10th International Congress, Ankara, pp.99–102.

EMO (2007). Aegean Region Production Transmission and Dispatching. Technics, EMO Izmir city Branch Energy Commision, May, 2007.

Evrenosoglu C.Y., and Abur A. (2005). Travelling Wave Based Fault Location for Teed Circuits, *IEEE Transac Power Deliv*, 20:1115–1121.

Faig J., Melendez J, Herraiz S, and Sánchez J. (2010). Analysis of Faults in Power Distribution Systems With Distributed Generation. International Conference on Renewable Energies and Power Quality (ICREPQ'10), Granada, Spain, 23th to 25th March, 2010.

Gopalakrishnan A., Kezunovic M., McKenna S.M., and Hamai D.M. (2000). Fault Location Using the Distributed Parameter Transmission Line Model. *IEEE Transac Power Deliv*, 15:1169-1174.

Hambley, A.R. Electrical engineering: principles and applications. Prentice Hall. pp. 637, ISBN 9780131470460, Retrieved 20 April 2011.

IAEA (1995). Expansion Planning for Electrical Generating Systems, A Guidebook, Technical Reports Series No. 241 1984 or User's Manual of WASP-III Plus, Computer Manual Series, No. 8, 1995.

Kamkaratug P. (2011). Redution of Over Line Current in Power System from Short Circuit Effect Using Static Synchronous Series Compensator. *Am J Appl Sci*, 8:129–133.

Kasikci I. (2002). Short Circuits in Power Systems: A Practical Guide to IEC 60 909. Wiley-VCH, Weinheim, Germany.

Maslo K., and Vnoucek S. (2001). Short Circuit Calculation Analysis. Paper accepted for presentation at PPT 2001, IEEE Porto Power Tech Conference 10th -13th September, Porto, Portugal, 2001.

Miroshnik R. (2000). The probabilistic model of the dynamic of the cables under short-circuit current. Comp Meths Appl Mech Eng, 187:201–211.

Onal E., and Dikun J. (2013). Short-Time Fourier Transform for Different Impulse Measurements, Balkan *Journal of Electrical & Computer Engineering*, Vol.1, No.1, pp.44-47.

Pamuk N. (2011). Modelling and analysing of electrical transmission meshwork in Sakarya by being used matlab/simulink programs. *Erciyes University Science Institute Periodical*, 27:19–39.

Paska J. (2007). Methodologies and Tools for Electric Power System Reliability Assessment on HL I and HL II Levels, 9th International Conference-Electrical power Quality and Utilisation, Barcelona, October 9–11, 2007.

Patel R., Bhatti T.S., and Kothari D.P. (2002). MATLAB/Simulink-based transient stability analysis of a multimachine power system. *Int J Electrical Eng Educ*, 39:320–336.

PDH Online. Introduction to Short Circuits Analysis. www.pdhonline.org/cgi-in/quiz/courses/courselist.cgi?class_name=*e*204:Introduction, 18/03/2013.

Schneider Electric (2005). Calculation of Short-Circuit Currents. Cahier Technique No.158.

Seker S., Akinci T.C., and Taskin S. (2012). Spectral and Statistical Analysis for Ferroresonance Phenomenon in Electric Power System, Electrical Engineering-Springer 2012, Vol..94, No..2, pp.117-124.

Serrican A.C., Ozdemir A, and Kaypmaz A. (2010). Short circuit analyzes of power system of PETKIM petrochemical aliaga complex. Online *J Electron Elec Eng (OJEEE),* 336–340.

Smeets R.P.P. (2010). Lathouwers AGA. Short-circuit withstand of T&D components, CEPSI Proceedings of the 18th Conference on the Electronic Power

Supply Industry, Taipei, Taiwan, October 24–28, 2010.
TEIAS: Transmission and Dispatching System-Transmission System. http://www.teias.gov.tr/apkuretim/iletimdagitim.htm. 08/04/2011.
TEIAS: Turkey Electricity Production- Dispatching Statistics 2008, http://www.teias.gov.tr/istatistik2008/index.htm. 08/04/2011.
TEIAS: Load Dispatch Chamber Headship Management Function Reports. http://www.teias.gov.tr/yukdagitim/yillik_menu.htm. 08/04/2011.
TEIAS: 9th Dispatching Facility and Management Group Directorship 380 Kv-ENH List. www.teias.gov.tr/Gr9/eihatlariliste.xls. 08/04/2011.
TEIAS: Load Dispatch Management Headship. http://www.teias.gov.tr/haritayukOK.htm. 09.04.2011.
Tekin K. (2006). Short Circuit and Interaction Examination in Electrical Systems Containing Wind Energy Facility. Master's Thesis, Istanbul Technical University, Istanbul, Turkey.
Unal A. (1996). Determination of mathematical model of an electric power system using linear graph. *Math Comput Appl*, 1:134–139.
Vaseghi V.S. (1996). Advanced Signal Processing and Digital Noise Reduction, John Wiley, New York, USA.
Yuhai S., Guangjian W., and Xiangguo C. (2007). Fault Detection and Analysis of Distributed Power System Short-circuit Using Wavelet Fractal Network, The Eighth International Conference on Electronic Measurement and Instruments.
Závodný I.M (2005). Power Electric System Transient Simulation Using Matlab-Simulink. Konference a soutež Student EEICT.

Received 30 October 2013; revised 17 March 2015

Erratum

In Volume 26 Number 1, the paper titled: A comparative study of the stochastic models and harmonically coupled stochastic models in the analysis and forecasting of solar radiation data by Edmore Ranganai and Mphiliseni B Nzuza was published on pages 125–137.

The corrections for the normality test in Figure 8 and the corresponding text was incorrect, and a reference was omitted. The replacement text, table and figure are as follows:

5.2 SARIMA and HCSARIMA modelling

Both SARIMA and HCSARIMA models with significant (p-values< 0.05) parameters were fitted on all four data series (see Appendices A and B, respectively) via maximum likelihood (ML) estimation. To check the adequacy of these models, tables of residual analysis based the Box-Ljung statistics (p-values> 0.05) for no serial correlation and; histograms (bell-shaped) of residuals, Q-Q plots (approximately straight line), and the Kolmogorov-Smirnov, Cramer-von Mises and the Anderson-Darling normality tests (p-values > 0.05) for normality of residuals. Satisfying all criteria in parenthesis constitute adequacy. For brevity, only results for model A are given in Appendix C.

Table 14: Fitted normal distribution for RESIDUALS

Goodness-of-fit tests for normal distribution				
Test	*Statistic*		*p value*	
Kolmogorov-Smirnov	D	0.05231706	Pr > D	>0.150
Cramer-von Mises	W-Sq	0.10654126	Pr > W-Sq	0.094
Anderson-Darling	A-Sq	0.73446188	Pr > A-Sq	0.056

Details of authors

Safdar Ali *B Sc M Sc M.S*
College of Engineering, Department of Computer Engineering, Jeju National University Republic of Korea
E-mail: safdar.ali.sannan@gmail.com
Safdar Ali received his B Sc, M Sc and M.S degrees in computer science from Peshawar University Pakistan in 2001, 2003 and NUCES FAST Islamabad Pakistan in 2010. He joined the Mobile Computing Lab, Jeju National University as a PhD student in 2011. His area of interest is M2M, energy management, optimization and prediction in building sector.

Tahir Cetin Akinci *B Eng (Electrical,) M Sc (Electrical Edu) PhD (Electrical Edu)*
Associate Professor: Electrical & Electronics Engineering
Kirklareli University, Faculty of Engineering
39100, Kirklareli, Turkey
Phone: +90 288 214 05 14
Fax: +90 288 214 05 16
E-mail: cetinakinci@hotmail.com
Tahir Cetin Akinci is an electrical engineer with M Sc and PhD degrees from the Marmara University, Electrical Education Department. He is currently associate professor of electrical & electronics engineering at Kirklareli University. His research interests are electrical energy systems, signal processing, soft computing and condition monitoring techniques.

A Valan Arasu *B E (Mech) M E (Thermal Eng) PhD*
Boyscast Fellow
Associate Professor, Department of Mechanical Engineering,
Thiagarajar College of Engineering, Madurai, Tamilnadu, India
Tel: +91 98653 16125
Fax: +9145224 83427
E-mail: avamech@tce.edu
A. Valan Arasu is currently Associate Professor in the Department of Mechanical Engineering of Thiagarajar College of Engineering, Madurai, India. He obtained his B.E. degree from Thiagarajar College of Engineering, Madurai, India. He received his M.E degree in Thermal Engineering & Ph.D. from Anna University, Chennai, India. He completed PDF in the area of energy storage with phase change materials at NUS, Singapore, under BOYSCAST Fellowship from the Department of Science and Technology, Government of India.
He has about 20 years of teaching experience. His area of research is thermal energy engineering and has published many technical papers in refereed international journals and conferences. He has carried out several sponsored research project works and consultancy works. He has authored three books viz. Turbomachines, Thermal Engineering and Thermodynamics. He is listed in Marquis Who's Who in the World 2009.

Hasan Aydogan *PhD*
Assist. Prof (Dr) Mechanical Engineering Department
Selcuk University, Technology Faculty, Mechanical Engineering Department, Campus, Selcuklu, Konya 42075 TURKEY
Tel: +90 332 223 33 39
Fax: +90 332 241 21 79
E-mail: haydogan@selcuk.edu.tr
Hasan Aydogan has a PhD in Mechanical Engineering. His major is renewable energy and biodiesel. Currently he is appointed as an Assistant Professor in the Mechanical Engineering Department of the Technology Faculty, Selcuk University.

Sunil Chirayath
Associate Director, Nuclear Security Science & Policy Institute (NSSPI), Texas A&M University (TAMU); and Assistant Professor, TAMU Nuclear Engineering Department
Dr Sunil Chirayath is an expert in the area of nuclear safety, security and safeguards research and education. He teaches courses on nuclear fuel cycle, nuclear material safeguards, nuclear security and Monte Carlo radiation transport. His research interests include safeguards approaches for nuclear fuel cycle, proliferation resistance quantification & analysis, nuclear forensics, nuclear security insider threat analysis, fast breeder reactor analysis and small modular reactor neutronics coupling with thermal hydraulics. In the NSSPI, he manages projects funded by USDHS (Domestic Nuclear Detection Office), USDOE (National Nuclear Security Administration and Nuclear Energy),

USDOS (Partnership for Nuclear Security) and nuclear utility companies. Prior to his appointment in NSSPI, he served at the Indian Atomic Energy Regulatory Board (AERB) in the capacity of Scientific Assistant (1991-1998) and Scientific Officer (1998-2007) with the responsibility for the regulatory review of Indian nuclear fuel cycle facilities. He earned his PhD and M Sc in Physics respectively from the University of Madras and University of Calicut (India). He has over 100 technical publications and about 25 in refereed journals and 80 in national and international conference proceedings, with citations of more than 100.

Jelena Dikun
Lecturer, Electrical Engineering Faculty, Klaipeda University, Lithuania
Jelena Dikun was born in Klaipeda, Lithuania. She received P.B. from Klaipeda Business and Technology College in Electrical Engineering Faculty (2005-2009) and a B.Sc. from Klaipeda University in Electrical Engineering Faculty (2009 – 2011). In present, she is lecturer in Electrical Engineering Faculty of Klaipeda University. She visited as a trainee of Istanbul Technical University from 21 October, to 22 November, 2012 that was provided by projects JUREIVIS and 'Lithuanian Maritime Sectors' Technologies and Environmental Research Development'. Her areas of interest are the study of electric and magnetic fields.

Marina du Toit *M Eng (Nuclear)*
Eskom, PO Box 19447, Noordbrug, Potchefstroom, 2522, South Africa
Tel: +27 84 4991 263
Fax: +27 86 6648 796
E-mail: skapiemarina@gmail.com
Marina du Toit is a PhD student at the Post Graduate School for Nuclear Science and Engineering, North West University. The subject of her PhD project is 'Design analysis of European Pressurized water Reactor (EPR) with the introduction of thorium-uranium in the core. '
She completed my Master's degree in Nuclear Engineering in 2012. She has been working as an Engineer at Eskom since the start of 2013. Some of her experience includes training at Koeberg Nuclear Power Station.

Vedat Esen *B (Electrical Education) M Sc (Electrical Education)*
Lecturer: Department of Electricity
Arel University, Vocational High School, Department of Electricity,
Istanbul, Turkey
Phone: +90 212 540 96 96
Fax: +90 212 540 97 97
E-mail: vedatesen@arel.edu.tr
Vedat Esen graduated from Marmara University, Technical Education Faculty, İstanbul, in 2009 and received his M Sc degree from Marmara University, Institute of of Electrical and Electronics Engineering, Marmara University, Institute of Pure and Applied Sciences in 2011. He is currently an instructor at İstanbul Arel University. His current interests are electrical power systems, energy policy and control sytems.

Kenneth Joseph Gondwe *B Sc (Mech) Eng M Eng (Systems)*
Senior Lecturer, Mechanical Engineering
University of Malawi, The Polytechnic, Mechanical Engineering Department,
P/Bag, 303, Chichiri, Blantyre 3, Malawi
Cell: +2658 8851 5050/ +2659 9473 0531
Emails: kgondwe@poly.ac.mw/ gondwekj@gmail.com
Mr. Gondwe holds a Master's degree in Systems Engineering from Oklahoma State University in the USA and a B Sc (Mechanical) Engineering with Distinction from University of Malawi- The Polytechnic. He is also a fellow of Leadership for Environment and Development (LEAD). Mr. Gondwe is currently working as the Director of Polytechnic Commercial Technical Services Centre and Senior Lecturer in Mechanical Engineering at the Polytechnic. Mr. Gondwe is a seasoned energy and climate change researcher and consultant. He has been involved in various areas of climate change: national communication to UNFCCC, training programmes, greenhouse gas inventories, vulnerability and adaptation assessment, national inventories, state of environment reports, national adaptation programmes of action (NAPAs), CDM project evaluations, Nationally Appropriate Mitigations Actions (NAMAs) as well as policy and strategies. In the energy sector, he has undertaken a number of energy baseline studies, project evaluations and energy technology research and development in the area of renewable and sustainable energy options.

Shantanu Kelkar *PhD*
Research Engineer, Michigan State University
219 Farrall Hall East Lansing MI 48823, USA
Tel: +1 517 507 0540
E-mail: shant121@gmail.com
Shantanu Kelkar obtained his PhD in Chemical Engineering from Michigan State University and currently works at DuPont. He has worked and conducted research in the areas of food process development, bioenergy, catalysis and bioseparations.

Do-Hyeun Kim *B.S M.S PhD*
College of Engineering, Department of Computer Engineering, Jeju National University Republic of Korea
E-mail: kimdh@jejunu.ac.kr

Do-Hyeun Kim received the B.S. degree in electronics engineering from the Kyungpook National University, Korea, in 1988, and the M.S. and Ph.D. degrees in information telecommunication the Kyungpook National University, Korea, in 1990 and 2000, respectively. He joined the Agency of Defence Development (ADD), from Match 1990 to April 1995. Since 2004, he has been with the Jeju National University, Korea, where he is currently a Professor in the Department of Computer Engineering. From 2008 to 2009, he has been at the Queensland University of Technology, Australia, as a visiting researcher. His research interests include sensor networks, M2M/IOT, energy optimization and prediction, intelligent service, and mobile computing.

Theodore Mwata Kipepe *B Eng (Met) M Tech (Met)*
Student researcher: Energy Efficiency
University of Johannesburg
PO Box 524, Auckland Park, 2006, South Africa
Cell: +27 78 014 4921
Alternative cell: +27 73 694 9130
E-mail: tkipepe@gmail.com
Theodore Mwata Kipepe is a Metallurgical engineer with a Master's degree in Technology in Engineering Metallurgy. He has been a member of the SAIMM and SAIF since 2014. He got a Certificate in Supervisory Management and is currently studying the online course of Mineral Project Management with the University of Arizona and University of British Columbia. He has been tutoring Physical Metallurgy at the University of Johannesburg for almost 2 years, and is currently seeking a job in extraction metallurgy and energy sustainability.

Zhenglong Li *B.S. (Env Eng) M Sc (Env Eng) PhD (Chem Eng)*
Postdoc Research Associate: Materials Science & Technology Division, Oak Ridge National Lab
One Bethel Valley Road, Oak Ridge, TN 37909, United States
Tel: +1 517 290 9941
E-mail: lizhenglong1982@gmail.com
Zhenglong Li got his PhD degree in Chemical Engineering and Biosystems Engineering from Michigan State University. He also has B.S. degree and M.S. degrees in Environmental Engineering. He has developed strong expertise in Biomass thermochemical conversion, bio-oil electrocatalytic upgrading, heterogeneous catalysis and kinetics during his PhD and postdoc research. Currently he is appointed as a postdoc research associate in Materials Science and Technology Division at Oak Ridge National Lab, where he is working on biomass derived alcohols conversion to hydrocarbon blend-stock, which can be blended with petroleum gasoline, diesel and jet fuels.

Andrea Lombard *BA (Development and Environment) BA Hons (GIS) MA (Geography and Environmental Studies)*
Lecturer: Geography
Department of Geography, University of South Africa (UNISA)
Private Bag X6, Florida, Roodepoort, 1710, South Africa
Tel: +27 11 471 2352
Fax: +27 11 471 3216
E-mail: lombae1@unisa.ac.za
Andrea Lombard is a Geographer with a Master's degree in Geography and Environmental Studies from the University of Stellenbosch where she is also currently registered for her PhD focusing on the evolution of rural regions in South Africa as a result of macro-scale renewable energy infrastructure development. Andrea has been involved in a number of GIS related consultancy projects in the past while based at Stellenbosch University and is a qualified GIS mapping practitioner. She has recently been appointed as a lecturer in the Department of the Geography at the University of South Africa (UNISA) and is now based at the Science Campus of UNISA in Florida, Roodepoort.

Misagh Moradali *B Eng (Mech) M Sc (Mech)*
Graduated Student: Engineering Faculty, South Tehran Branch, Islamic Azad University, Tehran, Iran
Tel: +98 912 513 0309
Fax: +98 21 337 17140
E-mail: misagh-moradali@yahoo.com
Misagh Moradali is a mechanical engineer with a Master's degree in mechanical engineering. Since 2010 he has worked in a variety of industry sectors in Iran in the field of thermal engineering.

Edmund C Okoroigwe *B Eng (Agric Eng) M Eng (Mech Eng) PhD (Mech Eng)*
Senior Research Fellow: National Centre for Energy Research and Development University of Nigeria, Nsukka, Enugu State, Nigeria
Tel: +234 8064 879825, +234 8057156223
E-mail: Edmund.okoroigwe@unn.edu.ng
Edmund Okoroigwe is an Agricultural engineer with Masters and PhD degrees in mechanical engineering. Since 2006 he has worked as a renewable energy researcher in biomass conversion to energy at the National Centre for Energy Research and Development (NCERD), University of Nigeria, Nsukka. He lectures in the Department of Mechanical Engineering, University of Nigeria, Nsukka.He was a Fulbright Visiting Researcher at Michigan State University, East Lansing, USA. In 2014, he joined the Energy Research Centre (ERC),

University of Cape Town, as a Postdoctoral Fellow and researcher working on application of renewable energy resources in gas turbine technology under the ERAfrica Project.

Emel Onal *M Sc PhD*
Assistant Professor, Electrical Engineering Department, Istanbul Technical University
E-mail: eonal@itu.edu.tr
Emel Onal was born in Istanbul, Turkey. She received her B Sc., M Sc. and PhD degrees from Istanbul Technical University (ITU) in the Electrical and Electronics Faculty in Istanbul, Turkey. She worked as a visiting researcher at IEH Stuttgart University about GIS technology and transformers between 2006 and 2007. Her interest areas are in the areas of discharge phenomena, generation and measurement of high voltages. She is currently working as assistant professor in the Electrical Engineering Department at ITU.

Samuel O. Onyegegbu *BSE (Mech Eng) MSE (Mech Eng) PhD (Mech Eng)*
Professor: Mechanical Engineering
Dept of Mechanical Engineering, University of Nigeria, Nsukka, Enugu State, Nigieria
Tel: +234- 8033 949542
E-mail: samuel_onyegegbu@yahoo.co.uk
(http://www.unn.edu.ng/profile/professor-samuel-onuorah-onyegegbu)
Samuel Onyegegbu is a mechanical engineer with Masters and PhD degrees in mechanical engineering from the University of Michigan, Ann Arbor, USA. He was former Dean of School of Postgraduate Studies, and former Dean of Faculty of Engineering, former Director of National Centre for Energy Research and Development (NCERD) and many times Head of Department of Mechanical Engineering. His expertise and skills are on heat and mass transfer, solar energy and renewable energy.

Bulent Oral *B (Electrical Education) M Sc (Electrical Education) PhD (Electrical Edu.)*
Associate Professor: Electrical & Electronics Engineering
Marmara University, Faculty of the Technology 34722, Goztepe, Istanbul, Turkey
Phone: +90 216 336 57 70 ext 129
Fax: +90 216 337 89 87
E-mail: boral@marmara.edu.tr
Bülent Oral graduated from Marmara University, Technical Education Faculty, Istanbul, in 1994, and received MS and PhD degrees from Marmara University, Institute of Pure and Applied Sciences, in Istanbul, Turkey, in 1997 and 2004 respectively. He has been employed as a research assistant, lecturer and assistant professor in the Technical Education Faculty between 1994 to 2012. Presently Dr. Oral is an Associate Professor in the Technology Faculty, in the Electrical and Electronics Engineering Department at Marmara University. His special fields of interest include energy policy, electricity market and renewable energy systems.

Xiaowei Pan *B Sc (metallurgy) (Kunming University of Science and Technology) M Sc (metallurgy) (Beijing University of Science and Technology) PhD (metallurgy) (Wits)*
Dr Xiaowei Pan has worked for more than 30 years as a production engineer, lecturer and project manager with Kumming Heavy Machinery, Beijing University of Science and Technology, BHP Billiton Process Research, De Beers Technology Centre and Rand Controls (Pty) Ltd. From 2011 until now, he is lecturing at the Metallurgy Department, University of Johannesburg, supervising more than 10 postgraduate students with research interests in process improvement for industries of mining, alloy smelting and metal casting. Xiaowei Pan has been a member of organization committees for more than 6 international conferences, and has been invited as a peer reviewer for various conferences and journals, and is a member of an editorial board for an international journal in the USA. More than 50 papers have been presented and published on various conferences and journals internationally. More than 20 papers have been published in the last 3 years, and have been rewarded with accreditation by the Department of Higher Education and Training (DHET). He has been member of Executive Committees for various institutes, including NFTN of DTI, MCTS of Tia/DST, HCDP of DST, etc. He is currently a senate member of the University of Johannesburg.

Ghanshyam Purohit *BSc, MSc (Physics), Ph D (Physics)*
Professor: Physics
Associate Dean – Research
Sir Padampat Singhania University
Bhatewar, Udaipur – 313601, India
Tel: +91 2957 226095 to 100 (6 lines)
Fax: +91 2957 226094
E-mail: ghanshyam.purohit@spsu.ac.in
Dr. Ghanshyam Purohit is an Associate Dean – Research and Professor of Physics at Sir Padampat Singhania University, Udaipur, India. He is also a Visiting Professor at Sophia University, Tokyo, Japan. He obtained his PhD degree in theoretical atomic physics. His research interest includes Atomic & Molecular Physics, electron-atom / ion collision, Non-linear electronic circuits, quantum information theory, quantum computation, solar energy etc. He has over 40 research publications in the field of atomic physics, non-linear dynamics and chaos, MPPT techniques for solar panels. Dr. Purohit has visited ICTP, Trieste (Italy), Max Planck

Institute for Nuclear Sciences, Heidelberg (Germany), ITAMP, Harvard University, Cambridge (USA), ISSP, Tokyo University, Japan and Kitasato University, Sagamihara (Japan) as a visiting scientist. Besides this, he has presented research work at various international conferences held in the UK, USA, Japan, Germany, France, Austria, Italy, Sweden, Ireland, Switzerland and China.

A. Samuel Raja *B Sc (Chem) B Tech (Auto Eng) M E (Int Comb Eng)*
Assistant Professor, Department of Mechanical Engineering,
Thiagarajar College of Engineering, Madurai, Tamilnadu, India
Tel: +91 99430 87376
Fax: +91 45224 83427
E-mail: samuel1973@tce.edu
A. Samuel Raja is an automobile engineer with A Master's degree in internal combustion engineering. Since 1999, he has worked in various capacities in different educational institutions in India and abroad. He has handled various theoretical and practical courses on automobile engineering and has guided many projects in undergraduate and post graduate programmes. Currently, he is Assistant Professor in the Department of Mechanical Engineering, Thiagarajar College of Engineering, Madurai, Tamilnadu, India. His research interests include cold-start emission control in S.I. Engines, coolant heat and exhaust heat recovery, and simulation of IC engine processes.

Christopher M Saffron *Ph.D.*
Assistant Professor
Michigan State University
Dept. of Biosystems and Agricultural Engineering
Dept. of Chemical Engineering and Materials Science
Dept. of Forestry
524 S. Shaw Ln., 204 Farrall Hall
East Lansing, MI 48824
Tel: (517) 432-7414
Christopher M Saffron is a chemical engineer and possesses a PhD in chemical engineering. His areas of expertise includes process synthesis and techno-economic analysis of catalytic strategies for biofuels; upgrading lignin by pyrolysis and electrocatalysis.

Adoniya Sebitosi *B Sc (Eng)(Hons)(Nairobi) PhD (Cape Town) CEng REng MIET MIEEE MIDiagE MIEK*
Professor, Centre for Renewable and Sustainable Energy Studies
University of Stellenbosch
P/Bag X1, Matieland, 7602 South Africa
E-mail: sebitosi@sun.ac.za
Professor Sebitosi obtained his B Sc (Eng) with honours in electrical engineering from the University of Nairobi. He then joined industry and obtained extensive technical and managerial experience. His responsibilities included industrial quality assurance and training of service engineers in various countries in sub-Saharan Africa. He consequently attained various professional qualifications including Registered Engineer of Kenya and Chartered Engineer of the United Kingdom. In 2001 he joined the Department of Electrical Engineering at the University of Cape Town and subsequently obtained an M Sc (Eng) and PhD degrees with distinction.

He was nominee for the Joseph Arenow best PhD award in 2005. He was on the teaching staff of the Department of Electrical Engineering, at UCT between 2005 and 2008. He then joined Stellenbosch University in 2009 as senior lecturer and is currently Professor, Centre for Renewable and Sustainable Studies, in the Department of Mechanical and Mechatronic Engineering, Stellenbosch University. He is rated by the National Research Fund (NRF) of South Africa, as Established Researcher. He has published 30 papers in refereed international journals including Elsevier's Energy Policy, Energy Conversion and Management and IEEE Transactions on Energy Conversion as well as 29 refereed conference proceedings. He has co-published 1 book and 2 book chapters and 4 contract reports. He was lead coordinator for energy curriculum development for the Pan African University for water and energy. He is also a reviewer and editorial board member for several international energy journals and the National Research Fund (NRF) of South Africa. He is a recipient of the Rector's award 2010 Stellenbosch University. His research and professional interests include rational use of energy, (incorporating energy conversion, renewable energy, and water-energy nexus), energy policy, rural energisation, industrial quality assurance and power quality.

Ross Dane Schultz *B Sc (Physics and Chemistry), BSc Hons (Physics) MSc (Physics).*
Nelson Mandela Metropolitan University (NMMU)
Centre for Energy Research, PO Box 77000,
Nelson Mandela Metropolitan University, Port Elizabeth, 6031
Tel: +27 41 504 4860
E-mail: ross.schultz@nmmu.ac.za
Web: http://energy.nmmu.ac.za
Ross Schultz obtained his M Sc in Physics at the Nelson Mandela Metropolitan University in 2012 and is currently awaiting the results of his PhD. As a graduate from Nelson Mandela Metropolitan University, he was employed as a Research Assistant in 2014 at the Centre for Energy Research. During this position, he worked on projects such as the further development of CPV technologies, meteorological and solar resource monitoring, PV

system design, performance simulations and monitoring of popular Photovoltaic technologies. Mr Schultz's principal area of specialisation lies in Concentrator Photovoltaics (CPV) and flat plate photovoltaics, specifically the development and analysis of new modules and systems. He has published two scientific journal articles in the field of Photovoltaics and has authored or co-authored and has presented his research at one international and twelve national conferences.

Dinesh K Sharma *B Eng (Electro. & Commn. Engg.) M Eng (Electrical Eng) PhD (Solar PV)*
Assistant Professor: Electronics & Commn. Engg.
School of Engineering, Sir Padampat Singhania University
Udaipur-313601 (Rajasthan), India
Tel: +91-2957-226095 to 100 (6 lines) (Ext. 344)
Mobile. No. +91-7568912396
Fax: +91 2957 226094
E-mail: mail2dksharma@gmail.com
Dinesh K. Sharma received his B.Eng. degree in Electronics & comm. Engg. in 2003 from MJP Rohilkhand University, Bareilly (India) and an M. Eng. degree in Power Electronics, Electrical Machines & Drives in 2006 from M.D. University, Rohtak (India). He has submitted his thesis titled: Optimization of Efficiency of Solar Photovoltaic Systems using improved MPPT. Since 2010, he is working as an Assistant Professor in the ECE Department at Sir Padampat Singhania University, Udaipur (India). His research interests are solar energy systems including solar PV systems, Power electronics for renewable energy technologies, Solar Passive architecture, Green buildings and Sustainable energy development.
He has published more than 7 peer-reviewed research papers. He has recently presented two research papers at the 6th World Conference on Photovoltaic Energy Conversion (WCPEC-6) held at Kyoto, Japan, during November 23-27, 2014. He is the reviewer of the following International Journals: International Journal of Sustainable Engineering (IJSE), Taylor and Francis Group, UK; International Journal of Energy Engineering (IJEE), Scientific and Academic Publishing (SAP), USA; Journal of Clean Energy Technology (JOCET), Singapore; American Journal of Energy and Environment (AJEE), and Scientific and Academic Publishing (SAP), USA. He is a member of the International Association of Engineers (IAENG), Hong Kong.

Randall Spalding-Fecher *BA (Biology, Harvard) MALD (Intl Env Policy & Dev Econ, Fletcher School/Tufts)*
Senior Advisor: Carbon & Energy, Carbon Limits AS (Norway)
45 Station Road, Amherst, MA 01002 USA
Tel: +1 413 320 9810
E-mail: Randall.Spaldingfecher@gmail.com
Randall Spalding-Fecher has 18 years' experience in energy and climate change analysis. He has special expertise in Clean Development Mechanism (CDM) methodology and project development, energy economics, mitigation analysis, and energy efficiency analysis. His experience includes leading the 'Impact of CDM' research for the High Level Panel on the CDM Policy Dialogue, reviewing and consolidating more than 40 CDM baseline and monitoring methodologies, as well as serving as a consultant to the UNFCCC on additionality testing, technical guidelines for baseline methodologies, energy efficiency methodologies, and analysing requests for registration of CDM projects.

John L Taulo *B Sc (Mech) Eng M Sc Eng (Mech) AMIE*
Department of Mechanical and Mechatronic Engineering
Stellenbosch University
P/Bag X1, Matieland, 7602 South Africa
Tel: +27 78985 4929
E-mail: johntaulo@sun.ac.za
John Taulo received his bachelor's degree in mechanical engineering from the University of Malawi, in 1994, and the master's degree in mechanical engineering from University of Cape Town in 2008. He joined industry in 1996 where he worked in various capacities as Plant Engineer, Projects Engineer, and Production Engineer. In 2000 he joined the Malawi Industrial Research and Technology Development Centre as Research Officer and later on promoted to Senior Research Officer then rising to the position of Deputy Director responsible for research and development.
He is currently a Research Fellow and Head of Research and Development at the Malawi University of Science and Technology. His research interests include energy optimization, energy modelling and power productions systems. He is currently a PhD candidate at Stellenbosch University, working on multi-objective optimization of the tea industry with sustainability considerations.

Ernest E van Dyk *B Sc (Physics and Applied Mathematics) B Sc Hons (Physics) M Sc (Physics) PhD (Physics), Pr.Nat.Sci. Pr.Phys.*
Professor of Physics, Nelson Mandela Metropolitan University (NMMU)
Director: Centre for Energy Research, NMMU
Centre for Energy Research, PO Box 77000, Nelson Mandela Metropolitan University, Port Elizabeth, 6031
Tel: +27 41 504 2259
Fax: +27 41 504 1959
E-mail: ernest.vandyk@nmmu.ac.za

Website: http://energy.nmmu.ac.za
Professor Ernest van Dyk obtained his PhD in Physics at the University of Port Elizabeth in 1994. He teaches Physics at the NMMU and is also Director of the Centre for Energy Research (CER) at the NMMU since 2006. The CER is involved with several renewable energy research projects for industry and government agencies. Prof van Dyk's research interests are in the field of Solar Energy, specialising in Photovoltaics and Solar Thermal research. He has supervised 17 M Sc and 7 PhD student projects to completion and is currently supervising 6 PhD students. He has published forty-nine scientific journal articles in the field of Photovoltaics and has authored or co-authored 39 international conference papers and 128 national conference presentations. Prof van Dyk has a passion for teaching Physics and researching Renewable Energy Technologies. He also regularly consults on Photovoltaics and Solar Energy to national and international companies.

Frederik J Vorster *B Sc (Physics, Mathematics), M Sc (Physics), PhD (Physics)*
Senior Lecturer: Physics
Senior Researcher: Centre for Renewable Energy, Nelson Mandela Metropolitan University
PO Box 770002, Nelson Mandela Metropolitan University, Port Elizabeth, 6031, South Africa
Tel: +27 41 504 3051
Fax: +27 41 504 2573
E-mail: Frederik.vorster@nmmu.ac.za
Frederik Vorster is a physicist with PhD specialising in photovoltaics. He teaches Physics and Engineering subjects at the NMMU and is closely involved with the management and development of various projects at of the Centre for Energy Research. He is currently a Senior Lecturer at the NMMU and actively involved with supervision of several Physics and Engineering masters and doctoral students. Dr Vorster's broad research interests include solar energy, heat engines and micro wind turbine development. His principal area of specialisation lies in concentrator and flat plate photovoltaics, specifically the development on new characterisation techniques for photovoltaic materials, modules and systems. He has consulted to a variety of industry and public sectors in South Africa in the fields of photovoltaics and domestic solar water heating.

Masoud Yousefi *B Eng (Mech) M Sc (Mech)*
Lecturer: Fluid Mechanics, Thermodynamics and Heat Transfer
Student Deputy: Engineering Faculty, South Tehran Branch, Islamic Azad University, Tehran, Iran
Tel: +98 912 216 0771
Fax: +98 21 337 17140
E-mail: yousefi.masoud4@gmail.com
Masoud Yousefi is a mechanical engineer with a Master's degree in mechanical engineering. Since 2000 he has consulted to a variety of industry sectors in Iran in the fields of thermal engineering and natural gas systems for vehicles. Currently he is appointed as Deputy of Student Affairs in the Engineering Faculty of South Tehran Branch, Islamic Azad University, where he is also a full time lecturer in Mechanical Engineering.

INFORMATION FOR AUTHORS

The *Journal of Energy in Southern Africa* publishes papers covering the technical, economic, policy, environmental and social aspects of energy research and development carried out in, or relevant to, Southern Africa. Contributions from those working in these fields are welcome.

Submissions
All contributions should be submitted in English.

Only original work will be accepted, and by submitting an original work for publication the author grants the publisher a worldwide, non-exclusive, royalty-free and perpetual licence to reproduce, publish and distribute the author's work in any format or medium.

The suggested length for full-length articles is 3 000 to 5 000 words. All full-length articles are refereed, and amendments to scripts and formats may be required before final acceptance. The Editor reserves the right to make editorial changes to contributions.

The following shorter items are also welcome, but are not refereed:

- Research notes, Shorter communications and Case studies (500–2 500 words)
- Conference reports (100–1 500 words)
- Book reviews (800–1 000 words)

Format
Contributions should be in electronic format, and submitted either on disk or via e-mail. They should preferably be in a format compatible with MS Word. The Editor might also request the submission of a printed version.

Text should be single-spaced, with a wide left-hand margin. Standard international (SI) units must be used throughout.

An abstract of the article should be provided, not exceeding 500 words, resuming the contents and conclusions of the article. A maximum of six keywords should be included, reflecting the entries the author(s) would like to see in the annual Subject Index published in the last issue for the year. The keywords may consist of more than one word each, but the entire concept should not be more than 30 characters long.

References must be made according to the Harvard (author, date) system. See articles in the JESA for examples of this and of other aspects of its house style.

Notes, where unavoidable, should *not* be automatically embedded, but gathered at the end of the article and indicated in the text by means of sequential arabic numbers in superscript.

Numbers for headings, captions for tables and figures, etc should be manually inserted, rather than automatically generated.

Illustrations and tables
If the contribution is accepted, original electronic versions of graphs must be supplied; produced, where possible, with MS Office programmes (Excel, PowerPoint). The quality of the illustrations must be acceptable to the Editor. For photographs and non-electronically produced drawings, the originals will have to be provided, or scans of an acceptable quality (minimum 300DPI). Straight screen-grabs are never acceptable. All illustrations must be provided in monochrome, and readable as such (colour photographs can be converted by us).

Illustrations and tables should appear in their proper places in the submitted document (not gathered at the end). All should be referred to in the text, numbered sequentially (manually rather than automatically), and with accompanying captions. Tables must be submitted as text, rather than as images.

General
No material will be returned to the author(s) following publication unless this is requested by at the time of original submission.

At the time of submission, the author(s) must state that the contribution has not been published and is not being considered for publication elsewhere, and will not be submitted for publication elsewhere unless rejected by the *Journal of Energy in Southern Africa* or withdrawn by the author(s).

Authors must supply a brief CV (maximum of 500 words), which includes the following personal information (for the Details of authors section): surname, initials, address, contact telephone/fax numbers, email address, qualifications, occupation and/or employment.

Authors of accepted contributions will receive a free copy of the issue in which their contribution appears as well as a PDF version.

Neither the Editorial Committee nor the Publisher accepts responsibility for the opinions or viewpoints expressed, or for the correctness of facts and figures.

All contributions and enquiries should be addressed to: The Editor, Journal of Energy in Southern Africa, Energy Research Centre, University of Cape Town, Private Bag, Rondebosch 7701, South Africa. E-mail: richard.drummond@uct.ac.za